HYDROSILOXANES: EFFICIENT AGENTS FOR CONTROLLED GENERATION AND NUCLEATION OF NOBLE METAL NANOPARTICLES

BY

RAJESH SARDAR

A dissertation submitted to the Graduate Faculty in Chemistry in partial fulfillment of the requirements for the degree of Doctor of Philosophy, The City University of New York.

2006

UMI Number: 3287102



UMI Microform 3287102

Copyright 2008 by ProQuest Information and Learning Company.
All rights reserved. This microform edition is protected against unauthorized copying under Title 17, United States Code.

ProQuest Information and Learning Company
300 North Zeeb Road
P.O. Box 1346
Ann Arbor, MI 48106-1346

This manuscript has been read and accepted for the Graduate Faculty in Chemistry in satisfaction of the dissertation requirement for the degree of Doctor of Philosophy.

	Dr. Bhanu P. S. Chauhan
Date	Chair of Examining Committee
	Prof. Gerald Koeppl
Date	Executive Officer
	Prof. Nan-Loh Yang
	Dr. Chwen Yang Shew
	Dr. Kenrick Martin Lewis

Supervisory Committee

THE CITY UNIVERSITY OF NEW YORK

Abstract

HYDROSILOXANES; EFFICIENT AGENTS FOR CONTROLLED GENERATION AND NUCLEATION OF NOBLE METAL NANOPARTICLES

By

Rajesh Sardar

Advisor: Professor Bhanu P. S. Chauhan

We have developed a new synthetic route where silver nanoparticles can be generated in organic solvent using polyhydrosiloxane as a reducing and stabilizing agent. We have also achieved the silver self-assembled silver nanonecklaces and nanocluster by varying the molar ratio of stabilizing agent. To extend the research, we have also investigated the role of counter anions on the particle morphology, stability and rate of the reaction. Different counter anions, ranging from organic to inorganic and hard to soft was studied in this investigation. It was observed that the under similar reduction condition, the rate of reduction, particle size and its stability varies from one silver salts to others. We also able functionalize the silver nanoparticle surface with thiol containing alkoxy to generates functionalize silver organosols.

We disclose a new high yielding synthetic method of SAMs of silver and gold nanoparticles. The synthesis was carried out using the oligomericsilane, heptamethyltrisiloxane in toluene. The method permits to obtain the SAMs of almost all the commercially available silver salts. The synthesized SAMs show remarkable stability at room temperature. The SAMs of silver nanoparticles also allow to do the redispersion

and solvent exchange study. The SAMs of gold nanoparticles permits the ligand exchange study on its surface.

A chemical method for large quantity of different shaped gold nanocrystals synthesis is described here. The method enable us the routine formation of gold nanoparticles, nanoprisms, and nanorods from the reduction of $HAuCl_4$ by simply varying the molar concentrations of reducing agent (PMHS) and surfactant (TOA). The different nanostructures has distinct optical properties and stable at room temperature. The synthesize nanoprisms has very low edge length and the nanorods has low aspect ratio. The gold nanoprisms are also achieved from the reduction of Et_3PAuCl salt and the edge length of the prisms can be controlled by varying the concentrations of TOA. The nanoprisms are then successfully converted to the gold nanocubes.

This thesis is dedicated to my parents for setting the foundation for me to make my goals such as this degree attainable. Their encouragement and mental support throughout my graduate study make my path easier

Acknowledgments

Obtaining a Ph.D degree is a long process requiring assistance from many people along the way. I would like to extend my gratitude to my mentor Professor Bhanu P. S. Chauhan for his enthusiasm, patience and encouragement throughout my dissertation research and I feel very fortunate to have had him. He has provided invaluable assistance in the development of my research and always managed to find time for our interactions, for which I am very grateful. I would also like to thank my dissertation committee- Professor Nan-Loh Yang, Professor Shwen-Yang Shew at College of Staten Island, and Dr. Ken Lewis at G. E, for their sound advice and warm support through all stages of my research. I would also like to thank Professor William L'Amourax at College of Staten Island for his help in EM analysis. I would also thank Dr. James E. Helt, Dr. Raja at College of Staten Island and Dr. Moni Chauhan at Queens borough Community College for their valuable comments and suggestions on thesis writing.

Thanks all the faculty, stuff, and graduate students of the chemistry department who have contributed to an extraordinary friendly and helpful working environment. I also want to thank my fellow graduate students Jitendra S Rathore, Alok Sarkar, Narayan Mukherjee, and Dr. Bharathi Balagam for their help in these Years and also all the undergraduate students in the lab. I would like to give my special thanks to Umar Latif, Manik Mandal, and Sukanta Dolai for their useful suggestions in the thesis writing. I would like to thank my two undergrads student, Victor Cheung, and Prashant Sharma for their hard work in the research projects. I am also thankful to all my friends Debarshi, Rajarshi, Nihar, Binita, and Suman for their encouragement and moral support during my research.

Finally, without naming each one individually, I would like to thank all of my family members for their encouragement and understanding during this “busy” time period of graduate study. Most important, I owe a special thanks to my incredible wife Moumita for all her love, patience, and support throughout my degree program and making our memories of Staten Island much more special.

Table of Contents

Chapter 1: Nanomaterials: Synthesis Stabilization, and Applications

1.1 Introduction……2

1.2 Properties of the noble metal nanoparticles…….…..3

1.3 Commonly available synthetic routes……....6

1.3.1 Reduction of transition metal salts…….……...7

1.3.2 Thermal, photochemical, and sonochemical methods……15

1.3.3 Metal vapor synthesis……..18

1.3.4 Electrochemical synthesis…….……..19

1.4 Stabilization of nanomaterials…….….21

1.4.1 Electrostatic stabilization…….22

1.4.2 Stabilization by ligand or solvent…….……...23

1.4.3 Stabilization by dendrimer…….……..…25

1.4.4 Polymer stabilized nanoparticles……..…27

1.4.5 Electrosteric stabilization…….29

1.5 Applications of the nanosized metal particles……..…30

1.5.1 Surface enhanced Raman Spectroscopy…….…..…30

1.5.2 DNA-Gold nanoparticles assemblies and sensors……...31

1.5.3 Au, AgNanoparticles as an effective catalysts…….36

1.6 Challenges of the solution phase synthesis……..…...40

1.7 Aim and objective of our research……...…42

1.7.1 To investigate the ability of Si-H bonds for the reduction of silver and gold metal salts……. ……42

1.7.2 To Utilize the Polymethylhydrosiloxanes (PMHS) and their Oligomeric Counter Parts, Heptamethyltrisiloxane (HMTS) as Reducing Agents……43

1.7.3 To Investigate, if it is Possible to Control the Nucleation and Growth of Metal Particles Under our Reaction Conditions……..45

1.7.4 To Investigate, if it is Possible to Control the Shape of the Synthesized Nanoparticles……...47

1.8 References and notes…….……...48

Chapter 2: The Ability of the Si-H bonds for the reduction of silver metal salts to silver nanoparticles

Part A: Self-assembled silver nanoclusters and nanonecklace formation: Poly(methylhydrosiloxane)-mediated one-pot route to organosols

2.1 Introduction……..62

2.2 Results and Discussions……...64

2.3 Conclusions……..71

Part B: Role of Polyhydrosiloxanes and counter anions in the self-assembly of silver nanoclusters

2.4 Introduction……..……72

2.5 Results and Discussions……..…..75

2.5.1 Synthesis of Ag(0) by PMHS in the presence of different molar ratios of TOA……...76

2.5.2 Rate of reaction and stability of nanoparticles from silver salts having inorganic counter anions..…….……...82

2.5.3 Study the rate of the reaction for organic counter anions……....83

2.5.4 Role of TOA in the reaction rate and synthesized particles…….…...84

2.6 Conclusions……..…...91

Part C: Silicon Thiol Stabilized Silver Nanoparticles: Functionalized Silver Organosols

2.7 Introduction……..……92

2.8 Results and discussions……94

2.8.1 Synthesis and characterization of Ag-thiol complex……...94

2.8.2 Reduction of Ag-thiol complex by PMHS …….……98

2.8.3 Thiol capped Ag(0) with different topologies…….……...100

2.9 Conclusions……...……..103

2.10 Experimental section……..….103

2.11 References……..…….….107

Chapter 3: Monohysiloxane Induced Formation of Noble Metal nanoparticles: A New Route to Self-Assembled Monolayers (SAMs)

Part A: Self-Assembled Monolayers (SAMs) of Silver Nanoparticles

3.1 Introduction……....111

3.2 Results and Discussion: Formation of SAMs…….……...114

3.2.1 Synthesis of self-assembled monolayers…….....115

3.2.2 UV-vis absorption spectroscopy studies…….…..…116

3.2.3 Characterization studies by TEM…….....118

3.2.4 Redispersion studies in organic solvents……...….122

3.2.5 Solvent exchange studies…….…129

3.3 Conclusion……..…132

Part B: Self-assembled monolayers (SAMs) of gold nanoparticles

3.4 Introduction…….…...133

3.5 Results and Discussions…….....135

3.6 Place Exchange studies..……....145

3.7 Conclusions…….…...154

3.8 Experimental section……..…154

3.9 References……..…158

Chapter 4: Polyhydrosiloxane an efficient reagent to control the nucleation and growth of metal nanoparticles: Shape control synthesis of gold nanoclusters

Part A: Polymethylhydrosiloxane mediated one-pot synthesis of spherical, prismatic, and rod shaped gold nanocrystals

4.1 Introduction…….……..….163

4.2 Results and discussions…….....165

4.3 Mechanistic proposal for different shaped gold nanocrystals…….…..179

4.4 Conclusions……181

Part B: Morphological conversion of gold nanoprisms to gold nanocubes

4.5 Introduction……....182

4.6 Results and discussion…….……..183

4.7 Conclusion……..……...191

4.8 Experimental section……..…....192

4.9 References…….…....196

Chapter 5: Solventfree Synthesis of monodispersed silver nanoparticles

5.1 Introduction…….…..199

5.2 Results and discussions…….…....201

5.3 Conclusions…….……..218

5.4 Experimental sections…….…..218

5.5 References…….……221

List of Schemes

Chapter 1

Scheme 1.1 Major routes to metal nanoparticle synthesis……..7

Scheme 1.2 Schematic representation of the formation of metallic nanoparticles in alcoholic media……..……...9

Scheme 1.3 Synthesis of metal colloidal particle proposed by Bonneman……...11

Scheme 1.4 Modified Colloid Synthesis Proposed by Bonneman……....12

Scheme 1.5 Hydrazine reduction of silver metal salt to silver nanoparticles……..….12

Scheme 1.6 Generation of silver nanoparticles by DMF reduction method….……....13

Scheme 1.7 Brust method of two-phase synthesis for gold nanoparticles…….…..…..14

Scheme 1.8 Generation of metal nanoparticles by radiolytic methods…….……16

Scheme 1.9 Sonochemical formation of metal nanoparticles…….……..17

Scheme 1.10 Electrochemical formation of $NR_4^+Cl^-$ stabilized nanometals…….…….20

Scheme 1.11 Schematic representation of electrostatic stabilization of metal nanoparticles……...22

Scheme 1.12 Surface capping of metal nanoparticles with surfactant and solvent……23

Scheme 1.13 Schematic representation of steric stabilization of metal Nanoparticles…….....25

Scheme 1.14 Dendrimer encapsulated metal nanoparticles……...….26

Scheme 1.15 Schematic representation for the synthesis of polymer-coated gold nanoprticles by surface-initiated living radical polymerization…....27

Scheme 1.16 Hydrosilylation of 1-hexyne promoted by gold nanoparticles…….…....37

Scheme 1.17 Silver nanoclusters assisted Wolff rearrangement of diazoketones……..39

Scheme 1.18 Polysiloxane-Pd" nanoconjugate assisted silesterification of PMHS and the corresponding poisoning study in presence of dodecanethiol…….……41

Scheme 1.19 Polyhydrosiloxane induced generation and stabilization of noble metal nanoparticles……..……44

Scheme 1.20 Surfactant exchange reaction on polysiloxane-metal nanocomposite…...44

Scheme 1.21 Formation of metal nanoparticles by PMHS reduction method……46

Chapter 2

Scheme 2.1 Synthetic strategy to polysiloxane stabilized silver sols and their surface grafting……..……..…...64

Scheme 2.2 Synthesis of silver thiol complex in toluene…….…….....94

Scheme 2.3 Reduction of silver thiol complex by PMHS to thiol functionalized silver nanoparticles……..……..98

Scheme 2.4 Functionalization of presynthesized silver nanoparticles by MPS……..100

Chapter 3

Scheme 3.1 Synthetic strategy to HMTS induced reduction of silver salts to self-assembled silver nanoparticles…….114

Scheme 3.2 Brust method of two-phase synthesis for gold nanoparticles…….....133

Scheme 3.3 Synthetic strategy of the formation of gold amine complex……..….136

Scheme 3.4 Reduction of gold-amine complex…….....136

Scheme 3.5 Schematic illustration of the formation of self-assembled monolayers of gold nanoparticles……....141

Scheme 3.6 Place-exchange reaction on the surface of amine protected Au nanoparticles……..…146

Chapter 4

Scheme 4.1 Schematic illustration of the formation of spherical and prismatic gold nanostructures in the presence of different amount of TOA…….…..……165

Scheme 4.2 Synthetic strategy to polyhydrosiloxane templated gold nanorods…..….176

Scheme 4.3 Synthetic strategy for the generation of gold nanoprisms fom Et_3PAuCl salt…….…..…...184

Scheme 4.4 Synthetic strategy for the generation of gold nanocubes from gold nanoprisms……..…..…189

Chapter 5

Scheme 5.1 Synthetic strategy to polysiloxane-Ag(0) nanocomposite and its transformation to soluble organosols……..……...203

Scheme 5.2 Schematic representation of processing of Ag(0) powder and its dispersion in coordinating solvents…….…208

Scheme 5.3 Functionalization of polysiloxane-Ag(0) nanocomposite with different surfactants……..…..213

List of Tables

Chapter 1

Table 1.1 A selective of reactions relevant to chemical processing catalyzed by supported gold (0)……...……..38

Chapter 2

Table 2.1 The comparative analysis data for silver nanoparticle synthesis from five different silver salts……..….88

Chapter 3

Table 3.1 Comparison of UV-vis absorption maxima and particle size analysis of SAMs of different silver salts…….…122

Table 3.2 The presence of different elements in the brown solid from EDX analysis…….…….125

Table 3.3 Comparison of UV-vis absorption maxima and particle size, and interparticle separation analysis for different redispersion step of synthesized SAMs of silver nanoparticles…….…….128

Table 3.4 Comparison of UV-vis absorption maxima and particle size analysis of TOA capped silver nanoclusters in solvent varying refractive indices…….....130

Table 3.5 Comparison of UV-vis absorption maxima and particle size analysis of HMTS induced formation of SAMs of gold nanoparticles…….……..142

Table 3.6 The presence of different elements in the brown solid from

EDX analysis……..…149

Table 3.7 Comparison of UV-vis absorption maxima and particle size analysis of gold nanoparticles in the presence of different surfactant…….....153

Chapter 4

Table 4.1 Comparison of UV-vis absorption maxima, populations and average edge lengths of gold nanoprisms at different stages of reactions…….171

Table 4.2 Shapes of gold nanoparticles and corresponding reaction condition……....174

Chapter 5

Table 5.1 Comparison of absorption maxima and particle size analysis of silver nanoparticles in different solvents……..…207

Table 5.2 Comparison of UV-vis absorption maxima and particle size of silver nanoparticles in the presence of different surfactants…….....216

List of Illustrations

Chapter 2

Fig. 2.1 UV-vis spectra monitoring of the absorption changes at different time intervals and TEM analysis and its corresponding histogram ……..……66

Fig. 2.2 TEM images, UV-vis absorption spectra, Particle Size analysis and the ring size analysis of resulting nanonecklaces……..……..….69

Fig. 2.3 UV-vis spectrum, TEM images, and Particle size analysis of the of reaction mixture in presence of six equivalents of amine……..……..….70

Fig. 2.4 Time evolved UV-vis absorption spectra (1A), TEM image (1B) and the corresponding histogram (1C) of silver nanocluster of polysiloxane stabilized silver nanoparticles obtained from silver nitrate reduction in presence of catalytic amounts of TOA……..77

Fig. 2.5 UV-vis spectra monitoring the absorption changes at different time intervals (2A) and TEM analysis (2B) of the silver nanonecklaces obtained from silver nitrate reduction in presence of 2 equiv of TOA……...78

Fig. 2.6 Tapping mode AFM image of polysiloxane stabilized silver nanonecklaces obtained from silver nitrate reduction in presence of 2 equiv of TOA……....79

Fig. 2.7 EDX spectra and elemental Ag map of synthesized silver nanonecklaces……..…79

Fig. 2.8 UV-vis spectrum (3A) of the reaction mixture in presence

of six equiv of amine and TEM image (3B) and the corresponding histogram (3C) of silver nanocluster……..…80

Fig. 2.9 Schematic illustration of the counter anion effect on the formation, rate of reaction and the stability of the synthesized particles in the process……....81

Fig. 2.10 TEM image, UV-vis spectrum, and the corresponding histogram of silver nanoparticles obtained from silver perchlorate reduction with catalytic amounts of TOA……..…83

Fig. 2.11 Time evolution of the absorbance at λ = 420 nm for the various silver salt reduction by polysiloxane in the presence of 2 equivalents of TOA…….……...…85

Fig. 2.12 TEM image of silver nanoclusters obtained from silver tetrafluoroborate reduction in presence of 2 equiv of TOA……....86

Fig. 2.13 UV-vis spectrum, TEM image of silver nanoparticles obtained from silver perchlorate reduction in presence of 6 equiv of amine……....87

Fig. 2.14 Figure 7 represents the TEM of silver nanoparticles and the corresponding histogram obtained form heptafluorobutyrate reduction in the presence of 6 equiv of TOA……..…….…..87

Fig. 2.15 EDX of silver nanoclusters……89

Fig. 2.16 SEM image and elemental Ag map of synthesized silver nanoclusters…….89

Fig. 2.17 Schematic representation of functionalization of silver nanoparticles by MPS…….…..93

Fig. 2.18 ^{1}H NMR spectra in chloroform-d at 25^{0} C of (a) pure MPS and

(b) complexed MPS in toluene when the AgOAc: MPS ratio was 1:1……..…96

Fig. 2.19 ^{13}C NMR spectra in chloroform-d at 25^0 C of (a) pure MPS and

(b) complexed MPS in toluene when the AgOAc: MPS ratio was 1:2……..….97

Fig. 2.20 TGA of Silver-MPS complex…….…....97

Fig. 2.21 UV-vis spectra of MPS stabilized silver nanocrystals

synthesized by in-situ reduction method…….……...99

Fig. 2.22 TEM and corresponding histogram of MPS stabilized silver

nanocrystals synthesized by in-situ reduction method……...….99

Fig. 2.23 UV-vis spectra and TEM of MPS stabilized silver nanocrystals

synthesized by ex-situ reduction method after 12h, when

AgOAc: PMHS: MPS concentration was 1:6:4. Scale bar is 100 nm……..101

Fig. 2.24 TEM of MPS stabilized silver nanocrystals synthesized by

ex-situ reduction method after 12h, when AgOAc: PMHS: MPS

concentration was 1:6:2……...102

Chapter 3

Fig. 3.1 Schematic illustration of formation, characterization, and property profiling of self-assembled silver nanoclusters…….……..116

Fig. 3.2 UV-vis absorption spectra and the kinetics of nanoparticle

formation from silver acetate reduction……117

Fig. 3.3 Time evolution of the UV-vis absorption spectra of the

solution for different silver salts reduction; (A) $AgNO_3$

(B) $AgClO_4$, (C) $AgBF_4$, and (D) $AgF_7C_4O_2$……....118

Fig. 3.4 TEM micrograph and the corresponding histogram of self-assembled silver nanoparticles for different silver salts, Silver acetate (A1, A2), Silver nitrate (B1, B2), Silver tetrafluoroborate (C1, C2), and silver heptafluorobutyrate (D1, D2) respectively……..….121

Fig. 3.5 X-ray photoelectron spectra of the Ag 3d transition……..……..123

Fig. 3.6 SEM image of the solid product after solvent evaporation…….……..124

Fig. 3.7 EDX spectra from brown solid using SEM……..…….125

Fig. 3.8 Elemental map obtained using EDX analysis……...….125

Fig. 3.9 UV-vis absorption spectra of silver nanoparticles arrays: (A) nanoparticles of freshly prepared solution, (B) 1st step redispersion, (C) 2nd step redispersion, and (D) 3rd step redispersion in toluene…….126

Fig. 3.10 TEM micrograph of silver nanoparticles arrays: (A) nanoparticles of freshly prepared solution, (B) 1st step redispersion, (B) 2nd step redispersion, and (D) 3rd step redispersion in toluene. Scale bar is 100 nm……127

Fig. 3.11 Comparison of particle size and interparticle spacing for different stages of redispersion. (A) nanoparticles of freshly prepared solution, (B) 1st step redispersion, (C) 2nd step redispersion, and (D) 3rd step redispersion in toluene…….…..128

Fig. 3.12 The surface plasmon band of redisperse silver nanoclusters
in different solvents……..….130

Fig. 3.13 TEM images of redisperse silver nanoclusters
in (A) DCM, (B) THF, (C) cyclohexane, and (D) benzene…….….131

Fig. 3.14 ^{1}H NMR comparison of gold-TOA complex where (a) pure TOA,
(b) gold-TOA 1:1 complex and (c) is gold-TOA 1:2 complex……..…137

Fig. 3.15 TEM image, corresponding histogram and the UV-vis spectra
represent the HMTS induced formation of gold nanoparticles
in acetonitrile……138

Fig. 3.16 Time dependent UV-vis spectra; TEM image and the
corresponding histogram of HMTS induced formation of 3.6 nm
self-assembled gold nanoparticles in the presence
of 4 equivalent of TOA……..139

Fig. 3.17 Time dependent UV-vis spectra; TEM image and the
corresponding histogram of HMTS induced formation of 3.5
nm self-assembled gold nanoparticles in the presence of
6 equivalent of TOA……...140

Fig. 3.18 Comparison of UV-vis absorption maxima for different
gold amine complex reduction…….143

Fig. 3.19 X-ray photoelectron spectra for TOA-capped gold nanocrystals…….....144

Fig. 3.20 SEM image of the solid product after particle precipitation……....144

Fig. 3.21 Representative ^{31}P NMR spectra of TPP and the
corresponding TPP-stabilized gold nanoparticles…….……...….148

Fig. 3.22 X-ray photoelectron spectra for TPP-capped gold nanocrystals……..148

Fig. 3.23 EDX spectra from purple solid using SEM and the elemental P and Au map obtained using EDX…….……149

Fig. 3.24 TPP stabilized gold nanoparticles and the corresponding histogram……...150

Fig. 3.25 Comparison of UV-vis absorption maxima for gold nanoparticles in the presence of different surfactants……...……151

Fig. 3.26 DPPP stabilized gold nanoparticles and the corresponding histogram……....152

Fig. 3.27 Representative ^{31}P NMR spectra of DPPP and the corresponding DPPP-stabilized gold nanoparticles…….……....…152

Fig. 3.28 DPPE stabilized gold nanoparticles and the corresponding histogram……153

Chapter 4

Fig. 4.1 (A) UV-vis absorption spectra, (B) AFM image, and TEM analysis and edge length calculations of nanoprism formation at different stages of reaction: after (C) 25 min (D) 40 min (E) 50 min and (F) 90 min of PMHS addition. Scale bar is 100 nm…….……..169

Fig. 4.2 TEM analysis of the synthesized gold nanoprisms after 90 min of the addition of PMHS at different scale bar (A) 500 nm, (B) 200 nm, and (C) 20 nm. (D) The abundance of the nanoprisms at different time interval of reaction after PMHS addition…….……..170

Fig. 4.3 UV-vis absorption spectra and TEM image of gold nanoprisms dispersed in water…….……....172

Fig. 4.4 UV-vis spectra of gold nanoclusters formed by PMHS reduction

in presence of 2 equiv of TOA……..173

Fig. 4.5 TEM image, particles size analysis, and AFM image of gold nanoclusters formed by PMHS reduction in presence of 2 equiv of TOA…….....174

Fig. 4.6 TEM image, particles size analysis, and UV-vis absorption spectra of gold nanoclusters formed by PMHS reduction in presence of 6 equiv of TOA…….....175

Fig. 4.7 UV-vis absorption spectra of synthesized gold nanorods…….....177

Fig. 4.8 TEM image and the average length of synthesized gold nanorods……..…178

Fig. 4.9 Mechanistic proposal for formation of different shapes gold nanocrystals at different monomer concentration……..…181

Fig. 4.10 UV-vis absorption spectra of the formation of gold nanoprisms from the reduction of Et_3PAuCl salt…….……185

Fig. 4.11 Time resolved ^{31}P NMR of the gold nanoprism solution……..…185

Fig. 4.12 TEM image and the corresponding histogram for edge length calculation of gold nanoprisms synthesized from Et_3PAuCl in the presence of 5 equivalent of TOA…….186

Fig. 4.13 AFM image of gold nanoprisms synthesized from Et_3PAuCl in the presence of 5 equivalent of TOA……..186

Fig. 4.14 TEM image and the corresponding histogram for edge length calculation of gold nanoprisms synthesized from Et_3PAuCl in the presence of 2 equivalent of TOA…….187

Fig. 4.15 Comparison of UV-vis absorbance maxima……..……189

Fig. 4.16 TEM image of the gold nanocubes at different
magnification; (A) 200 nm, (B) 100 nm, and (C) 50 nm scale bar.
(D) the histogram of the nanocubes at 100 nm scale bar…….190

Chapter 5

Fig. 5.1 FT-IR spectra of the yellowish brawn color semisolid product…….……..….202

Fig. 5.2 UV-vis absorption spectra of disperse silver nanoparticles in
different solvent…….203

Fig. 5.3 TEM image and the corresponding histogram of acetonitrile
stabilized silver nanoparticles……..……...204

Fig. 5.4 AFM image of acetonitrile stabilized silver nanoparticles……...….205

Fig. 5.5 ^{1}H NMR of THF stabilized silver nanoparticles…….……..….205

Fig. 5.6 TEM image and the corresponding histogram of
THF stabilized silver nanoparticles……...…206

Fig. 5.7 Solid state FT-IR of the brown solid after washing with hexane…..……..…208

Fig. 5.8 XPS spectra of brown solid…….……...….209

Fig. 5.9 EDS analysis of the brown solid…….....210

Fig. 5.10 SEM image of brown powder……...…210

Fig. 5.11 UV-vis abs maxima of brown powder in acetonitrile(A) and THF(B)…...….211

Fig. 5.12 TEM image and the corresponding histogram of acetonitrile

stabilized brown powder…….…….212

Fig. 5.13 FTIR comparison of pure oleylamine (A) and the amine capped nanoparticles……..……..215

Fig. 5.14 UV-vis absorption maxima of silver organosols in the presence of different surfactant…….……..….215

Fig. 5.15 TEM images of different surfactant capped silver nanoparticles. (A) OA, (B) DDA, (C) TPP, and (D) MHDA……..…217

List of Abbreviations

2D	two-dimensional
3D	three-dimensional
AFM	Atomic force microscopy
AuNP	gold nanoparticle
CVD	chemical vapor deposition
DCM	dichloromethane
DDA	dodecanoic acid
DEN	dendrimer
DLVO	Derjaguin-Landau-Verwey-Overbeek
DNA	deoxyribonucleic acid
DMF	N, N-dimethylformamide
DPPP	1,2-bis(diphenylphosphino) propane
EDX	energy-disperse X-ray
FTIR	Fourier transforms infrared
HMTS	1,1,1,3,5,5,5 heptamethyltrisiloxane
MHDA	16-mercaptohexadecanoic acid
MPS	3-mercaptopropyl triethoxy silane
MUN	11-mercapto-1-undecanol
NMR	nuclear magnetic resonance
OA	oleylamine
PAMAM	polyamidoamine
PMHS	poly(methylhydrosiloxane

PRB	plasmon resonance band
PS-PVP	polystyrene-block-poly(4-vinylpyridine)
RT	room temperature
SAM	self-assembled monolayer
SEM	scanning electron microscopy
SERS	surface-enhanced Raman scattering
SMAD	solvated metal atom dispersion
SP	surface plasmon
SPB	surface plasmon band
TEM	transmission electron microscopy
TGA	thermogravimetric analysis
THF	tetrahydrofuran
TOA	trioctylamine
TPP	triphenylphosphine
UV-vis	ultraviolet-visible
XPS	X-ray photoelectron spectroscopy

Chapter 1

Nanomaterials: Synthesis, Stabilization, and Applications

1.1 Introduction

Preparation of colloidal metals in a two-phase system was first introduced by Faraday,[1] who reduced an aqueous solution of a gold salt with phosphorus in carbon disulfide and obtained a ruby red colored solution of dispersed gold particles. Since then, ultrafine metal particles have been the subject of intense scientific interest. These ultrafine materials are also called nanoscale, nanostructured and nanosized.

Nanoscale materials typically, though not exclusively, have at least one dimension smaller than 100 nanometers (100 x 10^{-9} meter). Atomic diameters of metals range from about 1 to about 4 Angstroms (that is, 1 x10^{-10} to 4 x 10^{-10} meter). Thus, nanoscale metals consist of tens of thousands of atoms clustered together. Interest in these materials stems from the radical property changes, which accompany size reduction from the micro scale to the nano scale. The increase in surface to volume ratio (*S/V*) alters physical properties (for example, melting, hardness and magnetism) and chemical properties (for example, catalytic reactivity). Consequently, nanoscale materials serve as model systems to experimentally probe the effects of quantum confinement on electronic, magnetic, and other related properties.[2] They have been widely exploited for use in photography,[3] catalysis,[4] biological labeling,[5] photonics,[6] optoelectronics,[7] information storage,[8] surface enhanced Raman spectroscopy (SERS),[9] and formulation of magnetic ferrofluids.[10]

The intrinsic properties of a metal nanoparticle are mainly determined by its surface to volume ratio, size, shape, composition, crystallinity, and structure.[11] In principle, one could control any one of these parameters to fine tune the properties of the nanoparticle. This dissertation project investigates the reducing properties of poly(methylhydrosiloxanes) (PMHS) and its oligomeric counterparts for the reduction of

silver and gold metal salts to the corresponding metal nanoparticles. The polymer was chosen to investigate its effects on the nucleation and growth process of the synthesized metal nanoclusters. In addition, the morphological property profile of the well shaped nanoclusters is also investigated.

1.2 Properties of the Noble Metal Nanoparticles

Physicists predicted that nanoparticles in the diameter range 1-10 nm (intermediate between the size of small molecules and that of bulk metal) would display electronic structures, reflecting the electronic band structure of the nanoparticles, owing to quantum-mechanical rules. The resulting physical properties are neither those of bulk metal nor those of molecular compounds, but they strongly depend on the particle size, interparticle distance, nature of the protecting organic shell, and shape of the nanoparticles.[11,12] The few "last metallic electrons" are used for tunneling processes between neighboring particles, an effect that can be detected by impedance measurements that distinguish intra- and intermolecular processes. The *quantum size effect* is involved when the de Broglie wavelength of the valence electrons is of the same order as the size of the particle itself. Then, the particles behave electronically as zero-dimensional quantum dots (or quantum boxes) relevant to quantum-mechanical rules. Freely mobile electrons are trapped in such metal boxes and show a characteristic collective oscillation frequency of the plasma resonance, giving rise to the so-called plasmon resonance band (PRB) observed near 530 nm in the 5-20 nm diameter range for gold nanoparticles and 400-420 nm in the 5-10 nm diameter for silver nanoparticles. In nanoparticles, there is a gap between the valence band and the conduction band, unlike in bulk metals.

The frequency and width of the surface plasmon absorption depends on the size and shape of the metal nanoparticles as well as on the dielectric constant of the metal itself and the surrounding medium.[13] Noble metals such as copper, silver, and gold have a strong visible-light plasmon resonance, whereas most other transition metals show only a broad and poorly resolved absorption band in the ultraviolet region.[11a, 12a] This difference is attributed to the strong coupling between the plasmon transition and the interband excitation. In addition, the conduction band electrons of the noble metals can move freely, independently from the ionic background, and the ions act only as scattering centers. This gives the electrons in the noble metals a higher polarizability, which shifts the plasmon resonance to lower frequencies with a sharp bandwidth. The surface plasmon resonance was theoretically explained by Mie in 1908, including linear optical properties such as extinction and scattering of small spherical metal particles.[14]

Mie's theory and experimental spectra agree well in the size regime >20 nm until the normal incidence absorption no longer shows a plasmon resonance for bulk metals. The spectrum is composed of the sum of size-dependent absorption and scattering modes. Higher order modes become more dominant with increasing particle size, causing the plasmon absorption band to red shift and resulting in increased bandwidth, because for larger particles, the light cannot polarize the nanoparticles homogeneously and retardation effects lead to the excitation of higher order modes. The optical absorption spectra depend directly on the size of the nanoparticles, which is called the extrinsic size effect.[15]

Two key factors controlling the properties of nanomaterials are the size and surface characteristics of nanoparticles.[16] These two factors are interrelated because the S/V ratio

increases as the size decreases. For a spherical particle, the S/V ratio is inversely proportional to its radius, R ($S/V = 3/R$). Full-shell clusters are built up by hexagonal (hcp) or cubic (ccp) close-packed atoms. It is clear that the surface of nanoparticles plays an important role in their fundamental properties, from structural transformation via light emission to solubility. The surface atoms are chemically more active compared to the bulk atoms because they usually have fewer adjacent coordinate atoms and unsaturated sites or more dangling bonds. At the same time, the imperfection of the particle surface induces additional electronic states in the band gap, which act as electron or hole trap centers. At high densities of surface defects, a decrease in the observed transition energy and a red-shifted emission band can be observed due to defect band formation. As the size of the materials decreases, the surface to-volume ratio increases and the surface effects become more apparent and thereby easier to explore. In addition, the surface states near the gap can mix with the intrinsic states to a substantial extent, and these effects may also influence the spacing of the energy levels of nanoparticles. In a system containing only a few hundred atoms, a large fraction of these atoms will be located on the surface. Because surface atoms tend to be coordinatively unsaturated, there is a large energy associated with this surface. The smaller the nanocrystal, the larger the contribution made by the surface energy to the overall energy of the system and, thus, the more dramatic the melting temperature depression occurred.

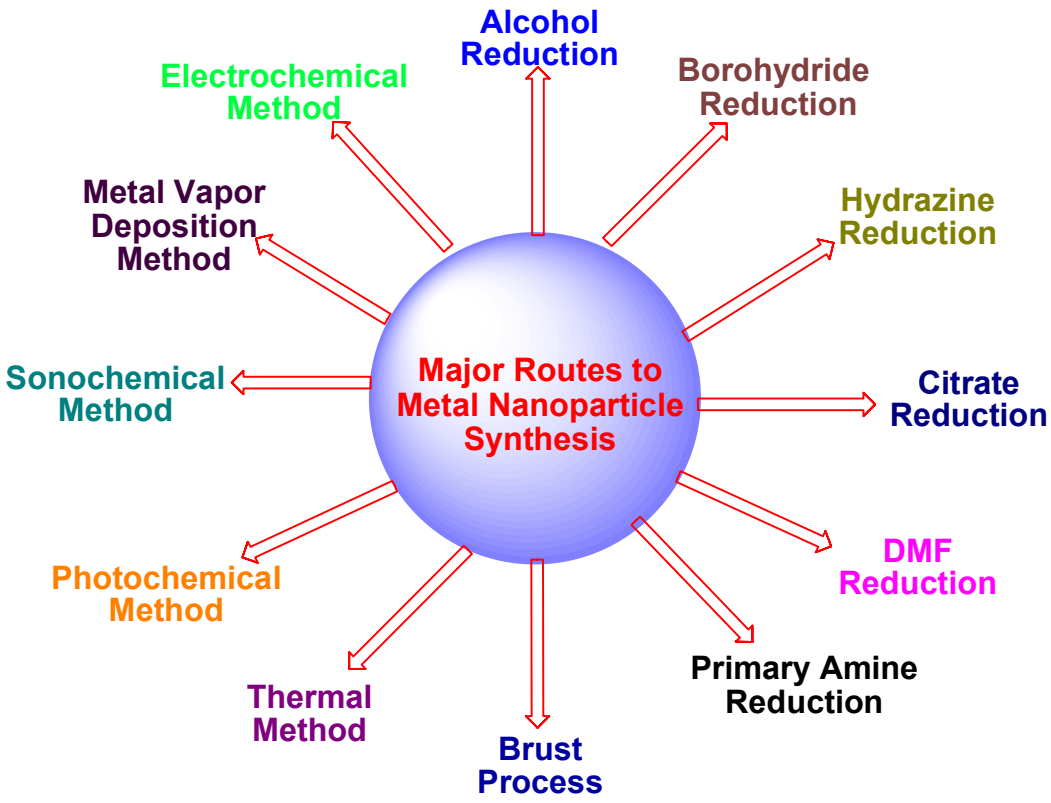
Fluorescence studies of metal nanoparticles have been carried out under various conditions including femtosecond emission and steady-state investigation of the interaction between thiolate ligands and the metalcore.[17] In this regard, gold nanoparticles are well studied metal nanoclusters Capping fluorescent groups are pyrenyl,[18]

polyoctylthiophenyl,[19] fluorenyl,[20] and other probes.[21] Indeed, resonant energy transfer was observed in fluorescent ligand-capped gold nanoparticles, this phenomenon being of great interest in biophotonics[22] and materials science.[23] Both radiative and nonradiative rates critically depend on the size and shape of the gold nanoclusters the distance between the dye molecules, the orientation of the dipole with respect to the dye-nanoparticle axis, and the overlap of the molecule's emission with the nanoparticle's absorption spectrum. Orders-of-magnitude higher efficiencies were obtained with nanometer-dimension metal samples. The observed increase in the fluorescence yield reflected the suppression of the nonradiative decay upon binding to Au nanoparticles. Visible luminescence has been reported for water-soluble Au nanoparticles, for which a hypothetical mechanism involving $5d^{10}$ to $6(sp)^1$ interband transition has been suggested.[24] On the basis of the ability of discrete photoisomeric states of spiropyrans to exhibit distinct physical properties, photo switchable Au nanoparticle assemblies of various amino acids were designed by anchoring spiropyrans to allow the release of the outer sphere of amino acids on irradiation.[25]

1.3 Commonly Available Synthetic Routes

Commonly available methods for the synthesis of metal nanoparticles in solution are summarized in Scheme 1.1. Average particle size and particle size distributions vary with the method used. In most of the methods, the presence of a stabilizing agent is necessary to prevent the aggregation of the colloids formed into larger particles. The following five general synthetic methods are most often used to synthesize transition metal colloids: (i) reduction of transition metal salts by alcohol, borohydride, hydrazine,

DMF, primary amine, ii) Brust Method. iii) thermal, photochemical, or sonochemical decomposition, (iv) vapor deposition methods, which include chemical vapor deposition and physical vapor deposition, and (v) electrochemical reduction.



Scheme 1.1: Major routes to metal nanoparticle synthesis.

1.3.1 Reduction of Transition Metal Salts

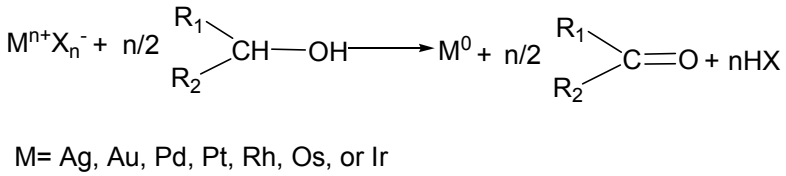
The solution phase synthesis of transition metal nanoparticles is the most widely used method to generate colloidal suspensions of metals. In fact, this method is generally very simple to implement. A wide range of reducing agents has been used to synthesize metal nanoparticles. They include gases such as hydrogen or carbon monoxide, orgabic

compounds like glucose and sorbitol, hydrides such as sodium borohydride, salts such as sodium citrate, and even oxidizable solvents such as alcohols and polyols. Some transition metal nanoparticles can be obtained in refluxing alcohol from the corresponding metal salts. In this process, the alcohol acts both as solvent and reducing agent. The alcohols, which are useful reducing agents, contain α-hydrogen adjacent to the hydroxyl functionality. In this context, alcohols such as methanol, ethanol, or 2-propanol are good reducing agents, whereas *tert*butyl alcohol is not effective. During the reduction, the alcohols are oxidized to the corresponding carbonyl compounds. This reaction often requires the presence of water to be effective.

Aqueous alcohol has been extensively used as the reducing agent in the synthesis of colloidal transition metals such as Rh, Pt, Pd, Os, or Ir. All of these metal nanoparticles were stabilized by organic polymers or oligomers such as polyvinylic alcohol (PVA), polyvinylpyrrolidinone (PVP), polyvinylic ether (PVE), or by cavitands such as cyclodextrin.[26] Other kinds of polymers were used for the stabilization of colloids formed during the metallic salt reduction. The use of various polyacids,[27] polyelectrolytes,[28] or block copolymers,[29] to stabilize Pd, Pt, and Au[30] nanoparticles has been largely studied. In the same way, after reductive synthesis in aqueous alcohol, Pt colloids were stabilized by poly(*N*-isopropylacrylamide) (PNIPAAm),[31] poly(*N*-sulfonatopropyl-*p*-benzamide),[32] or PVA/PVP copolymers.[33]

Recently, several groups investigated the influence of various parameters on the particle size distribution of the particles synthesized. The variation of stabilizing agent quantity,[34] structure and quantity of alcohol,[35] metallic precursor,[36] as well as the addition of base[37] were studied. For example, When the reduction of H_2PdCl_4,[34] H_2PtCl_6,[35] or

$RhCl_3$ [38] was carried out in higher boiling point alcohol, nanoparticles with narrow size distribution are produced. In the same way, the addition of NaOH during the reduction of H_2PtCl_6 or $PdCl_2$ with methanol allows decrease in the size of the particles formed.[37] Recently, Xia and coworkers elaborated the polyol method for the synthesis of noble metal (for example, Pt, Pd, and Ag) nanoclusters. They were able to control the nucleation and growth of nanoclusters to achieve different shaped nanoarchitectures.[40]



Scheme 1.2: Schematic representation of the formation of metallic nanoparticles in alcoholic media (scheme was adapted from ref [40]).

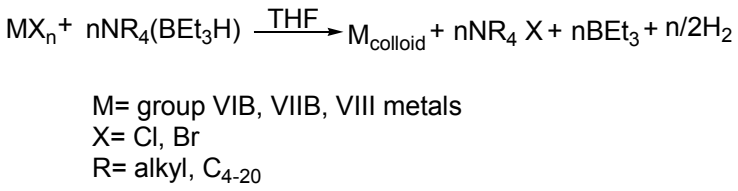
In some cases, the effects of heating were also studied.[39] For example, rapid microwave heating of an aqueous alcoholic solution of H_2PtCl_6 allows the production of nearly monodispersed Pt nanoparticles.

The borohydrides ($NaBH_4$ or KBH_4) reduction of transition metal salts is the most widely used method for the generation of metal nanoparticles. The stabilizing agents used in these cases are generally surfactants or water-soluble polymers. With this method Cu nanoparticles were generated in the presence of PVP, PVE, PVA, or various polysaccharides.[41] Pt colloids were also stabilized by PVP with this method. The aqueous phase reduction of Ag, Au, Pt, or Pd salts has been carried out by KBH_4 and the resulting nanoparticles were stabilized by polymer molecules.[42] In this context, cationic polyelectrolytes, polyacids, nonionic polymers, and block copolymers were investigated.

Recently, $NaBH_4$ reduction was used to synthesize Au, Ag, Pt, Pd, or Cu nanoparticles and the resulting nanoparticles were stabilized by dendrimers (polyamidoamine or PAMAM).[43] These macromolecules help to obtain nearly monodispersed particles. Dimethylamineborane has been also used to prepare gold nanoparticles stabilized by hydrophobically modified PAMAM in organic solvent, toluene or chloroform.[44]

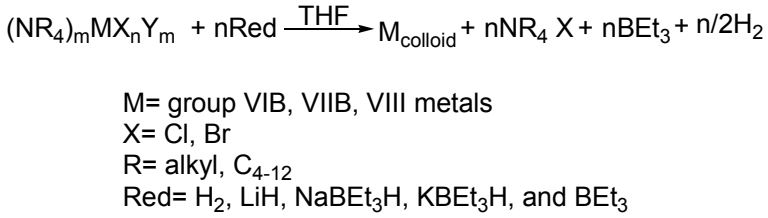
Surfactants are generally used as stabilizers of aqueous colloidal suspensions of transition metal reduced by $NaBH_4$ or KBH_4. They can be cationic, anionic, or nonionic. The synthetic method is available for generation of Ru, Rh, Pd, Pt, Ag, or Au nanoparticles stabilized by quaternary ammonium, sulfates, or poly(ethylene glycol).[45] Aliquat (trioctylmethylammonium chloride) and CTAB or glycerol monooleate also show stabilization in water/oil microemulsions containing Pd[46] or Cu[47] nanoparticles. Borohydrides have also been used to obtain aqueous suspensions of colloidal Rh stabilized by a trisulfonated surfactant.[48]

Several authors applied the borohydride reduction of transition metal salts to the preparation of colloidal suspensions of transition metals in organic media.[49] The first approach consists of reducing a metallic salt in aqueous phase by $NaBH_4$. The water is then evaporated and the solid obtained is redispersed in an organic solvent. A range of methods for the phase transfer of particles has been also reported, with most studies focusing on the transfer from aqueous to organic media.[50] The classical approach consists of reducing transition metal salts in an organic phase. So, Bönnemann used tetraalkylammonium hydrotriorganoborates ($NR_4(BEt_3H)$) in THF solution to reduce a wide range of Group VIB, VIIB, VIII, and IB metal halide salts (Scheme 1.3).[51]



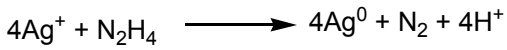
Scheme 1.3: Synthesis of metal colloidal particle proposed by Bonneman (scheme was adapted from ref [51a]).

The reported particle size is generally between 1 and 10 nm, and by using appropriately substituted tetraalkylammonium salts, the colloidal metal nanoparticles can be solubilized in organic media. The advantages of this system include the large-scale preparation and the wide range of metal nanoclusters available, but the main disadvantage is a lack of exact compositional characterization of the resultant colloid materials. Indeed, boron from the initial BEt_3H^- reductant is found as a 1-2% impurity in the resultant colloids.[52] In this process, both the stabilizing agent (the NR_4^+ group) and the reducing group are coupled in the same reagent. A high local concentration of stabilizer is present during the reduction process, thus limiting the growth of the nanoparticles. Nevertheless, the reducing agents had to be generated, and this step is not straightforward. The alternative developed by Bönnemann consists of coupling the reducing agent with the transition metal salt, as depicted in Scheme 1.4. This new compound is then reduced by hydrides (superhydride, lithium hydride...) to yield colloidal metal particles.



Scheme 1.4: Modified Colloid Synthesis Proposed by Bonneman (scheme was adapted from scheme [51a]).

Other reducing agents such as hydrazine have been used efficiently in metal nanoparticle synthesis. Hydrazine can be used in all its forms to reduce transition metals. This one is a pH dependent reduction. The reduction takes place at pH>8. Therefore, it is very important to adjust the pH at this region. NaOH is used to adjust the pH, but it indirectly inhibits the reaction rate. In addition, this reaction is also inhibited because of the release of the protons (Scheme 1.5).

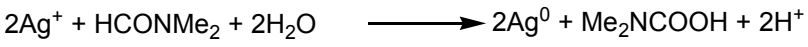


Scheme 1.5: Hydrazine reduction of silver metal salt to silver nanoparticles.

Hydrazine hydrochloride[53] or sulfate[54] was tested successfully for the preparation of metal nanoclusters. Gold nanoparticles can be synthesized by hydrazine in the presence of cationic or nonionic surfactants.[55] The use of hydrazine as reducing agent and block copolymers as stabilizing agents was recently reported in the literature, where Au, Pd, Ag, or Rh nanoparticles were stabilized by block copolymers such as polystyrene-*b*-polyvinylpyridine, polystyrene-*b*poly- *m*-vinyltriphenylphosphine, or poly(ethylene

oxide)-polyethyleneimine. Several polymer-stabilized systems have high thermal stability and can be used in drastic conditions.[56]

Sodium citrate was also used as reducing agent to obtain colloidal suspension of transition metals. Turkevitch and co-workers[57] studied the nucleation and growth of Au nanoparticles reduced by sodium citrate. In this case, the citrate is not only a reducing agent but also an ionic stabilizer. The citrate was also found to be an effective agent for reduction and stabilization of silver nanoparticles.[58] Citrate reduction has also been used to prepare Ir,[59] and Pt[60] nanoparticles. However, citrate anion is a noninnocent ligand and has one significant disadvantage because of the simultaneous formation of the intermediate acetone dicarboxylic acid. The unavoidable result is compositionally ill-defined colloids in opposition to focused modern nanoparticles. Finke and co-workers[61] have recently performed fundamental studies around this research area. DMF reduction of metal salt to metal nanoparticles is also synthetic route for the generation of metal nanoclusters. In this reduction process (Scheme 1.6), DMF acts both as a solvent and reducing agent.[62]

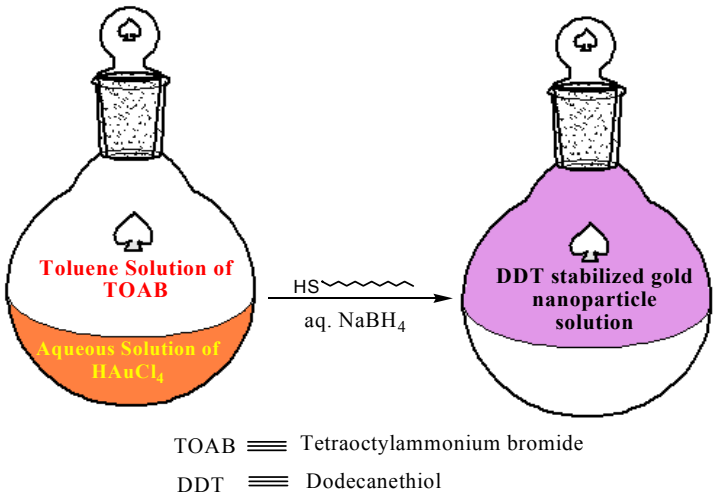


Scheme 1.6: Generation of silver nanoparticles by DMF reduction method (scheme was adopted from ref[62]).

Recently primary amines were found to be effective reducing agents for the reduction of silver and gold metal salts in both organic and aqueous media.[63] The synthesized particles were monodisperse and stable for long periods of time. The synthesized nanoclusters were also allowed to do ligand exchange on their surfaces.[64]

Dragieva and coworkers[65] have developed a new synthetic route for monodisperse metal colloids by the solvated metal atom dispersion method (SMAD). The SMAD method involves vaporization of a metal under vacuum and co-deposition of the atoms with the vapors of a solvent on the wall of a reactor at 77 K. After the warm up stage, the particles are stabilized both sterically (by solvation) and electrostatically.

The most popular method is the two phase synthesis introduced by Brust *et al.* It involves the transfer of $[AuCl_4]^-$ into toluene with the use of tetraalkylammonium bromide and subsequent reduction with $NaBH_4$ in presence of alkanethiols.[66] As mentioned previously, the Brust method produces nanoparticles with wide size dispersity. To obtain a self-assembled ordered system of metallic nanoparticles, it is very essential to have a low polydispersity of the synthesized particles. Moreover, the impurity that is introduced by the use of surfactant and the restriction of carrying out the reduction in the presence of functionalize stabilizing agent put limitations of this nanomaterials for further applications.



Scheme 1.7: Brust method of two-phase synthesis for gold nanoparticles.

1.3.2 Thermal, Photochemical, and Sonochemical Methods

Photochemical synthesis of metallic nanoparticles can be obtained either by (i) transition metal salt reduction by radiolytically produced reducing agents or (ii) degradation of an organometallic complex by radiolysis. The goal of these synthetic procedures is to obtain zerovalent metals under conditions, which prevent the formation of bulk metal. Ionizing radiation is generated with X- or γ-ray sources. UV-visible irradiation is generated with a Hg or Xe lamp. One advantage of radiolytic methods is that a large number of atoms is homogeneously and instantaneously produced during the irradiation thus providing favorable conditions for the formation of nearly monodispersed particles (<15% dispersion calculated by TEM imaging and NIH Image software counting of 300 particles).[67]

Over the past 20 years, a wide range of transition metal nanoparticles such as Ag, Au, Ir, Pt, Pd, or Cu colloids were prepared by radiolytic method.[68] Several reducing agents can be generated during radiolytic procedure. Thus, the radiolysis of aqueous suspension of transition metal salts produced solvated electrons or H• and OH• originating from water radiolysis. These species can react with the molecules in solution to give new radicals able to reduce metal salts. Irradiating a solution of copper perchlorate (Cu-$(ClO_4)_2$) containing sodium formate produced Cu nanoparticles via h the reduction of Cu^{2+} by both solvated electrons and CO^{2-} generated during radiolysis.[69] Similarly, the radiolysis of an aqueous solution of $Pd(NH_3)_4Cl_2$ and 2-propanol also results in the formation of Pd colloids by both solvated electrons and 1-hydroxy-1-

ethylmethyl radicals ($(CH_3)_2^{\cdot}COH\bullet$) generated by the reaction of H• and OH• with 2-propanol.[70] In an original example of radiolytic Pt colloid synthesis,[771] both the nanoparticles and the protecting polymer are produced simultaneously by radiolysis of a solution containing the monomer (acrylamide) and the metal salt (H_2PtCl_6). The radiolytic preparation of transition metal nanoparticles is also possible in organized environments such as micelles or micoemulsions.[72]

The photolysis of metal salts is also an efficient method to prepare transition metal colloids. Thus, the UV-visible irradiation of Au,[73] Ag,[74] or salts in reverse microemulsions in the presence of surfactants or polymers yielded metallic nanoparticles.[75] Toshima, et al. prepared Pt[76] and Pd[77] colloids in the presence of micelles of a wide range of surfactants by photolysis and hydrogen reduction. They reported that the UV-visible irradiation yields smaller and better dispersed nanoparticles.

Active species generation:

$$H_2O \longrightarrow H^{\bullet}, {}^{\bullet}OH, e_s^{-}\ H_3O^{+}, H_2, H_2O_2$$

$$OH^{\bullet}(H^{\bullet}) + RH \longrightarrow R^{\bullet} + H_2O\ (H_2)$$

Metal reduction:

$$M^{n+} + nR^{\bullet} \longrightarrow M^0$$

$$M^{n+} + ne_s^{-} \longrightarrow M^0$$

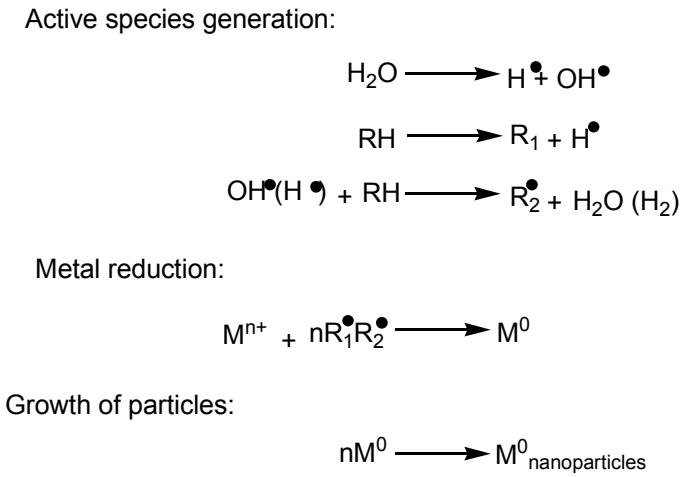
Growth of particles:

$$nM^0 \longrightarrow M^0_{nanoparticles}$$

Scheme 1.8: Generation of metal nanoparticles by radiolytic methods (scheme was adopted from ref[76]).

Fendler and coworkers, who used UV-visible irradiation to encapsulate Pt nanoparticles into polymerized vesicles, described another aspect.[78] The vesicle reticulation and the

colloid formation occur simultaneously during irradiation. Mayer and Esumi reported the UV-visible photolytic synthesis of Au nanoparticles stabilized by block copolymers, polyelectrolytes, or dendrimers (polyamidoamine: PAMAM).[79]



Scheme 1.9: Sonochemical formation of metal nanoparticles (scheme was adapted from ref[81]).

Sonochemistry is due to acoustic cavitation phenomena causing the formation, the growth, and the explosion of bubbles in a liquid media. The very high temperature (>5000 K), the pressure (>20 MPa), and the cooling rate (>107 K s^{-1}) reached during cavitation gave unique properties to sonicated solutions. These extreme conditions were used by Suslick and coworkers to obtain Fe particles,[80] or Co alloys[81] by reduction of metal salts. In the same way, Gedanken, et al. reported the preparation of nanosized Ni,[82] Cu,[83] Pd,[84] Fe,[85] and Fe oxide.[86]

The sonochemical reduction of transition metal salts occurs in three steps: the generation of the active species, the reduction of the metal, and the growth of the colloids. These three steps occur in different compartments: (i) In gaseous phase into the

cavitation bubbles where high temperature and pressure allow water pyrolysis to form H• and OH•, (ii) at the interface between the cavitation bubbles and the solution, and finally (iii) in the solution. This synthetic procedure was applied to colloidal synthesis and a wide range of surfactant or polymer stabilized transition metal nanoparticles such as Au[87] or Ag, Au, Pt, Pd[88] were generated. The kinetics of nanoparticle formation was also investigated based on the influence of stabilizing agent and of the addition of alcohol.[89] Finally, quaternary ammonium stabilized Pd colloids was prepared and solubilized in an organic solvent (THF).[90]

1.3.3 Metal Vapor Synthesis

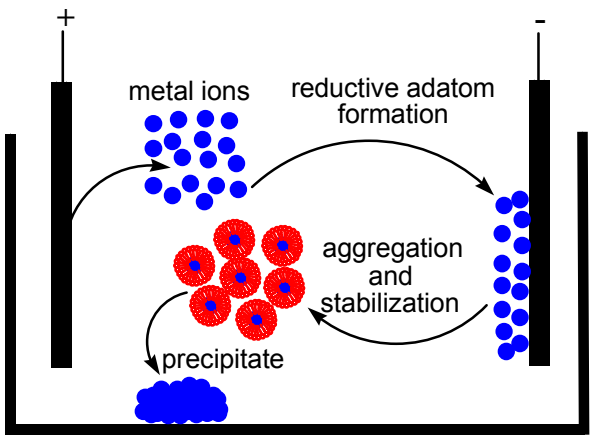
The metal vapors co-condensed with organic vapors are a known method for generation of metal nanoparticles. This method consists of the evaporation at reduced pressure of relatively volatile metals and a subsequent co-condensation at low temperature of these metals with the vapors of organic solvents. A colloidal dispersion of the metal was then obtained by warming the frozen metal/organic mixture. The colloidal particles nucleate and grow as the frozen mixture is warmed to melting. This synthetic procedure can be conducted either in a rotating[91] or in a static reactor.[92] Generally, the metal vapors are generated from a resistively heated hearth or an electron beam furnace and condensed on the walls of the reactor together with the organic solvent vapors. This process resolves the problems of volatile solvents. All these systems allow the synthesis of the suspension of transition metal colloids. The various suspensions of Au and Pd can be prepared by co-condensation of metal vapors in acetone, the particle sizes were varies between 5 and 30 nm.[93] An analogous procedure was used to condense Au in solution of

polystyrene,[94] poly(methyl methacrylate),[95] or polyacetylene to obtain Au colloids of 2 to 15 nm. Colloidal metals could also be generated by metal vapor condensation in fluorinated solvents.[96] Five nanometer Co colloids[97] stabilized by surfactants were also generated in toluene by metal vapor condensation. Smaller particles of Pd, Cu, Ni, Pt, Pr, Yb, or Er with a size about to 2 nm were obtained by co-condensation of metal vapor into solvents for the stabilization such as methylcyclohexane and *iso*butylaluminoxane.[98] The development of metal vapor routes to transition metal colloids is often limited by the apparatus. The advantage of this metal atom method is to generate zero-valent nanoparticles stable for several months, but the main disadvantage is the control of the size. This parameter is essential for reproducible catalytic applications and can require sophisticated metal vapor reactor for the control of the preparative conditions such as inert gas and gas pressure.

1.3.4 Electrochemical Synthesis

The electrochemical method for the preparation of transition metal nanoparticles is well-established and well defined.[99] This large-scale synthetic procedure allows one to obtain size-controlled particles. A sacrificial anode is used as a metal source. This anode is oxidized in the presence of quaternary ammonium salt, which is both the electrolyte and the stabilizing agent. The ions are then reduced at the cathode to yield the metallic nanoparticles. With this process, it is easy to generate acetonitrile/THF dispersed Pd colloids with various sizes.[100] The mechanism for the generation of nanoclusters consists of (i) dissolution of the anode to form metal ions (oxidation of Pd to Pd^{2+}); (ii) migration of the metal ions to the cathode; (iii) reduction of the metal ions at the surface of the

cathode; (iv) aggregation of the particles stabilized by the ammonium ions around the metal cores; and then (v) precipitation of the Pd nanoparticles.



Scheme 1.10: Electrochemical formation of $NR_4^+Cl^-$ stabilized nanometals (adapted from ref.[99]).

This process presents several advantages: (i) particle size can be controlled by varying the current intensity and the particle size is inversely proportional to current density, (ii) isolation of the nanoparticles is simple as they precipitate out of the solvent when formed; and finally (iii) the synthesis occurs with good yields (>95%). This synthetic procedure can be applied to easily oxidized transition metals such as Ni or Cu. The solubility of the nanoparticles obtained can be tuned from nonpolar solvents such as pentane to polar solvents as water by changing the polarity of the protecting agent [101] For less easily oxidized metals such as Pt, Rh, or Ru, the anode and cathode used are made of Pt and the metallic precursor is a transition metal salt.[101] In this new process the anode is no more sacrificed and the metallic precursor is reduced by electrolysis in the presence of a quaternary ammonium salt, which is both the electrolyte and the stabilizing agent.

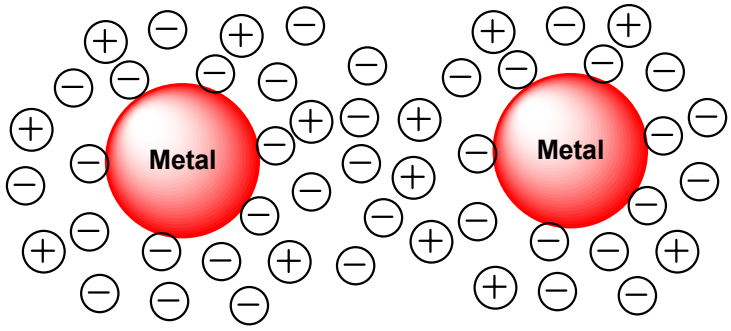
1.4 Stabilization of Metal Nanoclusters

The essential feature of nanoclusters is their small size. Owing to their small size, these metallic nanoparticles are unstable with respect to agglomeration into bulk materials. This aggregation leads to decrease of surface area and to the loss of the advantageous physical and chemical properties associated with the ultrafine state of these metallic particles. For example, during catalysis the coagulation of metallic nanoparticles used as catalyst can lead to a significant loss of activity as well as selectivity. The stabilization of metallic colloids, and thus the means to preserve their finely dispersed state, is a crucial aspect to consider during their synthesis. Several general discussions have already been reported on the stability of colloids and nanoclusters.[102] At short interparticle distances, the van der Waals forces will attract two metallic particles to each other. These forces vary inversely as the sixth power of the distance between their surfaces. In the absence of repulsive forces opposed to the van der Waals forces, the colloidal metal particles will aggregate. Consequently, the use of a stabilizing agent able to induce a repulsive force opposed to the van der Waals forces is necessary to provide stable nanoparticles in solution.[103]

The general stabilization mechanisms of colloidal materials have been described in Derjaguin-Landau-Verwey-Overbeek (DLVO) theory.[104] Nanocluster stabilization is categorized into three main types; (i) electrostatic stabilization, (ii) steric stabilization,[105] and (iii) electrostatic stabilization.[106] The steric stabilization of metallic nanoclusters has been widely studied and is the most common method used for nanoclusters stabilization. This kind of stabilization is generally done with ligands, solvents, dendrimers, and polymers.

1.4.1 Electrostatic Stabilization

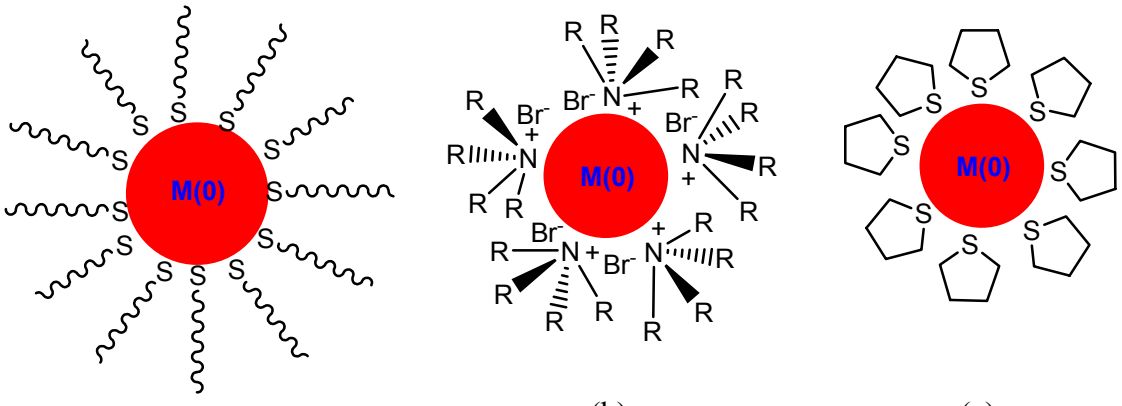
Ionic compounds such as halides, carboxylates, or polyoxoanions, dissolved in (generally aqueous) solution can provide the electrostatic stabilization. The adsorption of these compounds and their related counterions on the metallic surface will render an electrical double-layer around the particles (Scheme 1.11). This results in a Coulombic repulsion between the particles. If the electric potential associated with the double layer is high enough, then the electrostatic repulsion will prevent particle aggregation. Colloidal suspensions stabilized by electrostatic repulsion are very sensitive to any phenomenon able to disrupt the double layer like ionic strength or thermal motion. So the control of these parameters is essential to insure an effective electrostatic stabilization.



Scheme1.11: Schematic representation of electrostatic stabilization of metal nanoparticles (scheme was adopted from ref[51a]).

1.4.2 Stabilization by Ligand or Solvent

In this section we discuss about the stabilization of metal nanoparticles by ligands, or solvent, scheme 1.12. This stabilization occurs by the coordination of metallic nanoparticles with ligands such as phosphines,[107] thiols,[108] amines,[109] or carbon monoxide.[110] In the literature, reports are available in which Au, Pt, Pd, and Ni nanoclusters were stabilized by phosphines.[111] The phenanthroline and its derivatives[112] and octanethiol[113] have also been used to prepare Pt and Pd colloids. Recent reports disclose solvent-stabilized metal nanoparticles. Thus, Ti[114] and Ru[115] nanoparticles were synthesized in tetrahydrofuran or thioethers without adding steric or electrostatic stabilizers. However, in both cases, it has not been established that there is no coordination of the heteroatoms of the solvents with the metallic surface. Moreover, proof of the absence of stabilizing agents such as anions or cations is lacking. Sometimes, elemental analysis shows that potentially coordinating bromide or chloride anions still remain.[116]

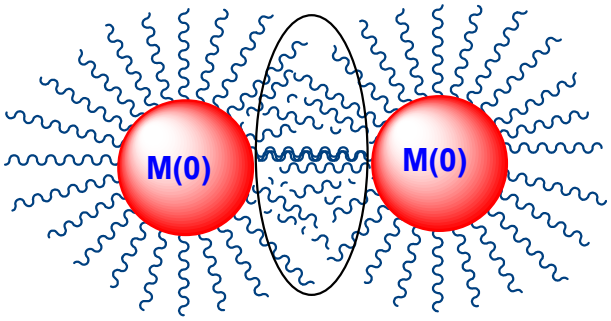


(a) (b) (c)

Scheme 1.12: Surface capping of metal nanoparticles with surfactant and solvent (Scheme was adapted from ref[51e]).

Scheme 1.12 corresponds to the stabilization of metal nanoclusters by strong coordinating ligand, thiol (a) or lipophilic or cationic type surfactant tetraoctylylammonium bromide (TOAB) (b). Both the thiol and TOAB were found highly efficient surfactant for nanometals giving very stable organosols. Tetrahydrothiophene has been used as stabilizing agent to protect metal nanoparticles from agglomeration (c). In the regard, Bonnemann has extensively studied the stabilization process of metal nanoclusters by above-mentioned stabilizing agents.[51e]

The adsorption of these molecules at the surfaces of the particles will provide a protective layer. The way in which these large adsorbed molecules prevent aggregation can be explained in a simplified manner by visualizing the approach of two metallic colloids. In the interparticle space, adsorbed molecules will be restricted in motion, which causes a decrease in entropy and thus an increase in free energy. A second effect is due to the local increase in concentration of adsorbed macromolecules as the two protective layers begin to interpenetrate. This result in an osmotic repulsion as the solvent will reestablish the equilibrium by diluting the surfactant and thus separating the particles. By contrast with the electrostatic stabilization, which is mainly used in aqueous media, the steric stabilization can be used in organic or in aqueous phase. Nevertheless, the length and/or the nature of the macromolecules adsorbed influence the thickness of the protective layer and can thus modify the stability of the colloidal metal particles. Scheme 1.13 represents the steric stabilization of metal nanoparticles by ligand. From the scheme it is clear that that when the surfactants were absorbed on the metal nanocluster surface, it is not allow the particles to come closer, which results fine dispersed metal organosols.



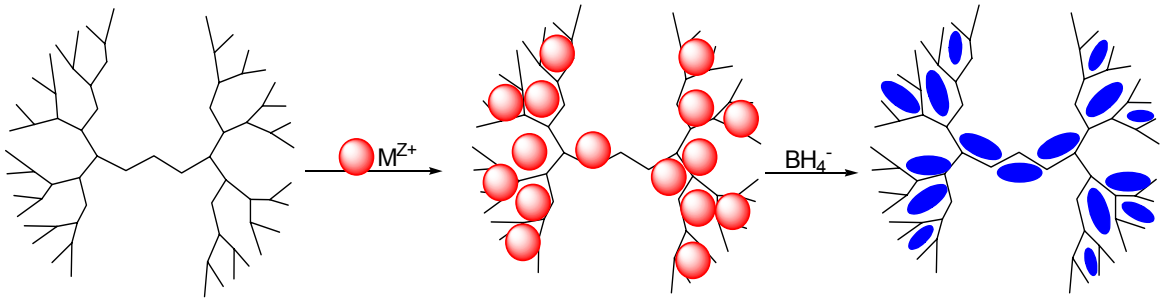
Scheme 1.13: Schematic representation of steric stabilization of metal nanoparticles (Scheme adapted from ref.[51a])

1.4.3 Stabilization by Dendrimer

Chemical routes to stable metal nanoparticles typically involve the reduction of metal salts and capping of the resulting nanoparticles with polymers or surfactants to stop growth and prevent agglomeration.[117] Alternatively, templates can be used to synthesize nanoparticles having well-defined sizes and shapes: examples of templates include porous alumina and track-etched membranes,[118] and reverse micelles.[119] These methods generally yield nanoparticles that are passivated by steric or electrostatic stabilizers, which limits their use for applications in fields such as catalysis. That is, one cannot have catalytic activity without access to surface sites, but removal of stabilizers to allow such access usually leads to aggregation. Dendrimers (DENs) address this issue, because the dendrimer allows for kinetic (templated) control of the nanoparticle size (and possibly shape), but it also prevents aggregation of the nanoparticles without passivating all of the active sites on the nanoparticle surface. There are three other potentially useful properties of DENs. First, it is easy to control the chemical composition of the peripheral groups on the dendrimer,[120] and this provides a means for attaching DENs to supports and for

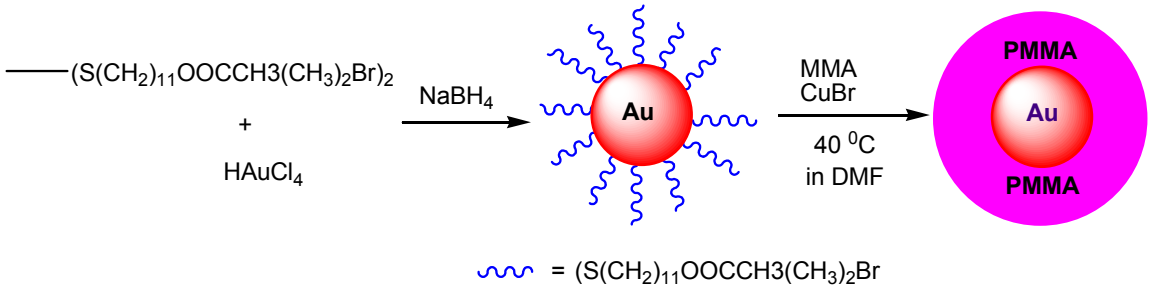
solubilizing them in nearly any solvent. Second, the dendrimer periphery can function as a size-and-shape selective molecular filter, thereby providing a means for introducing selectivity to intrinsically nonselective metal catalysts.[122] Third, the dendrimer can, in some cases, provide a means for controlling product selectivity.[123]

A variety of assemblies between PAMAM dendrimers and gold nanoparticles has been reported in which the nanoparticles were stabilized by dendrimers that acted as both a polymer and a ligand. Dendrimer-stabilized gold nanoparticles were synthesized by using the Brust technique; the dendrons were functionalized with thiols at the focal point.[125] PAMAM-dendrimer-gold nanoparticle composites were used as chemiresistor sensors for the detection of volatile organic compounds and studied by specular neutron reflectometry. Crooks *et al*. synthesized bimetallic Au-Pd nanoparticles from PAMAM-dendrimer-Pd nanoparticles assemblies for catalytic purpose.[126]



Scheme 1.14: Dendrimer encapsulated metal nanoparticles ((Scheme adapted from ref [126b]).

1.4.4 Polymer Stabilized Nanoparticles



Scheme 1.15: Schematic representation for the synthesis of polymer-coated gold nanoprticles by surface-initiated living radical polymerization (scheme was adopted from ref[117b]).

Polymers can also use as stabilizers to achieve polymer stabilized metal nanoparticles. The most commonly used polymers for the stabilization of metal nanoparticles are PVP, polyethylene glycol, and polystyrene.[127] Although there are a variety of ways to achieve nanoparticle-polymer composites,[128] two main approaches dominate. The first one consists of the in situ synthesis of the nanoparticles in the polymer matrix either by reduction of the metal salts dissolved in that matrix[129] or by evaporation of the metals on the heated polymer surface.[130] The second one, less frequently used, involves polymerization of the matrix around the nanoparticles.[131] Recently, however, blending of *presynthesized* AuNPs into a *pre*synthesized polystyrene polymer (synthesized by anionic polymerization) bound to a thiol group was also reported.[132] Whereas the physical process involving mechanical crushing or pulverization of bulk metals and arc discharge yielded large nanoparticles with a wide size distribution, nanoparticles prepared by reduction of metal salts are small, with a narrow size distribution. This reduction processes most often use a reagent such as $NaBH_4$,[133] which

is added in situ, or the reductant can also be the solvent, such as an alcohol.[134] For instance, $HAuCl_4$ gives stable AuNPs upon refluxing in methanol/water in the presence of PVP, even if NaOH is added subsequently to the preparation of the AuNPs.[135] In poly(acrylamide), $AuCl_4^-$ cannot be reduced by alcohol, but it can be reduced by $NaBH_4$.[136] The polymer-nanoparticle composite can be generated from solution (the classic mode) or can involve the immobilization by a solid polymer such as poly(acrylic acid), poly(vinyl alcohol), or PVP frequently used. Reduction of metal ions in the presence of the polymer is most often chosen because the complexation of the metal cations by the ligand atoms of the polymer is crucial before reduction. In particular, it dramatically limits the particle size.[137] The most important role of the stabilizing polymer is to protect the nanoparticles from coagulation. Toshima has expressed this function quantitatively by the "gold number", i.e. the number of milligrams of protective polymer that just prevents 10 mL of a red gold sol from changing color to violet upon addition of 1 mL of 10% aqueous NaCl. The "gold number" is smaller for protective polymers that are better stabilizers. Core-shell PVP-stabilized Au/Pd[138] and Au/Pt[139] nanoparticles were prepared by Yonezawa and Toshima by simultaneous alcohol reduction of the two corresponding metal salts and characterized by EXAFS. The relative order of reduction in alcohol/water is seemingly controlled by the relative redox potentials, $HAuCl_4$ being reduced more rapidly than $Pd(OH)_2$ and $PtCl_6^{2-}$. The AuNPs form first, and then the Pd or Pt shell forms around the AuNPs to produce the core-shell bimetallic particles. In fact, the Pd^0 formed reduces $AuCl_4^-$ to Au^0 and thus acts as a mediator or redox catalyst for the reduction of $AuCl_4^-$, as long as any $AuCl_4^-$ is left in the solution.[140] Attempts to synthesize Pd-core/Au shell bimetallic particles led instead to a remarkable cluster-in-

cluster structure because of this redox priority.[141] Nanosized domains of block copolymers can be used as nanoreactors to synthesize AuNPs by expansion of the nanosized domains and period of block copolymers, such as polystyrene-*block*-poly(4-vinylpyridine) (PS-PVP) diblock copolymers.[142] Self-assemblies of AuNPs/polymer multilayer films have been formed using surface functionalization.[143] AuNPs of average size between 1 and 50 nm have also been stabilized by many water-soluble polymers, and some of then have been shown to be stable after 9 months in air. The most stable ones were obtained with polymers possessing hydrophobic backbones and side groups, allowing good interactions with the $AuCl_4^-$ ion. The preparations were carried out using either UV irradiation or KBH_4 to reduce $HAuCl_4$ in the presence of a mass ratio of polymer: gold 25:1.[144]

1.4.5 Electosteric Stabilization

The electrostatic and steric stabilization can be combined to maintain metallic nanoparticles stable in solution. This kind of stabilization is generally provided by means of ionic surfactants. These compounds bear a polar head group able to generate an electric double layer and a lypophilic side chain able to provide steric repulsion. The electrosteric stabilization can be also obtained from polyoxoanions such as the couple ammonium (Bu_4N^+)/polyoxoanion ($P_2W_{15}Nb_3O_{62}^{9-}$). The significant steric repulsion of the associated bulky Bu_4N^+ countercations associated with the highly charged polyoxoanion (Coulombic repulsion) provide an efficient electrosteric stability against agglomeration in solution of the resultant nanoclusters.[106]

1.5 Applications of the Nanosized Metal Particles

1.5.1. Surface Enhance Raman Spectroscopy (SERS)

Surface-enhanced Raman scattering (SERS) is a powerful analytical tool to determine chemical information for molecules on metallic substrates.[145] In general, there are two traditional operational mechanisms to describe the overall SERS effect: electromagnetic and chemical enhancement mechanisms. Electromagnetic enhancement is enhancement of the local electromagnetic field incident on an adsorbed molecule at a metallic surface. Chemical enhancement results from electronic resonance/charge transfer between a molecule and a metal surface, which leads to an increase in the polarizability of the molecule.[146] Since the introduction of the SERS phenomenon on roughened silver electrodes,[147] much attention has turned to SERS on spherical colloidal substrates of either gold or silver and maximizing Raman signals.[148] Colloidal nanoparticles are of interest as SERS substrates not only because they are strong light scatterers, but also because of their tunable optical properties, which depend on nanoparticle size, shape, and aggregation state.[149] Silver colloids as active surfaces for surface-enhanced Raman scattering (SERS) spectroscopy possess several distinct features as compared to e.g. silver electrodes and films. It is now well known that the surface enhancement of Raman scattering works most effectively for aggregated colloids.[149] Aggregation is induced either by the adsorbate itself or by a preaggregation agent. The conditions under which the aggregation of the colloid occurs have, in many cases, to be tailored for each particular adsorbate. The aggregation *can* be easily monitored by UV/vis absorption

spectroscopy via the changes in the surface plasmon absorption of the colloid induced by aggregation. A substantial amount of information about the relationship between the state of aggregation and SERS activity of the Ag colloid/adsorbate system can thus be obtained.[149] Spheroidal or rod-shaped nanoparticles are of significant interest as SERS substrates because of their tunable longitudinal plasmon bands and the "lightning rod" effect on surface enhancement.[150] Whereas electric field enhancement is observed for 10-200 nm metallic particles, even greater local field enhancements are observed at sharp surface features, for example, at the tips of needle-shaped nanorods, where the curvature radius is much smaller than the size of the nanoparticle. This phenomenon is known as the lightning rod effect. Despite the desirable characteristics of metallic nanorods and nanowires as SERS substrates, only a few reports exist for SERS on rod- or wire-shaped nanoparticles.[151]

1.5.2 DNA-Gold Nanoparticles Assemblies and Sensors

Not all molecular fluorophores are suitable probes in biodiagnostic assays, nor do all nanomaterials offer advantages in biodetection. Certain nanomaterials are attractive probe candidates because of their small-size (1-100 nm) and correspondingly large surface-to-volume ratio, chemically tailorable physical properties, which directly relate to size, composition and shape, unusual target binding properties, and **(4)** overall structural robustness. The size of a nanomaterial can be an advantage over a bulk structure, simply because a target binding event involving the nanomaterial can have a significant effect on its physical and chemical properties, thereby providing a mode of signal transduction not necessarily available with a bulk structure made of the same material. Tailorable physical

properties are a very important aspect of nanomaterials. Indeed, in this regard, nanomaterials and biology have a long history as nanoparticles have been used in bioconjugation and as cellular labeling agents for the past four decades.[152] However, new synthesis, fabrication, and characterization methods for nanomaterials have evolved to the point that deliberate modulation of their size, shape, and composition is possible, thereby allowing exquisite control of their properties.

The ability to carefully tailor the physical properties of nanomaterials is essential for their application in biodetection.[153] Specifically, the sizes, shapes, and compositions of metal nanoparticles and quantum dots can now be systematically varied to produce materials with specific emissive, absorptive, and light-scattering properties, which make these materials ideal for multiplexed analysis detectors;[153, 154] the composition of nanowires and nanotubes also can be controlled, thus allowing for measurement and variation of their conductive properties in the presence of target analytes.[155] Additionally, tools and techniques for surface modification and patterning have advanced to a point that now allows generation of nanoscale arrays of biomacromolecules and small molecules on surfaces.[156] Along with synthetic advances for varying the size, shape, and composition of nanostructured materials has come the ability to tailor their binding affinities for various biomolecules through surface modification and engineering.[157] Each of these capabilities allows researchers to design materials that can potentially be implemented into new assays having improved modes of signal transduction that can compete favorably with the molecular fluorophore-dominated methods of PCR and ELISA.

Conjugates of AuNPs-oligonucleotides are of great current interest because of the potential use of the programmability of DNA base-pairing to organize nanocrystals in space and the multiple ways of providing a signature for the detection of precise DNA sequences. Applications in the fields of biosensors, disease diagnosis, and gene expression are clearly called for. Intensive research has been carried out with gold nanoparticles functionalized with oligonucleotides. Mirkin and coworkers[158] have used DNA as a linker to form macroscopic assemblies consisting of discrete 13 nm diameter particles. The DNA attached to the nanoparticles retained its ability to hybridize with complementary DNA, and the annealing process was thermally reversible and nondestructive. The reaction was sequence-specific. Alivisatos[159] has used DNA as a template to prepare nanocrystal molecules consisting of two or three 1.4 nm diameter particles on a single oligonucleotide strand. DNA-driven assemblies of AuNPs have indeed attracted considerable interest,[160] and a new colorimetric technique based on the sensitivity of the SPB (surface plasmon band) to monitor DNA modification was designed by the Mirkin-Letsinger group. In this strategy, gold nanoparticles are used as building blocks, allowing the assembly of alkanethiol-capped oligonucleotides such as single-stranded DNA and complementary linker oligonucleotide (DNA) strands. Aggregation of AuNPs linked by the oligonucleotides provokes a red-to-blue color change (red shift from 520 to 600 nm of the SPB) that is most useful for this DNA-sensing method. The parameters that are controlled are the AuNP composition, the periodicity, and the aggregate thermal stability. These parameters are organized in order to influence the optical, mechanical, and electrical properties of the gold nanoparticles. In particular, the optical properties due to the SPB of gold nanoparticles from 13 to 17 nm

diameter led to the development of a highly selective diagnostic method for DNA, based on the distance-related SPB of AuNPs. The effect of the length of the DNA strands that control the interparticle distance was studied, and it was found that the SPB frequency changes are inversely dependent on the oligonucleotide linker length (between 24 and 72 base pairs, i.e., from 80 to 24 Å). An interesting result was that the most important parameter that controls the SPB shift of these AuNPs-DNA materials is the aggregate size. This aggregate size is under kinetic control, and it is the growth rate that depends on the linker length. Annealing of the kinetic structures formed at temperatures just below their melting points lead to a SPB shift. This growth, leading to the red shift of the SPB, occurs through an Oswald ripening mechanism whereby larger aggregates grow at the expense of smaller ones.

Another important characteristic of the gold nanoparticles based pair detection is the "melting" transition of the complementary DNA strand. The gold nanoparticles are linked in the presence of the complementary strand. These H-bonded connections of the links are broken at sufficiently high temperatures, which unzips the oligonucleotides, "melting" the DNA and releasing the particles.[158] Calculations using AuNP polarizabilities determined from Mie theory, an iterative conjugate-gradient solution algorithm, and fast Fourier transform methods for efficient solution of the electrodynamics of interacting AuNP equations show that the UV extinction lowering and the shift and broadening of the SPB of the DNA-linked AuNPs are explained as the collective electromagnetic response of thousands of AuNPs.[158]

Immunolabeling with AuNPs and imaging of cells, biomolecules, and other biological components have been extensively reviewed in the book edited by Hayat in

1989,[127] and this area continues to attract the attention of biochemists and biophysicists.[161] The recognition of proteins has been for some time the subject of research on biodevices for diagnostics based on the interaction between AuNP-antibody conjugates and their antigens. Only recent progress is reviewed here. The great sensitivity of the SPB by AuNP adsorption led to their use in bioassay applications. The investigated AuNP-protein conjugate architectures involve either direct binding of antigen: AuNP-biocongugate to an antibody-modified surface or the exposure of an antibody-derived surface to free antigen and then to a secondary antibody-AuNP conjugate. This classic type of immunoassay allows the evaluation of AuNP tags in a standard mode of antigen detection.[162] Biosensors for immunoassays in human serum have been developed.[163]

AuNPs coupled with biomolecules are attracting increasing attention because of the potential applications of these new materials in biology-related challenges.[164] Mannose-encapsulated AuNPs have been shown by TEM to specifically bind FimH adhesin of bacterial type 1 pili in *Escherichia coli*, and to do so more strongly than free mannose in the competition assay. This process represents a new method of labeling specific proteins on the cell surface using carbohydrate-conjugated AuNPs, whereby the visualization of the target receptor on the cell surface is relatively easy under an electron microscope.[165] AuNPs functionalized with a monolayer of 11-thioacetateundecanol-derivatized neoglycoconjugates of lactose disaccharide and trisaccharide antigens can be used to mimic glycophosphinolipid clusters in plasma membranes in order to investigate a new mechanism of cell adhesion through carbohydrate-carbohydrate interactions.[166] Spontaneous formation of AuNPs was observed in aqueous solutions of sugar-persubstituted PAMAM dendrimers without the addition of any additional reductant.[167]

AuNPs coated with haptenated mercaptodextrans containing 15 mercapto groups bind specifically to paramagnetic beads coated with the corresponding antibody.[168] A mannose derivative has been self-assembled onto preformed, citrate-capped water-soluble AuNPs, and, through the use of a C2 tether, a rapid colorimetric detection test has been developed for the protein canavalinin A.[169] Multivalent interactions of glycono-AuNPs containing galactosyl and glucosyl headgroups with the HIV-associated recombinant glycoprotein gp 120 have been studied.[170]

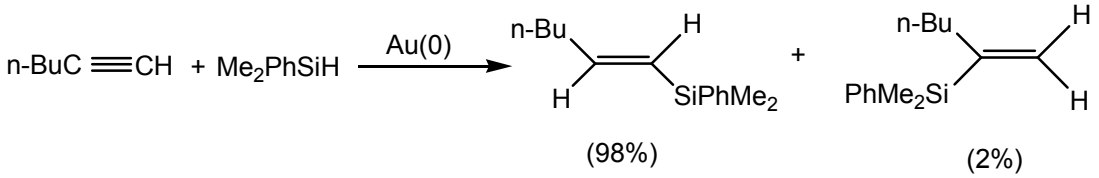
1.5.3 Au, Ag Nanoparticles as Effective Catalysts

Although nanoparticles find application in such diverse fields as photochemistry, nanoelectronics, or optics, their principal application in today's technology is in catalysis. As catalysts, these systems show a great potential because of the large surface area of the particles. Many chemists suggest that metal colloids are very efficient catalysts because of a great ratio of atoms remaining at the surface, and so available for chemical transformation of substrates. In fact, these catalysts are microheterogeneous systems bearing metal nanoparticles. Undoubtedly, many catalytic transformations have been carried out with microheterogeneous metal catalysts while chemists believed that they were performed via homogeneous catalysts. Since that time, modern methods to distinguish homogeneous from heterogeneous catalysts were described. The original catalytic approach is to use colloidal metallic particles finely dispersed in organic or aqueous solution or a solvent mixture. Generally, these suspensions must be stabilized with protective agents to prevent aggregation and/or to facilitate recycling. One disadvantage of soluble colloidal metals is the recovery of the catalyst from the reaction

products. This can be overcome by using aqueous/organic biphasic conditions or other immobilization systems such as, for instance, fluorinated solvents or thin films of liquids on porous supports.

In contrast to the catalytic potential of its neighbors silver and platinum, bulk gold metal appeared for long time as essentially useless material for catalysis.[171] Information on the catalytic chemistry of Au^0 was discovered when silica supported Au^0 catalyzed the hydrogenation of alkenes at 373 K.[172] Table 1.1 represents the various reactions performed with supported gold catalyst. The supported Au^0 was also found to be active for oxidation of CO to CO_2.[173] From the above two examples, it is quite clear that for gold catalyzed reactions, the presence of nanoparticles and the metal oxide such as Fe_2O_3, TiO_2, or CO_3O_4 support are the two key factors.[174]

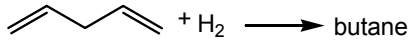
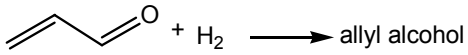
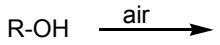
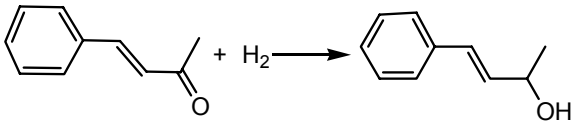
The hydrosilylation reaction is one of the most important ways to prepare silicone polymers. It was reported that acetone solvated gold nanoparticles can be successfully used for the hydrosilylation of 1-hexyne. The resulted product was highly regio-and



stereoselective, scheme 1.16.[175]

Scheme 1.16: Hydrosilylation of 1-hexyne promoted by gold nanoparticles (adapted from ref [175]).

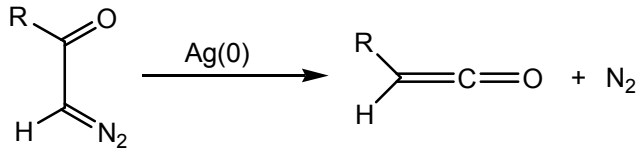
Table 1.1: A selection of reactions relevant to chemical processing, catalyzed by supported gold (0) (adapted from ref [174c]).

Entry	Reaction	Catalyst	Remarks
1		Au/S	gas phase
2		Au/ZrO_2	gas phase
3		Au/SiO_2	gas phase
4		Au/Fe_2O_3	liquid phase, ethanol 1 atm, 60 ^{0}C
5	D-glucose + O_2 ⟶ gluconic acid	Au/TiO_2	liquid phase, 1-3 atm, 70-80 ^{0}C
6	H_2 + O_2 ⟶ H_2O_2	$Au\text{-}pd/Al_2O_3$	liquid phase, methanol 97 atm, 2 ^{0}C

More recent investigations have shown that AuNPs that were adsorbed and dispersed on oxide support by reduction of $AuCl_4^-$ or $AuCl_3$, and then calcinated, were also efficient catalysts for other reactions, including hydrogenation of unsaturated substrates. For instance, such AuNPs of 1-5 nm diameter, supported on titania or zirconia, were active in the regioselective hydrogenation of acrolein to allylic alcohol at 180-280 °C (total pressure, 2 MPa), a particularly difficult reaction. Following TEM and EPR studies, it was suggested that the origin of the selectivity of CdO vs CdC hydrogenation might be attributed to quantum size effects that alter the electronic properties of sufficiently small AuNPs.[176] Active sites were identified as edges.[177] AuNPs were prepared by dispersion on an amorphous silica support, wherein silanol groups of

the surface of fumed silica spontaneously reduced $AuCl_4^-$ ions. These supported AuNPs were found to be catalytically active in the hydrogenation of cyclohexene at 80 °C and 200 psi H_2.[178] PVP-stabilized Au/Pd bimetallic nanoparticles showed high activity for the hydrogenation of cycloocta-1,3-diene (COD), with 100% selectivity for cyclooctene formation. The high activity was ascribed to electronic deficiency of the active surface Pd atoms (required for *ð* back-donation from the coordinated olefin) due to electron transfer to the gold atoms. Reduction of eosin by $NaBH_4$ at 29 °C was catalyzed by AuNPs of 10-46 nm diameter, prepared by a seed-mediated growth method, and the reaction rates were shown to increase both above and below 15 nm diameter.[179]

In situ-generated silver nanoclusters(Ag_n) during the reduction of either silver(I) oxide or other salts presumably catalyze the Wolff rearrangement of R-diazoketones. The electron donation by the additives to silver (I) compounds leads to the formation of silver nanoclusters (Ag*n*) during the reaction, which presumably catalyzes the reaction to the desired product.[180] Scheme 1.17 represents the Wolf rearrangement of diazoketones by silver nanoclusters.

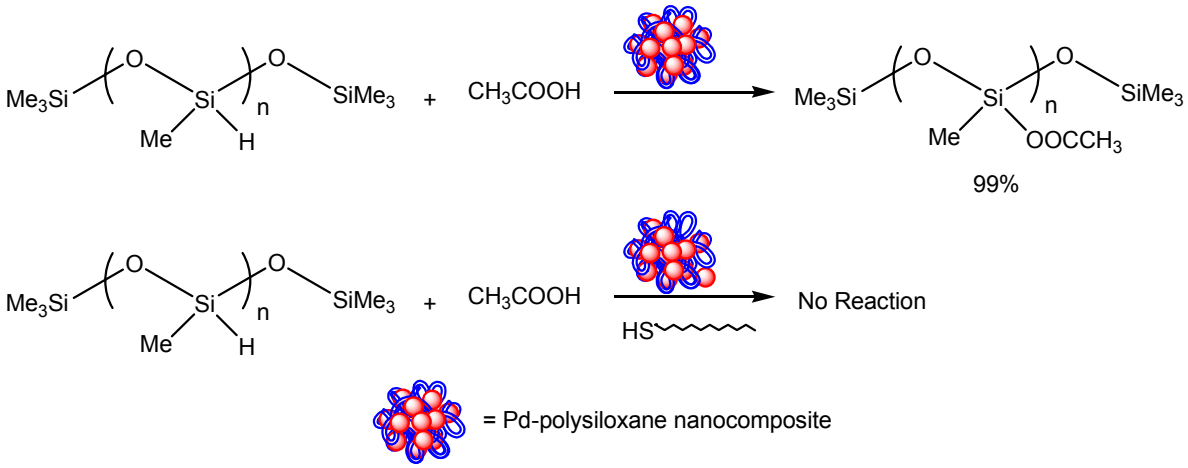


Scheme 1.17: Silver nanoclusters assisted Wolff rearrangement of diazoketones (adapted from ref [180]).

1.6 Challenges of the Solution Phase Synthesis

At present, the Brust-method and its various modifications are the most established schemes for Au and Ag nanoparticle synthesis, although other approaches are also available. However, the Brust method has some limitation: (i) first of all almost all the synthetic processes involves reduction of metal salts by $NaBH_4$ as a reducing agent. Because all of the four hydrogen atoms in the BH_4^- anion can take part in the reducing process, the resulting metal colloids are contaminated with borides. (ii) The size distribution is broad; the uniformity of size is necessary to obtain ordered assemblies. The resulting nanoparticles are coated with a monolayer of strong surfactant, thiol, which makes it difficult to carry out the surface modification and functionalization on nanoclusters surface. The capping materials should provide uniform protection of the surface without modification of essential structural and electronic properties of the nanoparticles.

Most of the reduction processes for synthesizing nanoparticles have been carried out in aqueous medium. On the other hand nanoparticle catalyzed reactions are typically performed in organic media. Eventually, there must be phase transfer between synthesis and the application of nanoparticles. Moreover the aqueous phase synthesis was carried out in the presence of different strong coordinating ligand. The strong coordinating surfactant then killed the active sites of the metal nanoclusters. Chauhan and coworkers[181] have successfully investigated the poisoning of different metal nanoclusters catalyzed reactions. They have found that thiolated ligand has strong ability to kill the active nanoparticle sites, resulting in very low yield of the desired product.



Scheme 1.18: "Polysiloxane-Pd" nanoconjugate assisted silaesterification of PMHS and the corresponding poisoning study in presence of dodecanethiol (scheme was adapted from ref [181a]).

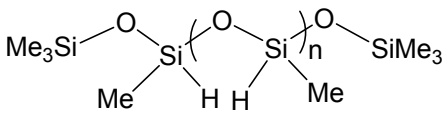
Scheme 1.18 represents the palladium nanoclusters catalyzed silaesterification of PMHS. When the similar reaction was carried out in the presence of strong coordinating ligand, thiol, the nanoclusters were inactive to perform the transformation. It happened because of the thiol molecules, which absorbed on the nanoclusters surface and killed the active sites of nanoparticles. These kinds of experiments are known as catalytic poisoning experiment. Other than thiol, phosphine ligands were also investigated for the poisoning experiments.

1.7 Aims and Objective of Our Research

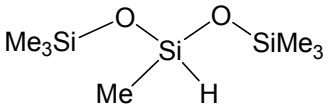
1.7.1 To Investigate the Ability of Si-H Bonds for Reduction of Silver and Gold Metal Salts

Polymethylhydrosiloxane (PMHS) is an attractive reducing reagent for environmentally benign reductive processes because it is inexpensive, non-toxic, and stable to air and moisture. This is in marked contrast to commonly used reducing agents such as lithium aluminium hydride, borane and hydrogen, which are all clearly hazardous. Although PMHS has been known and readily available for the past 50 years, it has only been used sparingly as a reagent for nanomaterials synthesis. Siloxane polymers are a very versatile class of polymer, which have been used as additives to produce or enhance a number of physical properties. PMHS is commercially available and is typically a colorless free flowing liquid, which is soluble in most organic solvents and is inert to air and moisture. The lack of reactivity in the absence of catalysts makes PMHS such an attractive reducing agent. Numerous types of catalysts have been used in combination with PMHS to reduce a wide range of organic functional groups. The most frequently used catalysts are tin, titanium and palladium species, which mediate reduction *via* the corresponding metal hydride species.[182] In these cases the catalysts act as sources of hydride transfer agents. Monomeric siloxanes are known reducing agents for the generation of Pt, Pd, and Rh nano-sized particles,[183] on the other hand investigation of polysiloxanes as reducing agent for the gereration of nano-sized silver and gold particles have not been explored. Though, their property profile may provide the means of

directing metallic particles into specific physicochemical enviroment in addition of the utility as reducing agent.



PMHS

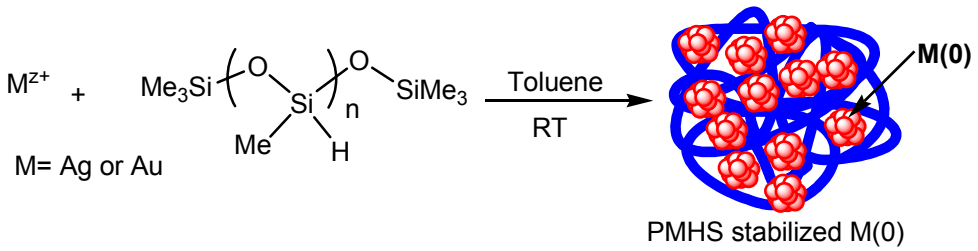


HMTS

1.7.2 To Utilize the Polymethylhydrosiloxanes (PMHS) and their Oligomeric Counterparts, Heptamethyltrisiloxane (HMTS) as Reducing Agents

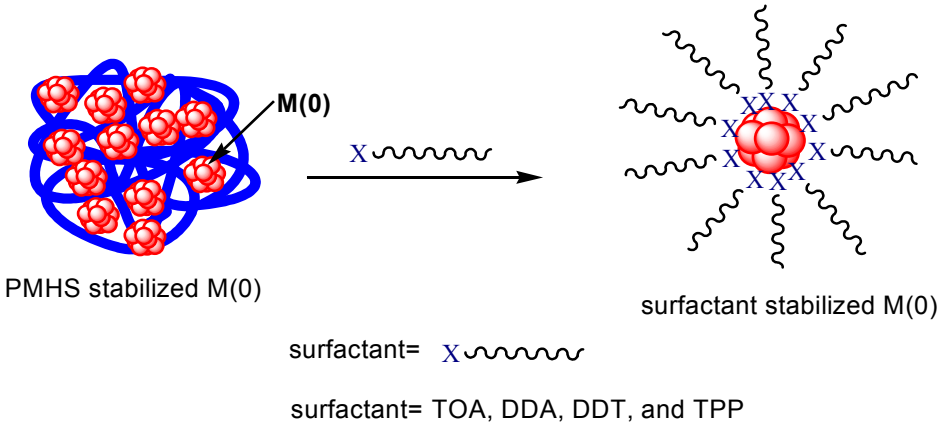
Polysiloxane are particularly well suitated for hosting metal nanoparticles for the following reasons:

- *The selected polysiloxane templates themselves are of fairly uniform composition and structure and therefore, they may yield well-defined nanoparticle replicas.*
- *Unusual freedom of rotation around the Si-O bond allows these polymers a high degree of flexibility while maintaining their integrity.*
- *Polysiloxanes with Si-H functionalities can act as reducing agent and thus can eliminate the need for extra reducing agent.*
- *The encapsulated nanoparticles are confined primarily by steric effects, and, therefore, a substantial fraction of their surface is unpassivated and available to participate in surface exchange and functionalization of nanoparticles.*



Scheme 1.19: Polyhydrosiloxane induced generation and stabilization of noble metal nanoparticles.

In our approach (Scheme 1.19), well-defined SiH-containing polymers are envisioned to act as reducing agent, as well as templates to control the size, stability and solubility of particles. The siloxane bonds in polysiloxanes are very flexible and encapsulated metal particles inside the polymer matrix The polymers can be easily removed from nanoparticle surface using strong capping agent, e.g.; thiol, amine, phosphine oxide and carboxylic acid. Scheme 1.20 represents the simple ligand exchange study on polymer stabilized metal nanoparticles.



Scheme 1.20: Surfactant exchange reaction on polysiloxane-metal nanocomposite.

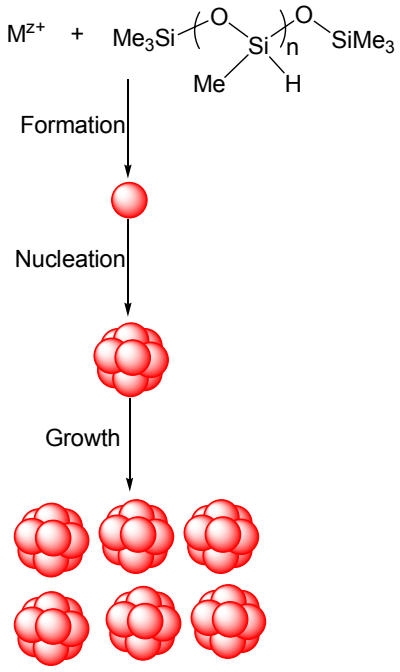
1.7.3 To Investigate, if it is Possible to Control the Nucleation and Growth of Metal Particles Under our Reaction Conditions

Most of the methods to make small metal clusters (1-5 nm) take advantage of the strong capping action of thiols. Varying the capping agent concentration allows for size control between 1 and 4 nm with good monodispersity, but any attempts to make larger size particles (>5 nm) with these procedures lead to a wider particle size distribution (standard deviation 25- 100%), and further narrowing of size distribution is required. Occasionally, aging, annealing, or ligand exchange improves size dispersion, but at the expense of small particle size.[184] Difficulty in controlling the nucleation and growth steps occurring at intermediate stages of particle formation results in a broad particle size distribution.

For the citrate reduction method, citrate acts both as a reducing agent and as a capping agent,[57,58] and due to its weak reducing and capping character, the average size is relatively large.[185] In comparison, the Brust method uses a strong reducing agent ($NaBH_4$), causing more nucleation, and a strong capping agent (alkanethiol), which drastically inhibits growth. Another common approach for controlling the size of nanoparticles is seeding growth. In seeding growth methods, small metal particles are prepared first and later used as seeds (nucleation centers) for the preparation of larger size particles. Recently, seeding growth methods were developed for size control of Au, Ag, Ir, Pd, and Pt particles. Providing a controlled number of preformed seeds (as nucleation centers) and a growth condition that inhibits any secondary nucleation, the particle size can be controlled simply by varying the ratio of seed to metal salt. However, difficulty in

finding a suitable growth condition that inhibits additional nucleation during the growth stage limits the application of such methods. In general, these conditions include using a reducing agent too weak to reduce the metal salt (in the growth stage) without the presence of seeds.

PMHS and its oligomeric counter parts might be the best suitable reducing agent for the generation of small metal nanoparticles with narrow size distribution. Due to their mild reducing character, the nucleation process is controllable. The long chain polysiloxane can also act as a stabilizing agent, which will not hinder the growth process. In the hydrosiloxane reduction, the small metal nanoparticles are formed at the beginning, which can act as a nucleation center for the preparation of larger particles. In the siloxane reduction process, the nucleation and growth occur simultaneously and the particle size can be controlled simply by varying the molar ratio of reducing agent.



Scheme 1.21: Formation of metal nanoparticles by PMHS reduction method.

1.7.4 To Investigate, if it is Possible to Control the Shape of the Synthesized Nanoparticles

The nucleation stage for the growth of anisotropic shapes plays a key role in determining the size/shape of the resulting nanocrystals. The critical nuclei can be much smaller than the ones for the synthesis of dots. In the extremely small size range, the relative chemical potential is highly size-dependent, and even very sensitive to the configuration of the nuclei. Thermodynamically, all of the nanocrystals will grow toward the shape having the lowest energy at equilibrium, which is governed by the classic theory. However, the formation dynamics can affect the shape of the formed nanocrystals. Indeed, the formation of nanocrystals is found to be a highly kinetics driven process. In principle, before the reaction reaches the equilibrium stage, tuning the reaction conditions can arrest any metastable nanocrystal shapes. Even spherical or dot-shaped nanocrystals are not thermodynamically stable unless they are arrested or capped by different protecting groups, which is true in the case of most nanocrystal systems. Essentially at low monomer concentrations or long enough growth time, all nanocrystals grow toward the lowest chemical potential environment, and this leads to the generation of only dots. On the other hand, a median monomer concentration can support only an isotropic growth in a three-dimensional growth stage and produces prismatic shaped nanocrystals. At high monomer concentrations, the magic-sized nanoclusters promote the formation of rods or other elongated structures having metastability. PMHS and its oligomeric counter parts are mild reducing agent, and the rate of nanoparticle formation could be easily controlled by simply varying the amount of PMHS in the reaction mixture.

1.8 References and Notes

1. Faraday, M. *Phil. Trans. Roy. Soc*. **1857**, *147*, 145.

2. (a) Alivisatos, A. P. *Science* **1996**, *271*, 933. (b) Brus, L. E. *J. Chem. Phys*. **1986**, *90*, 2555. (c) Majetich, S. A.; Jin, Y. *Science* **1999**, *284*, 470. (d) Murray, C. B.; Kagan, C. R.; Bawendi, M. G. *Science* **1995**, *270*, 1335. (e) Hyeon, T. *J. Chem. Soc., Chem. Commun*. **2003**, 927.

3. Mostafavi, M.; Marignier, J. L.; Amblard, J.; Belloni, J. *J. Radiat. Phys. Chem*. **1989**, *34*, 605.

4. (a) Lewis, L. N. *Chem. Rev*. **1993**, *93*, 2693, (b) Schmid, G. *Chem. Rev*. **1992**, *92*, 1709.

5. Park, S.-J.; Taton, T. A.; Mirkin, C. A. *Science* **2002**, *295*, 1503.

6. (a) Ditlbacher, H.; Krenn, J. R.; Schider, G.; Leitner, A.; Auessenegg, F. R. *Appl. Phys. Lett*. **2002**, *81*, 1762. (b) Wang, W.; Asher, S. A. *J. Am. Chem. Soc*. **2001**, *123*, 12528.

7. Thomas, K. G.; Kamat, P. V. *Acc. Chem. Res*. **2003**, *36*, 888.

8. (a) Black, C. T.; Murray, C. B.; Sandstrom, R. L.; Sun, S. *Science* **2000**, *290*, 1311, (b) Sun, S.; Murray, C. B.; Weller, D.; Folks, L.; Moser, A. *Science* **2000**, *287*, 1989.

9. (a) Matejka, P.; Vlckova, B.; Vohlidal, J.; Pancoska, P.; Baumrunk, V. *J. Phys. Chem*. **1992**, *96*, 13612.

10. Giersig, M.; Hilgendorff, M. *Eur. J. Inorg. Chem*. **2005**, 3571.

11. (a) Link, S.; El-Sayed, M. A. *Annu. Rev. Phys. Chem*. **2003**, *54*, 331. (b) Malinsky, M. D.; Kelly, K. L.; Schatz, G. C. *J. Am. Chem. Soc*. **2001**, *123*, 1471.

12. (a) Sanedrin, R.; Georganopoulou, D. G.; Park, S.; Mirkin, C. A. *Adv. Mater*. **2005**, *17*, 1027. (b) Metraux, G.; Mirkin, C. A.; *Adv. Mater*. **2005**, *17*, 412. (c) Pileni, M. P. *Nat. Mat*. **2003**, *2*, 145. (d) Shankar, S. S.; Rai, A.; Ankamwar, B.; Singh, A.; Ahmad, A.; Sastry, M. *Nat. Mat*. **2004**, *3*, 482. (e) Yu, D.; Yam, V. W.-W. *J. Am. Chem. Soc*. 2004, *126*, 13200. (f) Jin, R.; Egusa, S.; Schere, N. F. *J. Am. Chem. Soc*. **2004**, *126*, 9900. (g) Kim, F.; Song, J. H.; Yang, P. *J. Am. Chem. Soc*. **2002**, *124*, 14314. (h) Pastoriza-Santos, I.; Liz-Marzan, L. M. *Nano Lett*. **2002**, *2*, 903. (i) Caswell, K. K.; Benden, C. M.; Murphy, C. J. *Nano L*ett. **2003**, *3*, 667. (j) Im Hyuk, S.; Lee, Y. T.; Wiley, B.; Xia, Y. *Angew. Chem. Int. Ed*. **2005**, *4*4, 2154. (k) Ahmadi, T. S.; Wang, Z. L.; Green, T. C.; Hehlein, S.; El-Sayed. M. A. *Science* **1996**, *272*, 1924.

13. (a) Link, S.; El-Sayed, M. A. *Int. Rev. Phys. Chem*. **2000**, *19*, 409. (b) Thomas, K. G.; Zajicek, J.; Kamat, P. V. *Langmuir* **2002**, *18*, 3722. (c) Linnert, T.; Mulvaney, P.; Henglein, A. *J. Phys. Chem*. **1993**, *97*, 679. (d) Averitt, R. D.; Westcott, S. L.; Oldenburg, S. J.; Lee, T. R.; Halas, N. J. *Langmuir* **1998**, *14*, 5396.

14. Mie, G. *Ann. Phys*. **1908**, *25*, 329.

15. Kreibig, U.; Vollmer, M. *Optical Properties of Metal Clusters*; Springer: Berlin, Germany, 1995.

16. (a) Schmid, G. Metals. *In Nanoscale Materials in Chemistry*; Klabunde, K. J., Ed.; Wiley-Interscience: New York, 2001; Chapter 2, p 15. (b) Nirmal, M.; Brus, L. *Acc. Chem. Res*. **1999**, *32*, 407. (c) Alivisatos, A. P. *Endeavour* **1997**, *21*, 56. (d) Murray, C. B.; Norris, D. J.; Bawendi, M. G. *J. Am. Chem. Soc*. **1993**, *115*, 8706.

17. Hu, J.; Zhang, D.; Lui, F.; Kittredge, K.; Whitesell, J. K.; Fox, M. A. *J. Am. Chem. Soc*. **2001**, *123*, 1464.

18. Thomas, K. G.; Kamat, P. V. *J. Am. Chem. Soc*. **2000**, *122*, 2655.

19. Xu, P.; Yanagi, H. *Chem. Mater*. **1999**, *11*, 2626.

20. Dubbbertret, B.; Calame, M.; Libchaber, A. J. *Nat. Biotechnol*. **2001**, *19*, 365.

21. (a) Sarathy, V. K.; Narayan, K. S.; Kim, J.; White, J. O. *Chem. Phys. Lett*. **2000**, *318*, 543. (b) Makarova, O. V.; Ostafin, A. E.; Miyoshi, H.; Norris, J. R., Jr.; Meisel, D. *J. Phys. Chem. B* **1999**, *103*, 9080. (c) Gu, T.; whitesell, J. K.; Fox, M. A. *Chem. Mater*. **2003**, *15*, 1358.

22. Imahori, H.; Fukuzumi, S. *Adv. Mater*. **2001**, *13*, 1197.

23. (a) Imahori, H.; Arimura, M.; Hanada, T.; Nishimura, Y.; Yamazaki, I.; Sakata, Y.; Fukuzumi, S. *J. Am. Chem. Soc*. **2001**, *123*, 335. (b) Wilcoxon, J. P.; Martin, J. E.; Parsapour, F.; Wiedenman, B.; Kelley, D. F. *J. Chem. Phys*. **1998**, *108*, 9137.

24. Hwang, Y.-N.; Jeong, D. H.; Shin, H. J.; Kim, D.; Jeoung, S. C.; Han, S. H.; Lee, J.-S.; Cho, G. J. *J. Phys. Chem. B* **2002**, *106*, 7581.

25. Ipe, B. I.; Mahima, S.; Thomas, K. G. *J. Am. Chem. Soc*. **2003**, *125*, 7174.

26. (a) Hirai, H.; Nakao, Y.; Toshima, N. *J. Macromol. Sci., Chem*. **1978**, *A12*, 1117. (b) Borsla, A.; Wilhelm, A. M.; Delmas, H. *Catal. Today 2001*, *66*, 389. (c) Toshima, N.; Kuriyama, M.; Yamada, Y.; Hirai, H. *Chem. Lett*. **1981**, 793.

27. Mayer, A. B. R.; Mark, J. E.; Hausner, S. H. *J. Appl. Polym. Sci*. **1998**, *70*, 1209.

28. Mayer, A. B. R.; Mark, J. E. *J. Polym. Sci. A: Polym. Chem*. **1997**, *35*, 3151.

29. Mayer, A. B. R.; Mark, J. E. *Colloid Polym. Sci*. **1997**, *275*, 333.

30. Youk, J. H.; Locklin, J.; Xia, C.; Park, M. K.; Advincula, R. *Langmuir* **2001**, *17*, 4681.

31. (a) Chen, C.-W.; Akashi, M. *Langmuir* **1997**, *13*, 6465. (b) Chen, C.-W.; Takezako, T.; Yamamato, K.; Serizawa, T.; Akashi, M. *Colloids Surf., A* **2000**, *169*, 107. (c) Chen, C.-W.; Akashi, M. *J. Polym. Sci. A: Polym. Chem*. **1997**, *35*, 1329.

32. Dalmia, A.; Lineken, C. L.; Savinell, R. F. *J. Colloid Interface Sci*. **1998**, *205*, 535.

33. Meguro, K.; Nakamura, Y.; Hayashi, Y.; Torizuka, M.; Esumi, K. *Bull. Chem. Soc. Jpn*. **1988**, *61*, 347.

34. Teranishi, T.; Miyake, M. *Chem. Mater*. **1998**, *10*, 594.

35. Teranishi, T.; Hosoe, M.; Miyake, M. *Adv. Mater*. **1997**, *9*, 65.

36. Bonet, F.; Delmas, V; Grugeon, S.; Herrera Urbina, R.; Silvert, P.-Y.; Tekaia-Elhsissen, K. *Nanostruct. Mater*. **2000**, *11*, 1277.

37. Yu, W.; Liu, M.; Liu, H.; Zheng, J. *J. Colloid Interface Sci*. **1999**, *210*, 218.

38. Busser, G. W.; Van, Ommen, J. G.; Lercher, J. A. *Adv. Catal. Nanostruct. Mater*. **1996**, 213.

39. Yu, W.; Tu, W.; Liu, H. *Langmuir* **1999**, *15*, 6.

40. (a) Sun, Y.; Yin, Y.; Mayers, B. T.; Herricks, T.; Xia, Y. *Chem. Mater*. **2002**,*14*, 4736. (b) Wiley, B.; Herricks, T.; Sun, Y.; Xia, Y. Nano Lett. 2004, 4, 1733. (c) Xiong, Y.; Chen, J.; Wiley, B.; Xia, Y.; Yin, Y.; Li, Z.-Y. Nano Lett. 2005, 5, 1237. (c) Sun, Y.; Mayers, B.; Herricks, T.; Xia, Y. Nano Lett. 2003, 3, 955. (d) Sun, Y.; Mayers, B.; Xia, Y. Nano Lett. 2003, 3, 675. (e) Chen, J.; Herricks, T.; Geissler, M.; Xia, Y. *J. Am. Chem. Soc*. **2004**, *126*, 10854. (f) Sun, Y.; Xia, Y. *Science* **2002**, *298*, 2176.

41. Hirai, H.; Wakabayashi, H.; Komiyama, M. *Chem. Lett*. **1983**, 1047.

42. Mayer, A. B. R.; Antonietti, M. *Colloid Polym. Sci*. **1998**, *276*, 769 and references therein.

43. (a) Balogh, L.; Tomalia, D. A. *J. Am. Chem. Soc*. **1998**, *120*, 7355. (b) Zhao, M.; Sun, L.; Crooks, R. M. *J. Am. Chem. Soc*. **1998**, *120*, 4877. (c) Zhao, M.; Crooks, R. M.

Angew. Chem. Int. Ed. Engl. **1999**, *38*, 364. (d) Esumi, K.; Suzuki, A.; Yamahari, A.; Torigoe, K. *Langmui*r **2000**, *16*, 2604.

44. Esumi, K.; HoSoya, T.; Suzuki, A.; Torigoe, K. *J. Colloid Interface Sci*. **2000**, *229*, 303.

45. Nakao, Y.; Kaeriyama, K. *J. Colloid Interface Sci*. **1986**, *110*, 82.

46. Berkovich, Y.; Garti, N. *Colloids Surf., A* **1997**, *128*, 91.

47. Itoh, H.; Miura, M.; Okamoto, R.; Kikuchi, E. *Bull. Chem. Soc. Jpn*. **1991**, *64*, 333.

48. Larpent, C.; Brisse-Le Menn, F.; Patin, H. *J. Mol. Catal*. **1991**, *65*, L35.

49. Nakao, Y.; Kaeriyama, K. *Bull. Chem. Soc. Jpn*. **1987**, *60*, 4465.

50. (a) Liz-Marzan, L. M.; Lado-Tourina, I. *Langmuir* **1996**, *12*, 3585. (b) Wang, W.; Efrima, S.; Regov, O. *Langmuir* **1998**, *14*, 602.

51. (a) Bonnemann, H.; Richards, R. M. *Eur. J. Inorg. Chem*. **2001**, 2455. (b) Bonnemann, H.; Brijoux, W.; Brinkmann, R.; Dinjus, E.; Joussen, T.; Korall, B. *Angew. Chem. Int., Ed. Engl*. **1991**, *30*, 1312. (c) Bonnemann, H.; Brinkmann, R.; Koppler, R.; Neiteler, P.; Richter, J. *Adv. Mater*. **1992**, *4*, 804. (d) Bonnemann, H.; Brinkmann, R.; Koppler, R.; Neiteler, P. *Appl. Organomet. Chem*. **1994**, *8*, 361. (e) Bonnemann, H.; Braun, G.; Brijoux, W. Brinkmann, R.; Schulze-Tilling, A.; Seevogel, K.; Siepen, K. *J. Organomet. Chem*. **1996**, *520*, 143.

52. (a) Wonterghem, J. V.; Morup, S.; Koch, C. J. W.; Charles, S. W.; Wells, S. *Nature* **1986**, *322*, 622. (b) Glavee, G. N.; Klabunde, K. J.; Sorensen, C. M.; Dadjipanayis, S. *Inorg. Chem*. **1993**, *32*, 474.

53. Tan, C. K.; Newberry, V.; Webb, T. R.; McAuliffe, C. A. *J. Chem. Soc., Dalton Trans*. **1987**, 1299.

54. Kiwi, J.; Gratzel, M. *J. Am. Chem. Soc*. **1979**, *101*, 7214.

55. Esumi, K.; Sato, N.; Torigoe, K.; Meguro, K. *J. Colloid Interface Sci*. **1992**, *149*, 295.

56. (a) Chernyshov, D. M.; Bronstein, L. M.; Borner, H.; B.; Berton, B.; Antonietti, M. *Chem. Mater*. **2000**, *12*, 114. (b) Antonietti, M.; Wenz, E.; Bronstein, L.; Seregina, M. *Adv. Mater*. **1995**, *7*, 1000. (c) Klingelhofer, S.; Heitz, W.; Greiner, A.; Oestreich, S.; Forster, S. Antonietti, M. *J. Am. Chem. Soc*. **1997**, *119*, 10116. Le Bars, J.; Specht, U.; Bradley, J. S.; Blackmond, D. G. *Langmuir* **1999**, *15*, 7621.

57. Turkevitch, J.; Stevension, P. C.; Hillier, J. *Discuss. Faraday Soc*. **1951**, *11*, 55.

58. Henglein, A.; Giersig, M. *J. Phys. Chem. B* **1999**, *103*, 9355.

59. Harriman, A.; Thomas, J. M.; Millward, G. R.; *New J. Chem*. **1987**, *11*, 55.

60. Furlong, D. N.; Launikonis, A.; Sasse, W. H. F.; Sanders, J. V. *J. Chem. Soc. Faraday trans*. *1* **1984**, *80*, 571.

61. Ozkar, S.; Finke, R. G. *J. Am. Chem. Soc*. **2002**, *124*,

62. Pastoriza-Santos, I.; Liz-Marzan, L. M. *Langmuir* **1999**, *15*, 948.

63. (a) Manna, A.; Imae, T.; Iida, M.; Hisamatsu, N. *Langmuir* **2001**, *17*, 6000. (b) Selvakannan, P. R.; Kumar, P. S.; More, A. S.; Shingte, R. D.; Wadgaonkar, P. P.; Sastry, M. *Adv. Mater*. **2004**, *16*, 966. (c) Selvakannan, P. R.; Kumar, P. S.; More, A. S.; S.; Shingte, R. D.; Wadgaonkar, P. P.; Sastry, M. *Langmuir* **2004**, *20*, 295. (d) Swami, A.; Kumar, A.; Selvakannan, P. R.; Mandal, S.; Pasricha, R.; Sastry, M. *Chem. Mater*. **2003**, *15*, 17.

64. Hiramatsu, H.; Osterloch, F. E. *Chem. Mater*. **2004**, *16*, 2509.

65. Stoeva, S.; Klabunde, K. J.; Sorensen, C. M.; Dragieva, I. *J. Am. Chem. Soc*. **2002**, *124*, 2305.

66. Brust, M.; Walker, M.; Bethell, D.; Schiffrin, D. J.; Whyman, R. *J. Chem. Soc. Chem. Commun*. **1994**, 801.

67. Aiken, J. D., III; Finke, R. G. *J. Mol. Catal. A: Chem*. **1999**, *145*, 1.

68. (a) Henglein, A.; Tausch-Treml, R. *J. Colloid Interface Sci*. **1981**, *80*, 84. (b) Mosseri, S.; Henglein, A.; Janata, E. *J. Phys. Chem*. **1989**, *93*, 6791. (c) Mills, G.; Helglein, A. *Radiat. Phys. Chem*. **1985**, *26*, 385. (d) Delcourt, M. O.; Belloni, J.; Marignier, J. L.; Mory, C.; Colliex, C. *Radiat. Phys. Chem*. **1984**, *23*, 485.

69. Ershov, B. G.; Janata, E.; Michaelis, M.; Henglein, A. *J. Phys. Chem*. **1991**, *95*, 8996.

70. Michaelis, M.; Henglein, A. *J. Phys. Chem*. **1992**, *96*, 4719.

71. Rafaeloff, R.; Haruvy, Y.; Binenboym, J.; Baruch, G.; Rajbenbach, L. A. *J. Mol. Catal*. *1983*, *22*, 219.

72. Kurihara, K.; Kizling, J.; Stenius, P.; Fendler, J. H. *J. Am. Chem. Soc*. **1983**, *105*, 2574.

73. (a) Torigoe, K.; Esumi, K. *Langmuir* **1992**, *8*, 59. (b) Zhou, Y.; Wang, C. Y. R.; Chen, Z. Y. *Chem. Mater*. **1999**, *11*, 2310.

74. Sato, T.; Kuroda, S.; Takami, A.; Yonezawa, Y.; Hada, H. A. *Appl. Organomet. Chem*. **1991**, *5*, 261.

75. Toshima, N.; Takahashi, T.; Hirai, H. *Chem. Lett*. **1986**, 35.

76. Toshima, N.; Takahashi, T.; Hirai, H. *Chem. Lett*. **1985**, 1245.

77. Toshima, N.; Takahashi, T. *Bull. Chem*. **1992**, *65*, 400.

78. Kurihara, K.; Fendler, J. H.; Ravet, I.; Nagy, J. *J. Mol. Catal*. **1986**, *34*, 325.

79. Esumi, K.; Suzuki, A.; Aihara, N.; Usui, K.; Torigoe, K. *Langmuir* **1998**, *14*, 3157.

80. Suslick, K. S.; Choe, S. B.; Cichowlas, A. A.; Grinstaff, M. W. *Nature* **1991**, *253*, 414.

81. Suslick, K. S.; Hyeon, T.; Fang, M. *Chem. Mater*. **1996**, *8*, 2172.

82. Koltypin, Y.; Katabi, G.; Cao, X.; Prozorov, R.; Gedanken, A. *Noncryst. Solids* **1996**, *201*, 159.

83. Dhas, N. A.; Raj, C. P.; Gedanken, A. *Chem. Mater*. **1998**, *10*, 1446.

84. Dhas, N. A.; Cohen, H.; Gedanken, A. *J. Phys. Chem. B* **1997**, *101*, 6834.

85. Cao, X.; Koltypin, Y.; Kataby, G.; Prozorov, R.; Gedanken, A. *J. Mater. Res.* **1995**, *10*, 2952.

86. Cao, X.; Prozorov, R.; Koltypin, Y.; Kataby, G.; Felner, I.; Gedanken, A. *J. Mater. Res*. **1997**, *12*, 402.

87. Yeung, S. A.; Hobson, R.; Biggs, S.; Grieser, F. *J. Chem. Soc., Chem. Commun*. **1993**, 378.

88. (a) Nagata, Y.; Watanabe, Y.; Fujita, S.; Dohmaru, T.; Taniguchi, S. *J. Chem. Soc., Chem. Commun*. **1992**, 1620. (b) Caruso, R. A.; Ashok, K. M.; Grieser, F. *Colloids Surf., A* **2000**, *169*, 219. (c) Fujimoto, T.; Terauchi, S.; Umehara, H.; Kojima, I.; Henderson, W. *Chem. Mater*. **2001**, *13*, 1057. (d) Mizukoshi, Y.; Takagi, E.; Okuno, H.; Oshima, R.; Maeda, Y.; Nagata, Y. *Ultrason. Sonochem*. **2001**, *8*, 1.

89. (a) Mizukoshi, Y.; Oshima, R.; Maeda, Y.; Nagata, Y. *Langmuir* **1999**, *15*, 2733. (b) Okitsu, K.; Bandow, H.; Maeda, Y.; Nagata, Y. *Chem. Mater*. **1996**, *8*, 315.

90. Dhas, N. A.; Gedanken, A. *J. Mater. Chem*.**1998**, *8*, 445.

91. Benfield, F. W. S.; Green, M. L. H.; Ogden, J. S.; Young, D. *J. Chem. Soc., Chem. Commun*. **1973**, 866.

92. (a) Andrews, M.; Ozin, G. A.; Francis, C. G. *Inorg. Synth*. **1981**, *22*, 116. (b) Klabunde, K. J.; Timms, P.; Skell. P. S.; Ittel, S. D. *Inorg. Synth*. **1979**, *19*, 59.

93. (a) Lin, S. T.; Franklin, M. T.; Klabunde, K. J. *Langmuir* **1986**, *2*, 259. (b) Cardenas-Trivino, G.; Klabunde, K. J.; Brock Dale E. *Langmuir* **1987**, *3*, 986.

94. Klabunde, K. J.; Habdas, J.; Cardenas-Trivino, G. *Chem. Mater*. **1989**, *1*, 481.

95. Olsen, A. W.; Kafafi, Z. H. *J. Am. Chem. Soc*. **1991**, *113*, 7758.

96. Zuckerman, E. B.; Klabunde, K. J.; Olivier, B. J.; Sorensen, C. M. *Chem. Mater*. **1989**, *1*, 12.

97. Kilner, M.; Mason, N.; Lambrick, D.; Hooker, P. D.; Timms, P. L. *J. Am. Chem. Soc., Chem. Commun*. **1987**, 356.

98. Bradley, J. S.; Hill, E.; Leonowicz, M. E.; Witzke, H. *J. Mol. Catal*. **1987**, *41*, 59.

99. Reetz, M. T.; Helbig, W.; Quaiser, S. A. In *Active Metals: Preparation, Characterization, Applications;* Furstner, A., Ed.; VCH: New York, 1996; pp 279-297.

100. Reetz, M. T.; Helbig, W. J. Am. Chem. Soc. 1994, 116, 7401.

101. Reetz, M. T.; Quaiser, S. A. Angew. Chem., Int. Ed. Engl. 1995, 34, 2240.

102. (a) Finke, R. G. In *Metal Nanoparticles: Synthesis, Characterization and applications;* Feldheim, D. L., Foss, C. A., Jr., Eds.; Marcel Dekker: New York, 2002; Chapter 2, pp 17-54. (b) Aiken, J. D., III; Finke, R. G. *J. Mol. Catal. A: Chem.* **1999**, *145*, 1. (c) Aiken, J. D., III; Lin, Y.; Finke, R. G. *J. Mol. Catal. A: Chem.* **1996**, *114*, 29. (d)

103. Overbeek, J. T. G. In *Colloidal Dispersion*; Goodwin, J. W., Ed.; Royal Society of Chemistry: London, 1981; pp 1-23.

104. Evans, D. F.; Wennerstrom, H. In *The Colloidal Domain,* 2nd ed.; Wiley-VCH: New York, 1999.

105. Napper, D. H. In *Polymeric Stabilization of Colloidal Dispersion;* Academic Press: London, 1983.

106. Lin, Y.; Finke, R. G. *J. Am. Chem. Soc*. **1994**, *116*, 8335.

107. (a) Wang, W.; Murray, R. W. *Langmuir* **2005**, *21*, 7015. (b) Petroski, J.; Chou, M. H.; Creutz, C. *Inorg. Chem*. **2004**, *43*, 1597. (c) Tamura, M.; Fujihara, H. *J. Am. Chem. Soc*. **2003**, *125*, 15742. (d) Weare, W. W.; Reed, S. M.; Warner, M. G.; Hutchison, J. E. *J. Am. Chem. Soc*. **2004**, *122*, 12890. (e) Kim, S.-W.; Kim, S.; Tracy, J. B.; Jasanoff, A. Bawendi, M. G. *J. Am. Chem. Soc*. **2005**, *127*, 4556. (f) Son, S. U; Jang, Y.; Yoon, J. K.; Kang, E.; Hyeon, T. *Nano. Lett*. **2004**, *4*, 1147. (g) Yamamoto, M.; Nakamoto, M. *Chem. Lett*. **2003**, *32*, 452.

108. (a) Woehrle, G. H.; Warner, M. G.; Hutchison, J. E. *J. Phys. Chem. B* **2002**, *106*, 9979. (b) Rogach, A. L.; Kornowski, A.; Cao, M.; Eychmiller, A.; Weller, H. *J. Phys. Chem. B* **1999**, *103*, 3065. (c) Kimura, K.; Chen. S. *J. Phys. Chem. B* **2001**, *105*, 5397. (d) Balasubramanian, R.; Guo, R.; Mills, A. J.; Murray, R. W. *J. Am. Chem. Soc*. **2005**, *127*, 8126. (e) Woehrie, G. H.; Brown, L. O.; Hutchison, J. E. *J. Am. Chem. Soc*. **2005**, *127*, 2172. (f) Woehrie, G. H.; Hutchison, J. E. *Inorg. Chem*. **2005**, *44*, 6149. (g) Lin, S.-Y.; Tsai, Y.-T.; Chen, C.-C.; Lin, C.-M.; Chen, C.-H. *J. Phys. Chem. B* **2004**, *108*, 2134. (h) Sarathy, K. V.; Raina, G.; Yadav, R. T.; Kulkarni, G. U.; Rao, C. N. R. *J. Phys. Chem. B* **1997**, *101*, 9876. (i) Walker, C. H.; John, J. V. S.; Neilson, W. P. *J. Am. Chem. Soc*. **2001**, *123*, 3846. ((j) Wuelfing, W. P.; Gross, S. M.; Miles, D. T.; Murray, R. W. *J. Am. Chem. Soc*. **1998**, *120*, 12696. (k) Yang, J.; Lee, J. Y.; Deivaraj, T. C.; Too, H.-P. *Langmuir* **2003**, *19*, 10361. (l) Fujihara, H.; Nakai, H. *Langmuir* **2001**, *17*, 6393. (m) Kim, K.-S.; Demberelynyamba, D.; Lee, H. *Langmuir* **2004**, *20*, 556. (n) Choo, H.; Cutler, E.; Shon, Y.-S. *Langmuir* **2003**, *19*, 8555. (o) Shimmin, R. G.; Schoch, A. B.; Braun, P. V. *Langmuir* **2004**, *20*, 5613. (p) Maye, M. M.; Chun, S. C.; Rabinovich, D.; Zhong, C.-J. *J. Am. Chem. Soc*. **2002**, *124*, 4958. (q) Tan, Y.; Li, Y.; Zhu, D. *Langmuir* **2002**, *18*, 3392.

109. (a) Brown, L. O.; Hutchison, J. E. *J. Phys. Chem. B* **2001**, *105*, 8911. (b) Leff, D. V.; Brandt, L.; Heath, J. E. *Langmuir* **1996**, *12*, 4723. (c) Scott, R. W.; Wilson, O. M.; Crooks, R. M. *J. Phys. Chem. B* **2005**, *105*, 692 and references cited therein.

110. (a) Rodriguez, A.; Amiens, C.; Chaudret, B.; Casanove, M. J.; Lecante, P.; Bradley, J. S. *Chem. Mater*. **1996**, *8*, 1978.

111. (a) Amiens, C.; De Caro, D.; Chaudret, B.; Bradley, J. S.; Mazel, R.; Roucau, C. *J. Am. Chem. Soc*. **1993**, *115*, 11638. (b) Detuil, A.; Schmid, G.; Meyer-Zaika, W. *J. Chem. Soc., Chem. Comm*. **1995**, 31.

112. (a) Schmid, G.; Morun, B.; Malm, J. O. *Angew. Chem., Int. Ed. Engl*. **1989**, *28*, 778. (b) Schmid, G.; Maihack, V.; Lantermann, F.; Peschel, S. *J. Chem. Soc., Dalton Trans*. **1996**, *589*. (c) Schmid, G.; Emde, S.; Maihack, V.; Meyer-Zaika, W.; Peschel, S. *J. Mol. Catal. A: Chem*. **1996**, *107*, 95.

113. Chen, S.; Kimura, K. *J. Phys. Chem. B* **2001**, *105*, 5397.

11.4. (a) Franke, R.; Rothe, J.; Pollmann, J.; Hormes, J.; Bonnemann, H.; Brijoux, W.; Hindenburg, T. *J. Am. Chem. Soc*. **1996**, *118*, 12090. (b) Bonnemann, H.; Korall, B. *Angew. Chem., Int. Ed. Engl*. **1992**, *31*, 1490. (c) Bonnemann, H.; Brijoux, W. *Nanostruct. Mater*. **1995**, *5*, 135.

115. Vidoni, O.; Philippot, K.; Amiens, C.; Chaudret, B.; Balmes, O.; Malm, J. O.; Bovin, J. O.; Senocq, F.; Casanove, M. J. *Angew. Chem., Int. Ed. Engl*. **1999**, *38*, 3736.

116. Bonnemann, H.; Braun, G.; Brinkmann, R.; Schuize Tilling, A.; Seevogel, K.; Siepen, K. *J. Organomet. Chem*. **1996**, *520*, 143.

117. (a) Roucoux, A.; Schulz, J.; Patin, H. *Chem. Rev*. **2002**, *102*, 3757. (b) Daniel, M. C.; Astruc, D. *Chem. Rev*. **2004**, *104*, 293.

118. Hulteen, J. C.; Martin, C. R. In *Nanoparticles and Nanostructured Films*; Feldler, J. H., Ed.; Wiley- VCH: Weinheim, 1988; p 235.

119. Antonietti, M.; Forster, S.; Hartmann, J.; Ostreich, S. *Macromolecules* **1996**, *29*, 3800.

120. Vogtle, F.; Gestermann, S.; Kauffmann, C.; Ceroni, P.; Vicinelli, V.; Balzani, V. J. Am. Chem. Soc. 2000, 122, 10398.

121. Yeung, L. K.; Lee, C. T.; Jonhnston, K. P.; Crooks, R. M. *Chem. Commun*. **2001**, 2290.

122. (a) Crooks, R. M.; Zhao, M.; Sun, L.; Chechik, V.; Yeung, L. K. *Acc. Chem. Res*. **2001**, *34*, 181. (b) Niu, Y.; Yeung, L. K.; Crooks, R. M. *J. Am. Chem. Soc*. **2001**, *123*, 6840.

123. Yeung, L. K.; Crooks, R. M. *Nano Lett*. **2001**, *1*, 14.

124. Grohn, F.; Bauer, B. J.; Akpalu, Y. A.; Jackson, C. L.; Amis, E. J. *Macromolecules* **2000**, *33*, 6042.

125. (a) Daniel, M.-C.; Ruiz, J.; Nlate, S.; Palumbo, J.; Blais, J.-C.; Astruc, D. *Chem. Commun*. **2001**, 2000. (b) Daniel, M.-C.; Ruiz, J.; Nlate, S.; Blais, J.-C.; Astruc, D. *J. Am. Chem. Soc*. **2003**, *125*, 2617. (c) Wang, R.; Yang, J.; Zheng, Z.; Carducci, M. D.; Jiao, J.; Seraphin, S. *Angew. Chem., Int. Ed. Engl*. **2001**, *40*, 549. (d) Gopidas, K. R.; Whitesell, J. K.; Fox, M.-A. *J. Am. Chem. Soc*. **2003**, *125*, 6491.

126. (a) Zhao, M.; Crooks, R. M. *Chem. Mater*. **1999**, *11*, 3379. (b) Scott, R. W. J.; Ye, H.; Henriquez, R. R.; Crooks, R. M. *Chem. Meter*. **2003**, *15*, 3873

127. Hayat, M. A. *Colloidal Gold, Principles, Methods and Applications;* Academic Press: New York, 1989.

128. (a) Ziolo, R. F.; Giannelis, E. P.; Weinstein, B. A.; O'Horo, M. P.; Ganguly, B. N.; Mehrota, V.; Russel, M. W.; Huffman, D. R. *Science* **1992**, *257*, 219. (b) Jordan, R.; West, N.; Chou, Y.-M.; Nuyken, O. *Macromolecules* **2001**, *34*, 1606.

129. Selvan, S. T.; Spatz, J. P.; Klock, H.-A.; Moller, M.; *Adv. Mater*. **1998**, *10*, 132.

130. Sayo, K.; Deki, S.; Hayashi, S. *Eur. Phys. J. D* **1999**, *9*, 429.

131. Lee, J.; Sundar, V. C.; Heine, J. R.; Bawendi, M. G.; Jensen, K. F. *Adv. Mater*. **2000**, *12*, 1102.

132. Corbierre, M. K.; Cameron, N. S.; Sutton, M.; Mochrie, S. G. J.; Lurio, L B.; Ruhm, A.; Lennox, R. B.; *J. Am. Chem. Soc*. **2001**, *123*, 10411.

133. Kolb, U.; Quaiser, S. A.; Winter, M.; Reetz, M. T. *Chem. Mater*. **1996**, *8*, 1889.

134. Hirai, H.; Toshima, N. *In Polymer-Attached Catalysis*; Iwasawa, Y., Ed.; Kluwer: Dordrecht, 1986.

135. Hirai, H.; Nakao, Y.; Toshima, N. *J. Macromol. Sci. Chem*. **1979**, *A13*, 727.

136. Teranishi, T.; Miyake, M. *Hyomen* **1997**, *35*, 439.

137. Schaaf, T. G.; Whetten, R. L. *J. Phys. Chem. B* **2000**, *104*, 2630.

138. Toshima, N.; Harada, M.; Yamazaki, Y.; Asakura, K. *J. Phys. Chem*. **1993**, *97*, 5103.

139. Yonezawa, T.; Toshima, N. *J. Mol. Catal*. **1993**, *83*, 167.

140. Yonezawa, T.; Toshima, N. *J. Chem. Soc., Faraday Trans*. **1995**, *91*, 4111.

141. Harada, M.; Asakura, K.; Toshima, N. *J. Phys. Chem*. **1993**, *97*, 5103.

142. Sohn, B.-H.; Seo. B.-W.; Yoo, S.-I. *J. Mater. Chem*. **2002**, *12*, 1730.

143. Cant, N. e.; Critchley, K.; Zhang, H.-L.; Evans, S. D. *Thin Solid Films* **2003**, *426*, 31.

144. Mayer, A. B. R.; Mark, J. E. *Eur. Polym. J*. **1998**, *34*, 103.

145. Moskovits, M. Rev. Mod. Phys. 1985, 57, 783.

146. (a) Otto, A.; Mrozek, I.; Pettenkofer, C. *Surf. Sci*. **1990**, *238*, 192. (b) Schultz, S. G.; Janik-Czachor, M.; Van Duyne, R. P. *Sur. Sci*. **1984**, *104*, 419.

147. (a) Jeanmaire, D. L.; Van Duyne, R. P. *J. Electroanal. Chem*. **1977**, *84*, 1. (b) Albrecht, M. G.; Creigton, J. A. *J. Am. Chem. Soc*. **1977**, *99*, 5215.

148. (a) Nie, S. M.; Emery, S. R. *Science* **1997**, *275*, 1102. (b) Krug, J. T.; Wang, G. D.; Emory, S. R.; Nie, S. M. *J. Am. Chem. Soc*. **1999**, *121*, 9208. (c) Freeman, R. G.; Bright, R. M.; Hommer, M. B.; Natan, M. J. *J. Raman Spectrosc*. **1999**, *30*, 733. (d) Jesen, T. R.; Malinsky, M. D.; Haynes, C. L.; Van Duyne, R. P. *J. Phys. Chem. B* **2000**, *104*, 10549.

149. (a) El-Sayed, M. A. *Acc. Chem. Res*. **2001**, *34*, 257. (b) Kelly, L. L.; Coronado, E.; Zhao, L. L.; Schatz, G. C. *J. Phys. Chem. B* **2003**, *107*, 668.

150. (a) Schatz, G. C. *Acc. Chem. Res*. **1984**, *17*, 370. (b) Gersten, J. I. *J. Chem. Phys*. **1980**, *72*, 5779.

151. (a) Tao, A.; Kim, F.; Hess, C.; Goldberger, J.; He, R.; Sun, Y.; Xia, Y.; Yang, P. *Nano. Lett*. **2003**, *3*, 1229. (b) Jeong, D. H.; Zhang, Y. H.; Moskovits, M. *J. Phys. Chem. B* **2004**, *108*, 12724.

152. Baudhuin, P.; van der Smissen, P.; Beavois, S.; Courtoy, J. *Colloidal Gold: Principles, Methods, Applications* **1989**, *2*, 1.

153. Alivisatos, A. P. *Nat. Biotechnol*. **2004**, *22*, 47.

154. (a) Jin, R.; Cao, Y.; Mirkin, C. A.; Kelly, K. L.; Schatz, G. C.; Zheng, J. *Science* **2001**, *294*, 1901. (b) Jin, R.; Cao, Y.; Hao, E.; Metraux, G. S.; Schatz, G.; Mirkin, C. A. *Nature* **2003**, *425*, 487. (c) Sun, Y. G.; Xia, Y. N. *Science* **2002**, *298*, 2176.

155. Sau, T. K.; Murphy, C. J. *J. Am. Chem. Soc*. **2004**, *126*, 8648.

156. Ginger, D. S.; Zhang, H.; Mirkin, C. A. *Angew. Chem., Int. Ed*. **2004**, *43*, 30.

157. (a) Mirkin, C. A.; Letsinger, R. L.; Mucic, R. C.; Storhff, J. J. *Nature* **1996**, *382*, 607. (b) Chen, R. J.; Zhang, Y.; Wang, D.; Dai, H. *J. Am. Chem. Soc*. **2001**, *123*, 3838. (c) Mbindyo, J. K. N.; Reiss, B. D.; Martin, B. R.; Keating, C. D.; Natan, M. J.; Mallouk, T. E. *Adv. Mater*. **2001**, *13*, 249.

158. (a) Storhoff, J. J.; Mucic, R. C.; Mirkin, C. A. *J. Clust. Sci*. **1997**, *8*, 179. (b) Elghanian, R.; Storhoff, J. J.; Mucic, R. C.; Letsinger, R. L.; Mirkin, C. A. *Science*

1997, *277*, 1078. (c) Storhoff, J. J.; Elghanian, R.; Mucic, R. C.; Mirkin, C. A.; Letsinger, R. L. *J. Am. Chem. Soc*. **1998**, *120*, 1959. (d) Mucic, R. C.; Storhoff, J. J.; Mirkin, C. A.; Letsinger, R. L. *J. Am. Chem. Soc*. **1998**, *120*, 12675. (e) Mitchell, G. P.; Mirkin, C. A.; Letsinger, R. L. *J. Am. Chem. Soc*. **1999**, *121*, 8122. (f) Reynolds, R. A.; Mirkin, C. A.; Letsinger, R. L. *J. Am. Chem. Soc*. **2000**, *122*, 3795. (g) Storhoff, J. J.; Lazarides, A. A.; Mucic, R. C.; Mirkin, C. A.; Letsinger, R. L.; Schatz, G. C. *J. Am. Chem. Soc*. **2000**, *122*, 4640. (h) Taton, T. A.; Mucic, R. C.; Mirkin, C. A.; Letsinger, R. L. *J. Am. Chem. Soc*. **2000**, *122*, 6305.

159. Alivisatos, A. P.; Johnsson, K. P.; Peng, X. G.; Wilson, T. E.; Loweth, C. G.; Bruchez, M. P.; Schultz, P. G. *Nature* **1996**, *382*, 609.

160. (a) Storhoff, J. J.; Mirkin, C. A. *Chem. Rev*. **1999**, *99*, 1849. (b) Lazarides, A. A.; Schatz, G. C. *J. Phys. Chem. B* **2000**, *104*, 460. (c) Lazarides, A. A.; Schatz, G. C. *J. Chem. Phys*. **2000**, *112*, 2987. (c) Niemeyer, C. M.; Burger, W.; Peplies, J. *Angew. Chem., Int. Ed*. **1998**, *37*, 2265. (d) Park, S.-J.; Lazarides, A. A.; Mirkin, C. A.; Letsinger, R. L. *Angew. Chem., Int. Ed*. **2001**, *40*, 2909. (e) Harnack, O.; Ford, W. E.; Yasuda, A.; Wessels, J. M. *Nano. Lett*. **2002**, *2*, 919.

161. Niemeyer, C. M. *Angew. Chem., Int. Ed*. **2001**, *40*, 4128.

162. (a) Thanh, N. T. K.; Rosenzweig, Z. *Anal. Chem*. **2002**, *74*, 1624. (b) Zhang, C.; Zhang, Z.; Yu, B.; Shi, J.; Jhang, X. *Anal. Chem*. **2002**, *74*, 96.

163. (a) Schneider, B. H.; Dickinson, E. L.; Vach, M. D.; Hoijer, J. V.; Howard, L. V. *Biosens. Bioelectron*. **2000**, *15*, 13. (b) Schneider, B. H.; Dickinson, E. L.; Vach, M. D.; Hoijer, J. V.; Howard, L. V. *Biosens. Bioelectron*. **2000**, *15*, 497.

164. Taton, T. A. *Trends Biotechnol*. **2002**, *20*, 277.

165. Aslan, K.; Perez-Luna, V. H. *Langmuir* **2002**, *18*, 6059.

166. De la Fuente, J. M.; Barrientos, A. G.; Rojas, T. C.; Rojo, J.; Canada, A.; Fernandez, A.; Penades, S. *Angew. Chem., Int. Ed*. **2001**, *40*, 2257.

167. Esumi, K.; Hosoya, T.; Suzuki, A.; Torigoe, K. *Langmuir* **2000**, *16*, 2978.

168. Wilson, R. *Chem. Commun*. **2003**, 108.

169. Hone, D. C.; Haines, A. H.; Russel, D. A. *Langmuir* **2003**, *19*, 7141.

170. Nolting, B.; Yu, J.-J.; Liu, G.-y.; Cho, S.-J.; Kauzlarich, S.; Gervay-Hague, J. *Langmuir* **2003**, *19*, 6465.

171. (a) Bond, G. C.; Thomson, D. T. *Catal. Rev. Sci. Eng*. **1999**, *41*, 319. (b) Bond, G. C. *Catal. Today* **2002**, *72*, 5.

172. Bond, G. C. *Gold Bull*. **1971**, *5*, 11.

173. Haruta, M.; Tsuboda, S.; Kobayashi, T.; Kagehiama, H.; Genet, M. J.; Delmon, B. *J. Catal*. **1993**, *144*, 175.

174. (a) Schmid, G. *J. Chem. Soc., Dalton, Trans*. **1998**, 1077. (b) Valden, M.; Lai, X.; Goodman, D. W. *Science* **1998**, *281*, 1647. (c) Schmid, G.; Corain, B. *Eur. J. Inorg. Chem*. **2003**, 3081.

175. Caporusso, A. M.; Aronica, L. A.; Schiavi, E.; Martra, G.; Vitulli, G.; Salvadori, P. *J. Organomet. Chem*. **2005**, *690*, 1063.

176. Claus, P.; Bruckner, A.; Mohr, C.; Hofmeister, H. *J. Am. Chem. Soc*. **2000**, *122*, 11430.

177. Mohr, C.; Hofmeister, H.; Claus, P. *J. Catal*. **2002**, *213*, 86.

178. Mohr, C.; Hofmeister, H.; Radnik, J.; Claus, P. *J. Am. Chem. Soc*. **2003**, *125*, 1905.

179. Mukherjee, P.; Patra, C. R.; Ghosh, A.; Kumar, R.; Sastry, M. *Chem. Mater*. **2002**, *14*, 1678.

180. Sudrik, S. G.; Maddanimath, T.; Chaki, N. K.; Chavan, S. P.; Chavan, S. P.; Sonawane, H. R.; Vijayamohanan, K. *Org. Lett*. **2003**, *5*, 2355.

181. (a) Chauhan, B. P. S.; Rathore, J. S.; Chauhan, M.; Krawicz, A. *J. Am. Chem. Soc*. **2003**, *125*, 2876. (b) Chauhan, B. P. S.; Rathore, J. S. Bandoo, T. *J. Am. Chem. Soc*. *2004*, *126*, 8493. (c) Chauhan, B. P. S.; Rathore, J. S. Glloxhani, N. *Appl. Organometal. Chem*. **2005**, *19*, 542. (d) Chauhan, B. P. S.; Rathore, J. S. *J. Am. Chem. Soc*. **2005**, *127*, 5790.

182. Lawrence, N. J.; Drew, M. D.; Bushell, S. M. *J. Chem. Soc., Perkin Trans. 1,* **1999**, 3381

183. Lewis, L. N. *Chem. Rev*. **1993**, *93*, 2693 and references therein.

184. (a) Brown, L. O.; Hutchison, J. E. *J. Am. Chem. Soc.* **1999**, *121*, 882-883. (b) Zhong, C. J.; Zhang, W. X.; Leibowitz, F. L.; Eichelberger, H. H. *Chem. Commun.* **1999**, 1211-1212. (c) Lin, X. M.; Sorensen, C. M.; Klabunde, K. J. *J. Nanopart. Res.* **2000**, *2*, 157-164.

185. (a) Enustun, B. V.; Turkevich, J. *J. Am. Chem. Soc.* **1963**, *85*, 3317. (b) Turkevich, J.; Kim, G. *Science* **1970**, *169*, 873. (c) Lee, P. C.; Meisel, D. *J. Phys. Chem.* **1982**, *86*, 3391. (d) Kamat, P. V.; Flumiani, M.; Hartland, G. V. *J. Phys. Chem.* **1998**, *102*, 3123.

Chapter 2

The Ability of the Si-H Bonds for the Reduction of Silver Metal Salts to Silver Nanoparticles

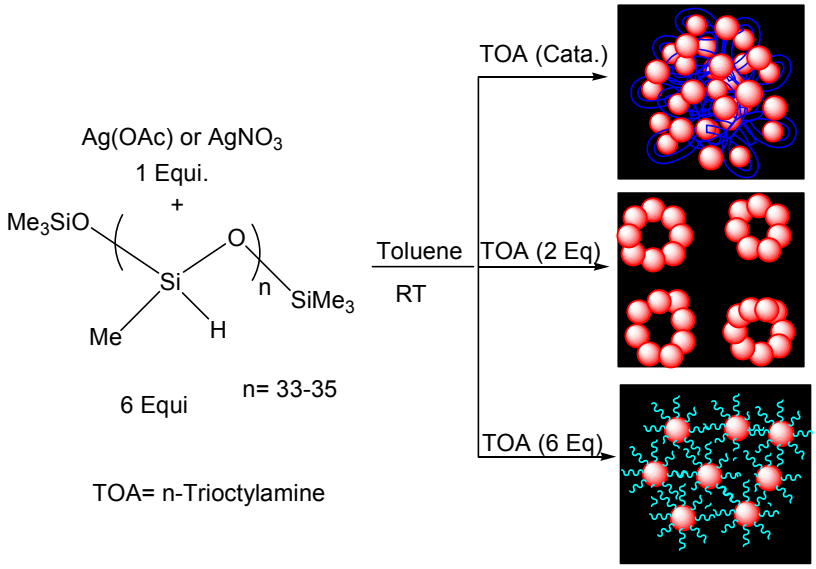
Part A: Self-Assembled Silver Nanoclusters and Nanonecklace Formation: Poly(methylhydrosiloxane)-Mediated One-Pot Route to Organosols

2.1 Introduction

Nanometer-sized particles of metals and semiconductors have been investigated intensively in recent years.[1] In this context, silver nanoparticles are of great interest due to their role in photographic processes,[2] their utility as substrates for surface-enhanced Raman spectroscopy (SERS),[3] and also their application in catalysis.[4] Silver nanocrystallites, mostly hydrosols, have been widely studied because of the ease of their preparation. Since most of the catalytic reactions are performed in organic solvents, it is desirable to design synthetic methods, which lead to the stabilization of metal nanoparticles in such solvents. Colloidal dispersions of silver in nonaqueous liquids (organosols) are rare and more difficult to prepare and stabilize. It has been observed that the stability, particle size, and properties of metal colloids strongly depend on the specific method of preparation and the experimental conditions applied. In most cases, nanoparticles are stabilized with strong coordinating surfactants to prevent the agglomeration and to provide specific surface properties.[5] On the other hand, utility and activity of such particles are compromised due to the difficulty in ligand exchange reactions in catalytic processes. In this context it is desirable to develop synthetic strategies to fabricate nanoparticles, which provide flexibility to functionalize nanoparticles according to the need and hence tailoring of nanoparticle surfaces.

Moreover, for catalytic applications such conjugates may have superior activity and selectivity over the nanoparticles passivated by strong coordinating ligands. Nanosized colloidal metal nanoparticles protected by polymers exhibit intriguing optical, catalytic, or electronic properties due to the "size effect" and additionally provide the option of influencing the materials' properties by selection of the polymeric matrix.[6,7] A large number of preparative methods for these colloidal metal dispersions involve the presence of the polymer during the reduction from the metal precursors. In this way, the polymer can profoundly influence the particle features of the resulting metal colloids as well as their long-term colloidal stability. Monomeric hydrosilanes are known reducing agents and have been successfully used for the generation of Pt, Pd, and Rh nanosized particles in the context of metal-catalyzed hydrosilylation of alkenes.[8] On the other hand, investigations of polymeric analogous such as polyhydrosilanes as reducing agents for the generation and in-situ stabilization of nanosized metal particles have not been explored. Though, their property profile may provide the means of directing metallic particles into specific physicochemical environments[9a] in addition to their utility as reducing agents. Moreover, combining the ease of processability of polysiloxane polymers with the improved mechanical and optical properties of metal nanoparticles is of practical use for the fabrication of many new devices.[9b] In this report, we describe a versatile method and first example of polyhydrosiloxane-induced generation and stabilization of functionalizable monodisperse silver sols (Scheme 1). This method enables routine formation of stable nanosilver reservoirs, avoiding particle aggregation during the storage as well as nucleation and growth process. We also demonstrate the

utility of such reservoirs in grafting the surface properties of nanosized silver particles by exchange reactions with trioctylamine.



Scheme 2.1: Synthetic strategy to polysiloxane stabilized silver sols and their surface grafting.

2.2 Results and Discussions

In an exploratory experiment, when poly(methylhydrosiloxane) (PMHS; 0.024 mL, 0.4 mmol, *M*w _ 2000, 33-35 Si-H units) was added to the 50 mL toluene suspension of silver acetate (0.032 g, 0.2 mmol), the mixture turned faint yellow and showed a very broad peak at 445 nm in UV-vis spectra, indicating formation of silver nanoparticles.[10] But, it was observed that the reduction process was very slow (24 h) and was accompanied by particles precipitation. To accelerate the reduction reaction, an amine catalyst was added to the reaction mixture. Amines are known to polarize the $Si^{\delta+}$-$H^{\delta-}$ bonds via intermediate formation of hypercoordinated silicon species.[11] Thus, in an optimized procedure, AgOAc (0.032 g, 0.2 mmol) was suspended in 50 mL of toluene and PMHS (0.072 mL, 1.2 mmol) was added while stirring gently at room temperature

under nitrogen. The solution was stirred for 1 h, and trioctylamine (TOA) (0.005 mL, 0.01 mmol) was added as a catalyst. The solution was stirred intermittently for around 5 min after every half an hour, and the formation of silver nanoparticles was probed by monitoring the absorption changes at different time intervals (Figure 2.1). The formation and stabilization process of polysiloxane-modified silver nanoparticles was traced by the UV-vis absorption method. Figure 1A shows the shifts of the peak positions and the shapes of the absorption spectra during the whole reduction process. Just after 10 min of the injection of the reducing agent, a very broad almost featureless UV-vis band was observed, which was very similar to the solution absorption spectrum before the reducing agent was added. When the reaction was continued for 3 h, a broad asymmetric peak centered at 445-448 nm appeared, indicating the formation of polydisperse nanoparticles. After 4 h of the reaction, the broad peak becomes more symmetric (indicating narrow size distribution) and blue shifts from 445 to 448 to 438 nm (indicating smaller particle size). After total 6 h of the reaction, the plasmon band (λ_{max}: 435 nm) becomes symmetric, and no further intensity increase was observed. At this juncture, the yellow solution was centrifuged and analyzed. One drop of the solution was deposited on a Formvar coated carbon grid and visualized by a transmission electron microscope (TEM), without any additional staining. TEM analysis demonstrated that indeed silver particles were formed. The average particle size was found to be 2 nm with a standard deviation of 0.6 nm (Figure 2.1). Careful visualization at higher resolution indicated that a lighter matrix, most probably polysiloxane, rapped all the particles. However, it was difficult to achieve enough contrast (PMHS is not visible at such resolutions) to conclude this observation. As prepared toluene solutions were found to be stable for 3 months. Because

of the stability of these particles, without any other stabilizing agent present, we infer that polysiloxane raps around the particles and prevents them from further agglomeration.

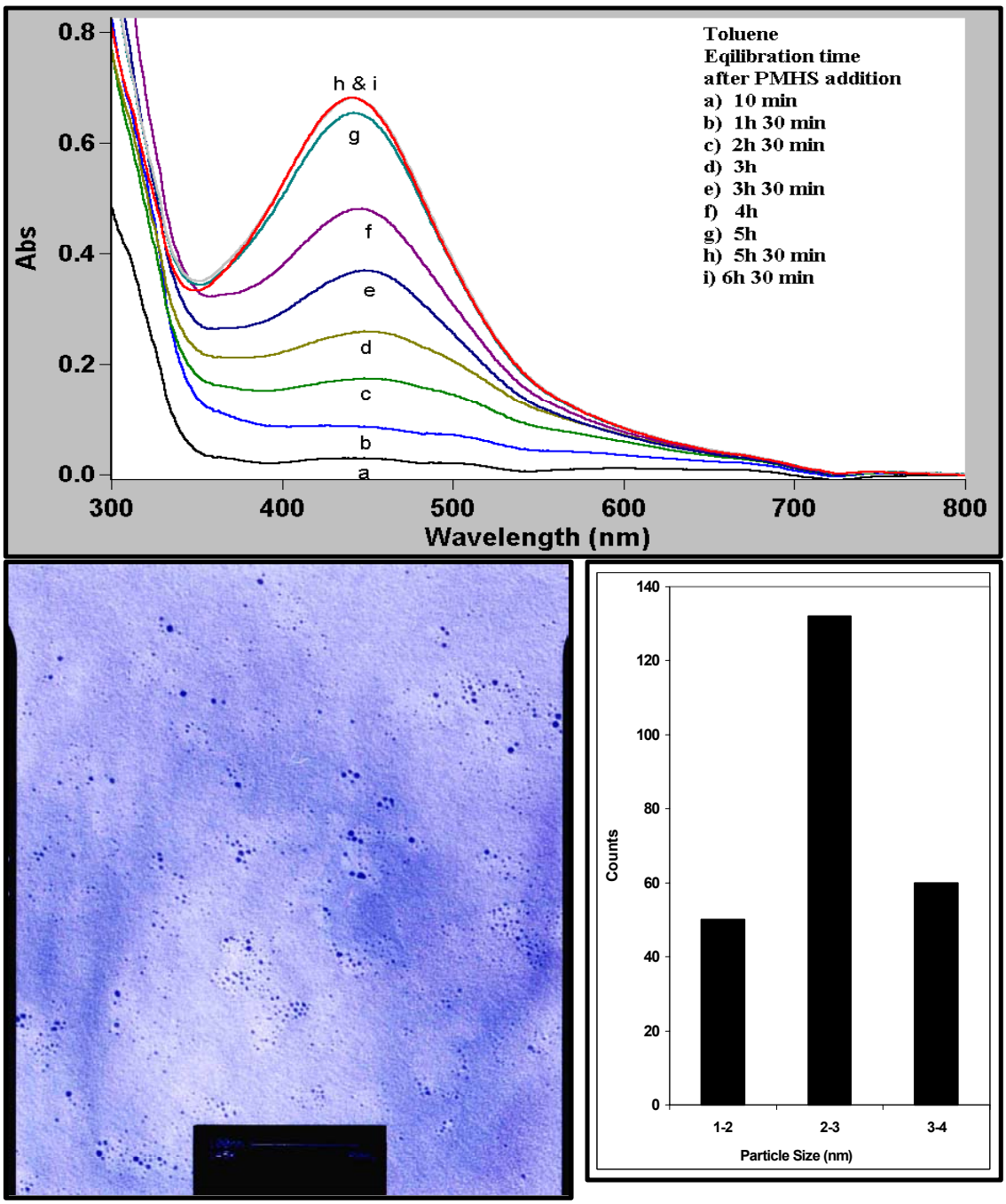
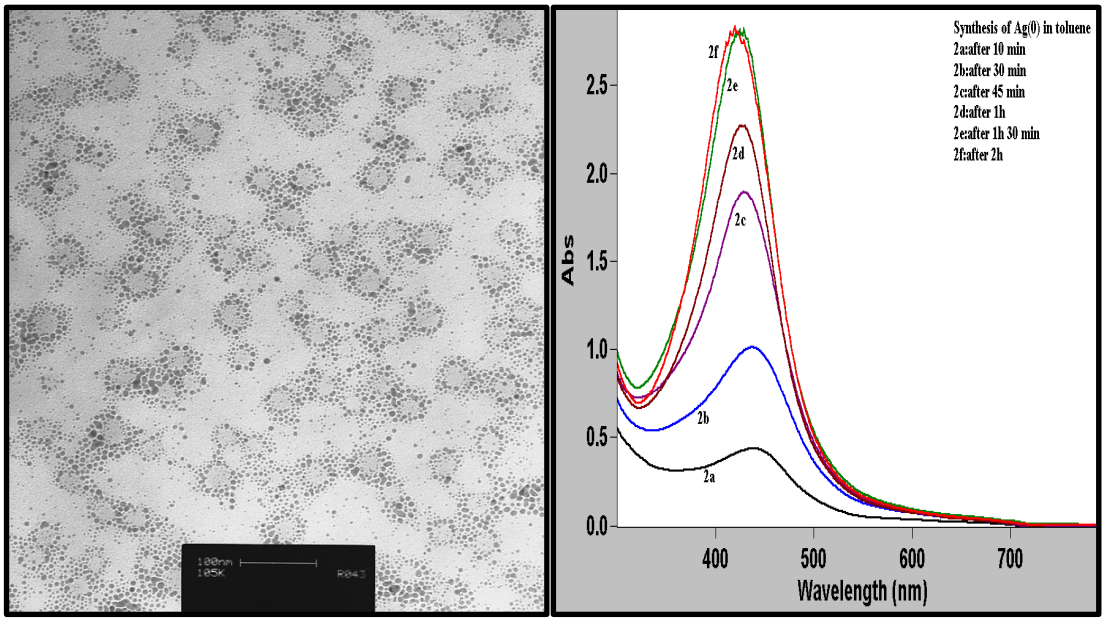


Figure 2.1 UV-vis spectra monitoring of the absorption changes at different time intervals, TEM analysis, and its corresponding histogram.

On the basis of these preliminary results, we can roughly elucidate the polysiloxane-induced generation, growth, and stabilization process as follows: At the beginning of the reaction silver ions which are reduced to atoms aggregate rapidly together to form small nanoparticles, which aggregate to become large nanoparticles due to the high density of the small nanoparticles. Formed large particles are not stable and are broken into small particles, which due to the protection provided by siloxane polymers become stable. Alternatively, it is also possible that the dynamics of the protection provided by siloxane polymer is such that it cannot wrap the particles in time, which allows nucleation growth phenomena to occur. On the basis of the preliminary UV-vis and TEM studies of the reaction mixture, the whole reduction process seems to be a dynamic one; that is, during the increase in the particle size there are some larger particles which decompose into smaller nanoparticles, and during the decrease in the particle size some smaller nanoparticles aggregate to become larger. However, more experimental and theoretical work is underway to understand the formation process.

After optimization of reaction conditions, the role of PMHS and catalyst TOA was examined in detail since both can also function as a stabilizing agent for nanoparticles. Reactions with varying amounts of TOA were performed. Thus, a suspension of AgOAc (0.2 mmol, 0.032 g) was prepared in 50 mL of toluene, and PMHS (1.2 mmol, 0.072 mL) was injected to this suspension at room temperature. Vigorous stirring was continued for 0.5 h, during which the color of the solution changed to faint yellow (UV-vis spectroscopy, λ_{max} at 444 nm). At this juncture TOA (0.4 mmol, 0.17 mL) was injected into the reaction mixture. After 10 min of addition of TOA, the color of the solution turned dark yellow (UV-vis spectroscopy, λ_{max} at 440 nm). After 2 h of total

reaction at room temperature, the mixture was centrifuged, and one drop of the reaction mixture was deposited on a carbon-coated grid and analyzed by TEM (Figure 2.2). Surprisingly, individual nanoparticles as observed in the case of catalytic amounts of TOA were self-assembled in the form of nanosized necklaces. Particle size (Figure 2.2) analysis of the individual nanoparticles showed the particles to be rather monodispersed in the 2-3 nm size regime. The ring diameter analysis (Figure 2C) showed that there were three types of necklaces (15-18, 19-22, and 23-26 nm) present in the reaction mixture. The calculated length of the PMHS (*n*= 33-35) used in this reduction process is approximately 12-13 nm. Incidentally, if one or two to three polysiloxane strands arranged in a spherical form, it will lead to the formation of such spheres. The existence of the pearl-necklace aggregates suggests that the reduced silver particles even in the presence of other stabilizing agents are in interaction with polysiloxane, leading to new types of nanoarchitectures.



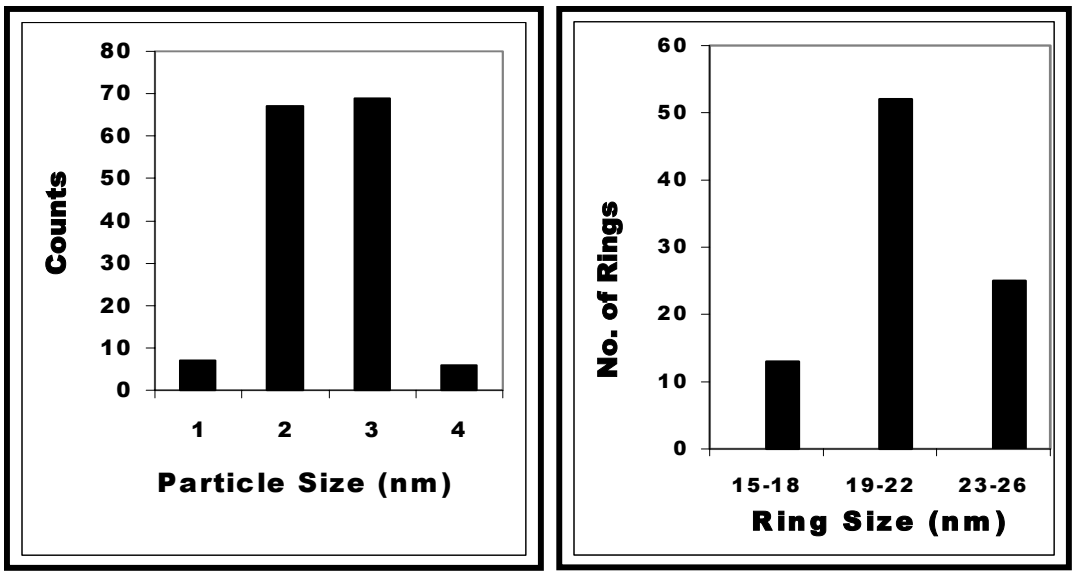
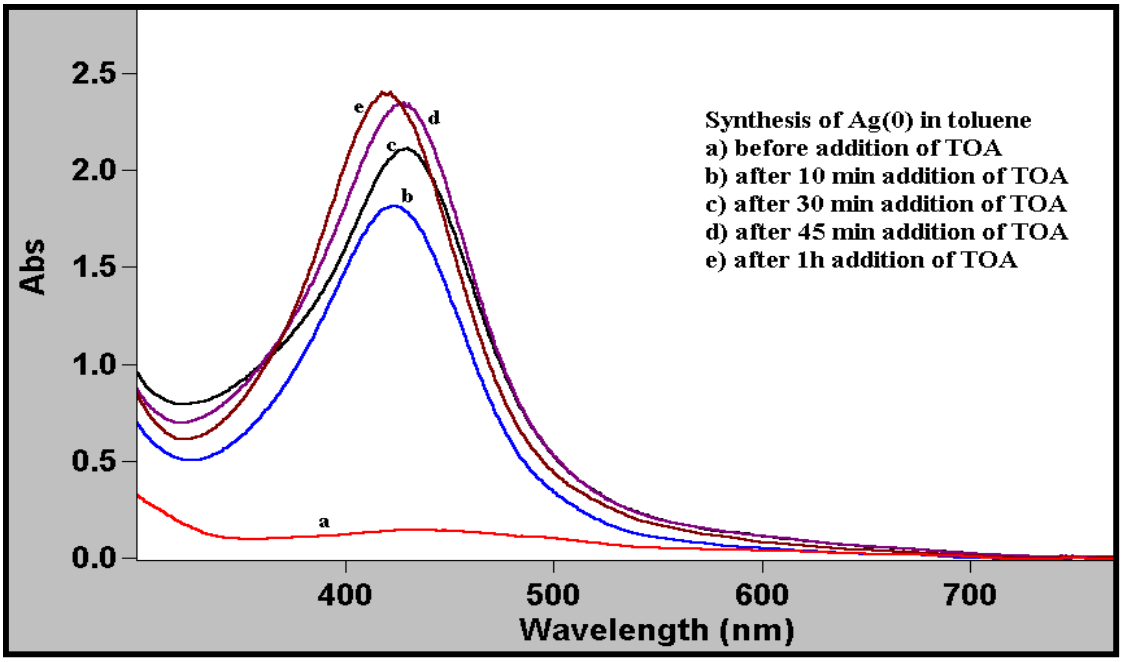


Figure 2.2: TEM images , UV-vis absorption spectra, particle Size analysis, and the ring size analysis of resulting nanonecklaces.



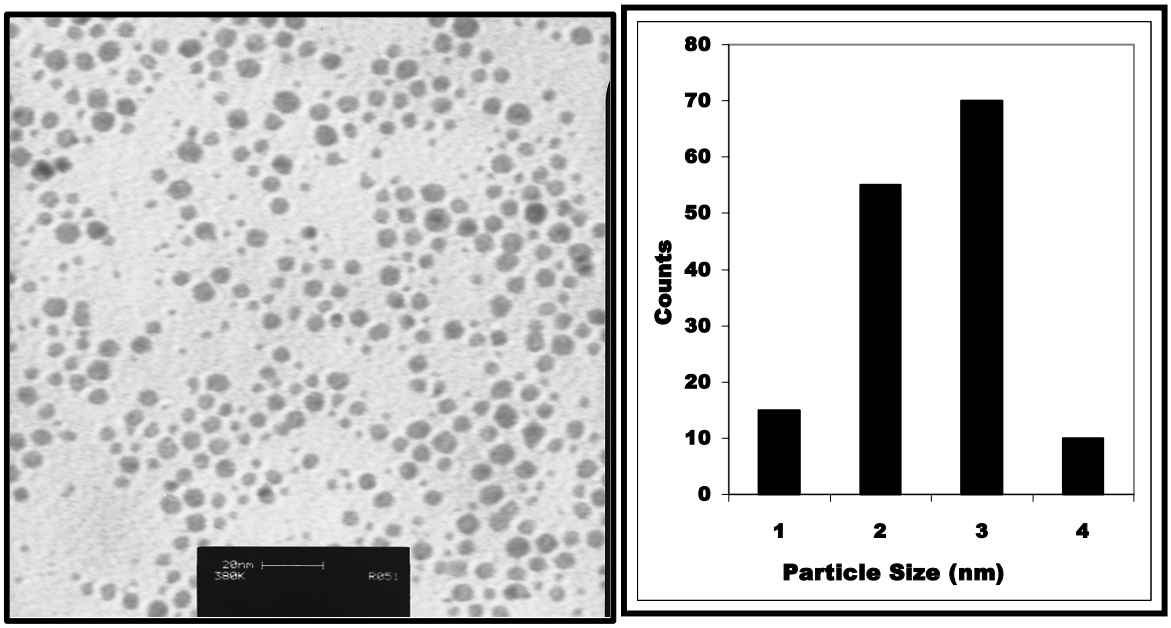


Figure 2.3: UV-vis spectrum, TEM images, and particle size analysis of the reaction mixture in presence of six equivalent of amine.

To validate this hypothesis, under identical reaction conditions and molar ratios of AgOAc and PMHS, an excess of TOA (6 equiv to AgOAc) was used. The reaction was significantly faster, and within 1 h reduction was complete (Figure 3A). After 1 h of the reaction, the mixture was centrifuged and analyzed by TEM (Figure 2.3). TEM analysis of the reaction mixture showed the formation of self-assembled individual nanoparticles in 3 nm size regimes, and the complete disappearance of nanosized necklaces was observed. This result shows that when enough coordinating (stabilizing) agents are present, PMHS is completely dissociated from the nanoparticle periphery and surfactant-stabilized nanoparticles are obtained. Further validity for this line of thought was obtained from the following experiment: In a separate experiment, when a solution showing necklace morphology was incubated with an excess of TOA, necklace

morphology disappeared completely, and an almost identical TEM image (as in the case of 6 equiv to AgOAc amine) showing self-assembly of individual nanoclusters was obtained. The stability of silver particles was also investigated in common organic solvents. PMHS- and TOA-stabilized yellow solutions of silver nanoparticles were found to be stable for months and always displayed an intense characteristic absorption peak around ~435 nm without any trailing at higher wavelengths.

2.3 Conclusions

In conclusion, a one-step conversion of silver acetate to stable nanosized silver particles is achieved under mild conditions in high yields. We have shown that the physicochemical and morphological property profile of polysiloxanes leads to controlled nucleation, growth, and stabilization of nanoparticles and provides new opportunities in nanoscale synthesis of metal particles. In addition, facile surface tailoring reactions open new possibilities in the field of surfactant exchange reactions.

Part B: Role of Polyhydrosiloxanes and Counter Anions in the Self-Assembly of Silver Nanoclusters

2.4 Introduction

Due to the importance of dimensionality on properties of nanoscale materials, there has been a significant effort in identifying routes to adjust their size and shape using various colloidal synthetic methods. Thus a large number of solution phase synthetic approaches have been applied with high degree of success to produce a variety of nanocrystal materials with controllable size and shape.[12] In these methods inorganic particles are controllably precipitated from molecular precursors in the presence of stabilizing agents such as polymers,[13] or strong coordinating ligands.[14]

One of the main characteristics of colloidal particles is their small size and due to which causes them to became unstable as they agglomerate in bulk. In most cases, this aggregation leads to the loss of properties associated with the colloidal state of these metallic particles. The stabilization of metallic nanoparticles to preserve their finely dispersed state is a crucial aspect to consider during their synthesis. Nanoclusters stabilization usually involves (i) charge stabilization by the surface adsorbed anions such as chloride or citrate, and (ii) steric stabilization by the presence of macromolecules such as polymers or oligomers, or (iii) ligand stabilization by coordinating with metal nanoparticles. The polymer or ligand is adsorbed on the nanocrystal surface and kinetically stabilize the colloidal growth by providing electrostatic or steric stabilization, thereby slowing the rate of particle agglomeration.[12] Thus the presence of polymer or a

ligand in preparative methods of nanoclusters dispersions profoundly influences the features of the resulting metal nanoparticles as well as their long-term colloidal stability.

Presently our group is interested in the synthesis of metal nanoclusters by using Polymethylhydrosiloxane as a stabilizing agent. The reasons for our interest are as follows: (i) siloxane polymers displayed unique properties due to their uniform composition and structure (ii) the unusual freedom of rotation around Si-O bond which allows these polymers a high degree of flexibility while maintaining their integrity, (iii) the polysiloxane with Si-H functionalities can act as reducing agent and thus the need for extra reducing agent can be avoided making the process more simple an economical (iv) the encapsulated nanoparticles are confined primarily by steric effects, and therefore a substantial fraction of their surface is unpassivated and accessible which can participate in surfactant exchange reactions to generate functionalize metal nanoparticles.

We recently disclosed a new strategy for generating Polysiloxane-stabilized Pd and Pt-colloids and demonstrated their utility as potent catalyst for selective silaesterification, hydrogenation, and hydrosilylation reactions.[7a,b,15] Silver nanocrystallites, mostly hydrosols, have been widely studied but the colloidal dispersions of silver in nonaqueous liquids (organosols) are rare and more difficult to prepare and stabilize. In a recent report by our group, we introduced a versatile method of polymethylhydrosiloxane (PMHS) induced generation and stabilization of functionalizable monodisperse silver sols.[16] The method has enabled the formation of stable silver nanoclusters reservoir without any particle aggregation or precipitation during its storage. In the report, we have also demonstrated the utility of such reservoirs in grafting the surface properties of nanosized silver particles by exchange reactions with

trioctylamine (TOA). The reduction of silver acetate in presence of 2 equivalent of TOA, led the silver particles to self-assemble in the form of nanonecklaces, which is due to their interaction with polysiloxane. On the other hand, with the increase in relative amount of TOA to 6 equivalents, surfactant stabilized self-assembly of individual Ag-nanopartcles are obtained with closed packed morphology.

To our knowledge, there are only one example present in the literature, where reduction of different silver salts were carried out in a specific reaction condition under identical molar ratios of reactants.[17] The authors have also conducted the kinetic study of nanoparticle formation for different silver salts. To date, no reports are available where reduction of different silver salts with a wide range of counter anion was carried out. As we know that for a given metal salt shows distinguishable chemical and physical properties such as texture, color, and solubility at ambient condition due to different counter anion attached to the metal ion. For example, silver acetate and silver heptafluorobutyrate has different solubility properties at room temperature in a particular solvent. Silver nanoparticles are particularly interested because of their use in photographic devices,[2] in surface enhance Raman scattering,[3] and as a catalyst.[4] It is essential to investigate a particular reduction process for where silver ions are attached to (i) week or strong chelating inorganic anions and (ii) short or long chain organic anions. In this section, we have investigated the activity profile of the counter anions from various silver salts AgX (X=NO_3^-, ClO_4^-, BF_4^-, AcO^- and $F_7C_4O_2^-$) on the silver nanoparticle synthesis, particle morphology and the rate of reaction and also demonstrated the role of TOA in the stabilization of silver nanoclusters during the synthesis. It was observed that the relative amounts of TOA as well as the different

counter anions of the silver salts influenced both the reaction rate and the morphology of the colloids obtained.

2.5 Results and Discussions

It has been observed that the different anions have different ability to allow the formation, stabilization, and property profile of metal nanoclusters formation reactions.[18] In some practical applications, environmentally or biologically compatible polymer matrixes are desired for dispersing the functionalized nanoprticles. In this context, in our previous communication, we have shown that the physicochemical and morphological property profile of polyhydrosiloxanes leads to controlled growth and stabilization of silver nanoparticles. Here we extend our studies for different silver salts such as $AgNO_3$, $AgClO_4$, $AgBF_4$, and $AgF_7C_4O_2$ to investigate the anion effect on the synthesis and stabilization of silver nanoparticles. In the present synthetic procedure, we have performed the following experiments to define the counter anion effect on the formation, rate of reaction and the stability of the synthesized particles in the process, see Figure 2.9: (i) synthesis of Ag(0) by PMHS in the presence of different molar ratios of TOA; (ii) rate of reaction and stability of nanoparticles from silver salts having inorganic counter anion ($AgNO_3$, $AgClO_4$, and $AgBF_4$); (iii) studies of the reaction rate for organic counter anion (AgOAc, and $AgF_7C_4O_2$) and (iv) role of TOA on the synthesized particles and reaction rate.

2.5.1 Synthesis of Ag(0) by PMHS in the presence of different molar ratios of TOA.

As described in our published article,[16] polymer (PMHS) stabilized silver nanoparticles were achieved in the presence of catalytic amount of TOA. The surfactant (TOA) capped Ag(0) was also synthesized when excess amount of TOA was used. In our present studies, we have synthesized silver nanoparticles from four different silver salts under similar reaction condition and identical molar ratios. In an exploratory experiment, when PMHS (0.072 ml, 1.2 mmol,) was added to in 50-ml toluene suspension of silver nitrate (0.033gm, 0.2 mmol,), there was no noticeable change of the solution color observed even after 24h of stirring. The UV-vis absorption spectrum showed a flat line curve, indicating no reduction of silver nitrate to silver nanoparticles. To optimize the reduction process, after 1 hour of catalytic amount of TOA (0.005 mL, 0.01mmol) was added in to the silver nitrate suspension. The stirring continued for another few hours and the formation of silver nanoparticles was probed by monitoring the absorption changes at different time intervals. Figure 2.4 shows the time evolution UV-vis absorption spectra, which depict the blue shifts of the peak positions (λ_{max}) and the shapes during the reduction process. When the reaction was continued for 0.5 h, a broad asymmetric peak centered at 431 nm indicating the formation of polydisperse nanoparticles. After 2.5 h of the reaction, the broad peak becomes more symmetric and blue shifts from 431 nm to 420 nm (indicating smaller particle size) After a total of 7h of the reaction, the plasmon band (λ_{max}: 418 nm) becomes symmetric and no further intensity increment was observed. At this juncture, the yellow reaction mixture was centrifuged and one drop was deposited on Formvar coated carbon grid and envisioned by a transmission electron microscope

(TEM). The TEM (Figure 2.4) analysis shows the formation of few silver nanonecklaces with diameter ~ 80nm. The average silver nanoparticle size in the ring was in the range of 2.7 ± 0.7 nm. The low population of nanonecklaces can be attributed to the slow reduction process of silver nitrate and formation of less number of nuclei in the reaction mixture. As a result the populations silver nanoparticle was also low. Under similar reaction condition and identical molar ratios of reactants, reduction of other silver salts was also inquired.

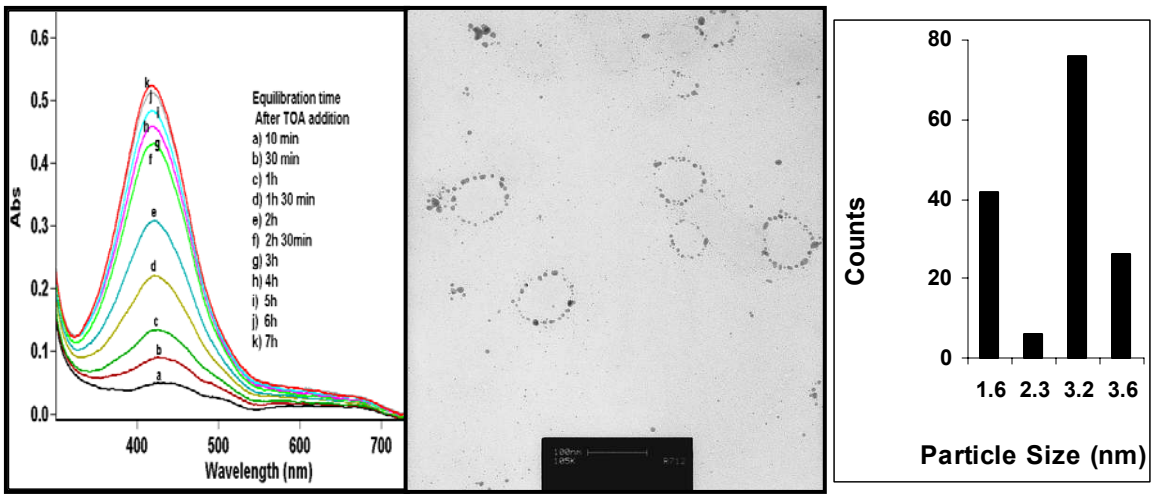


Figure 2.4: Time evolved UV-vis absorption spectra, TEM image, and the corresponding histogram of silver nanocluster of polysiloxane stabilized silver nanoparticles obtained from silver nitrate reduction in presence of catalytic amounts of TOA.

In order to examine the stabilizing effect of TOA, we performed experiments with varying amounts of TOA. Thus, a suspension of silver nitrate (0.033gm, 0.2 mmol) was prepared in 50 mL of toluene, and PMHS (0.072 ml, 1.2 mmol) was injected to this suspension at room temperature. Vigorous stirring was continued for 0.5h, during which no noticeable change of the solution color was observed. At this juncture TOA (0.4 mmol, 0.17 ml) was injected into the reaction mixture. After 30 min of addition of TOA, the color of the reaction mixture turned yellow (UV-vis spectroscopy, λ_{max} at 425 nm).

When the reaction was continued for another 3 h, the absorbance peak became more symmetrical and intense (Figure 2.4). After 3.5h, the color of the solution was yellowish brown and showed an intensive and symmetrical absorption peak at ~415 nm region. At this point the mixture was centrifuged and one drop was deposited on a TEM grid for morphological analysis. The TEM analysis showed the formation of nanoparticles in the form of nanosized necklaces (Figure 2.5). The particle size analysis of the individual nanoparticles showed the particles to be rather monodispersed in the 2-3 nm size regimes. The ring diameter analysis showed the average necklace diameter of 21-nm.

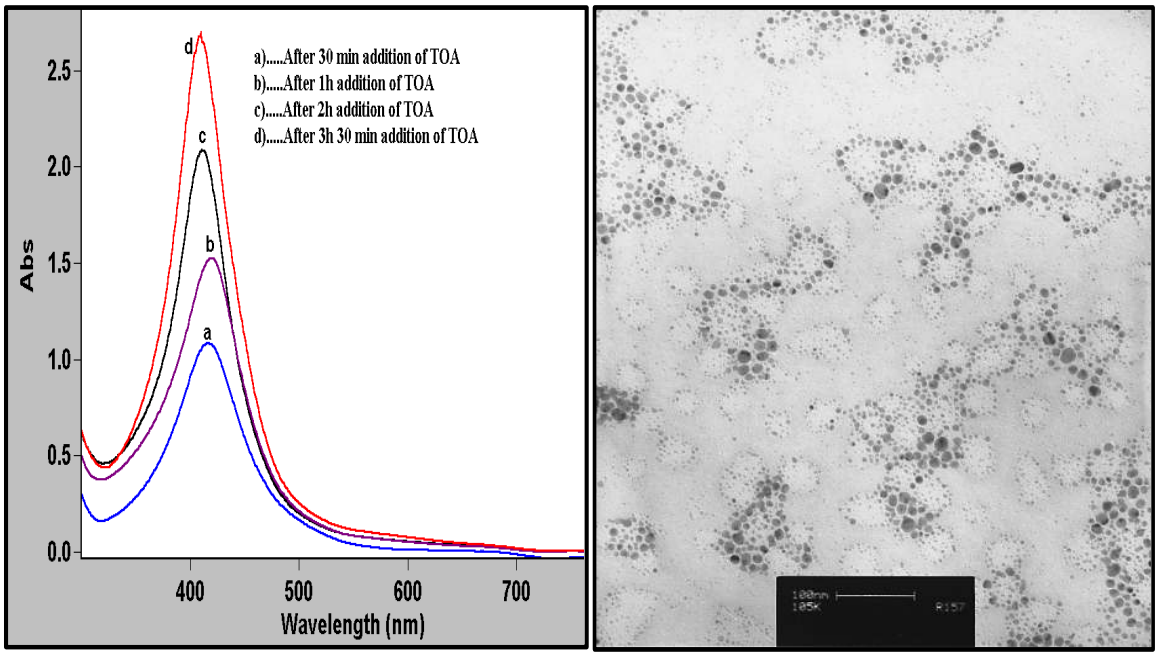


Figure 2.5:UV-vis spectra monitoring the absorption changes at different time intervals (2A) and TEM analysis (2B) of the silver nanonecklaces obtained from silver nitrate reduction in presence of 2 equiv of TOA.

The centrifuged solution was also analyzed by tapping mode AFM to investigate the morphology of silver nanoparticles. One drop of sample was spin coated on cleaned mica surface at 3000 r.p.m for 20 sec and then air dried for 3h and then analyzed by AFM. The experimental data showed the presence of necklaces with an average diameter

of 22 nm (Figure 2.6), which is comparable with the TEM analysis data of 21 nm. This result is very important in the sense that the nanonecklace morphology even subsisted on the solid surface and can be useful in future applications. When the same silver nanoparticle coated mica surface was analyzed by EDX for elemental analysis, only C, O, Si, and Ag were observed. It implied that the necklace morphology was composed by PMHS and silver nanoparticles.

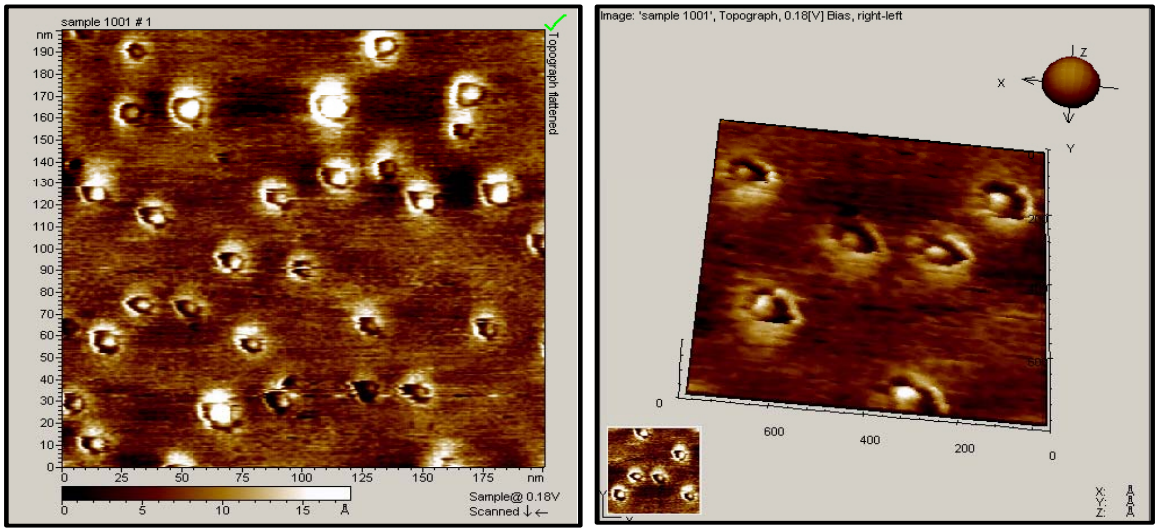


Figure 2.6 Tapping mode AFM image of polysiloxane stabilized silver nanonecklaces obtained from silver nitrate reduction in presence of 2 equiv of TOA.

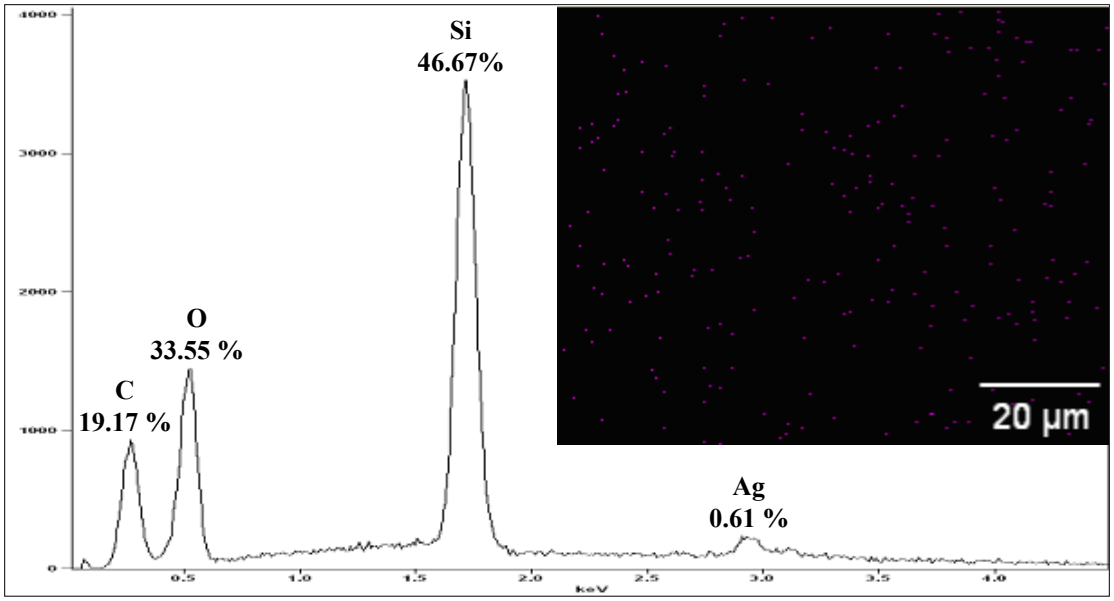


Figure 2.7: EDX spectra and elemental Ag map of synthesized silver nanonecklaces.

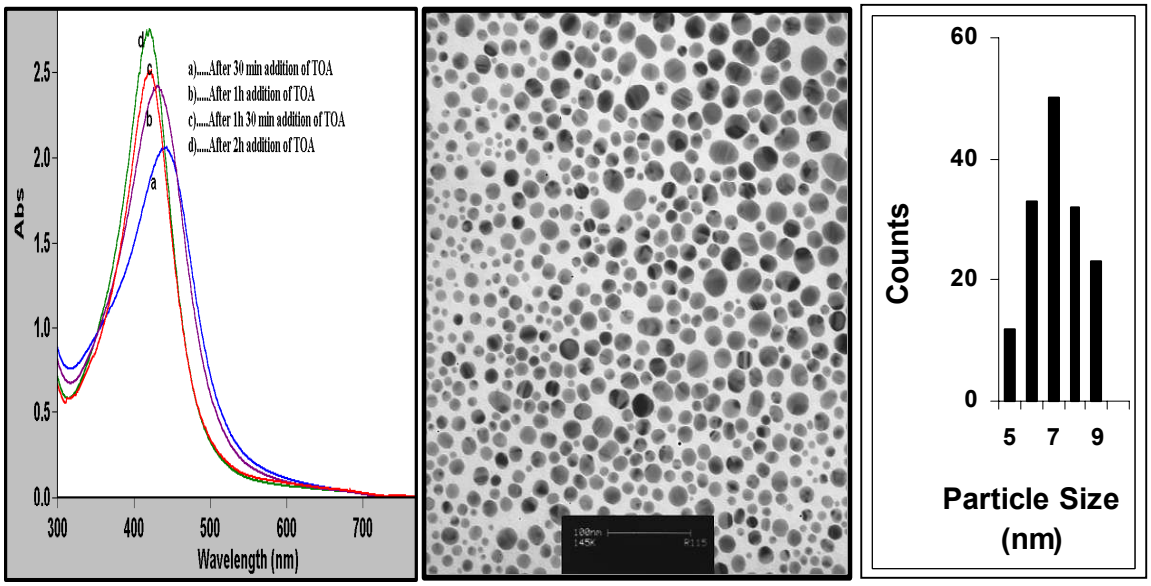
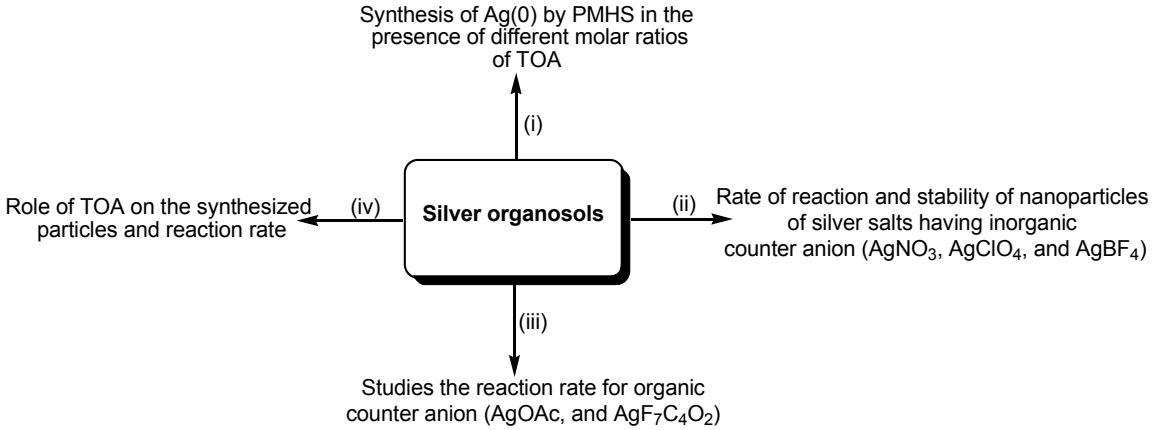


Figure 2.8 UV-vis spectrum (3A) of the reaction mixture in presence of six equiv of amine and TEM image (3B) and the corresponding histogram (3C) of silver nanocluster.

Under identical reaction conditions and molar ratios of $AgNO_3$ and PMHS, with an excess of TOA (6equivalents to $AgNO_3$ amount) the formation of nanoparticles were significantly faster, and after 2 h of stirring no other noticeable spectral changes were observed and the dark yellow solution was stable with a λ_{max} of 424 nm. At this point the reaction mixture was centrifuged and analyzed by TEM (Figure 2.8), which showed the formation of closed packed morphology of silver nanoparticles in 7 nm size regimes, and the complete disappearance of nanosized necklaces was observed. On the basis of these preliminary UV-vis and TEM results, we can elucidate the generation, growth, and stabilization process for the formation of silver nanonecklaces and self assembled individual nanoparticles as follows. During the reduction process with 2 equiv of TOA

(0.4 mmol), initially small oligomeric silver clusters are formed, which then grow in size to form bigger particles. These larger particles are not stable and are broken into small particles due to the protection provided by siloxane polymer. Finally the more stable nanoparticles are wrapped by polysiloxane chains to form spherical silver nanonecklaces. In this case as the particle formation is not vary rapid, the synthesized nanoparticles can easily interact with excess polysiloxane present in the reaction mixture to form nanonecklaces. The second growth process is very important for the formation of nanonecklaces. While in presence of 6 equiv TOA (1.2 mmol) the reduction is very fast and the metal nanoparticles react predominantly with the excess of amine molecules to form self-assembled closed packed nanoclusters. This result shows that when enough coordinating agents are present, PMHS is completely dissociated from the nanoparticle



periphery and surfactant-stabilized nanoparticles are obtained.

Figure 2.9 Schematic illustration of the counter anion effect on the formation, rate of reaction and the stability of the synthesized particles in the process.

Under similar reduction condition reduction of other silver salts was carried out in the presence of different amount of TOA. It has been observed that the rate of reaction

for five different salts are different from other and was strongly related on the amount of TOA present in the reaction mixture. The analysis results of nanoparticle synthesis from five different silver salts are summarized in table 2.1.

2.5.2 Rate of reaction and stability of nanoparticles from silver salts having inorganic counter anions

Finke and coworkers have been extensively studied the role of anions on the synthesis and its stabilizing ability towards nanoparticles. They have reported[19] an anionic series for controlled formation of nanoparticles and their stabilization ability based on five criterions. They have found that Bronsted basic polyoxoanions meets all the five criterions very well to be a suitable ligand, followed by the citrate and then other common anions used in nanoclusters synthesis. In our synthetic procedure, we have investigated the rate of reaction and stability of nanoparticles for silver salts having three different inorganic counter anions. It was found that the rate of particle formation and reduction of silver nitrate was very slow. The reduction of $AgNO_3$ did not happen with PMHS even until 24h at room temperature. To accelerate the reduction process, we had introduced TOA in the reaction mixture. The slow rate of particle formation of silver nitrate can be explained to the strong interaction between the silver ion and NO_3^-, which not allow the silver ion to convert the Ag(0). Unlike other anions with delocalized charges, NO_3^- is strongly coordinated to a silver ion through a chelation by two oxygen atoms and, therefore, the formation of silver nanoparticles becomes slow.[20] In the case of $AgClO_4$ and $AgBF_4$, the formation of silver nanoclusters was observed with addition of

PMHS, without addition of TOA. From our knowledge,[21] we know that ClO_4^- is a very week conjugate base; as a result, its stability in the solution will be high. Because of the high stability of perchlorate ion, it does allow the silver ion to get reduced to Ag(0). The similar explanation is also applicable for BF_4^-, which is also a weak conjugate base. Figure 2.10 represents the TEM image, UV-vis absorption spectra and particle size analysis when silver perchlorate reduction was carried out in the presence of catalytic amount of TOA.

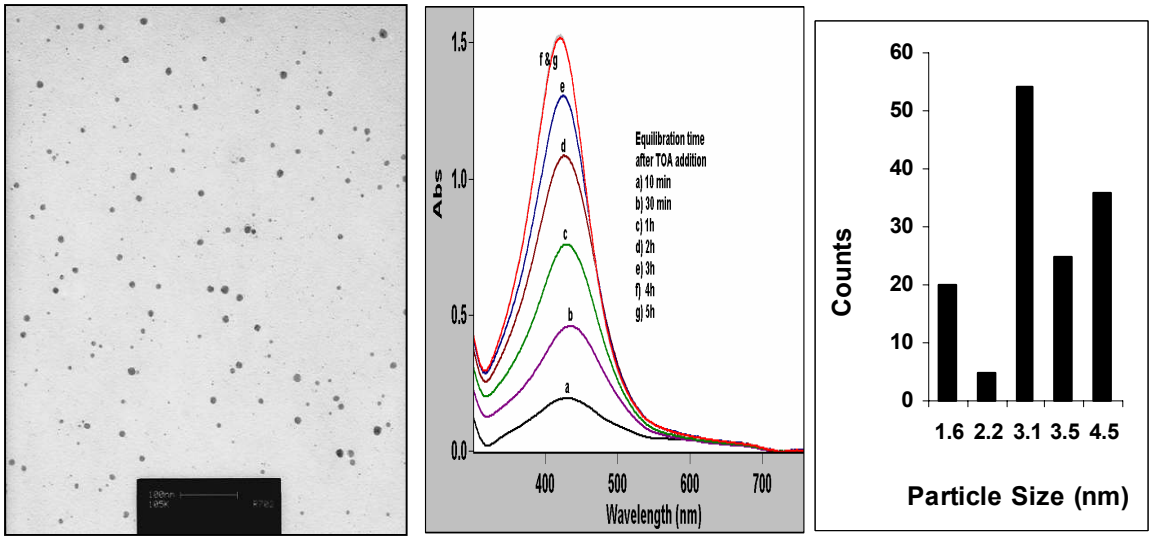


Figure 2.10 TEM image, UV-vis spectrum, and the corresponding histogram of silver nanoparticles obtained from silver perchlorate reduction with catalytic amounts of TOA.

2.5.3 Study of the rate of the reaction for organic counter anions

In this section, two different silver salts (AgOAc, and $AgF_7C_4O_2$), having organic anion were discussed to find out the role of counter anion on the rate of reaction and particle morphology. As we have mentioned in part A of this chapter that without TOA, the rate of reduction of silver acetate to silver nanoparticles was slow resulting in particle

precipitation. To make the reduction process successful, we have used different amount of TOA. First of all, the solubility of silver acetate in organic solvent is very poor, which makes the reduction process more difficult. Moreover, acetate ion cannot provide adequate stabilization for the synthesized nanoclusters. On the other hand, silver heptafluorobutyrate is completely soluble in toluene. The high solubility can be ascribed to increase ionic radius, which is associated with larger lattice structures and lower lattice energies of the complexes.[22] The high solubility of $AgF_7C_4O_2$ constructs the system easier, where silver ion can easily interact with the polysiloxane backbone. The rate of reduction of $AgF_7C_4O_2$ is very fast even without addition of TOA. In the presence of TOA, the reduction was completed within 1h of addition of TOA.

2.5.4 Role of TOA in the reaction rate and synthesized particles

The silver salts such as $AgClO_4$, $AgBF_4$, and $AgF_7C_4O_2$, were showed room temperature reduction without addition of TOA. The reaction is quite faster (4h) resulted in the formation of silver nanoparticles in the range of 3-4 nm. Other two salts silver acetate and nitrate had no reduction under this condition. In the presence of catalytic amount of TOA, silver acetate reduction resulted monodisperse silver nanoclustes with average diameter of 2.0 ±0.6 nm and silver nitrate produced 2-3 nm silver particles in the form of nanonecklaces. In this two cases, the reduction was completed within 6-7 h of TOA addition. Under identical molar ratios and reaction condition, reduction of $AgClO_4$, $AgBF_4$, and $AgF_7C_4O_2$ results the formation silver nanoparticles in the range of 2-4 nm in a 3-5h of time period. When the amount of TOA was increased to 2 equivalents, the rate

of reaction increased predominantly and completed within 3.5 h in case of $AgNO_3$ and AgOAc. The TEM analysis showed that the PMHS stabilized formation of nanoparticles, in the form of nanonecklaces. The average diameter of individual nanoparticle in necklaces was found be in the 3-4 nm regime and the average ring diameter was of 21-nm. In case of $AgClO_4$, $AgBF_4$, and $AgF_7C_4O_2$ under identical reaction conditions and molar ratio of reactants, the reaction takes place within 2h, with the formation of individual nanoparticles in the range of 2-5 nm. Figure 2.11 shows the time evolution of the absorbance at 420 nm for various silver salts in the presence of 2 equivalent of TOA. From the graph we can clearly see that, the rate of reduction of$AgClO_4$ and $AgBF_4$ is comparable where as, it was very fast for $AgF_7C_4O_2$ and completed within 1h of addition of TOA.

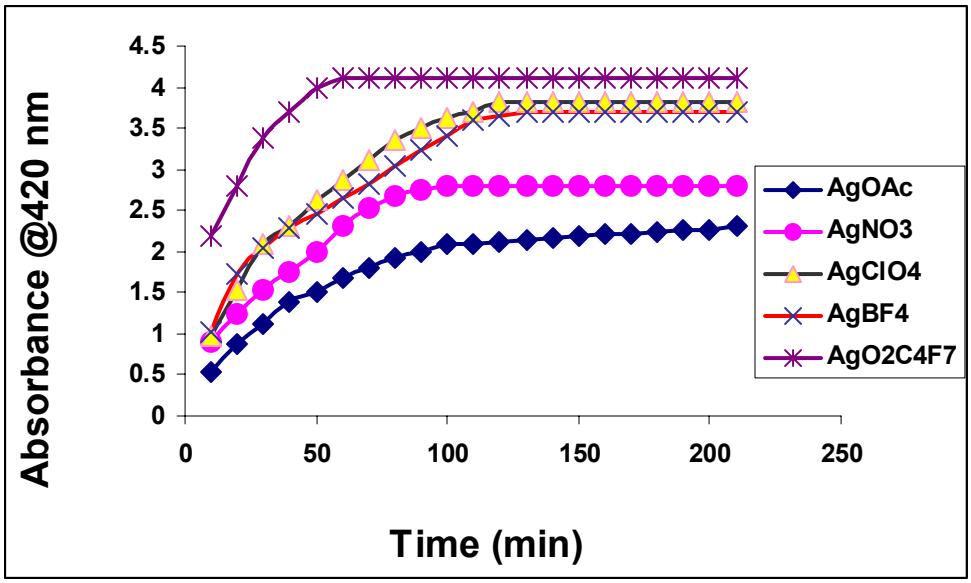


Figure 2.11 Time evolution of the absorbance at λ = 420 nm for the various silver salt reduction by polysiloxane in the presence of 2 equivalent of TOA.

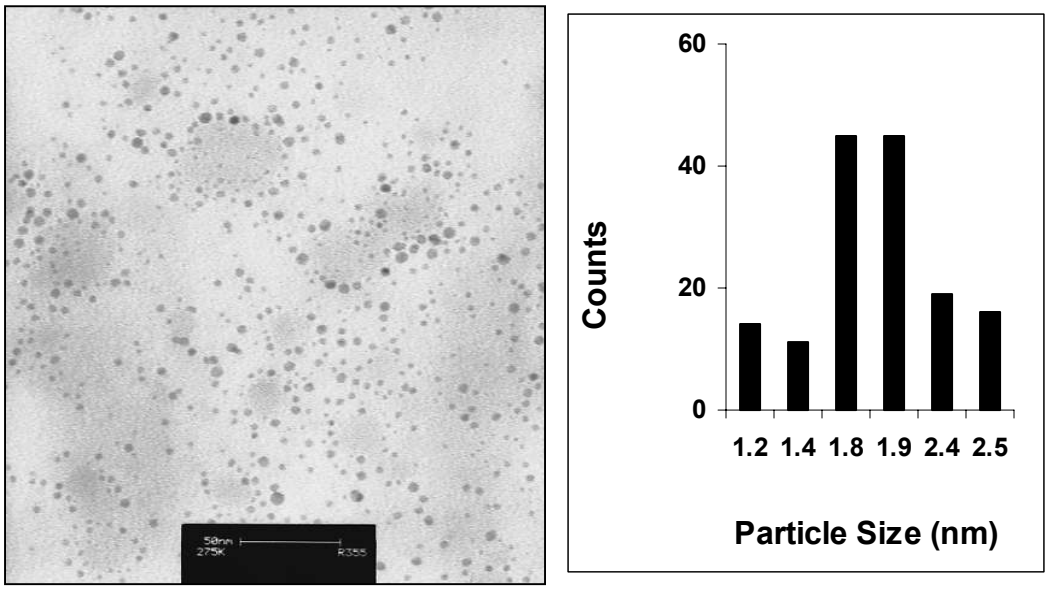


Figure 2.12 TEM image of silver nanoclusters obtained from silver tetrafluoroborate reduction in presence of 2 equiv of TOA.

It has been reported that,[23] polydimethylsiloxane, which is an analogue of polymethylhydrosiloxane, exhibits the lowest energy when it is in the trans conformation and formed a compact structure. The portion of the siloxane chain formed a closed loop structure consisting approximately eleven monomers. In the scientific point of view this data makes our hypothesis stronger that the nanonecklaces formation was because of loop structure of PMHS.

When enough coordinating surfactant (6 equivalent) was present in the reaction mixture, the particles were removed from polysiloxane periphery and attached to the TOA molecules. Because of this reason, all the silver salts produced self-assembled silver nanoclusters. The only differences observed was that the rate of reaction was faster compared to the reduction reaction where 2 equivalents of TOA were present. This

system open up a new avenue where surface exchange studies can be performed and is applicable to almost all the commercially available silver salts.

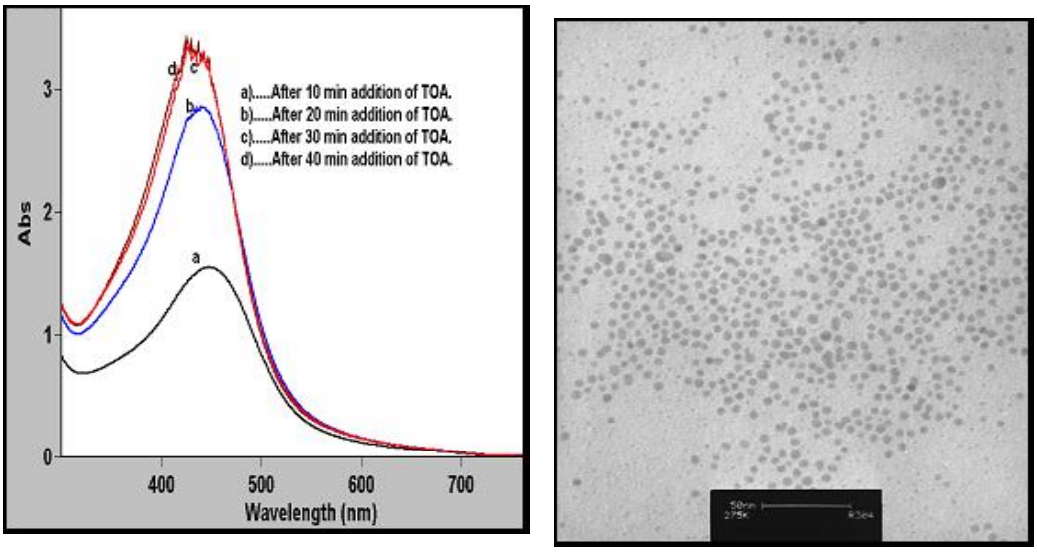


Figure 2.13: UV-vis spectrum, TEM image of silver nanoparticles obtained from silver perchlorate reduction in presence of 6 equiv of amine.

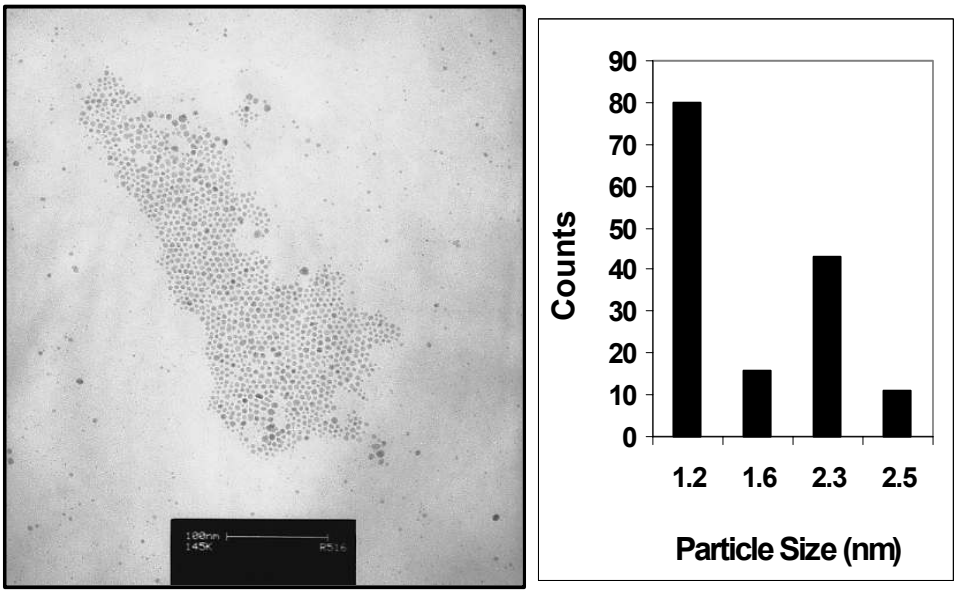


Figure 2.14: Figure 7 represents the TEM of silver nanoparticles and the corresponding histogram obtained form heptafluorobutyrate reduction in the presence of 6 equiv of TOA.

Table 2.1. The comparative analysis data for silver nanoparticle synthesis from five different silver salts.[a]

Entry	Silver Salt	Amount of TOA (eqiv)[b]	UV-vis absorption maxima (λ_{max}:nm)	Average Particle Size (nm)[c]
1	AgOAc	0.05[d]	435-440	2.0 (0.6)
2	AgOAc	2.0	425-440	3.0 (0.8)
3	AgOAc	6.0	420-434	2.8 (0.6)
4	$AgNO_3$	0.05	418-435	2.7 (0.7)
5	$AgNO_3$	2.0	408-417	3.8 (1.1)
6	$AgNO_3$	6.0	424-435	7.9 (1.1)
7	$AgClO_4$	None	421-425	3.1 (0.6)
8	$AgClO_4$	0.05	420-427	3.3 (0.9)
9	$AgClO_4$	2.0	425-430	4.3 (0.8)
10	$AgClO_4$	6.0	426-435	4.9 (0.6)
11	$AgBF_4$	None	425-433	3.6 (0.8)
12	$AgBF_4$	0.05	420-430	3.7 (0.8)
13	$AgBF_4$	2.0	415-427	1.9 (0.4)
14	$AgBF_4$	6.0	417-419	3.4 (0.5)
15	$AgF_7C_4O_2$	None	425-430	2.8 (0.9)
16	$AgF_7C_4O_2$	0.05	418-427	2.2 (1.1)
17	$AgF_7C_4O_2$	2.0	408-415	1.6 (0.6)
18	$AgF_7C_4O_2$	6.0	408-411	2.4 (0.3)

[a] In all the cases, ca. 150 particles were counted and then combined into histogram to obtain the size distribution. [b]Equivalent to silver salt (0.2 mmol). [c]The figures in the parenthesis indicate the standard deviation. [d]Catalytic amount of TOA.

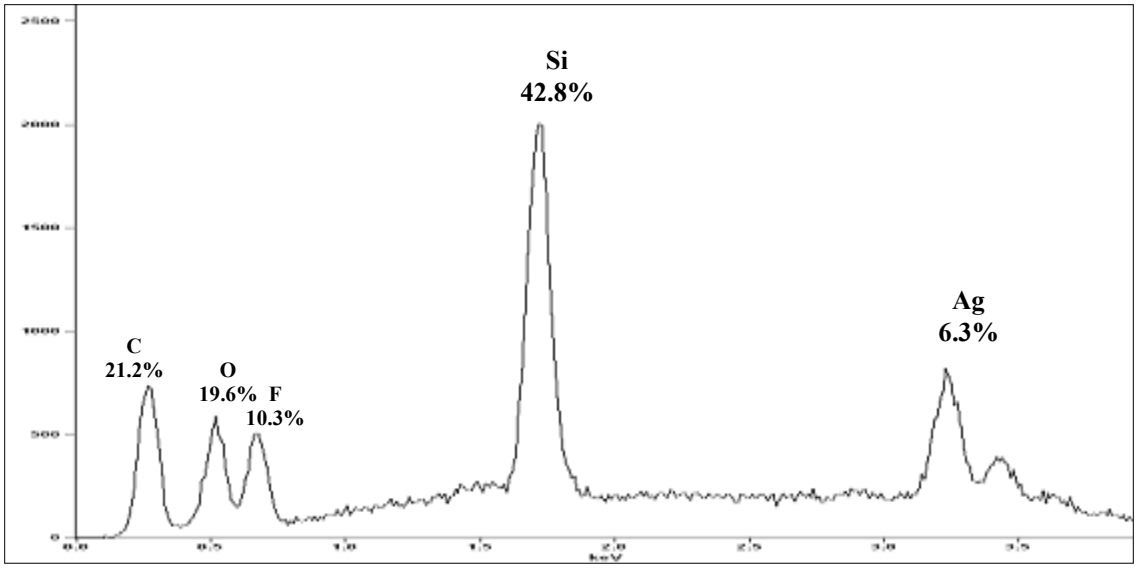


Figure 2.15: EDX of silver nanoclusters.

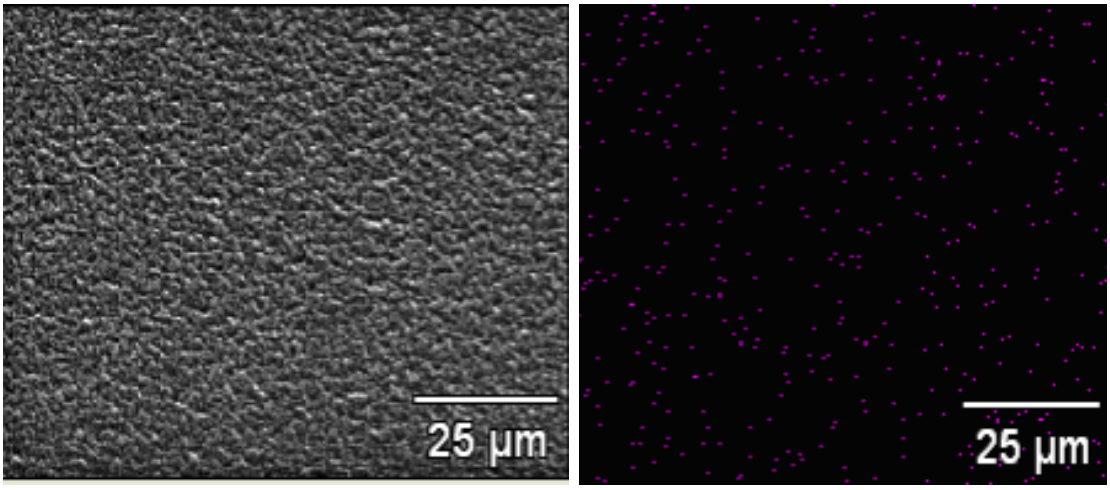


Figure 2.16: SEM image and elemental Ag map of synthesized silver nanoclusters.

The reaction rates and stabilization processes for different silver salts clearly prove that the anion of the silver salt plays a profound role in the rate of formation and stabilization of silver nanoparticle synthesis. The rates are fast, initially, but slow down after 30 minutes and reach to maximum absorbance within two hours for $AgClO_4$, Ag BF_4. On the other hand $AgNO_3$ and AgOAc show a gradual increase of absorbance and takes 3.5 hours to reach the maximum absorbance. These experimental results showed that the rate of reduction increases in the order of $AgNO_3$<AgOAc<$AgClO_4$≈Ag BF_4<$AgF_7C_4O_2$. The summery of the above experimental data is as follows: (i) silver salts such as $AgClO_4$, Ag BF_4, and $AgF_7C_4O_2$ display room temperature reduction with PMHS in the absence of TOA, on the other hand silver acetate and silver nitrate did not; (ii) the slow reduction processes with $AgNO_3$ and AgOAc result in the formation of PMHS stabilized silver nanonecklaces in presence of 2 equivalents of TOA and $AgClO_4$, Ag BF_4, and $AgF_7C_4O_2$ showed formation of individual silver nanoparticles; (iii) under fast reaction conditions, i.e., in presence of excess amounts of TOA (6 equivalents), all the silver salts result in the formation of surfactant stabilized silver nanoclusters in a closed packed morphology. On the basis of these experimental results we can hypothesize that when the particle formation is slow enough to be stabilized with PMHS, spherical polysiloxane strands form necklace morphology that wrap all the individual silver nanoparticles. In presence of excess of TOA, the particle formation is very fast and subsequently stabilized by TOA itself, resulting in the formation of self assembled close-packed morphology.

2.6 Conclusions

We have demonstrated that the counter anion of a silver salt plays a significant role on formation of silver nanoparticles. The order of reaction rates are as follows; $AgNO_3$<AgOAc<$AgClO_4$≈Ag BF_4<$AgF_7C_4O_2$. The silver salts, $AgNO_3$ and AgOAc resulted in the formation of PMHS stabilized silver nanonecklaces in presence of 2 equiv of TOA and $AgClO_4$, Ag BF_4 and $AgF_7C_4O_2$ produced individual nanoparticles. Under fast reaction conditions, i.e., in presence of excess amounts of TOA, result in the formation of surfactant stabilized self-assembled silver nanoparticles in a closed packed morphology. When the particle formation is slow enough to be stabilized with PMHS, all the individual silver nanoparticles are wrapped by spherical polysiloxane strands to form necklace morphology. In the presence of excess of TOA, the particle formation is very fast and subsequently stabilized by TOA itself, resulting in the formation of self assembled close-packed morphology.

Part C: Silicon Thiol Stabilized Silver Nanoparticles: Functionalized Silver Organosols

2.7 Introduction

Nanoclusters syntheses have received much attention due to unique size-dependent properties and new collective physical properties. However to fully exploit these properties nanocrystals functionalization is crucial and essential. In general, the key to functionalize nanoparticles is maintenance the original physical properties and in many cases, it is necessary to develop flexible nanocrystal surface chemistry, allowing further, subsequent functionalization. Generally the functionalization of small silver, and gold nanoparticles in the 1-10 nm size regime was carried out with alkanethiol,[24] thiol derivatives,[25] and polymers.[26]

The Brust method[27] is a well accepted and established synthetic route for the generation of thiol functionalized metal nanocrystals. Almost all the synthetic processes involve the reduction of metal salts using $NaBH_4$ as a reducing agent. The advantages of this method are (i) the particle size can be controlled by simple variation of the ratio of metal ion to ligand in the reaction condition, (ii) it is easy to introduce different surfactants to make functionalized nanoparticles, and (iii) it allows redispersion of the nanoparticles in a wide range of solvent. Because all of the four hydrogen atoms in the BH_4^- anion can take part in the reduction process, the resulting metal colloids are contaminated with borides.[28] Moreover, the reduction cannot be carried out in the presence of functional ligands. In this section, we present a simple one pot, high yield

route for the synthesis of functionalized silver nanoparticles using MPS (3-mercaptopropyl triethoxy silane) as a stabilizing agent. This methodology provides two different means to achieve functionalized silver nanoclustes with thiol, in toluene at room temperature. The two processes are, (a) synthesis of a silver mercaptosilane complex and subsequently reduction by PMHS and (b) formation of silver nanoparticles of average diameter of 2-3 nm by our standardized procedure[16] and then functionalized using mercaptosilane. Various topologies of nanosized silver particles were achieved by varying the concentration of both reducing and the stabilizing agents. The silane capping agent (3-mercaptopropyl)triethoxysilane (MPS) was selected because its thiol group has a high affinity for silver, leading to a stabilizing MPS monolayer on the silver surface. The method employs a mercaptosilane compound, which not only ensures the colloidal stability of silver particles but also provides them with alkoxysilane surface groups. The ethoxysilane groups of MPS can easily be hydrolyzed by making silica coated silver nanoparticles. The optical properties of the nanocrystalline dispersant are affected by the transparent silica encapsulated matrix.[29]

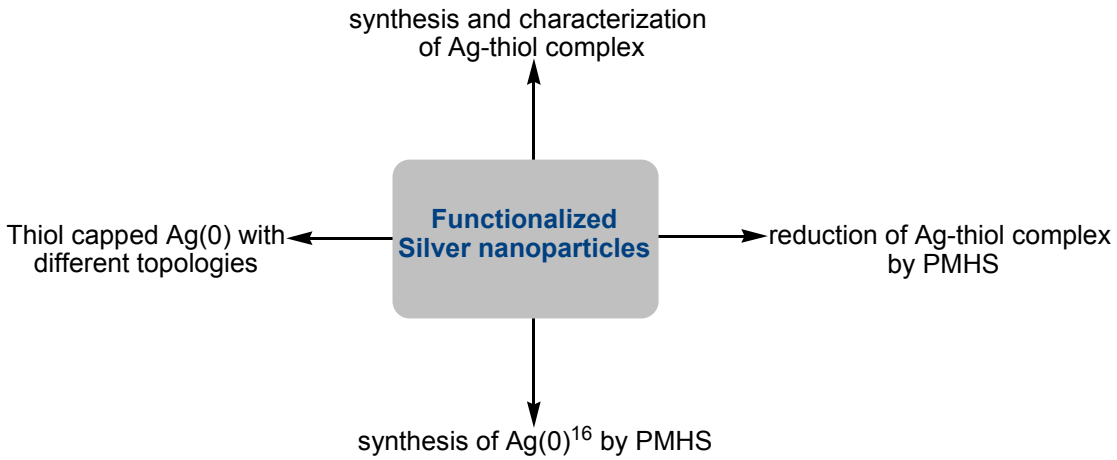
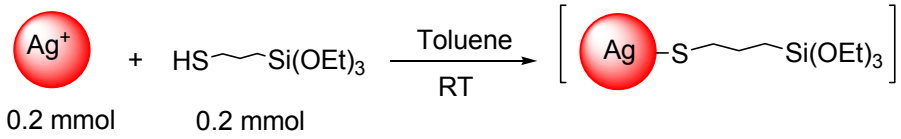


Figure 2.17: Schematic representation of functionalization of silver nanoparticles by MPS.

2.8 Results and Discussion

The organo-silane functionalized silver nanoparticles were prepared by polysiloxane reduction method.[16] We used different approaches to functionalize the nanoparticles. In the first approach, the presynthesized silver-thiol complex was reduced by PMHS, and in the second approach, the synthesized Ag(0) was functionalized with thiol. Figure 2.17 schematically presents a simple outline of the work presented in this section.

2.8.1 Synthesis and characterization of Ag-thiol complex



Scheme 2.2: Synthesis of silver thiol complex in toluene.

Before characterizing the MPS stabilized silver nanoparticles, it is necessary to find out whether the MPS moiety forming the complex with the monovalent silver ion selectively, when they are free in solution. The first step of our synthesis involved the production of a silver-thiol complex in toluene. In a typical experimental procedure, 50-ml silver acetate (0.2 mmol, 0.032 gm) suspension was prepared in toluene at room temperature with constant vigorous stirring. The suspension was stirred for 30 minutes and at this juncture MPS (0.2 mmol, 0.046 ml) was injected. After addition of MPS, the reaction mixture was stirred for another 1h. With 1h of stirring at room temperature, the silver acetate suspension solution was converted to a clear colorless homogeneous

solution. The clear solution was then evaporated under high vacuum and we obtained a yellow solid. The solid was then dissolved in $CDCl_3$ for NMR analysis. NMR spectroscopic investigations were carried out to quantitatively determine the details of the complexation of the ligand with the monovalent silver ion surface. The ^1H NMR spectra of MPS complex of silver acetate was investigated; see Figure 2.18. The MPS has two $–SCH_2$ protons with a characteristic resonance at 2.5 ppm. It was expected that the unimolecular mixture of these molecules would form a 1:1 complex in the solution. Consistent with this expectation, the $–SCH_2$ proton resonance are shifted downfield to 2.8 ppm. In similar reaction conditions two different AgOAc: MPS ratios (1:2 and 1:4) were also investigated. It was observed that in this two cases all the MPS molecules are not involved in the formation of a molecular complex with AgOAC. In 1:2 cases, the complexed and uncomplexed ratio of MPS was 1:1 and for 1:4 cases the ratio was 1:3. To reveal the phenomenon 1:2 silver acetate and MPS complex was analyzed by ^{13}C NMR spectra; see Figure 2.19. We concluded that the signal at δ 27.6 ppm corresponded to the free $–SCH_2$ carbon signal of MPS. Because of complexation to the silver ion it exhibits downfield shifts showing two peaks at δ 31.5 ppm and 34.0 ppm.

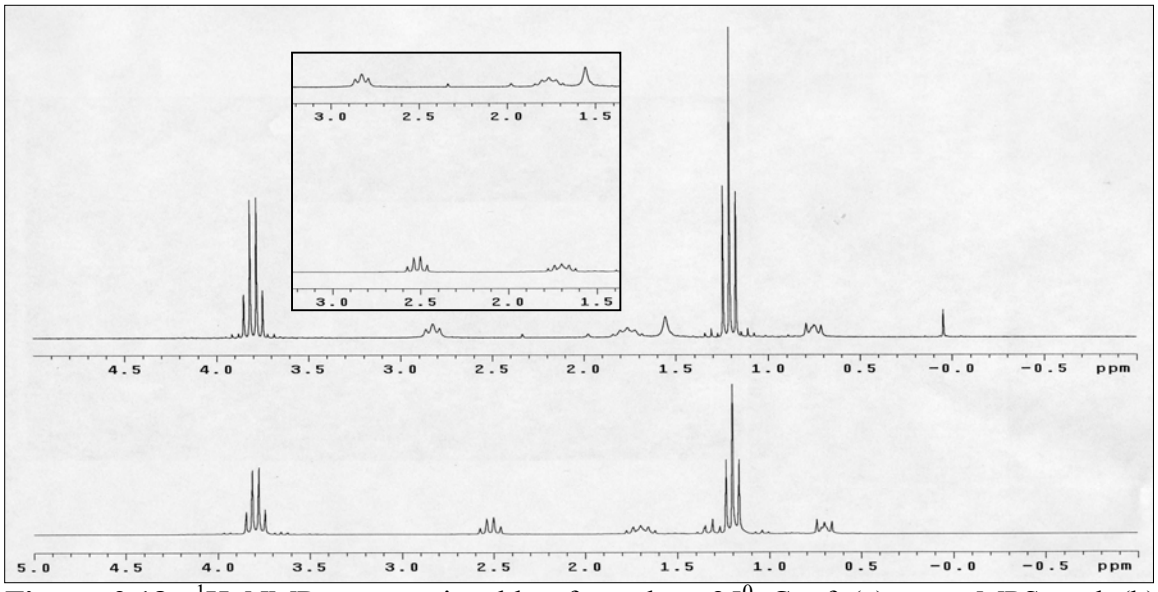


Figure 2.18: ^{1}H NMR spectra in chloroform-d at 25^{0} C of (a) pure MPS and (b) complexed MPS in toluene when the AgOAc: MPS ratio was 1:1.

From the above NMR spectra it is obvious that not all the MPS molecules are involved in complexation with the silver ions in solution. The solid mass was also analyzed by TGA under N_2 atmosphere. Figure 2.20 represents the thermogravimetric analysis of MPS capped silver ion. Considering the initial slow change in weight, the TG curve shows a sharp weight loss at 180-230 ^{0}C. Since the boiling point of MPS is at 210 ^{0}C, the above weight loss can be attributed due to the loss of the thiol molecule.

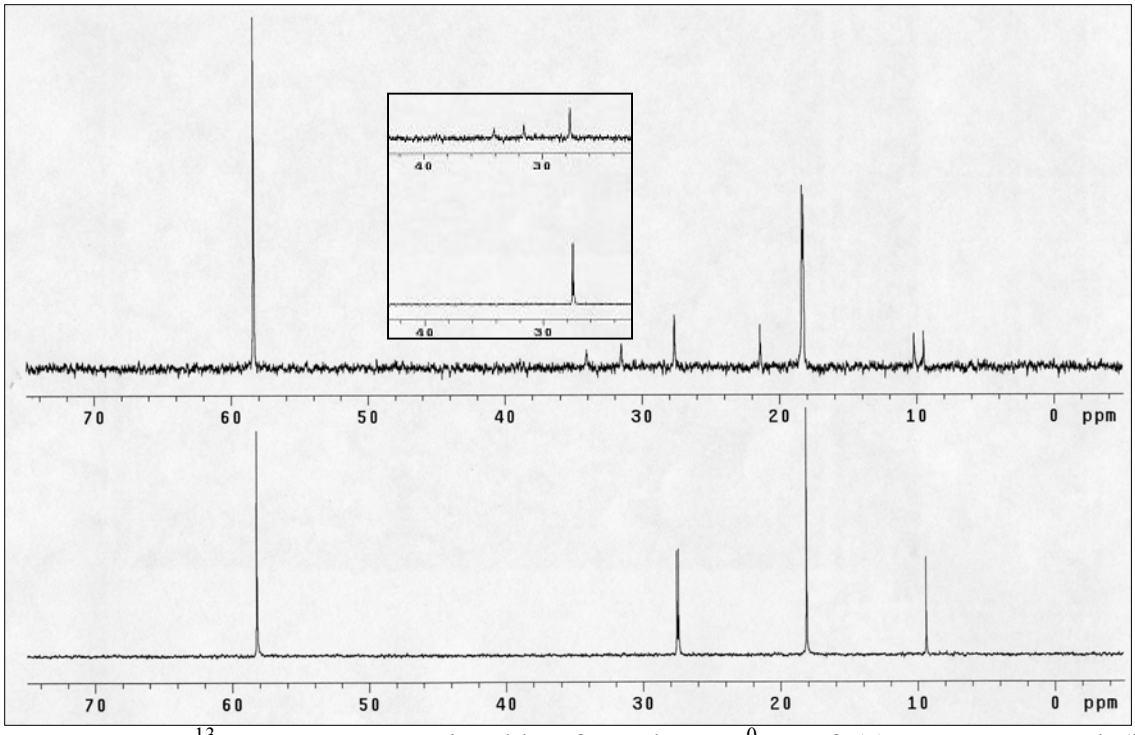


Figure 2.19: ^{13}C NMR spectra in chloroform-d at 25^0 C of (a) pure MPS and (b) complexed MPS in toluene when the AgOAc: MPS ratio was 1:2.

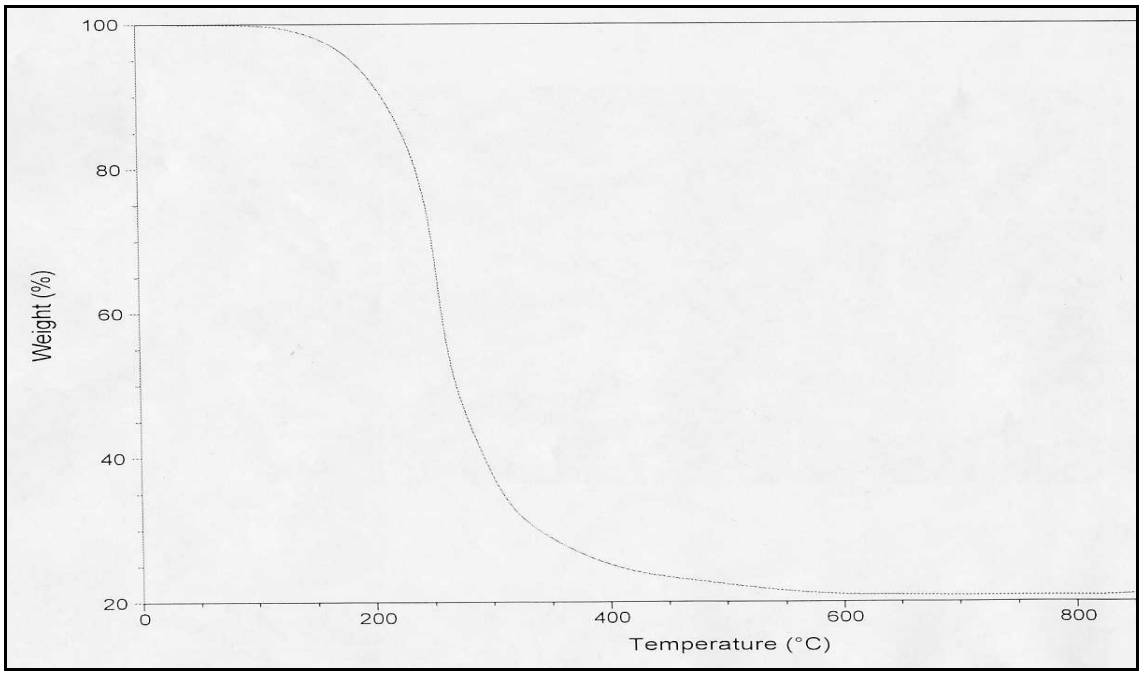
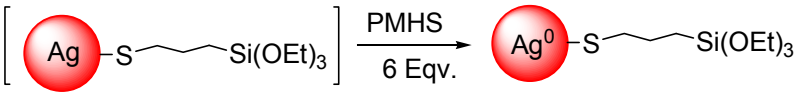


Figure 2.20: TGA of Silver-MPS complex.

2.8.2 Reduction of Ag-thiol complex by PMHS



Scheme 2.3: Reduction of silver thiol complex by PMHS to thiol functionalized silver nanoparticles.

The reduction of silver-MPS complex was carried out with different amount of PMHS at room temperature. We have already reported[7c] that the reduction of metal salt to metal nanoparticles is greatly influenced by the concentration of the reducing agent, PMHS. In the standardized procedure, 1.2 mmol (0.072 ml) of PMHS was added to the colorless silver-MPS solution. 30 minutes after the addition of PMHS, the color of the solution turned to golden yellow. The solution was then left at room temperature. After 12h, the color of the solution turned dark brown. The dark brown color solution exhibited a UV-vis absorbance in the ~ 480 nm region. The brown solution was then deposited on a copper grid and dried at ambient temperature and analyzed by TEM. The average particle size was found to be 2.9 nm with standard deviation 0.7 nm.

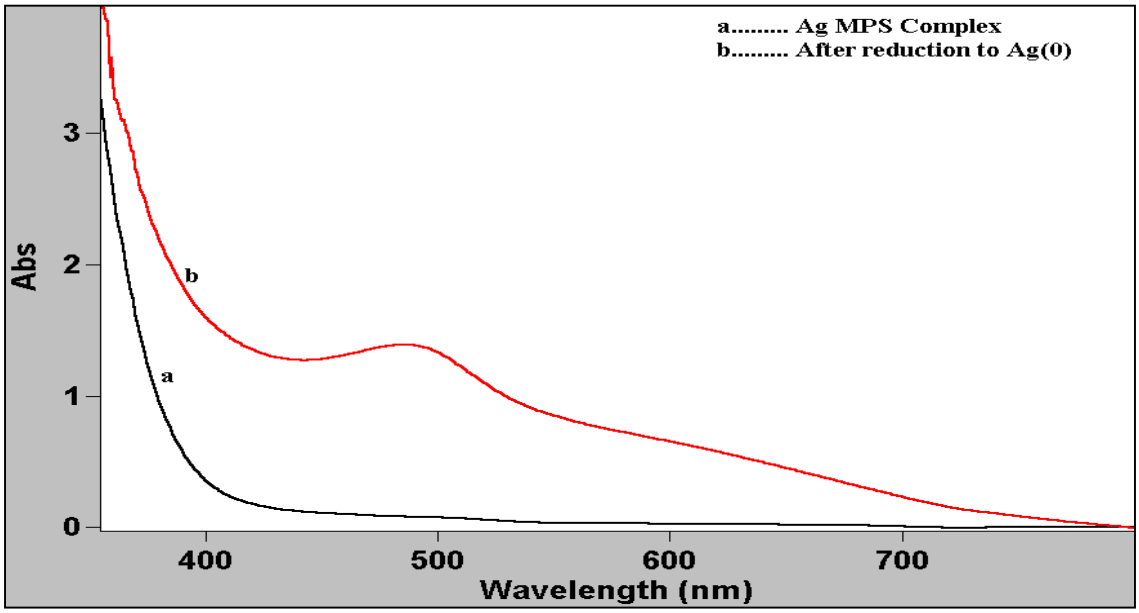


Figure 2.21: UV-vis spectra of MPS stabilized silver nanocrystals synthesized by in-situ reduction method.

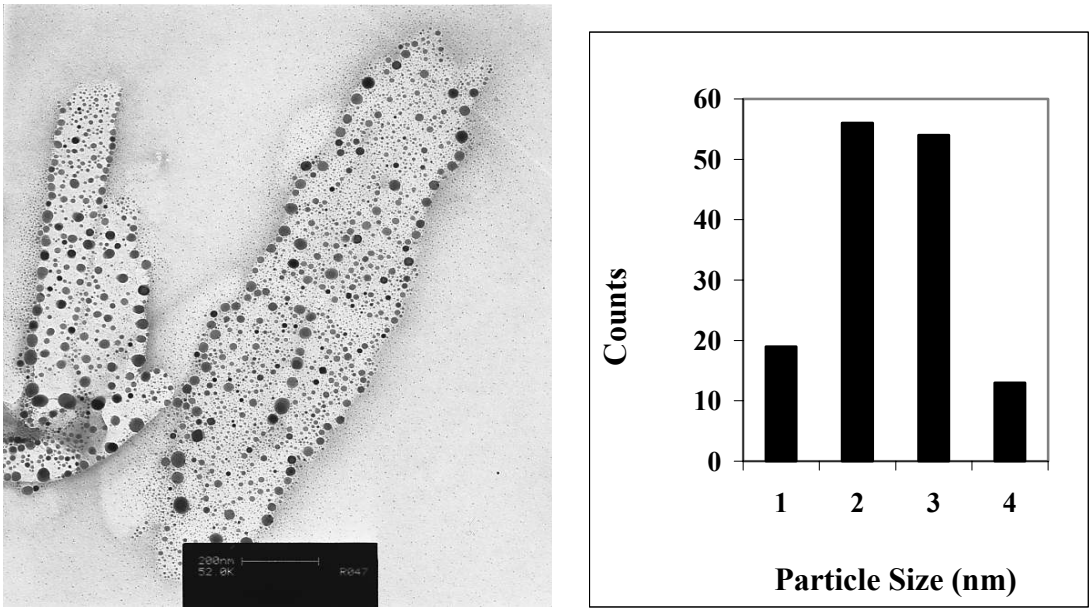
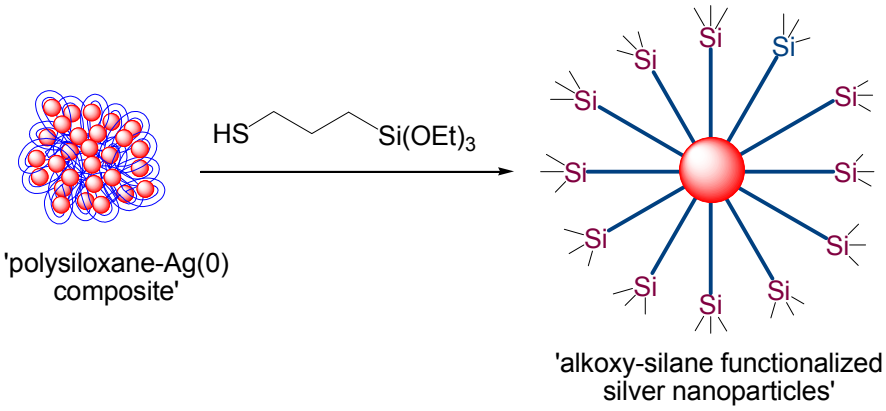


Figure 2.22: TEM and corresponding histogram of MPS stabilized silver nanocrystals synthesized by in-situ reduction method.

2.8.3 Thiol capped Ag(0) with different topologies



Scheme 2.4: Functionalization of presynthesized silver nanoparticles by MPS.

The ex-situ synthesis of thiol stabilized silver nanoparticles was also prepared in toluene. By using our standardized procedure,[16] the polysiloxane stabilized silver nanoparticles were synthesized in toluene (when TOA was in catalytic amount). To that solution different concentrations of MPS was added to investigate the occurrence of morphological changes of silver nanoparticles. It was found that a noticeable decrease in the concentration of silver led to a dramatic change in the shape of the particles. When the silver sols were synthesized in toluene, the average particle size was 2- 3 nm and it was a yellow color solution. After the addition of the capping agent to this solution, an optical change of the solution was also observed. After addition of thiol (MPS), the reaction mixture was monitored using UV- vis spectroscopy and the absorbance of the solution decreased with a 30 nm red shift. Before addition of thiol, the polysiloxane stabilized Ag(0) displayed an absorbance at 435 nm region. When MPS was added (Ag^0: MPS concentration was 1: 4), the color of the solution changed from yellow to light yellow.

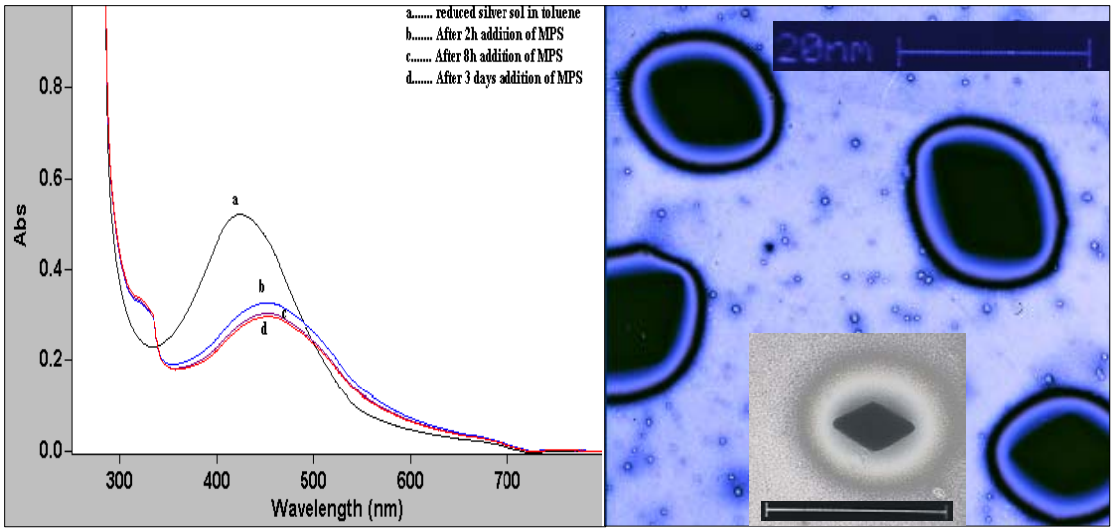


Figure 2.23: UV-vis spectra and TEM of MPS stabilized silver nanocrystals synthesized by ex-situ reduction method after 12h, when AgOAc: PMHS: MPS concentration was 1:6:4. Scale bar is 100 nm.

The absorbance of the solution still decreased until 8h of the thiol addition. After 3 days the solution was again monitored using UV-vis spectroscopy and it showed the same absorbance as it did after 8h of reaction; see Figure 2.23. The literature indicates that in the presence of thiol, the plasmon band of silver nanoparticles decreases in intensity and becomes broader with a red shift of the absorption maxima (λ_{max}).[30] Nothing is known at the present time about the nature or cause of this damping. The decrease in the UV-vis absorbance of the MPS stabilized Ag(0) can be attributed to the fact that the thiol group strongly interact with the nanoparticle surface which suppresses the collective oscillation of the silver nanoparticles. By observing the changes in the shape of the absorption band, one can determine whether adsorption of an additive has occurred. The changes can be brought about either because of changes in the refractive index of the medium surrounding the metal particles or because the dielectric property of the metal particles themselves are changed by chemisorption.

The reaction mixture (after 8h of addition of thiols) was then deposited on the TEM grid and dried at room temperature to investigate its morphology. Surprisingly, individual nanoparticles, as observed when synthesis was carried out in the presence of catalytic amounts of TOA, did not exist and instead were converted to silver nanocubes. In a recent paper,[31] the authors have mentioned that, when silver nanocubes were formed in water, there was no significant change of the surface plasmon excitation band in the UV-vis absorption spectroscopy respect to spherical silver nanocrystals. When 2 equivalent of MPS was added to the yellow color Ag(0) solution, we have observed the silver particle filled nanotubes. In this case the average particle size was in the range of 2-3 nm. This phenomenon indicates that, with an increase in the amount of capping agent, (MPS), the Ag(0) will be released from the polysiloxane shell and stabilized by the thiol group resulting in different morphologies.

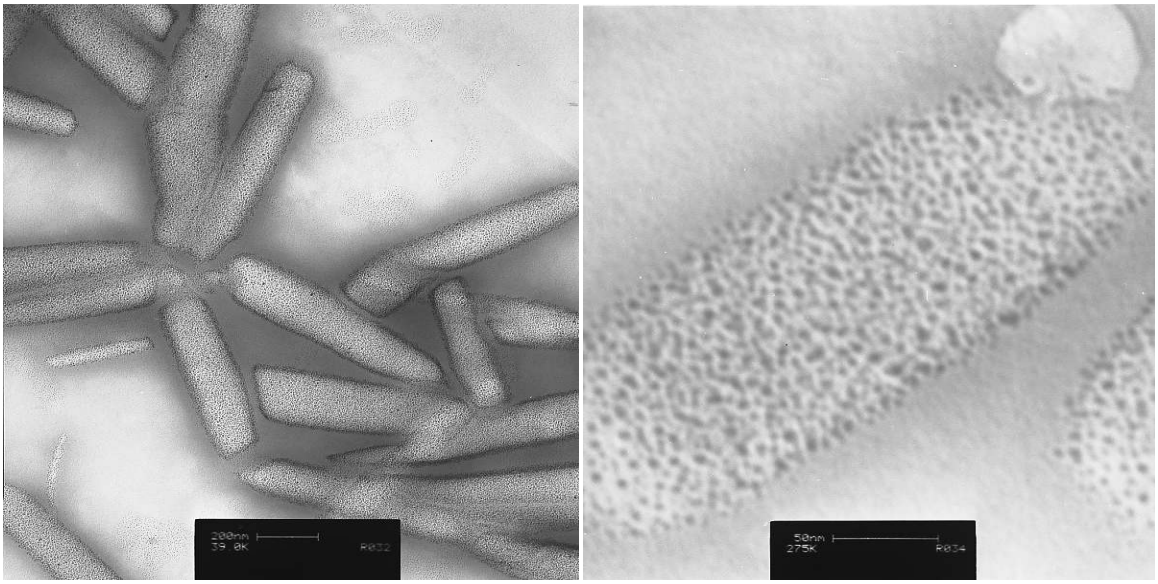


Figure 2.24: TEM of MPS stabilized silver nanocrystals synthesized by ex-situ reduction method after 12h, when AgOAc: PMHS: MPS concentration was 1:6:2.

2.9 Conclusions

In this section we have discussed the synthesis of functionalized silver nanoparticles. The method provided us the opportunity to obtain different orientations of silver nanoparticles in solution. We believe that this method is general and will be useful for synthesis of silane functionalized noble or magnetic nanoparticles. We expect that the siloxane group can be further used to graft other functional molecules for applications such as biolabelling,[32] and also in the fabrication of electronic devices.[33]

2.10 Experimental section

Chemicals:

Silver nitrate, silver perchlorate, silver tetrafluoroborate, silver heptafluorobutyrate, trioctylamine (TOA), and polymethylhydrosiloxane (PMHS, Mw = 2000, 33-35 Si-H units) were obtained from Aldrich Chemical Company and were used as received without further purification. Toluene, THF, and hexane were obtained from Fisher Scientific Company and distilled by using Innovative Technology instrument before being used. All the reactions were carried out at room temperature under positive pressure of nitrogen.

Characterization of Silver Nanoclusters:

UV-Visible absorption studies were carried out with a Varian Cary 50-scan spectrophotometer in a10-mm optical path length quartz cuvettes. The TEM micrographs were obtained with the help of a Philips CM-100 instrument operating at 80 Kv accelerating voltage. The10 μl centrifuged reaction mixture was deposited on a formver coated copper carbon grid, 150 mesh (Electron Microscopy Science, Port Washington,

PA) and allowed to dry at ambient temperature. The crude reaction mixtures were centrifuged for 10 minutes before deposition on the grid. Particle size analysis was performed with the use of the Scion Image Beta 4.02 Software (available on the Internet at http://www.scioncorp.com). Images, which have 100 nm scale bar, was chosen to do the particle size analysis. In Scion Image, after setting the unit and known distance the 'Analyze Particle' parameter was used to generate a table of particle diameter. This table was then exported into Microsoft Excel 2000 where statistical analysis and histogram plotting were performed. The AFM experiments were performed in tapping mode, using a silicon tip (CSC-12, molecular imaging, Tempe, AZ) under air and at room temperature by using Pico Scan plus instrument. For sample preparation, one drop of centrifuged reaction mixture was spin coated for 20 sec on 3000 r.p.m speeds on a clean mica surface and allowed to air dry for 3h.

Synthesis of Silver Nanoparticles:

Silver salt (0.2 mmol) suspension was prepared in 50-ml of toluene and stirred for 0.5h at room temperature. To this suspension, 1.2 mmol of PMHS (0.072 ml, 6 equiv) was added and continued stirring for another 0.5h, during which the color of the solution was changed from colorless to faint yellow. At this juncture TOA (0.05-6 equiv), was injected to the reaction mixture with constant stirring. After the additional stirring of another 1-3h, the color reaction mixture changes from dark yellow to yellowish brown. The formation of silver nanoparticles is monitored by UV-vis spectroscopy at different time intervals. At the highest absorption point, the stirring was stopped and the total solution was centrifuged. One drop of centrifuged solution was deposited on the TEM grid for morphology analysis. For silver nitrate reduction all the reactions were performed in the

dark by covering the round bottom flask with aluminum foil to avoid the possibility of photolytic reactions.

Preparation of Silver- Marcaptosilane Complex:

In a 500 ml round bottom flask, 50 ml AgOAc (0.032 gm, 0.2 mmol) suspension was prepared in toluene. The suspension was stirred vigorously at room temperature for 30 minutes. After 30 minutes of stirring, MPS (0.046 ml, 0.2 mmol) was injected to the reaction vessel. The stirring was continued for one more hour. At this point, it was a clear homogeneous solution. The clear solution was analyzed by UV-vis spectroscopy, but no peak was detected. The total solution was evaporated under high vacuum. After complete evaporation it was a light yellow color solid, which was redissolved in $CDCl_3$ for ^{1}H and ^{13}C NMR analysis. The yellow color solid was also analyzed by TGA. In the similar fashion and same reaction condition, different ratio of Ag: MPS was also investigated. The reaction mixture in each case was also analyzed by ^{1}H and ^{13}C NMR spectroscopy.

Synthesis of Thiol Stabilized Silver Nanoparticles by In-Situ Reduction:

After synthesis of silver-mercaptosilane complex, at room temperature. PMHS (0.072 ml, 1.2 mmol) was injected into the reaction mixture with constant stirring and it was continued for another 5 minutes. With 30 minutes of the addition of PMHS the color of the solution was turned to golden yellow. The solution was then left at room temperature. After 12h, the color of the solution turned to dark brown. The solution was then deposited on the copper grid and dried at ambient temperature. It was then analyzed by TEM The average particle size was 2.9 nm with standard deviation of 0.7 nm. The crude solution was also analyzed by UV-vis and IR spectroscopy.

Preparation of MPS stabilized Silver Sol by Ex-situ Method:

To the presynthesized Ag^0 solution,[16] MPS (0.18 ml, 0.8 mmol) was added with gentle stirring. There was no significant color changes were observed after immediate addition of MPS. The solution was then monitored by UV-vis spectroscopy in every 2h of interval. It was observed that after 8h of the addition of MPS, the peak position was constant. From this solution one drop was deposited on the copper grid for morphological analysis.

2.11 References

(1). (a) Ozin, G. A. *Adv. Mater*, **1992**, *4*, 612. (b) Alivisatos, A. P. *J. Phys. Chem*. **1996**, *100*, 13226. (c) Belloni, J. *Curr. Opin. Colloid Interface Sci.* **1996**, *2*, 184. (d) Brus, L. *Curr. Opin. Colloid, Interface Sci*. **1996**, *2*, 197. (e). Banin, U.; Lee, J. C.; Guzelian, A. A.; Kadavanich, A. V.; Alivisatos, A. P. *Superlattices Microstruct*. **1997**, *22*, 559. (f). Fendler, J. H.; Meldrum, F. C. *Adv. Mater*. **1995**, *7*, 607. (g) Bonnemann, H.; Richards, R. M. *Eur. J. Inorg. Chem*. **2001**, 2455.

(2). Mostafavi, M.; Marignier, J.L.; Amblard, J.; Belloni, J. *Radiat. Phys. Chem*. **1989**, *34*, 605.

(3). Matejka, P.; Vlckiva, B.; Vohlidal, J.; Pancoska, P.; Baumrunk, V. *J. Phys. Chem*. **1992**, *96*, 1361.

(4). (a) Sun, T.; Seff, K. *Chem. Rev*. **1994**, *94*, 857. (b) Verykios, X. E.; Stein, F. P.; Coughlin, R. W. *Catal. Rev.-Sci. Eng*. **1980**, *22*, 197.

(5). (a) Weller, H.; *Angew. Chem. Int. Ed. Engl*. **1993**, *32*, 41. (b) Schmidt, G. *Chem. Rev*. **1992**, *92*, 1709.

(6). (a) Karim, A.; Yurkeli, K.; Meredith, C.; Amis, E.; Krishnamoorti, R.; *Polym. Eng. Sci.* **2002**, *42*, 1836. (b) Schmidt, G.; Malwitz, M. M. *Curr. Opin. Colloid, Interface Sci*. **2003**, *8*, 103 and references therein. (c) Grohn, F.; Kim, G.; Bauer, A. J.; Amis, E. J. *Macromolecules* **2001**, *34*, 2179. (d) Crooks, R. M.; Zhao, M.; Sun, L.; Yeung, L. K. *Acc. Chem. Res*. **2001**, *34*, 181. (e) Jansen, J. F. G. A.; de Brabander-van den Berg, E. M. M.; Meijer, E. W. *Science* **1994**, *266*, 1226.

(7). (a) Chauhan, B. P. S.; Rathore, J. S.; Bandoo, T. *J. Am. Chem. Soc*. **2004**, *126*, 8493. (b). Chauhan, B. P. S.; Rathore, J. S.; Chauhan, M.; Krawicz, A. *J. Am. Chem. Soc*. **2003**, *125*, 2876. (c) Chauhan, B. P. S.; Rathore, J.; Sardar, R.; Tewari, P.; Latif, U.; *J. Organometal. Chem*. **2003**, *686*, 24. (d) Chauhan, B. P. S.; Sardar, R.; Tewari, P.; Sharma, P. Third International Workshop on Silicon-Containing Polymers, Troy, ISPO 2003, June 23-25, T-13.

(8). Lewis, L. N. *Chem. Rev*. **1993**, *93*, 2693 and references therein.

(9). (a) Ganicz, T.; Stanczyk, W. A. *Prog. Polym. Sci*. **2003**, *28*, 303. (b) Stucky, G. D.; Mcdougall, J. E. *Science* **1990**, *247*, 699.

(10). UV-vis absorption spectroscopy has been proved to be quite sensitive to elucidate the formation of silver colloids. An intense absorption peak at around 400-440 nm is generally observed and attributed to the surface plasmon absorption of Ag nanoparticles. Such resonance occurs when the incident photons frequencies match with the collective oscillations of the metal nanoparticles.

(11). (a) Corriu, R. J. P.; Lanneau, G. F.; Perrot, M. *Tetrahedron Lett*. **1988**, *29*, 1271. (b) Corriu, R. J. P.; Lanneau, G. F.; Perrot, M.; Mehta. V. D. *Tetrahedron Lett*. **1990**, *31*, 1585.

(12). (a) Sau, T. K.; Murphy, C. J. *J. Am. Chem. Soc*. **2004**, *126*, 8648. (b) Sun, Y.; Xia, Y. *Adv. Mater*. **2003**, *15*, 695. (b) Chen, S.; Carroll, D. L.; *Nano. Lett.* **2002**, *2*, 1003. (c) Jin, R.; Cao, Y.C.; Mirkin, C. A.; Kelly, K. L.; Schatz, G. C.; Zheng, J. G. *Science* **2001**, *294*, 1901. (d) Sun, Y.; Xia, Y. *Science* **2002**, *298*, 2176. (e) Ahmadi, T. S.; Wang, Z. L.; Green, T. C.; Heglein, A.; El-Sayed, M. A. *Science* **1996**, *272*, 1924. (f) Chen, J.; Herricks, T.; Geissler, M.; Xia, Y. *J. Am. Chem. Soc*. **2004**, *126*, 10854. (g) Puntes, V. F.; Krishnan, K. M.; Alivisatos, A. P. *Science* **2001**, *291*, 2115. (h) Ghezelbash, A.; Sigman, M. B.; Korgel, B. A. *Nano. Lett*. **2004**, *4*, 537. (i) Sun, Y.; Mayers, B.; Xia, Y. *Nano. Lett*. **2003**, *3*, 675. (j) Yu, D.; Yam, V. W.-W. *J. Am. Chem. Soc*. **2004**, *126*, 13200. (k) Jin, R.; Egusa, S.; Schere, N. F. *J. Am. Chem. Soc*. **2004**, *126*, 9900. (l) Jin, R.; Cao, Y. C.; Metraux, G. S.; Schatz, G. C.; Mirkin, C. A. *Nature* **2003**, *425*, 487.

(13). (a) Klingelhofer, S.; Heitz, W.; Greiner, A.; Oestreich, S.; Forster, S.; Antonietti, M. *J. Am. Chem. Soc.* **1997**, *119*, 10116. (b) Maclachlan, M. J.; Ginzburg, M.; Coombs, N.; Coyle, T. W.; Raju, N. P.; Greedan, J. E.; Ozin, G. A.; Manners, I. *Science* **2000**, *287*, 1460. (c) Walker, C. H.; John, J. V. S.; Wisian-Neilson, P. *J. Am. Chem. Soc.* **2001**, *123*, 3846. (d) Mossmer, S.; Spatz, J. P.; Moller, M.; Aberle, T.; Schmidt, J.; Burchard, W. *Macromolecules* **2000**, *33*, 4791. (e) Corbierre, M. K.; Cameron, N. S.; Sutton, M.; Mochrie, S. G. J.; Lurio, L. B.; Ruhm, A.; Lennox, R. B. *J. Am. Chem. Soc.* **2001**, *123*, 10411.

(14). (a) Kim, B.; Tripp, S. L.; Wei, A. *J. Am. Chem. Soc.* **2001**, *123*, 7955. (b) Son, S. U.; Jang, Y.; Yoon, K. Y.; Kang, E.; Hyeon, T. *Nano Lett.* **2004**, *4*, 1147. (c) Pal, T.; Sau, T. K.; Jana, N. R. *Langmuir* **1997**, *13*, 1481. (d) Chen, S.; Kimura, K. *J. Phys. Chem. B.* **2001**, *105*, 5397. (e) Tamura, M.; Fujihara, H. *J. Am. Chem. Soc.* **2003**, *125*, 15742. (f) Yang, J.; Deivaraj, T. C.; Too, H.-P.; Lee, J. Y. *J. Phys. Chem. B.* **2004**, *108*, 2181.

(15). Chauhan, B. P. S.; Rathore, J. S.; *J. Am. Chem. Soc.* **2005**, *127*, 5790.

(16). Chauhan, B. P. S.; Sardar, R. *Macromolecules* **2004**, *37*, 5136.

(17). Kim, H. S.; Ryu, J. H.; Jose, B.; Lee, B. G.; Ahn, B. S.; Kang, Y. S. *Langmuir* **2001**, *17*, 5817.

(18). (a) Finke, R. G. Transition-Metal Nanoclusters: Solution-Phase Synthesis, then Characterization and Mechanism of Formation, of Polyoxoanion- and Tetrabutylammonium-Stabilized Nanoclusters. *In Metal Nanoparticles: Synthesis, Characterization and Application*; Feldheim, D. L., Foss, C. A., Jr., Eds.; Marcel

Dekker: New York, 2002; Chapter 2, pp 17. (b) (a) Aiken, J. D., III; Finke, R. G. *J. Mol. Catal. A: Chem*. **1999**, *145*, 1.

(19). (a) Ozkar, S.; Finke, R. G. *Langmuir* **2002**, *18*, 7653. (b) Ozkar, S.; Finke, R. G. *J. Am. Chem. Soc*. **2002**, *124*, 5796.

(20). (a) Bu, X. H.; Xie, Y. B.; Li, J. R.; Zhang, R. H. *Inorg. Chem*. **2003**, *42*, 7422. (b) Sunderrajan, S.; Freeman, B. D.; Hall, C. K. *Ind. Eng. Chem. Res*. **1999**, *38*, 4051.

(21). Ebbing, D. D. General Chemistry; Houghton Mifflin Company: Boston, 1984.

(22). Blakeslee, A. E.; Hoard, J. L. *J. Am. Chem. Soc*. **1956**, *78*, 3029.

(23). Mark, J. E. *J. Chem. Edu*. **1981**, *58*, 898.

(24) (a) Harfenist, S. A.; Wang, Z. L.; Alvarez, M. M.; Vezmar, I.; Whetten, R. L. *J. Phys. Chem*. **1996**, *100*, 13904. (b) Ah, C. S. Han, H. S.; Kim, K.; Jang, D.-J. *J. Phys. Chem. B* **2000**, *104*, 8153. (c) Thomas, K. G.; Kamat, P. V. *Acc. Chem. Res*. **2003**, *36*, 888.

(25) (a) Lin, S. Y.; Tsai. Y. T.; Chen, C. C.; Lin, C. M.; Chen, C. H. *J. Phys. Chem. B* **2004**, *108*, 2134. (b) Shon, Y. S.; Cunter, E. *Langmuir* **2004**, *20*, 6626.

(26) Quaroni, L.; Chumanov, G. *J. Am. Chem. Soc*. **1999**, *121*, 10642.

(27) Brust, M.; Walker, M.; Bethell, D.; Schiffrin, D. J.; Whyman, R. *J. Chem. Soc. Chem. Commun*. **1994**, 801.

(28) Bonnemann, H.; Brijoux, W.; Brinkmann, R.; Fretzen, R.; Joussen, T.; Koppler, R.; Korall, B. K.; Neiteler, P.; Richter, J. *J. Mol. Catal*. **1994**, *86*, 129.

(29) Salgueirino-Maceira, V.; Caruso, F. Liz-Marzan, L. M. *J. Phys. Chem. B* **2003**, *107*, 10990.

(30) (a) linnert, T.; Mulvaney, P.; Henglein, A. *J. Phys. Chem*. **1993**, *97*, 679. (b) Henglein, A. *J. Phys. Chem*. **1993**, *97*, 5457.

(31) Yu, D.; Yam, V. W.-W. *J. Am. Chem. Soc*. **2004**, *126*, 13200.

(32) Bruchez, M.; Moronne, M.; Gin, P.; Weiss, S.; Alivisatos, A. P. *Science* **1998**, *281*, 2013.

(33) Chen, J.; Wang, W.; Klemic, J.; Reed, M.-A.; Axelrod, B. W.; Kaschak, D. M.; Rawlett, A. M.; Price, D, W.; Dirk, S. M.; Tour, J. M.; Grabisha, D. S.; Bennett, D. W. *Molecular Electronics II* **2002**, *960*, 69.

Chapter 3

Monohydrosiloxane Induced Formation of Noble Metal Nanoparticles: A New Route to Self-Assembled Monolayers (SAMs)

Part A
Self-Assembled Monolayers (SAMs) of Silver Nanoparticles

3.1 Introduction

In the recent literatures, various methods have been described for synthesis of metal or semiconductor nanocrystals.[1-6] A growing number of synthetic routes [7-12] have been explored for the self-assembly of 2D and 3D nanocluster supperlattices processing long range structural order. Fabrication of such ordered nanocrystals shows their potential application in optical filters, microelectronic devices, and optical gratings.[13-14] In this context, silver nanoparticles are of great interest due to their role in photographic processes,[15] application in catalysis,[16] substrates for surface enhanced Raman spectroscopy (SERS),[17] and in the field of biology.[18] The surfactant has the ability to control the size and shape of the growing particles. Through charge transfer, the surface tension is lowered and the growth can be controlled. In addition, the ligand layer prevents the agglomeration of particles and maintains the minimum interparticle separation. The prerequisites for a self-assembly route in macrostructure preparation are (i) availability of stable building blocks of metallic nanoparticles with well characterized monodisperse particle size and shape (ii) the presence of suitable capping materials (ligands or linkers), that concomitantly allow interparticle assembly, and preserve domination of repulsive forces between building block nanoparticles over irreversible aggregation.

At present, the method by Brust [19] and its various modifications [20] are the most established schemes in the field, with only a few other reports for the preparation of monodisperse metallic nanoparticles.[21] The Brust method is a biphasic process for which both nucleation and growth can only be possible at the interface of the two liquid phases. The Brust method is the most widely adopted synthetic approach and it is therefore instructive to review the benefits and limitations of this technique: (i) generally synthetic process involves reduction of metal salts by $NaBH_4$ as a reducing agent. Because all of the four hydrogen atoms in the BH_4^- anion can take part in the reducing process, the resulting metal colloids are contaminated with borides.[22] and (ii) the size distribution is broad; the uniformity of size is necessary to obtain ordered assemblies. (iii) The resulting nanoparticles are coated with a monolayer of a covalently bound surfactant e.g. alkanethiol, which makes it difficult to carry out the surface modification and functionalization on nanoclusters surface. The capping materials should provide uniform protection of the surface without modification of essential structural and electronic properties of the nanoparticles. The strong ligand used for nanoclusters synthesis should be avoided because they fix the activity of the monomers at a very low level. To avoid the boron contamination in the monodisperse metal nanoparticles, and single-phase nucleation and growth process, it is very important to formulate a synthetic route, where silver nanoclusters can be prepared by using organically soluble soft reducing agent.

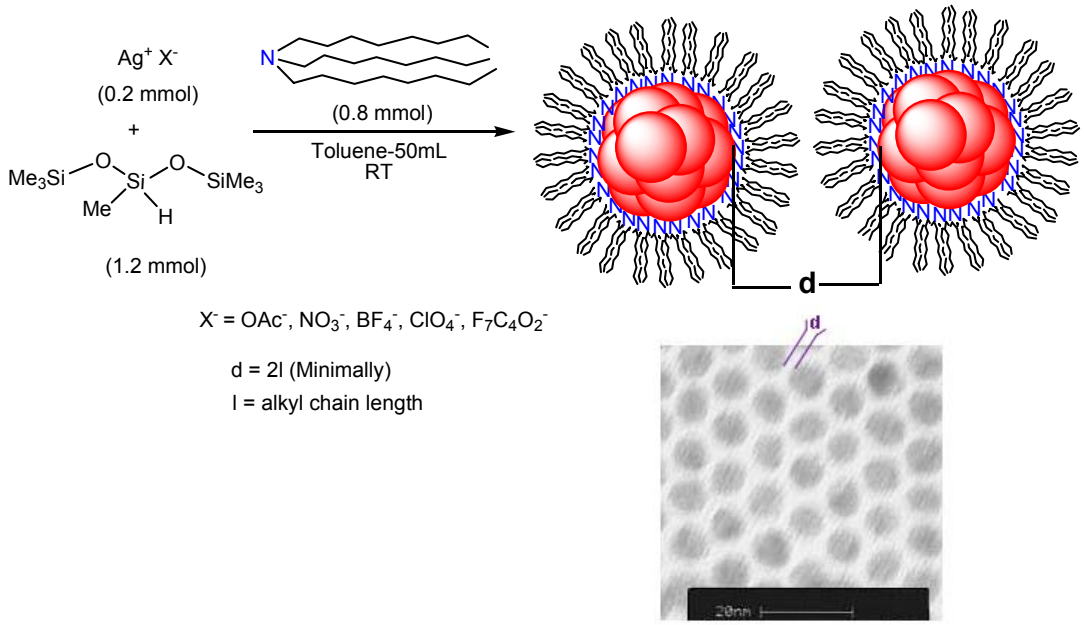
We have successfully investigated the reducing properties of polymethylhydrosiloxane (PMHS) for the reduction of different metal salts, such as silver, and palladium in organic solvent.[23] In chapter 2, we demonstrated how the property profile of siloxane polymers can influence the synthesis and morphology of

metal nanoparticles. In this chapter, we investigate the influence of the reducing polymer chain length on nanoparticle morphology, which broadens the scope of this synthetic approach.

Although the monomeric hydrosiloxane has been employed in the reduction of Pt or Pd metal complexes to generate nanosized particles,[6b] to date it has not been investigated as the reducing agent for silver nanoparticles synthesis demonstrated here. Hydrosiloxane monomers are promising candidates in such synthetic schemes because their property profile may provide the means of directing metallic particles into specific physiochemical environments in addition to their utility as reducing agent. In this chapter, we report for the first time, trioctylamine, (TOA), passivated one step in-situ synthesis of self-assembled monolayers (SAMs) of silver nanoparticles using heptamethyltrisiloxane (HMTS) as the reducing agent in toluene at room temperature. The synthetic approach described is applicable for most of the commercially available silver salts, AgX (X= AcO^-, NO_3^-, BF_4^-, ClO_4^-, and $F_7C_4O_2^-$). The synthesized SAMs show remarkable stability in organic solvent as well as when cast as films. The redispersibility studies are also possible on the synthesized 'silver-amine nanoconjugates' in toluene. The synthesized 2D nanoclusters also allow doing the solvent exchange for different organic solvents such as benzene, THF, cyclohexane and DCM, which opens up a new avenue for the product redispersion in a variety of organic solvents.

3.2 Results and Discussion: Formation of SAMs

The self-assembly process can be defined as the self-organization of components into structurally well-defined aggregates. In our approach, the synthesis of self-assembled monolayers of silver nanoparticles was carried out by a single step reduction of silver metal salts using HMTS in the presence of TOA. The reduction process is quite simple and was accomplished at room temperature. The yield of the synthesized particles was high and the self-assembled particles were stable in solution for greater than 3-4 weeks. The resulting solution leads to quantitative formation of self-assembled nanoparticles and unlike other methods, fractionation or any other purification steps were not required. No particle aggregation or precipitation was observed after long period of storage time. Scheme 3.1 represents the synthetic strategy for the formation of self-assembled monolayers of silver nanoparticles.



Scheme 3.1: Synthetic strategy to HMTS induced reduction of silver salts to self-assembled silver nanoparticles.

3.2.1 Synthesis of self-assembled monolayers

In a typical experimental procedure, a 50-ml toluene suspension of silver acetate was prepared at room temperature with constant stirring. After 10 minutes of stirring, HMTS (1.2mmol, 0.33mL) was injected. After another 10 minutes of stirring, TOA (0.8mmol, 0.35mL) was added and the reaction mixture was stirred at room temperature. After 30 minutes of addition of all the reagents, the mixture turned colorless to light yellow. At this stage the reaction progress was supervised by monitoring the absorbance change via UV-vis spectroscopy at different time intervals. After 2h of stirring, the color of the solution turned dark yellow and after that no increment of the absorption maxima in UV-vis spectra was observed. Under identical molar ratio and reaction conditions, reduction of other silver salts such as $AgNO_3$, $AgBF_4$, $AgF_7C_4O_2$, and $AgClO_4$ was investigated.

The following experiments were performed to study the formation of self-assembled ‘silver-amine nanoconjugates’ and their property profiling: (1) the kinetics of formation of silver nanoparticles was probed by monitoring UV-vis spectroscopy; (2) characterization studies by TEM; (3) redispersion studies of self-assembled 'silver-amine nanoconjugates' and (4) solvent exchange studies.

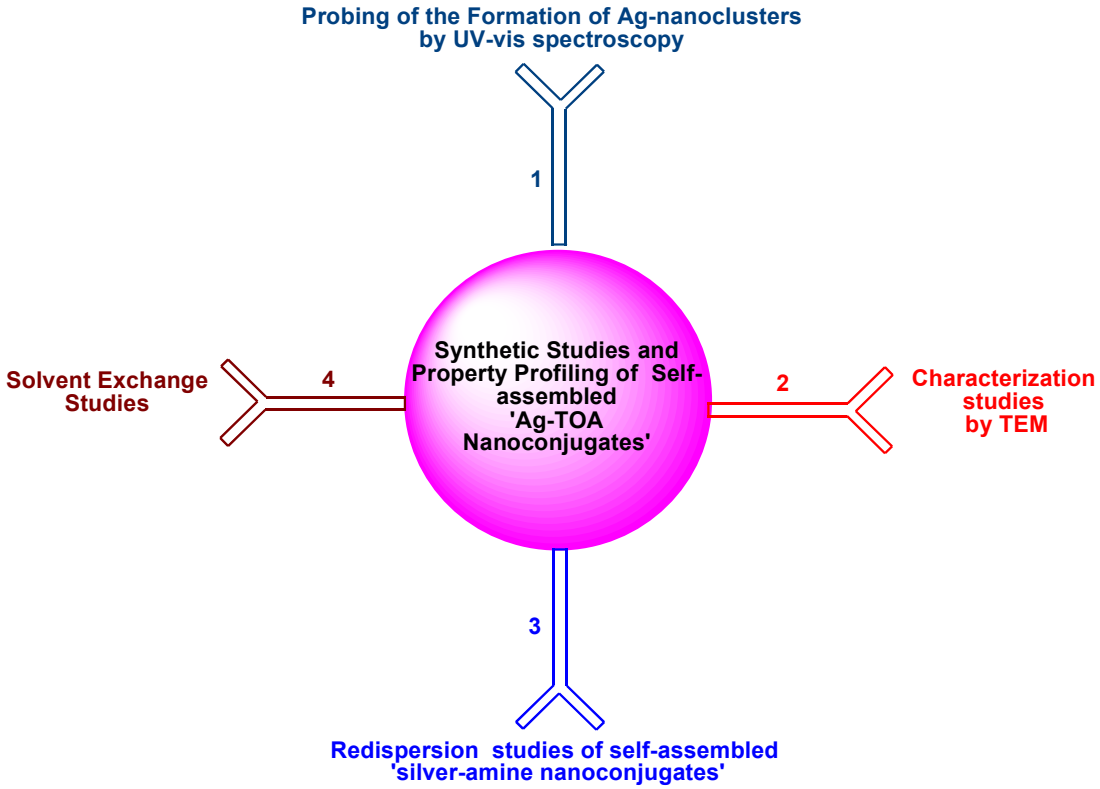


Figure 3.1: Schematic illustration of formation, characterization, and property profiling of self-assembled silver nanoclusters.

3.2.2 UV-vis absorption spectroscopy studies

When the silver acetate reduction was carried out using HMTS in the presence of TOA, 30 minutes after the addition of all the reagents, the color of the mixture turned yellow and evolution of the UV-vis absorption band (λ_{max}) at 450 nm was detected, which implied the formation of silver nanoparticles in solution. With respect to time an increase in the solutions absorbance, as well as, a λ_{max} blue shift was observed indicating that at the initial stage of reduction bigger particles were formed, which dissociates to smaller particles and form nano-ordered structures. After 2h of stirring, no other

noticeable spectral changes were observed and the dark yellow solution was stable for 6 months with a λ_{max} of 415 nm (Figure 3.2 A).

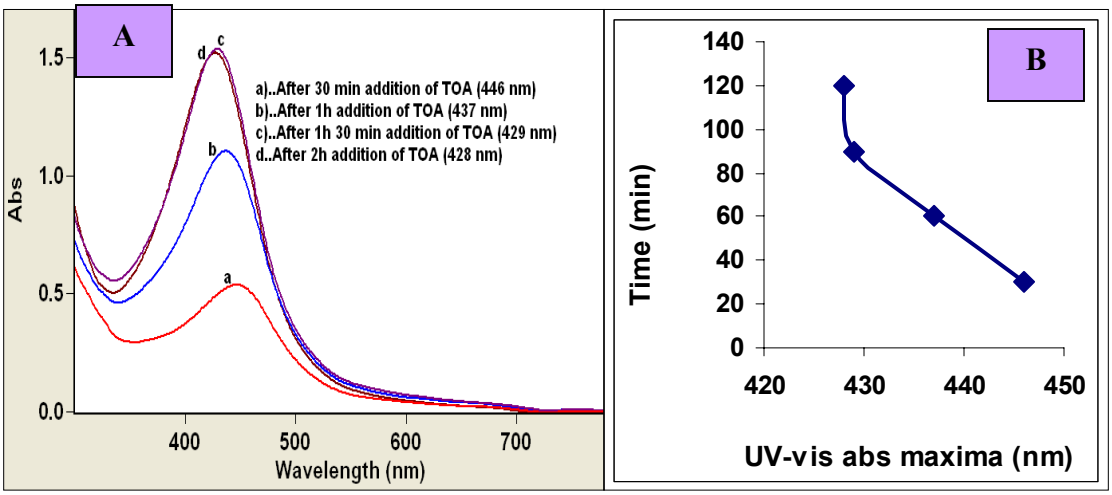


Figure 3.2: UV-vis absorption spectra (A) and the kinetics (B) of nanoparticle formation from silver acetate reduction.

The reduction of the other silver salts was carried out under similar conditions using identical molar ratios of reagents. In all cases, the final λ_{max} of each solution was observed to blue shift relative to the peak in absorption at the start of the synthesis. Such blue shifts are well established within the field of nanoparticles synthesis and are attributed to the surface plasmon absorption band. Figure 3.3 represents the time dependent UV-vis spectra of the reduction of different silver salts.

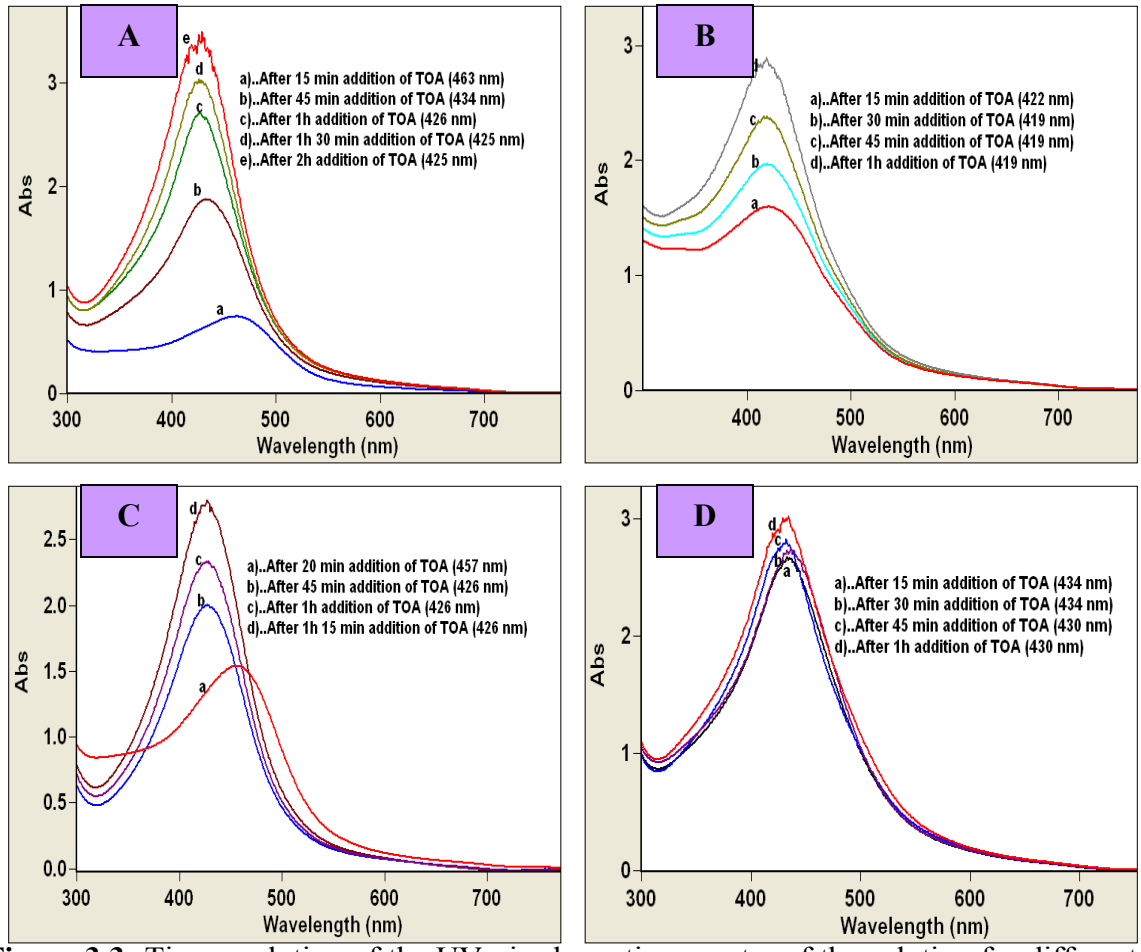


Figure 3.3: Time evolution of the UV-vis absorption spectra of the solution for different silver salts reduction; (A) $AgNO_3$ (B) $AgClO_4$, (C) $AgBF_4$, and (D) $AgF_7C_4O_2$.

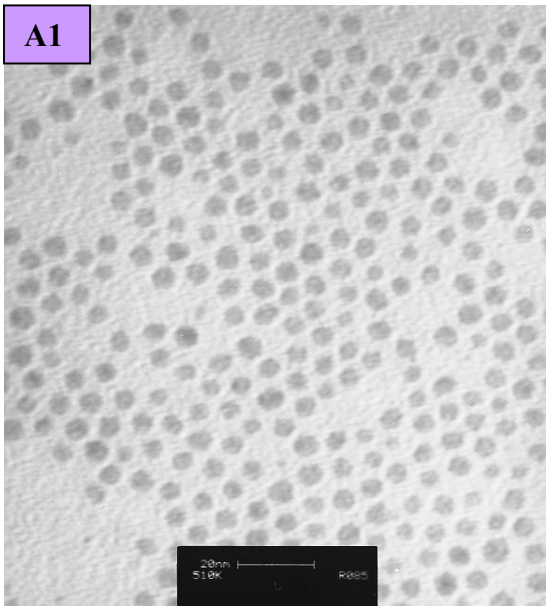
3.2.3 Characterization studies by TEM

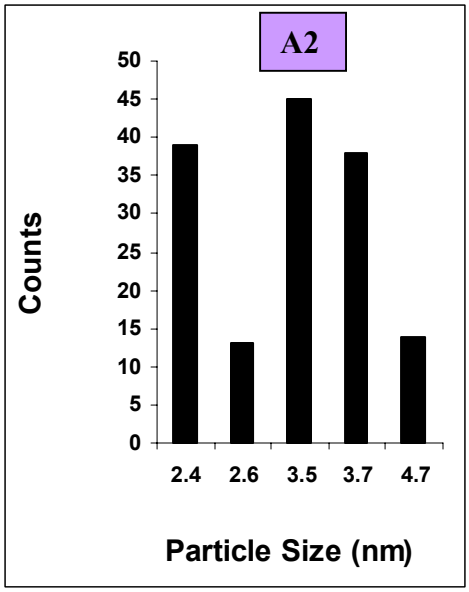
The size distribution and the morphology of the silver nanoparticles were determined by transmission electron microscopy. Figure 3.4. (A1) shows the electron micrograph obtained when silver acetate reduction was carried out in presence of TOA. Firmly uniform distributions of well-dispersed particles were obtained. The average particle size was 2.3 nm with standard deviation of 0.6 nm. The morphology for other silver salts such as $AgNO_3$, $AgBF_4$, $AgF_7C_4O_2$, and $AgClO_4$ were also investigated. In all

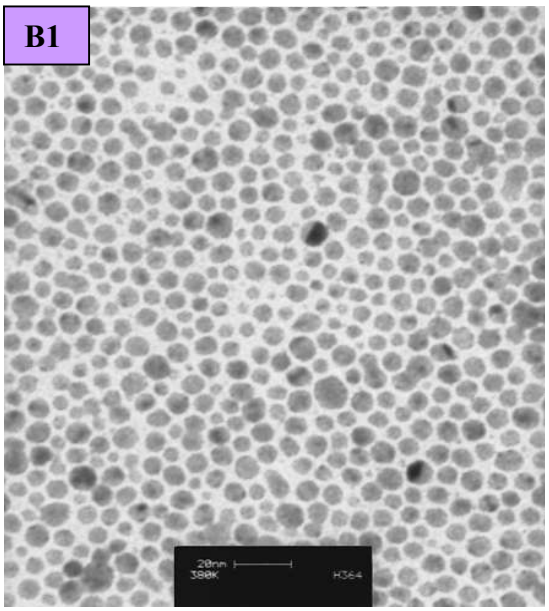
cases, the nanoparticles formed possessed similar, uniform size distributions. For comparison, the UV-vis spectral characteristics and particle size analysis is compiled in Table 3.1. When the silver nanoparticles were obtained from silver heptafluorobutyrate reduction, the TEM showed a remarkable degree of self- arrangement in regular arrays with a very uniform size distribution (3.9 ±0.3 nm). For instance, Figure 3.4 (D1) shows a typical two-dimensional stack in which the individual nanoparticles have acquired a pseudohexagonal close packed arrangement. The dimensional uniformity is generally achieved through a short nucleation period that generates all the particles at the end of the reaction followed by a self-sharpening growth process. Eventually almost monodisperse size distribution can be obtained at this stage by quenching the reaction quickly or by supplying capping group to keep a saturated condition during the course of the reaction. From UV-vis kinetic study of $AgF_7C_4O_2$ reduction (Figure 3.3.D), it is clear that 15 min after the addition of TOA, almost all the particles were formed and during the course of another 45 min, very slight increase in the absorption maxima was observed, which eventually leads to the uniform size distributions.

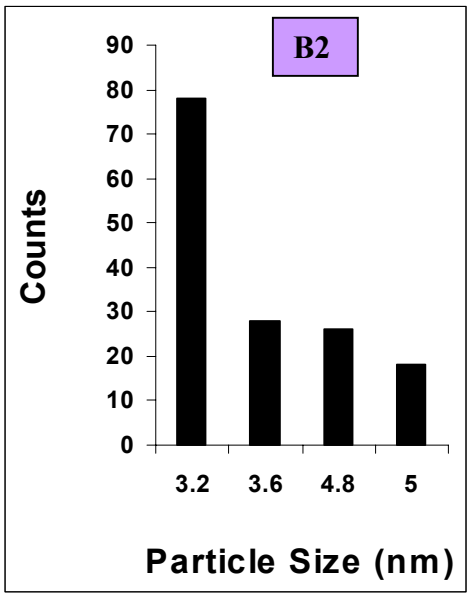
There are still gaps between the packed neighboring nanoparticles. It was observed that except silver heptafluorobutyrate, all the other salts resulted in a closed packed morphology of silver nanoparticles with 2.4-2.5 nm average spacing. The spacing was almost double the length of the TOA long hydrophobic alkyl chain. According to Bain's calculation,[24] the hydrocarbon length l = (0.25 + 0.127 n) nm, where n is the number of CH_2 groups; 0.25 nm takes into account the nitrogen and methyl terminated functional groups of trioctylamine, l = 1.2 nm.[25] The data presented suggests that each nanoparticle may be covered with a monolayer of the TOA molecules, most likely, with

its CH_2-N head group bound to the silver surface and its long alkyl hydrophobic chain faced outwards. It is the strong hydrophobic interactions between long alkyl chains on neighboring particles that probably cause the stacking of the nanoparticles. In case of $AgF_7C_4O_2$, the average interparticle spacing was 2.1 nm, which is approximately 0.3 nm shorter than the expected spacing between two particles. It indicates that TOA molecules are not oriented vertically at the silver nanoparticle surface but have an angle with the surface.









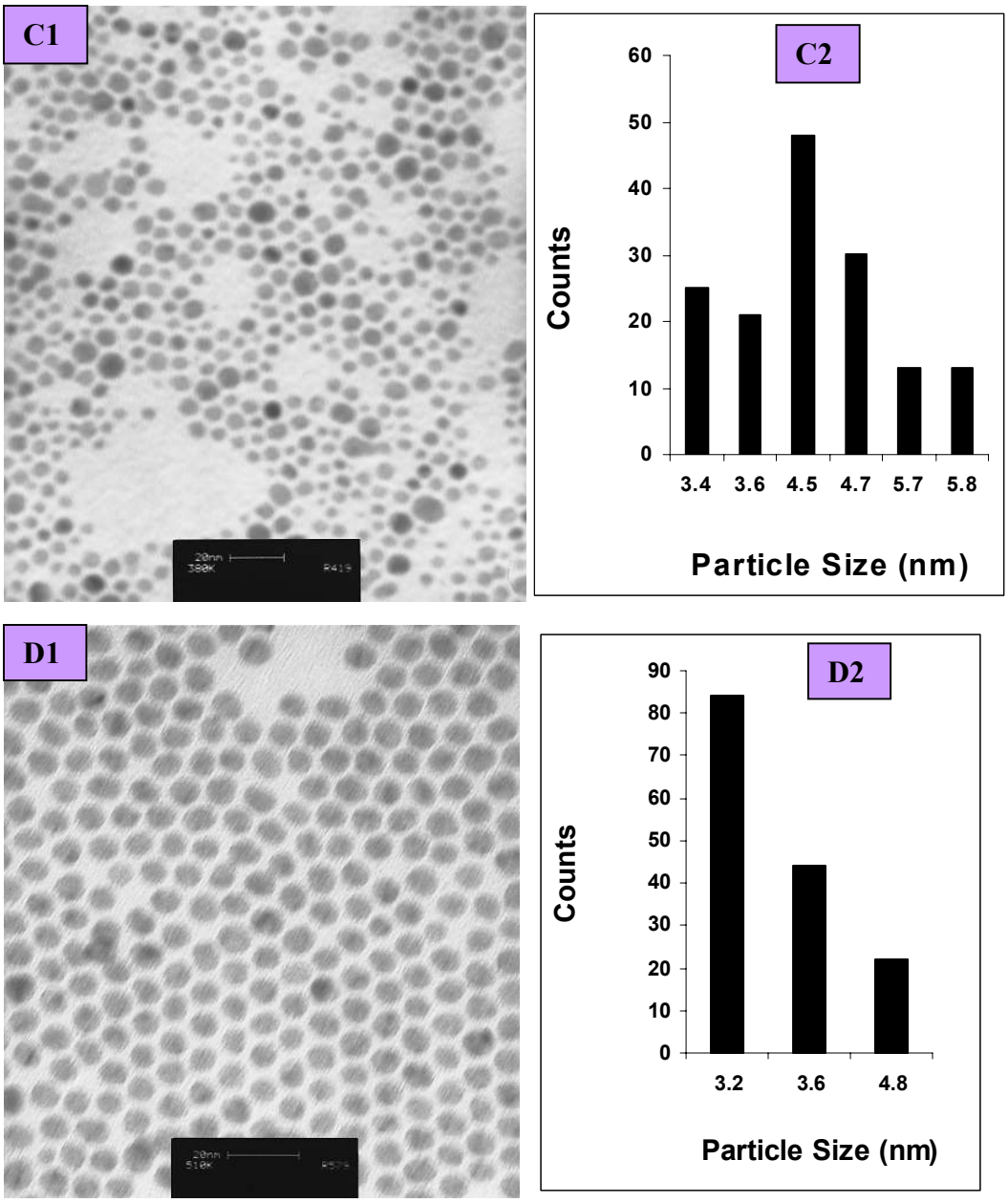


Figure 3.4: TEM micrographs and the corresponding histograms of self-assembled silver nanoparticles from different silver salts, silver acetate (A1, A2), silver nitrate (B1, B2), silver tetrafluoroborate (C1, C2), and silver heptafluorobutyrate (D1, D2) respectively.

Table 3.1. Comparison of UV-vis absorption maxima and particle size analysis of SAMs of different silver salts

Entry	Silver Salt	Reduction solution color	Absorption maxima (λ_{max}: nm)	Average particle Size[b](nm)	Int. particle spacing (nm)
1	AgOAc	Dark yellow	415-418 nm	3.3 (0.7)	2.4 (0.3)
2	$AgNO_3$	Reddish Brown	426-429 nm	3.7 (0.7)	2.5 (0.3)
3	$AgClO_4$	Dark Brown	420-424 nm	2.5 (0.4)	2.5 (0.2)
4	$AgBF_4$	Grey Brown	425-431 nm	4.4 (0.7)	2.4 (0.4)
5	$AgF_7C_4O_2$	Golden Brown	430-434 nm	3.9 (0.3)	2.1 (0.4)

3.2.4 Redispersion studies in organic solvents

It has been observed that the particle size, stability and morphology of metallic nanoparticles are strongly governed by the specific preparation method and experimental conditions applied. When solvents are removed from the metal nanoparticle surface, it is very difficult to redisperse the particles in the same solvent, even though the nanoclusters lose their activity and morphology. In this context, the amine stabilized self-assembled silver nanoparticles has given us the opportunity to explore the redispersion study in organic solvents. In a typical redispersion experiment, the 'silver-amine nanoconjugates' were prepared when $AgF_7C_4O_2$ (0.2 mmol, 0.064 gm) reduction was carried out in 50-ml toluene using HMTS (1.2mmol, 0.33mL) as a reducing agent in the presence of TOA (0.8mmol, 0.35mL). After 1h of reaction at room temperature, the UV-vis absorption

maxima was 430 nm and thereafter it remained constant. At this point, the total solution was evaporated using high vacuum resulting a brown color solid. The solid was then analyzed by X-ray photoelectron spectroscopy (XPS) for surface analysis because of the solvent evaporation, the surface of silver nanoparticles may be oxidized. Figure 3.5 shows the XPS spectrum obtained from brown solid. The signals of the XPS spectrum indicate the presence of C, Ag, and Si in the synthesized silver nanoparticles. A high resolution scan over the range 364-380 eV reveals a doublet of the Ag $3d_{5/2}$ peaks at 368.4 eV and the Ag $3d_{3/2}$ peaks at 374.4 eV corresponding to a peak to peak separation of 6 eV due to the presence of Ag^0. The line shapes and the peak-to-peak distance of the silver doublet are standard measurement of the silver zero oxidation state.[26]

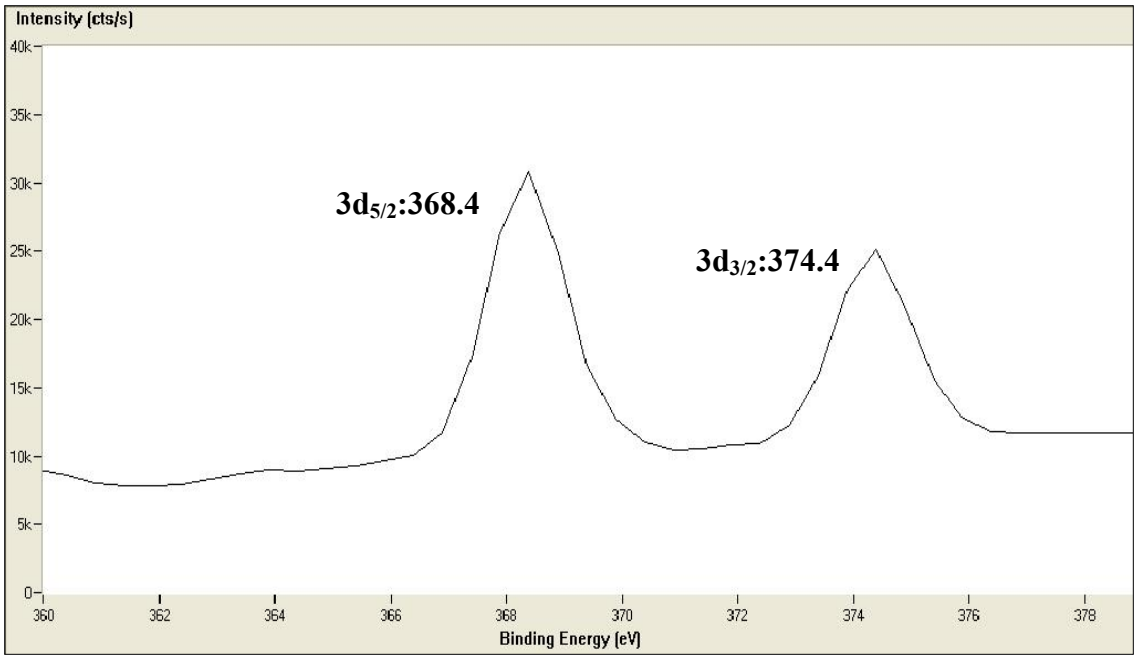


Figure 3.5: X-ray photoelectron spectra of the Ag 3d transition.

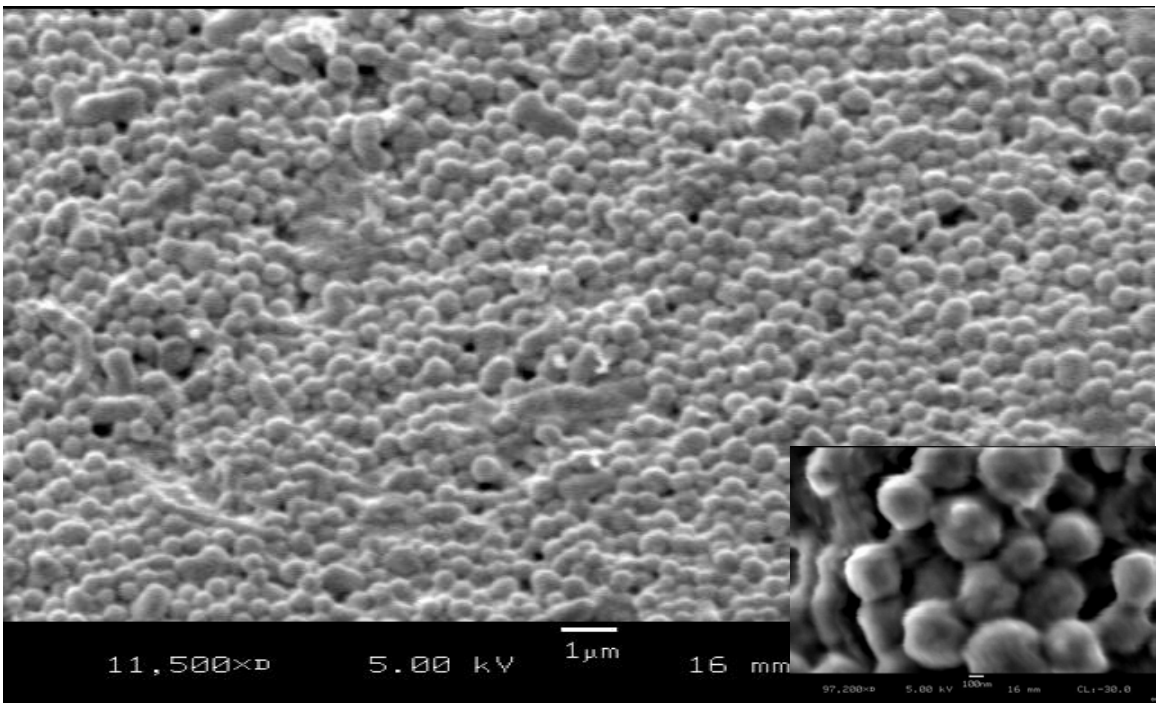


Figure 3.6: SEM image of the solid product after solvent evaporation.

Prior to the product being dispersed in solvents, it was analyzed by SEM to elucidate particle morphology. The solid analysis affirmed the presence of silver nanoclusters in the size regime of 328-381 nm, Figure 3.6. To characterize the nanoclusters array, the EDX analysis (Figure 3.7) of the brown solid was also carried out. 90.9 wt % of silver was revealed by EDS elemental analysis of the solid. Table 3.6 represents the percentages of elements presents in the solid.

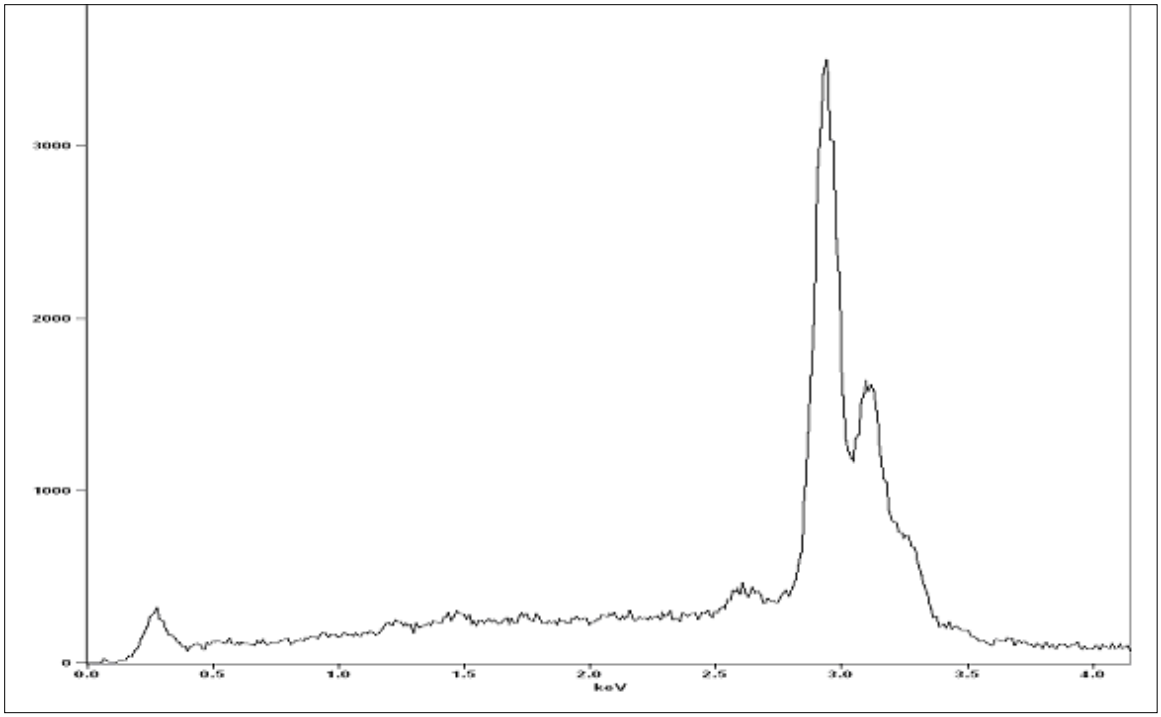


Figure 3.7: EDX spectra from brown solid using SEM.

Table 3.2: The presence of different elements in the brown solid from XPS analysis.

Element	Net count	Element Wt%	Atom%
C	2893	4.28	24.36
N	362	1.23	6.03
O	381	2.08	8.92
F	81	0.48	1.74
Si	418	0.34	0.84
Ag	62257	91.58	58.12

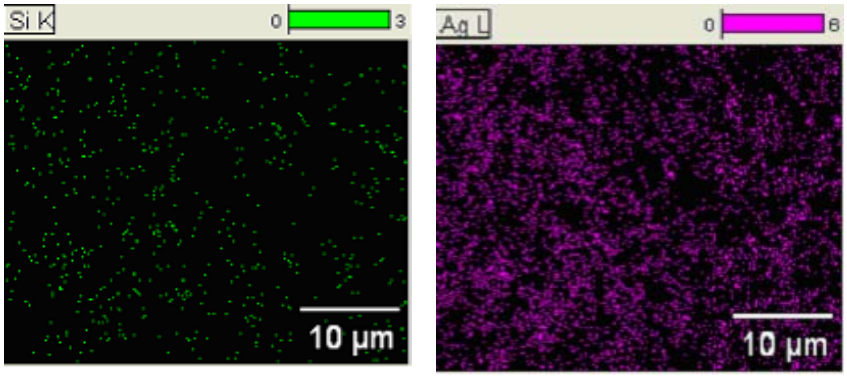


Figure 3.8: Elemental map obtained using EDX analysis.

50-ml toluene was added to that brown solid and after 2h of stirring at room temperature resulted dark brown solution. The dark brown solution was then analyzed by UV-vis absorption spectroscopy and TEM. The freshly prepared 'silver-amine nanoconjugates' in toluene displayed an intense absorption in UV-vis spectroscopy (λ_{max} at 430 nm), and after redispersion the peak intensity was almost constant but the blue shift of absorption maxima was observed (λ_{max} at 417 nm), Figure 3.9.

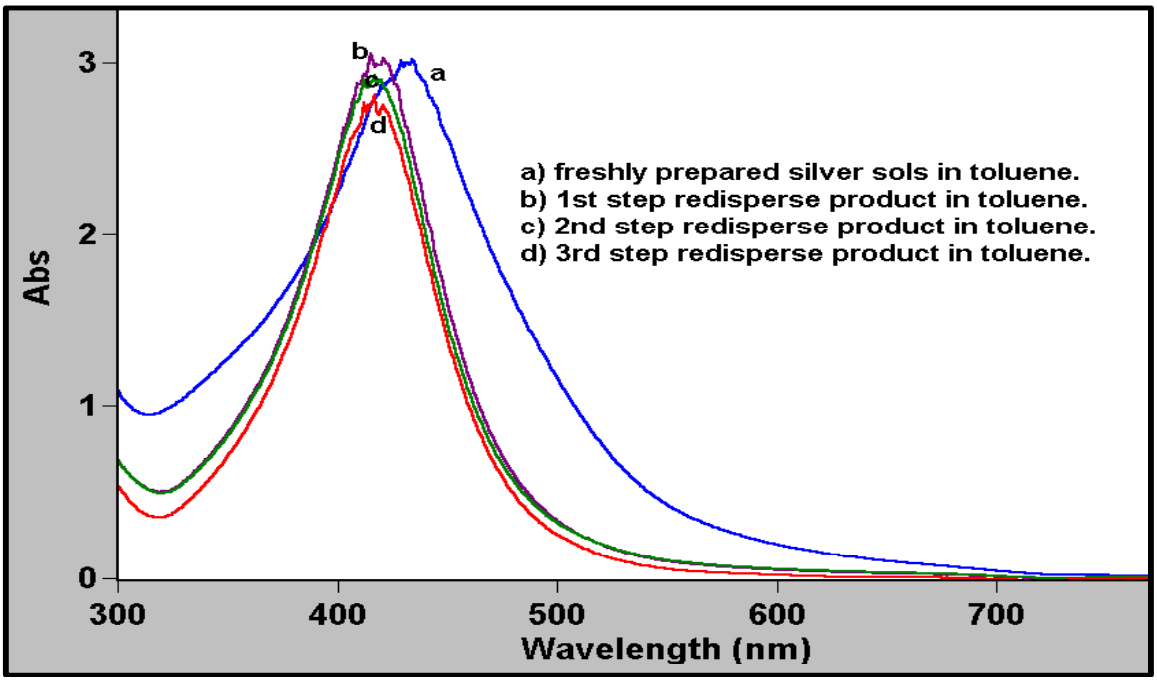


Figure 3.9: UV-vis absorption spectra of silver nanoparticles arrays: (A) nanoparticles of freshly prepared solution, (B) 1st step redispersion, (C) 2nd step redispersion, and (D) 3rd step redispersion in toluene.

The different step redispersion solutions were also analyzed by TEM. The TEM analysis showed even after 3rd step of dispersion (Figure 3.10 D), the nanoclusters were present in the form of self-assembly.

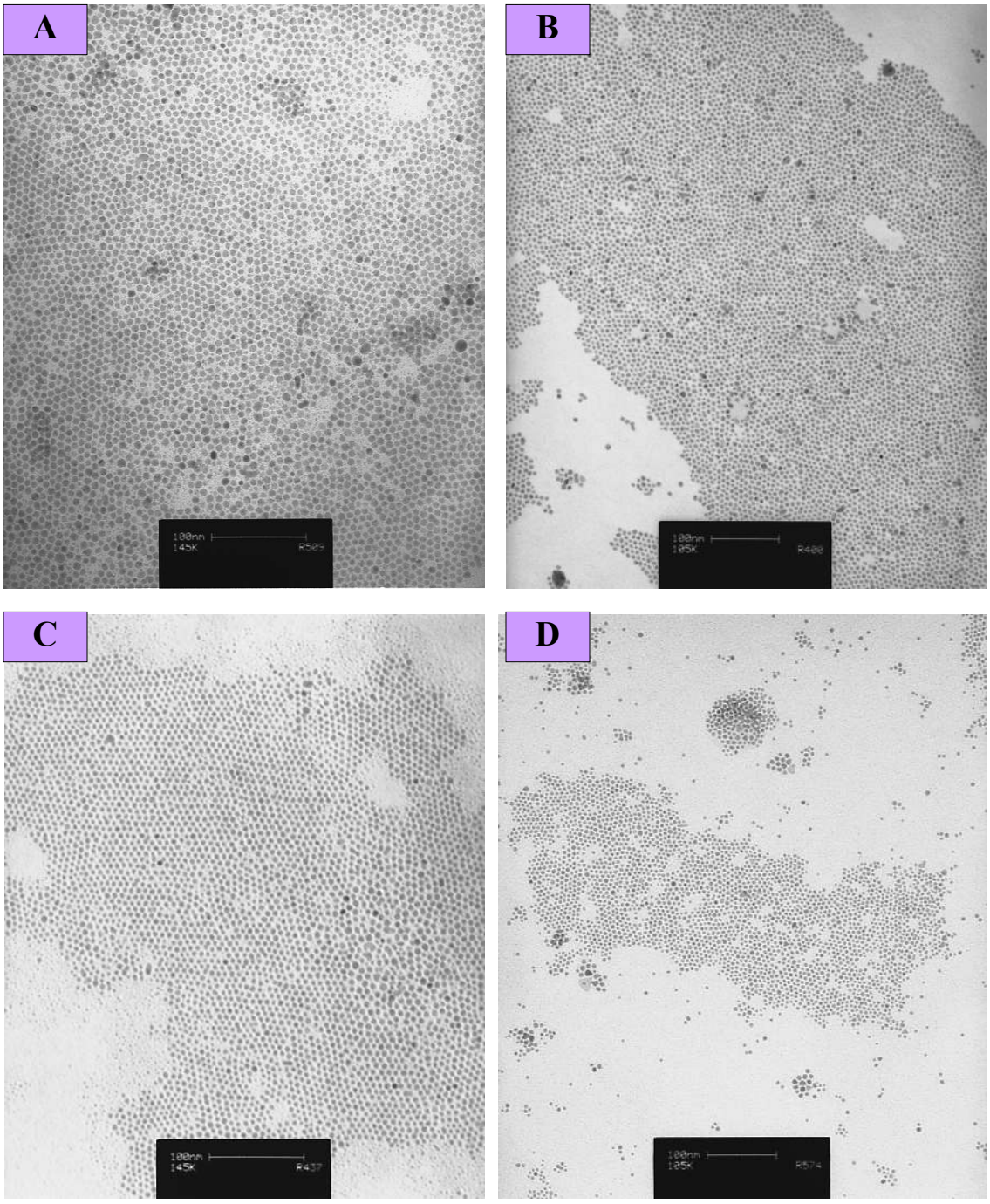


Figure 3.10: TEM micrograph of silver nanoparticles arrays: (A) nanoparticles in freshly prepared solution, (B) 1st step redispersion, (C) 2nd step redispersion, and (D) 3rd step redispersion in toluene. Scale bar is 100 nm.

Table 3.3. Comparison of UV-vis absorption maxima and particle size, and interparticle separation analysis for different redispersion step of synthesized SAMs of silver nanoparticles

Entry	Dispersion step	Abs. maxima (λ_{max}: nm)	Average particle Size[b](nm)	Int. particle spacing (nm)
1	Freshly prepared	430-434 nm	3.9 (0.3)	2.1
2	1st step	417-420 nm	2.8 (0.6)	2.4
3	2nd step	415-417 nm	2.5 (0.4)	2.4
4	3rd step	415-417 nm	2.5 (0.4)	2.5

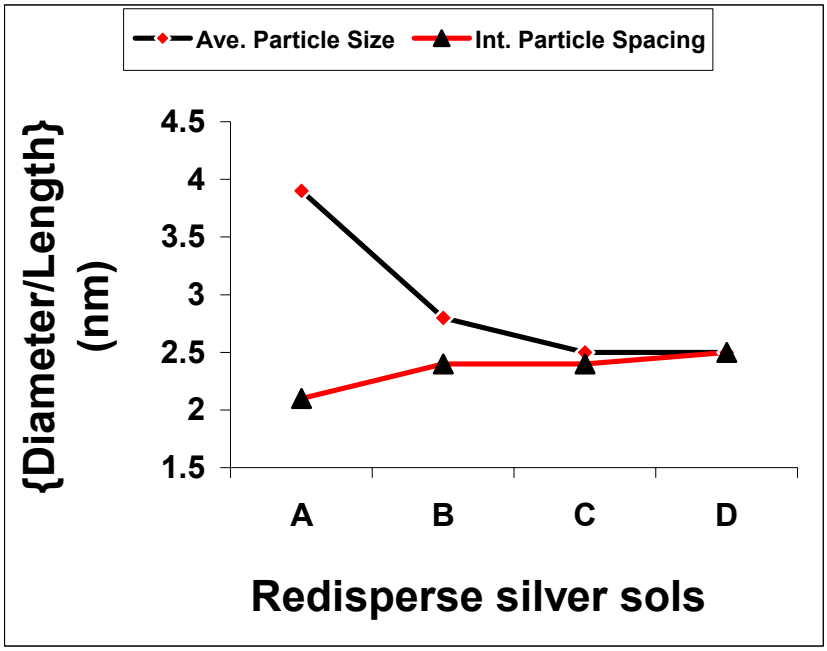


Figure 3.11: Comparison of particle size and interparticle spacing for different stages of redispersion. (A) nanoparticles in freshly prepared solution, (B) 1st step redispersion, (C) 2nd step redispersion, and (D) 3rd step redispersion in toluene

3.2.5 Solvent Exchange Studies

The position of the surface plasmon band of metal nanoparticles is greatly regulated by surrounding media,[27] depending on the surrounding media, the surface plasmon band oscillates between 400-450 nm for Ag nanoparticles. In a recent report, the authors have mentioned that the unmodified silver nanoparticles get structural changes when exposed to various solvents.[28] In the present study, we were able to investigate the solvent effects on the synthesized self-assembled silver nanoparticles. The SAMs of silver nanoparticles were easily redispersable in solvents of a wide range of refractive index without particle aggregation. For solvent exchange studies, a wide range of organic solvents such as benzene, dichloromethane (DCM), THF, and cyclohexane were chosen. Compare to solvents benzene, toluene, and cyclohexane, DCM has the highest refractive index, and in this case the highest maximum red shift of surface plasmon band was observed. Moreover, the particles were also bigger in size (4.0 ±0.7 nm) as compared to benzene, and cyclohexane. DCM, cyclohexane, and benzene do not have any active functional groups and remain inert, with no detectable chemical interaction with the silver surface. For these three solvents, we can see that the SAMs are present, but in the case of THF, the particles are bigger and randomly oriented. Figure 3.13 represents the TEM images of silver nanoparticles in different solvents. THF has an active coordinating atom and which was previously used to stabilize the nanoparticles.[5] In our system, it can be taken in to account that THF molecules coordinate with particle surface and disrupted the self-assembly of the silver nanoparticles. As a result formation of large truncated silver nanoparticles with 5.0±0.9 nm was observed. A comparative study of five different solvents is compiled in Table 3.4.

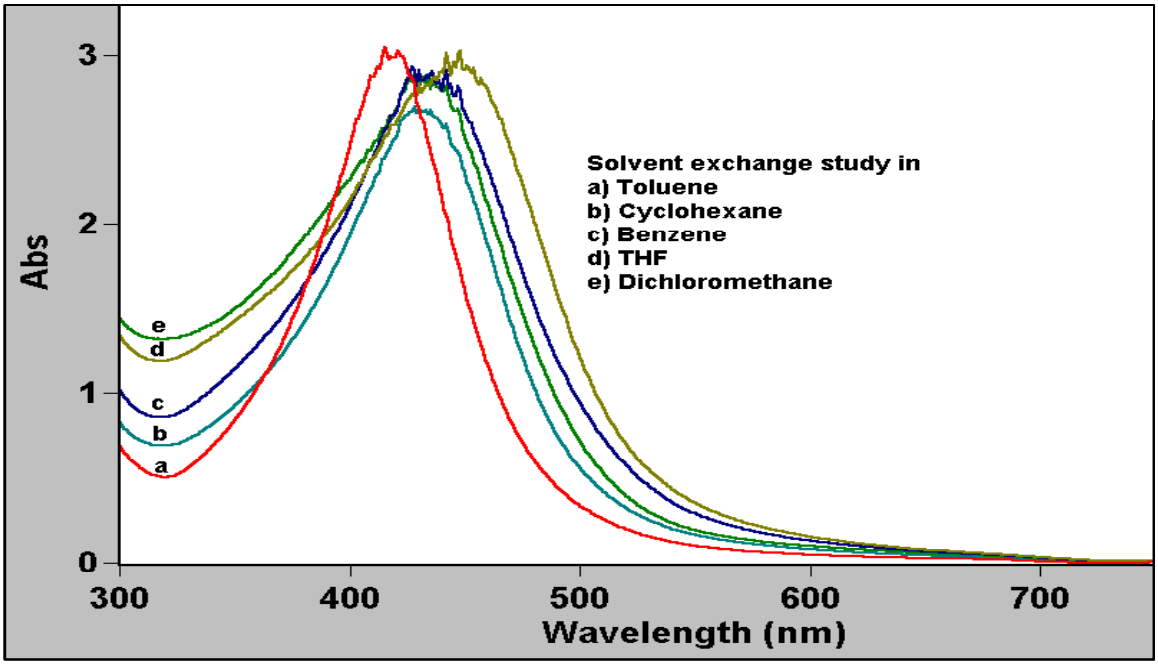


Figure 3.12: The surface plasmon band of redispersed silver nanoclusters in different solvents.

Table 3.4. Comparison of UV-Vis absorption maxima and particle size analysis[a] of TOA capped silver nanoclusters in solvents of varying refractive indices.

Entry	Solvents	Refra. Index (n)	Abs. maxima (λ_{max}: nm)	Ave. particle Size(nm)
1	Cyclohexane	1.426	425-430 nm	2.5 (0.3)
2	Toluene	1.496	417-420 nm	2.8 (0.6)
3	Benzene	1.501	428-435 nm	2.3 (0.3)
4	DCM	1.550	430-440nm	4.0 (0.7)
5	THF	1.407	435-450 nm	5.0 (0.9)

.

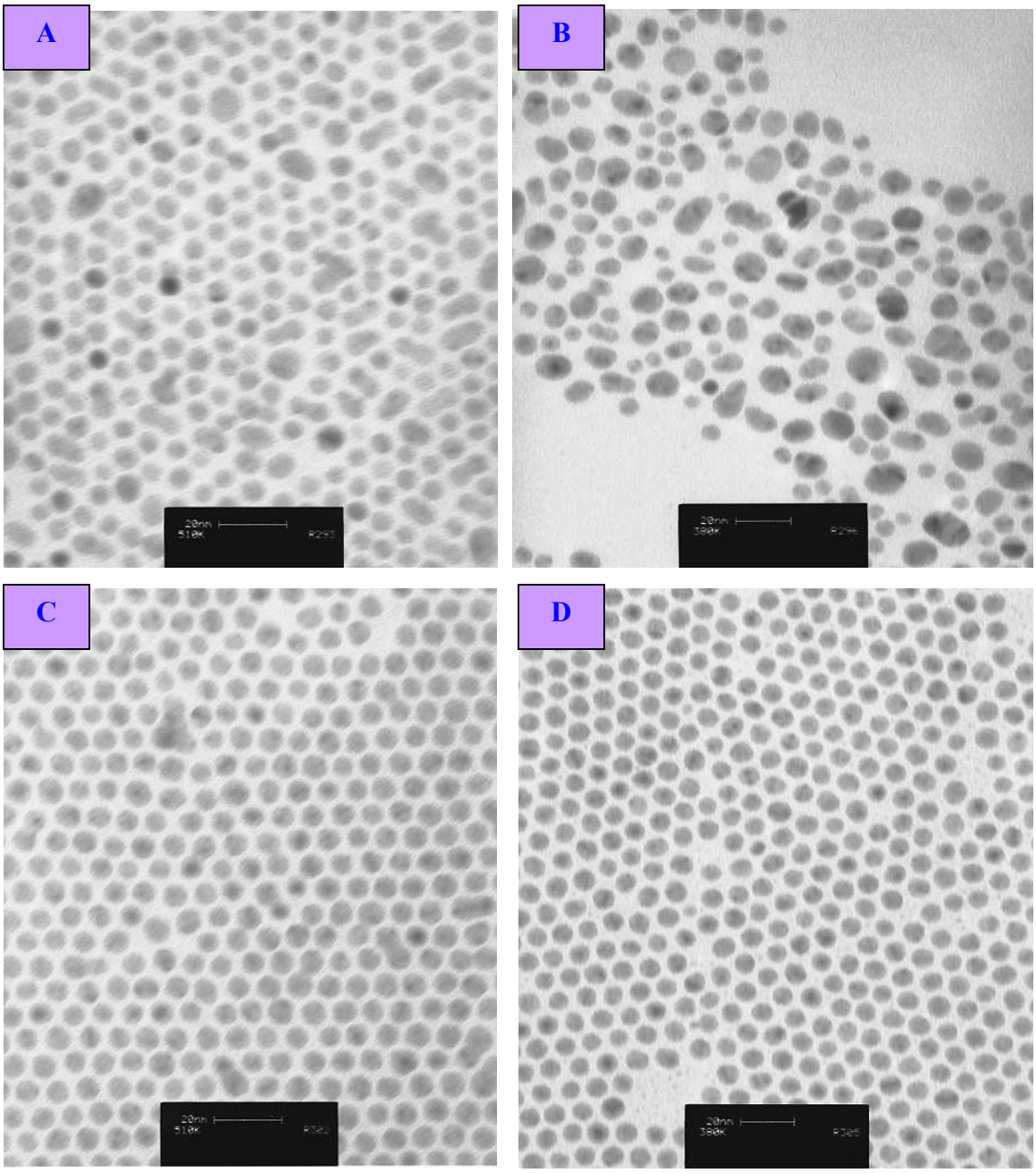


Figure 3.13: TEM images of redispersed silver nanoclusters in (A) DCM, (B) THF, (C) cyclohexane, and (D) benzene.

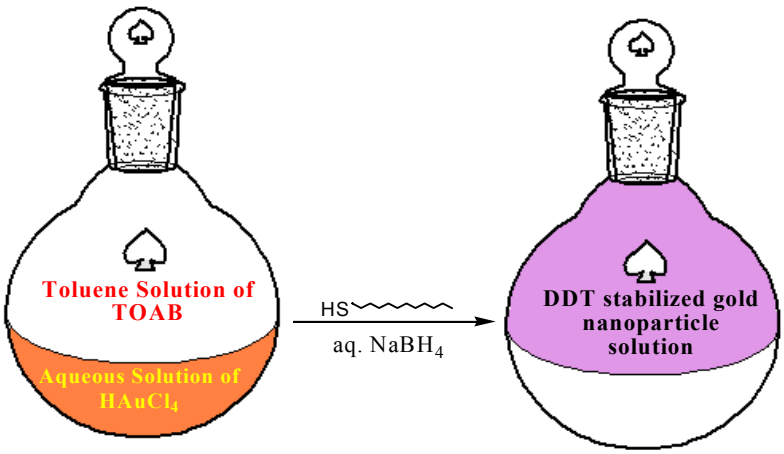
3.3 Conclusion

Ligand (TOA) stabilized self-assembled monolayers of silver nanoparticles are discussed for the first time from a synthetic point of view. The self-assembed 'silver-amine nanoconjugates' are achieved by heptamethyltrisiloxane (HMTS) reduction method at room temperature under mild reaction conditions with high yields. The reduction method is applicable for most of the commercially available silver salts AgX (X= AcO^-, NO_3^-, ClO_4^-, BF_4^-, and $F_7C_4O_2^-$). The redispersion and reproducibility studies are also carried out in toluene. The resulting 'silver-amine nanocomposites' can easily be redispersed and handled in other standard organic solvents such as benzene, tetrahydrofuran (THF), cyclohexane, and dichloromethane (DCM). The self-assembled silver nanoparticles were characterized by UV-vis absorption spectroscopy, transmission electron microscopy (TEM), scanning electron microscopy (SEM) attached with EDX and XPS.

Part B
Self-assembled monolayers (SAMs) of gold nanoparticles

3.4 Introduction

The preparation and characterization of supported, self-assembled monolayers (SAMs) of gold nanoparticles oriented by long chain organic molecules has generated model systems for the study of variety of interfacial phenomena.[29] Examples include catalysis,[30] lubrication,[31] corrosion,[32] adhesion,[33] adsorption of proteins at surface,[34] electrochemistry,[35] and electrical conduction,[36] among others. The most popular method is the two phase synthesis developed by Brust *et al.*, which involves the transfer of $[AuCl_4]^-$ into toluene with the use of tetraalkylammonium bromide and subsequent reduction with $NaBH_4$ in presence of alkanethiols.[19]



Scheme 3.2: Brust method of two-phase synthesis for gold nanoparticles.

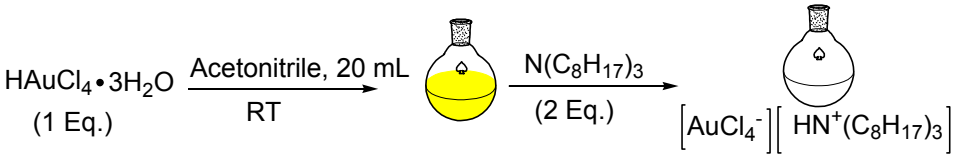
The Brust method produces nanoparticles with wide size dispersity. To obtain a self-assembeld ordered system of metallic nanoparticles, it is essential to have a low polydispersity of the synthesized particles. The impurity that is introduced by the use of surfactants and the restriction of performing the reduction in the presence of functionalized stabilizing agents. In the part A of this chapter 3, we discussed the utility of monomeric hydrosiloxane as an efficient reducing agent to obtain ordered self-assembled monolayers of silver nanoparticles in the presence of TOA. To explore this approach, in this section, we discuss about the heptamethyltrisoloxane (HMTS) induced reduction of $HAuCl_4$ to afford a simple one-pot route to stable self-assembled monolayers of gold nanoparticles in acetonitrile in the presence of trioctylamine (TOA). It has been reported that amines are not a suitable ligands for the formation of stable, closed packed monolayers on the gold surface.[24] In our synthetic strategy, the amine capped nanoparticles are very stable, moreover we can avoid the use of thiol surfactants, which makes difficulties to carry out the surface modification and functionalization needed for certain purpose. The method has several advantages include the fact that synthesized particles were stable for months without aggregation or precipitation. In addition, this methodology allows the easy surfactant exchange reactions by different phosphine ligands to furnish functionalized organogold nanocomposites.

3.5 Results and Discussion

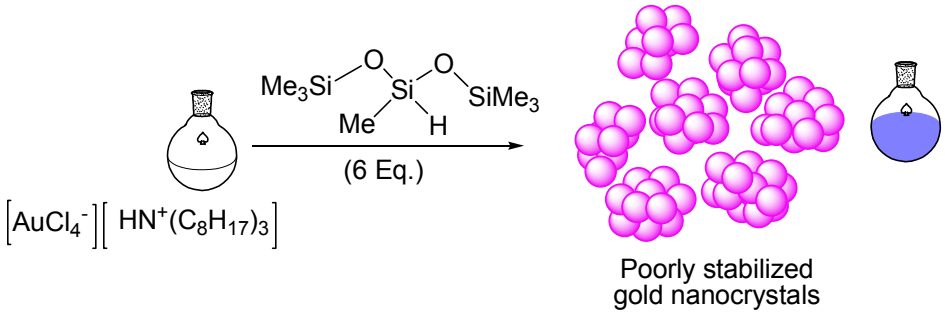
In order to gain insight, the HMTS induced reduction process was examined in detail. This reduction procedure examined in this section involves two distinct steps. (i) Generation of an amine gold complex and (ii) reduction of amine gold complex with HMTS without stabilizing surfactant. We assumed that the amount of amine present in the solution can act as a stabilizer. In the later part of the section, we discussed the role of TOA in the particle stabilization and its morphology. During the optimization studies, we have observed that this particular sequence is very important for achieving stable monodiaperse gold nanoclusters.

The $HAuCl_4$ (0.02 mmol, 0.008 gm)-TOA(0.02 mmol, 0.01 ml) complex was prepared in 20 ml acetonitrile. The gold tetrachloroaurate is completely soluble in acetonitrile and produces a yellow color solution with a strong plasmon absorption band, $\lambda_{max} \approx 322$ nm in UV-vis spectroscopy. Addition of TOA to yellow solution slowly leads to light yellow color and then turns completely colorless. The colorless solution has no UV-vis absorption. In the initial experiment, 1 equivalent of TOA was added with respect to Au^{+3} ion and the solution was analyzed by ^1H NMR spectroscopy, Figure 3.14. The data confirmed that a 1:1 complex formation between the gold ion and TOA, at this stage the color of the solution was light yellow indicating the presence of gold aurate. To the light yellow color solution, 1 more equivalent of TOA was injected. The light yellow color slowly turned to a colorless homogeneous solution indicating complete consumption of $HAuCl_4$.

Thus, under optimized reaction conditions, addition of 2 equivalents (0.04 mmol, 0.01 ml) of TOA to the yellow color gold aurate (0.02 mmol) solution of 20 ml acetonitrile leads to the formation of 1:2 ($HAuCl_4$: TOA) complex in 30 minutes at RT. The colorless solution was then evaporated under high vacuum and dissolved in C_6D_6 for NMR analysis. The $-NCH_2$ of TOA has a characteristic peak at 2.45 ppm, in ^1H NMR. After complexation with gold salt the signal due to NCH_2 group shifts to ~3.0 ppm (Figure 3.14). Higher molar ratio of TOA was also investigated but in all the cases the NMR studies indicated formation of 1:2 gold to amine complex. The Gold-TOA complex was found to be stable in air, and solution was used as precursor for reduction studies.



Scheme 3.3: Synthetic strategy of the formation of gold amine complex.



Scheme 3.4: Reduction of gold-amine complex.

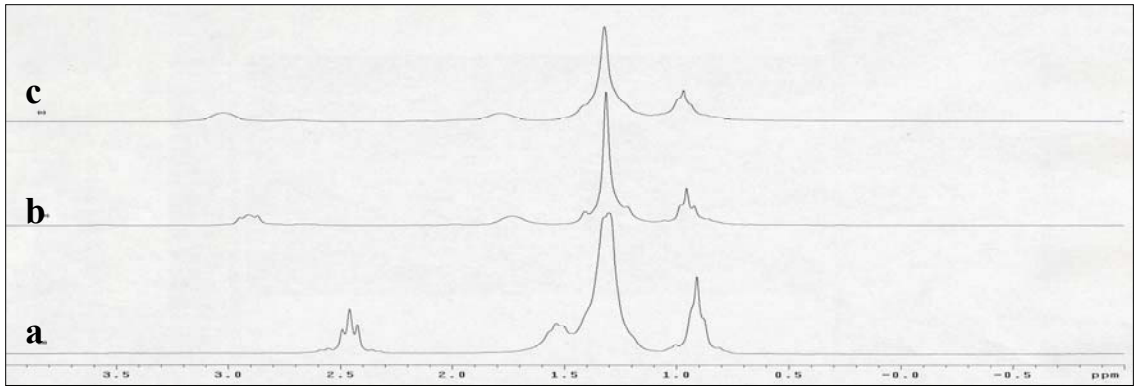


Figure 3.14: ^{1}H NMR comparison of gold-TOA complex where (a) pure TOA, (b) gold-TOA 1:1 complex and (c) is gold-TOA 1:2 complex.

Reduction of gold-amine complex was investigated in presence of HMTS. To the gold-TOA complex, 6 equivalents HMTS (0.12 mmol, 0.04 ml) was injected at RT. The formation of gold nanoparticles was monitored by UV-vis spectroscopy at different time intervals. After 1h of addition of HMTS, the formation of gold nanoparticles was observed and followed by appearance of a plasmon absorbance band at ~519-nm. With time, the peak intensity increased as the solution color got more intense. 2h and 30 minutes after addition of all the reagents, the peak position was at 550 nm, it remained constant for another five hours. The UV-visible spectrum of the reduction process is shown in Figure 3.15. It was observed that the plasmon peak gradually grows and red shifts (from 519 to 550-nm) over the course of 2h and 30 min. The increase in absorbance intensity, while the observed red shift is a result of aggregation that occurs as the particles become to large to be stabilized by 2 equivalent of TOA. After 1 day, the solution was completely colorless indicating total particle precipitation.

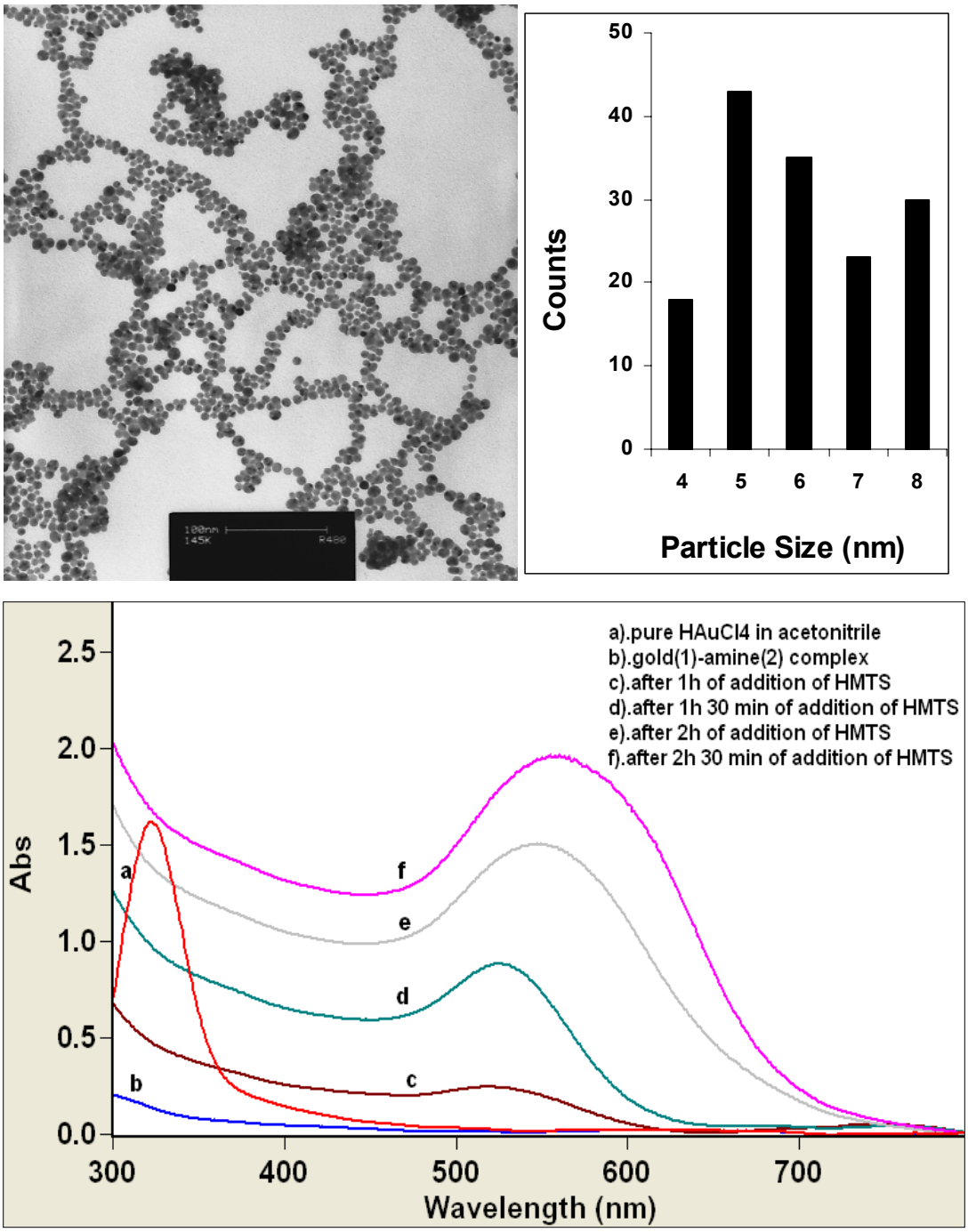


Figure 3.15: TEM image, corresponding histogram and the UV-vis spectra represents the HMTS induced formation of gold nanoparticles in acetonitrile.

The reaction mixture was then centrifuged and analyzed by TEM. A representative TEM image of nanoparticles is shown in Figure 3.15. The average particle size was 6.2 nm with standard deviation of 1.5 nm.

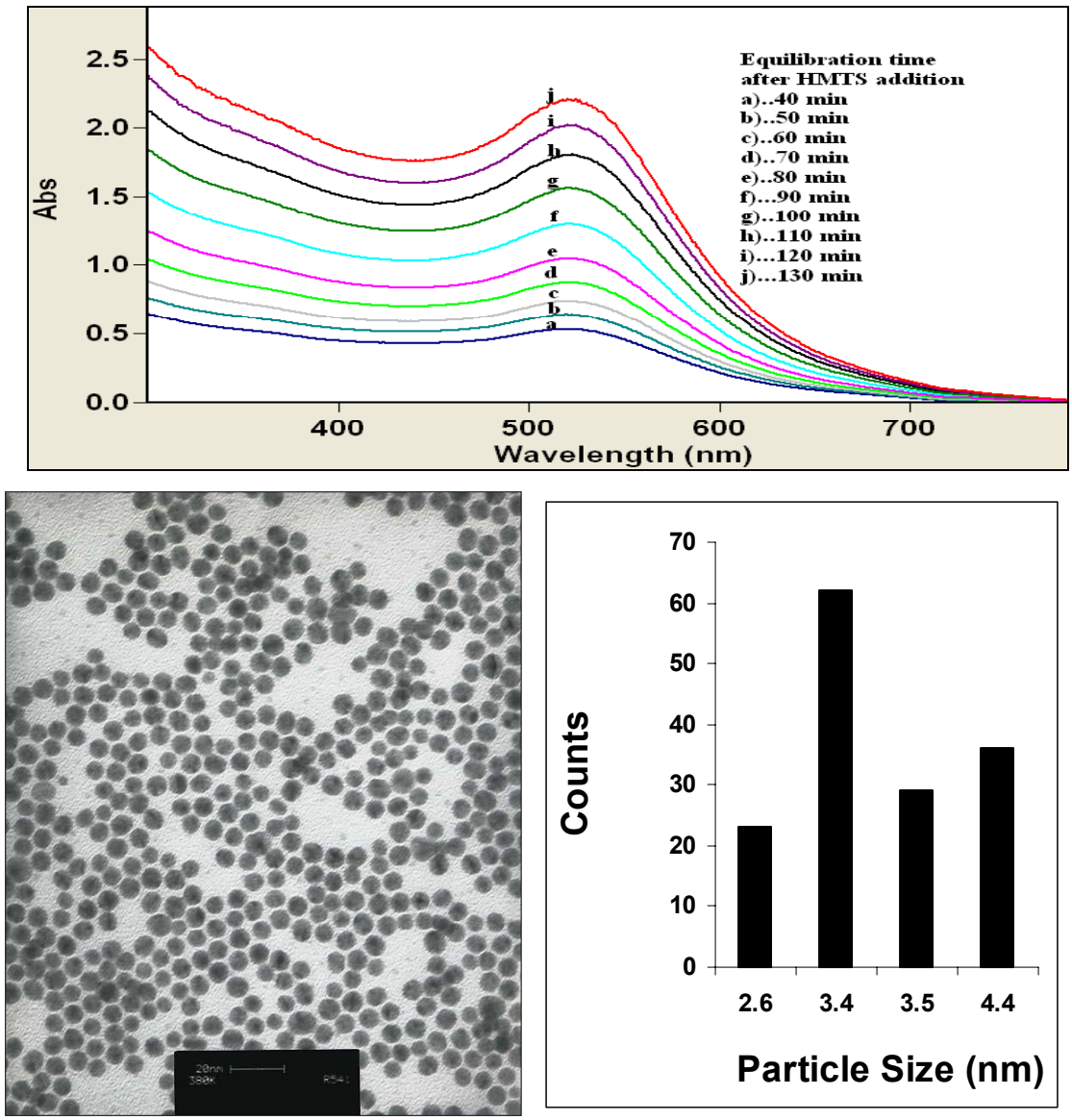


Figure 3.16: Time dependent UV-vis spectra; TEM image and the corresponding histogram of HMTS induced formation of 3.6 nm self-assembled gold nanoparticles in the presence of 4 equivalent of TOA.

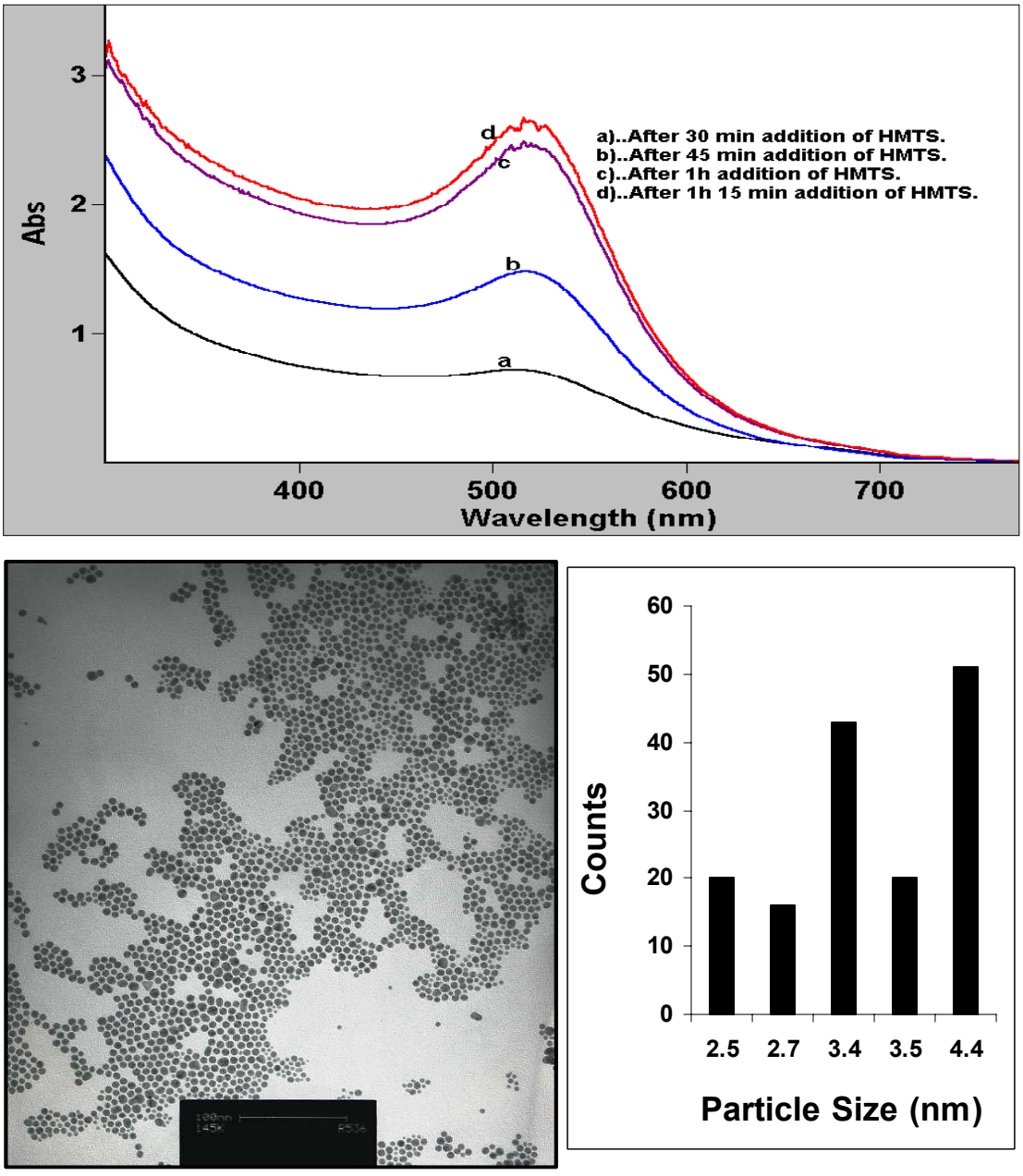
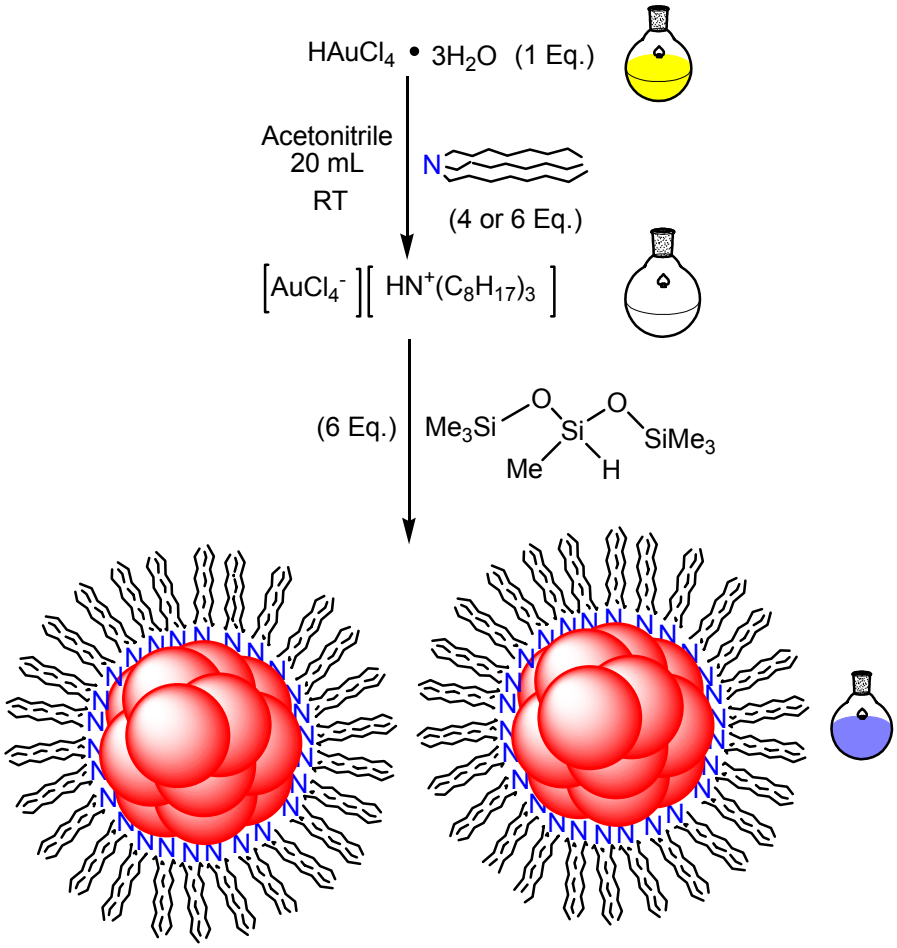


Figure 3.17: Time dependent UV-vis spectra; TEM image and the corresponding histogram of HMTS induced formation of 3.5 nm self-assembled gold nanoparticles in the presence of 6 equivalent of TOA.



Scheme 3.5: Schematic illustration of the formation of self-assembled monolayers of gold nanoparticles.

To explore the role of TOA in the reaction system, different concentrations of TOA were employed. When the amount of TOA in the reaction mixture was increased to 4 equivalents (0.08 mmol, 0.04 ml) from 2 equivalents, the self-assembled monolayers of spherical gold nanoparticles were achieved, Figure 3.16. A higher amount of TOA (6 equivalents) also resulted in self-assembled monolayers of gold nanoparticles, Figure 3.17. A comparative study was carried out to find out the rate of reaction, the position of SPB and the average particle size for the reduction of gold salt to gold nanoparticles in

the presence of different molar ratios of TOA, see Table 3.5. From the above result we can clearly see that, the SPB was dependent on the size of the synthesized gold nanoparticles. In particular, we showed how gold nanocrystals of specific size ranges could be obtained as self-assembled structures by simply alternating the initial metal-to-surfactant ratio (i.e., the $AuCl_4^-$/trioctylamine molar ratio). It has been reported that the blue shift of λ_{max} of the SPB occurred with the decreased of particle size.[37] The SPB maximum and bandwidth are also influenced by the particle shape, medium dielectric constant, and temperature of metal nanoparticles.[38] The refractive index of the solvent has been shown to influence a shift of the SPB. For gold nanoparticles of mean diameter of 9, 15, 22, 48, and 99 nm, the SPB maximum λ_{max} was observed at 517, 520, 521, 533, and 575 nm, respectively, in aqueous medium.[39] The shift is also especially significant with thiolate ligands, which are responsible for a strong ligand field interacting with the surface electron cloud. The synthetic method we have developed, the gold nanoparticles were capped with a monolayer of amine. The average interparticle separation of the self-assembled gold nanoparticles was also calculated and it was 2.3 nm, which is almost double the length of the one-triocltyamine length, which is comparable to the literature values.[24,25]

Table 3.5. Comparison of UV-vis absorption maxima and particle size analysis of HMTS induced formation of SAMs of gold nanoparticles.

Entry	Gold Sols	Amount of TOA (mmol)	Reaction time	Solution Color	UV-vis absorption (λ_{max}: nm)	Particle size (nm)
1	Au-HMTS	0.004	2h 30 min	purple	520-525	6.6 (1.0)
2	Au-HMTS	0.008	2h 10 min	Deep purple	516-519	3.6 (0.4)
3	Au-HMTS	0.012	1h 15 min	Deep purple	512-517	3.5 (0.7)

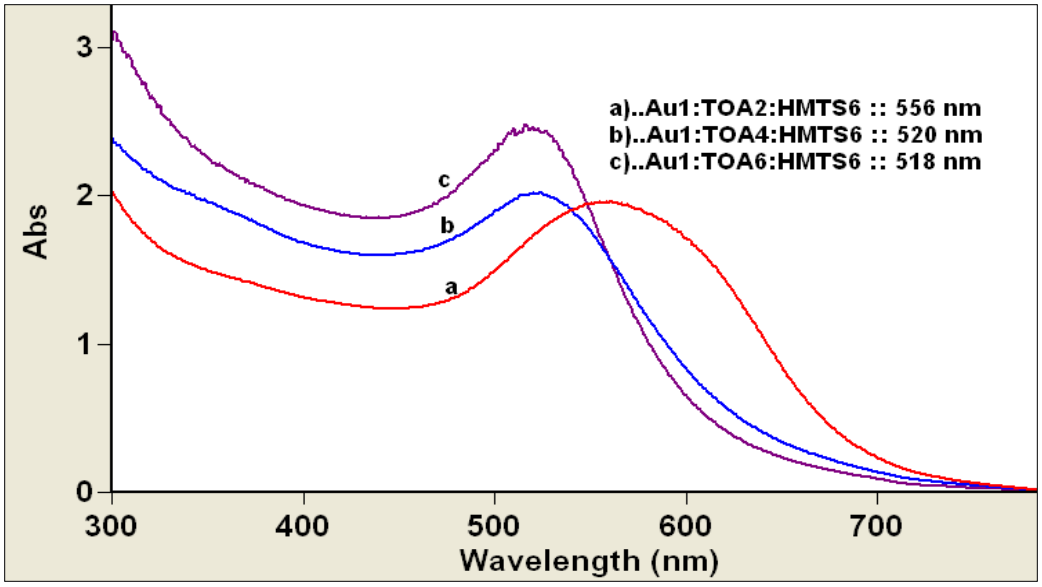


Figure 3.18: Comparison of UV-vis absorption maxima for different gold amine complex reduction.

When the solution showed static absorption maxima ; nanoparticle solution was reduced in volume to ≈5 mL by rotary evaporation. The particles were precipitated from acetonitrile by adding 100 ml of 95% ethanol followed by cooling to –40 ^{0}C for 12h. The solid was then analyzed by X-ray photoelectron spectroscope (XPS), and scanning electron microscope (SEM). In the spectrum, signals for gold ($4f_{7/2}$, $4f_{5/2}$, $4d_{5/2}$, $4d_{3/2}$, and $4p_{3/2}$ at ≈ 83, 87, 335, 354, and 347 eV, respectively), carbon (1s at ≈284.3 eV), and oxygen (1s at ≈531.8 eV) were observed. The Figure 3.19 represents the XPS signature of the Au 4f doublet ($4f_{7/2}$ and $4f_{5/2}$) for the particle produced by scheme 3.5. The peak position, line shapes, and peak-to-peak distance of Au 4f doublets are the standard measure of the gold oxidation state. The binding energies for the Au 4f doublets are 83.5 and 87.2 eV (peak-to-peak distance of 3.7 eV). These measurements are consistent with Au^{0} oxidation state and if Au^{3+} was present, it would be expected to show up as a peak or at least a shoulder near 84.9 eV.[40]

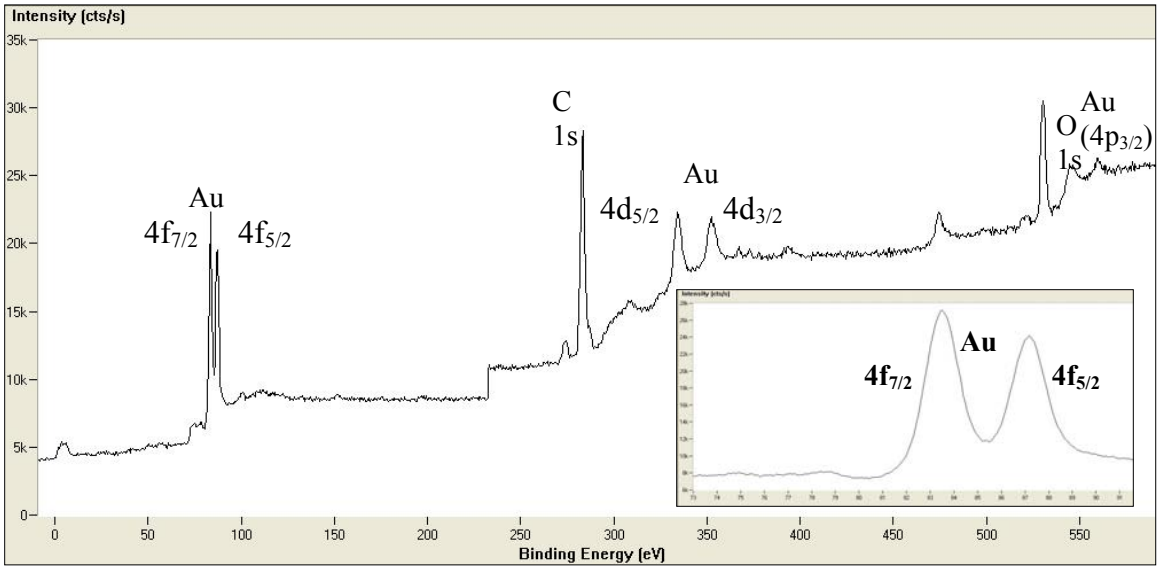


Figure 3.19: X-ray photoelectron spectra for TOA-capped gold nanocrystals synthesized by Scheme 4.2.

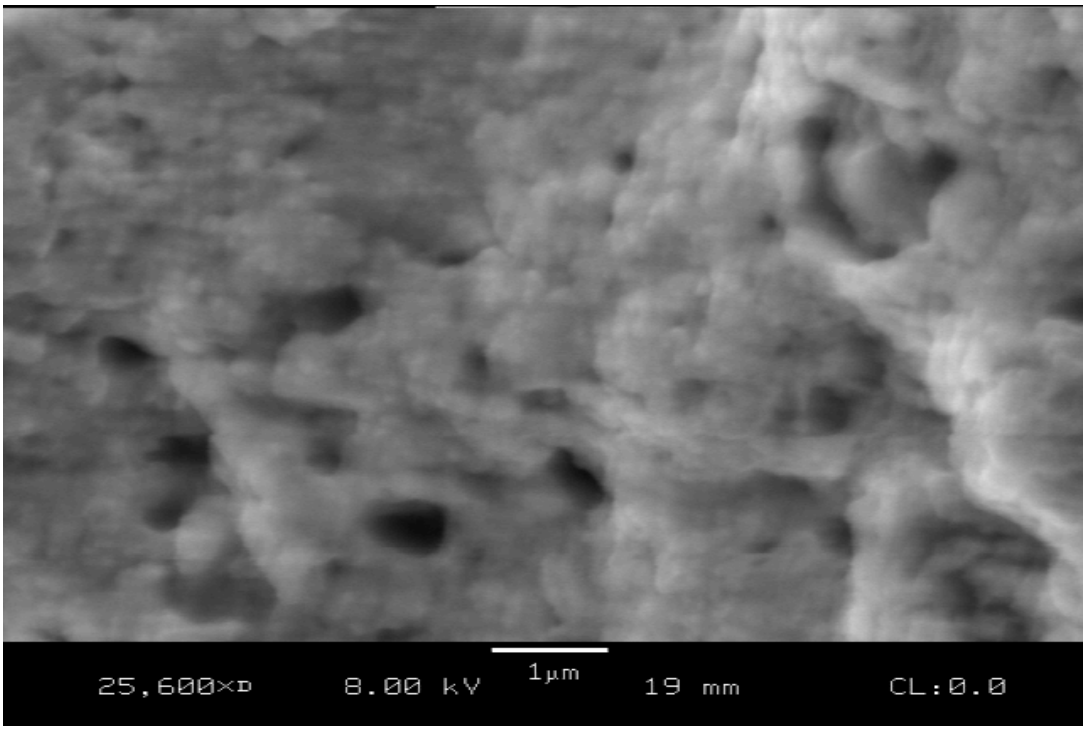
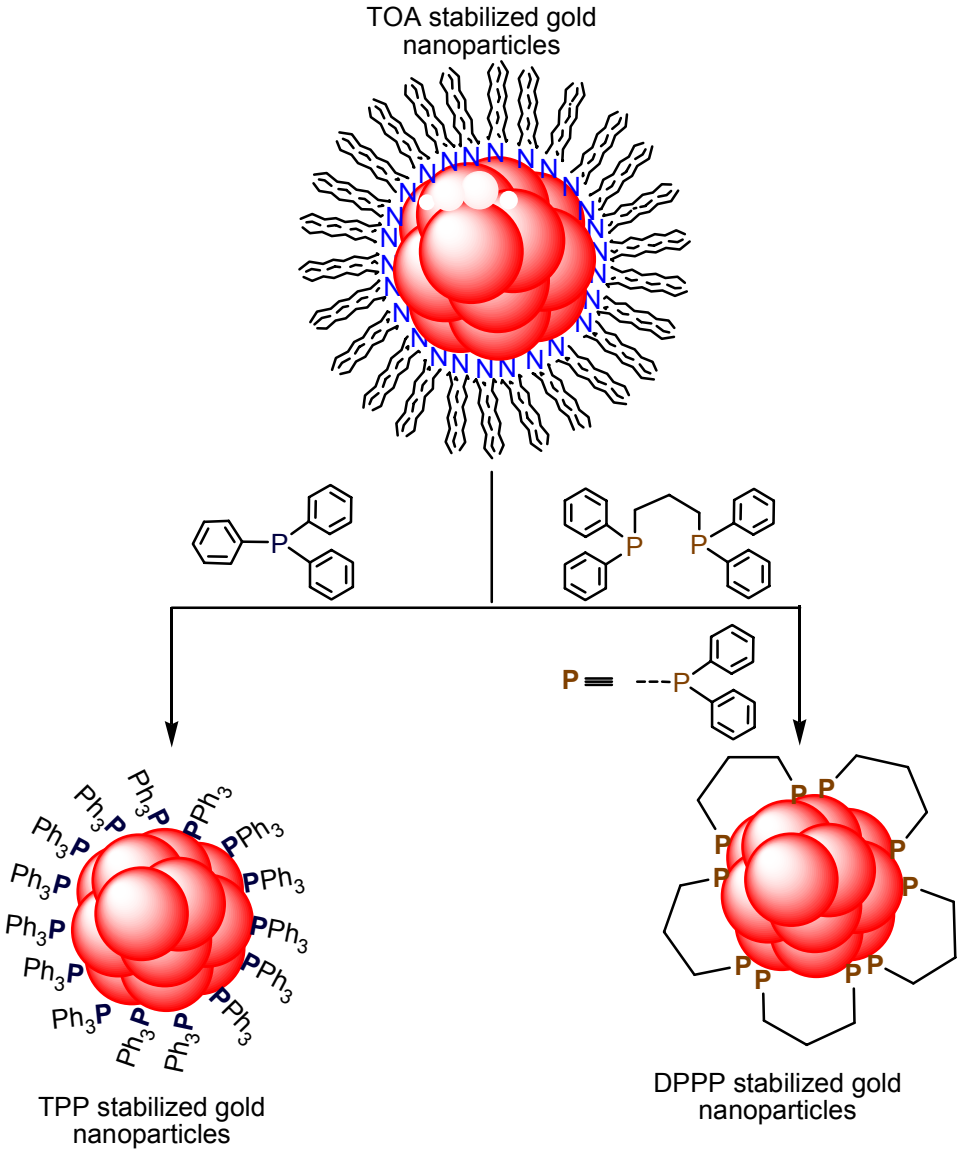


Figure 3.20 SEM image of the solid product after particle precipitation.

3.6 Place Exchange study

Ligand stabilized nanoparticles have been extensively studied for their large variety of applications in different fields.[41] For most applications and fundamental studies, it is desirable to be able to tailor the nanoparticle properties by controlling two key structural parameter: (1) the size and composition of the nanoparticle core,[39] and (2) the chemical nature of the stabilizing ligand shell.[42] Place-exchange reaction is an extremely versatile and important method for preparation of functionalized metal nanoparticles.[43] In this reaction, addition of pre-synthesized ligand-protected nanoparticles to a solution of another ligand effects partial replacement of the protecting shell on the nanoparticle surface. The reaction is most studied for thiol-protected Au nanoparticles; its simplicity and applicability to a wide range of different ligands made it a popular synthetic tool. The mechanism of the exchange reaction of Au nanoparticles with thiols was extensively studied by R. W. Murray and coworkers.[44] A small number of ligands were found to exchange rapidly; this initial fast reaction is then followed by a much slower process. Not all ligands can however be exchanged on the nanoparticle surface even at long reaction times. These observations point to the presence of different types of binding sites on the nanoparticle surface. Au nanoparticles are faceted, and it was postulated that vertex and edge sites are more reactive in exchange reaction than terrace sites.



Scheme 3.6: Place-exchange reaction on the surface of amine protected Au nanoparticles.

It has been reported that amine protected gold nanoparticles are more active in exchange reactions and allow rapid replacement of most of the ligand.[45] Phosphine stabilized gold nanoparticles have been widely studied because of their use as labeling reagents for bio-molecules in electron microscopy.[46] In this section, we describe the place

exchange study carried out on the pre-synthesized self-assembled monolayers of gold nanoparticles using different phosphine ligands, triphenyphosphine (TPP), 1,2-bis(diphenylphosphino) ethane (DPPE), propane (DPPP), and butane (DPPB) (Scheme 3.6). The phosphine stabilized gold nanoparticles were characterized by ^{31}P NMR spectroscopy, UV-vis spectroscopy, TEM, EDX and XPS.

In part B. section 3.5, we have described the synthetic route of self-assembled gold nanoparticle formation. Briefly, SAMs of gold nanoparticles were synthesized using 6 equivalents of HMTS, in the presence of 4 equivalent of TOA (Scheme 3.5). The particle size was 3.6 ±0.4 nm. To this pre-synthesized SAMs, 4 equivalents (0.08 mmol, 0.02 gm) of TPP were added followed by vigorous stirring at RT. After addition of TPP and stirring for 3h at room temperature, almost all the particles precipitated out from the solution. The particles were isolated by centrifugation, washed three times with 20 ml of acetonitrile. Drying under vacuum resulted a dark purple solid. To the resulting solid, 20-ml of distilled toluene was added; after 2h of stirring at room temperature produced blue color dispersion.

The coordination ability of phosphine ligands on gold nanoparticles was investigated by ^{31}P NMR spectroscopy. The dark purple color solid was dissolved in C_6D_6 and analyzed by ^{31}P NMR spectroscopy. The coordination of phosphine ligand on gold nanoparticles induce a downfield shift in the ^{31}P NMR peak. The ^{31}P NMR peak of TPP stabilized 4 nm sized gold nanoparticles appeared at 32. 22 ppm. In contrast, free TPP exhibited a peak at -4.08 ppm (figure 3.21). Almost similar observation was made when palladium nanoparticles were stabilized by TPP in aqueous medium.[47]

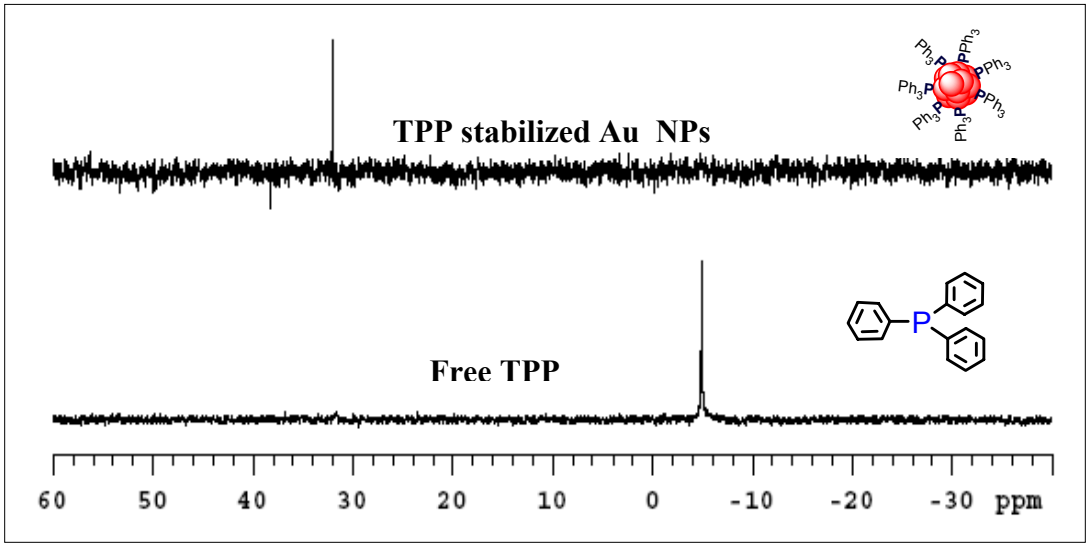


Figure 3.21: Representative ^{31}P NMR spectra of TPP and the corresponding TPP-stabilized gold nanoparticles.

The TPP stabilized dark purple solid was also analyzed by X-ray photoelectron spectroscopy (XPS). The binding energy of Phosphorus $2p_{3/2}$ is 132.6 eV and in the XPS spectra a peak at 132.1 eV is present, which confirmed the presence of phosphorus ligand in the exchange product (figure 3.22). [48]

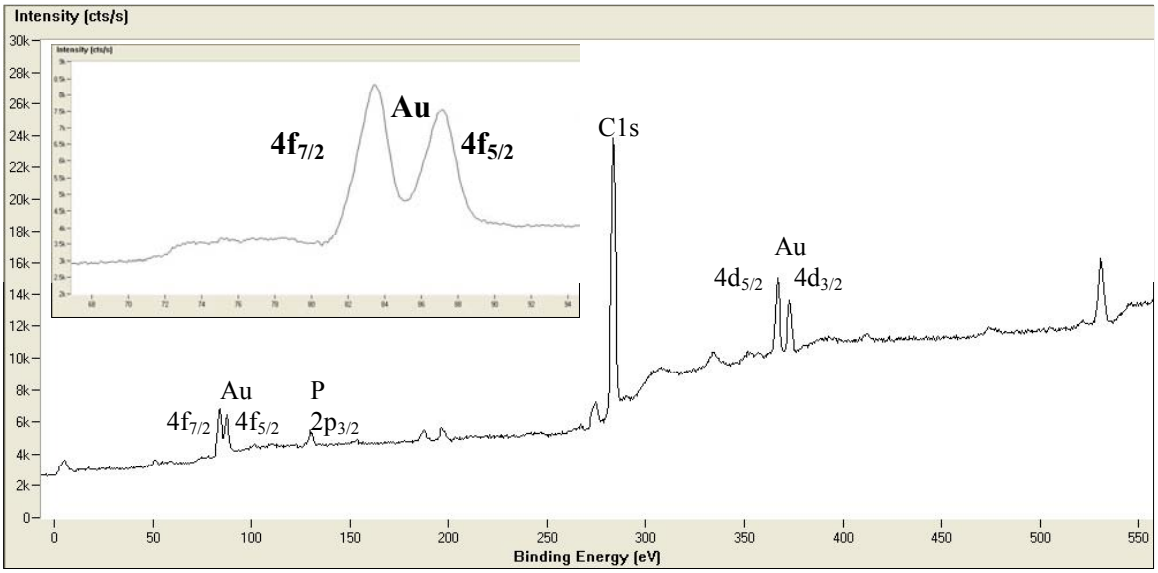


Figure 3.22: X-ray photoelectron spectra for TPP-capped gold nanocrystals.

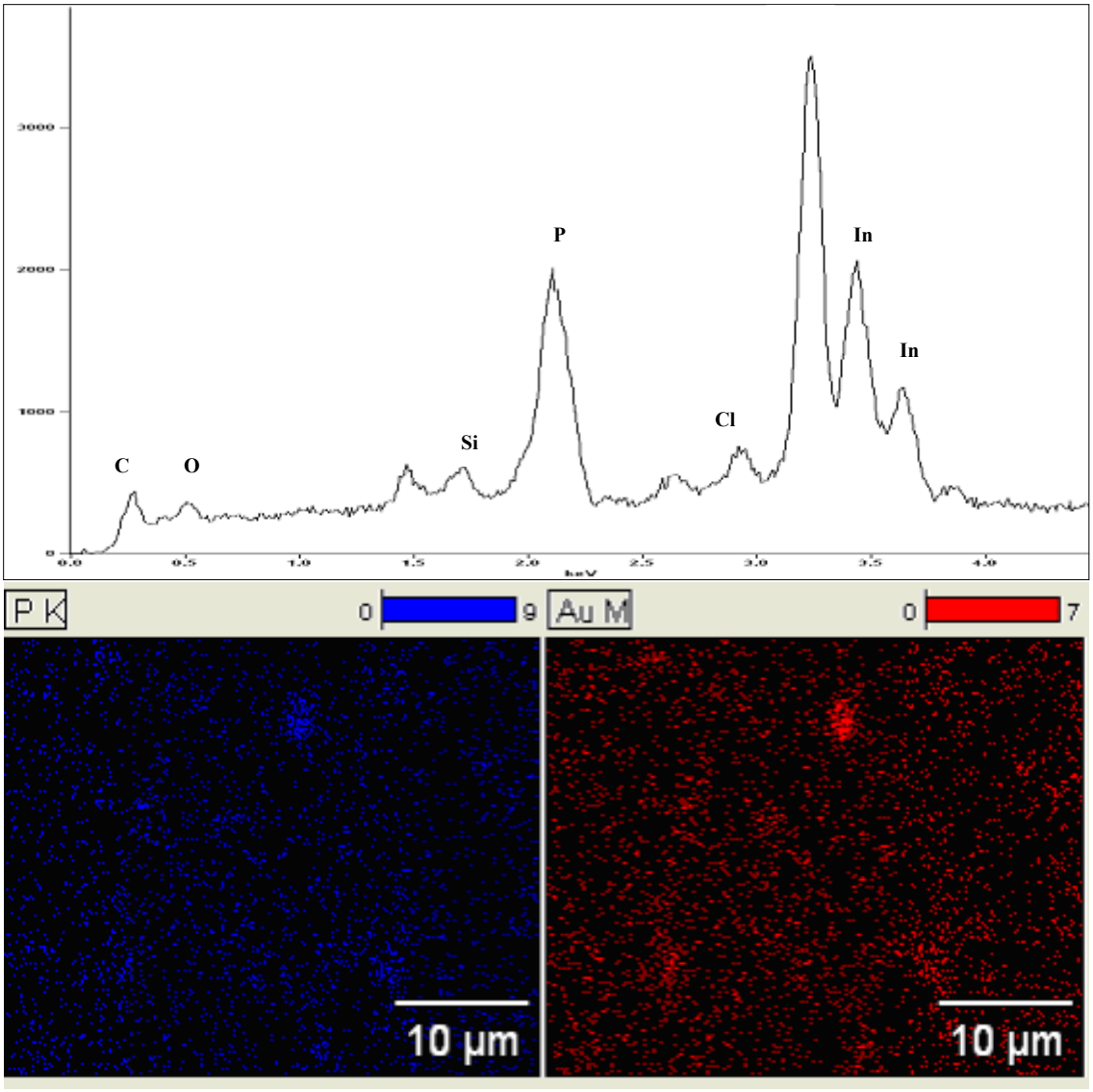


Figure 3.23: EDX spectra from purple solid using SEM and the elemental P and Au map obtained using EDX.

Table 3.6: The presence of different elements in the brown solid from EDX analysis.

Element	Net count	Element Wt%	Atom%
C	3567	11.55	36.87
N	1035	4.97	13.61
O	1642	8.58	20.56
Si	1951	1.14	1.56
P	8111	4.01	4.96
Cl	3999	1.99	2.15
In	76566	51.01	17.03
Au	21571	16.75	3.26

The TEM image, Figure 3.24, revealed that the TPP stabilized gold nanoparticles were still very monodisperse with a particle size of 3.9 ±0.4 nm. The particles also retained there self-assembly after the ligand exchange reaction. This result is very interesting, in the sense that the self-assembled monolayers of gold nanoparticles can hold its morphology after simple ligand exchange reaction. In some cases, the surfactant exchange reaction resulted in the deterioration of the quality of the nanoparticles, producing nanoparticles with deformed shapes and/or a broadened size distribution.[49]

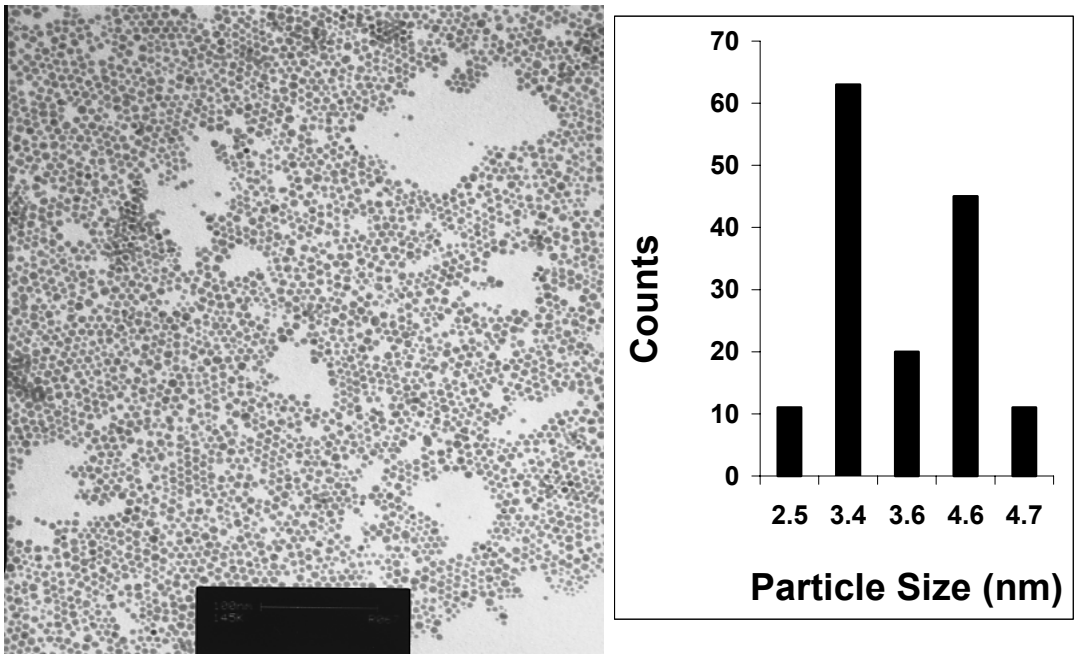


Figure 3.24: TPP stabilized gold nanoparticles and the corresponding histogram.

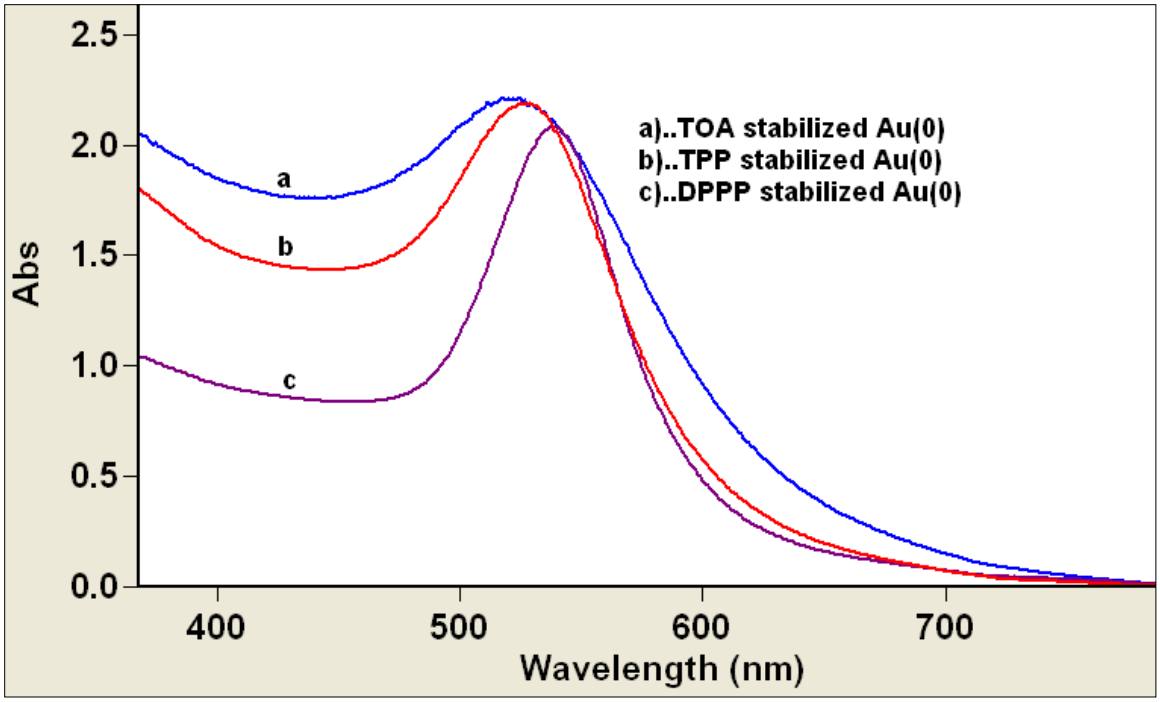


Figure 3.25: Comparison of UV-vis absorption maxima for gold nanoparticles in the presence of different surfactants.

The UV-vis spectrum of the redispersed dark purple solid in toluene was also analyzed. Optical spectra of the amine stabilized gold nanoparticles and exchange product is shown in Figure 3.25. A similar kind of ligand exchange reaction was also carried out using DPPP as a surfactant. In this case, we have achieved individual spherical gold nanoparticles of 3.3 ±0.6 nm in size. The particle population in the solution was relatively lower compared to TPP, which tells that the DPPP stabilized gold particles are not very stable in solvent compared to TPP stabilized gold nanoparticles. When the DPPP dispersion was analyzed by ^{31}P NMR, the data showed DPPP ligands were on nanoparticle surface, Figure 3.27. Table 3.7 represents the comparison studies of UV-vis absorption maxima and average particle size analysis of the gold nanoparticles before (TOA stabilized) and after (TPP and DPPP stabilized) ligand exchange study.

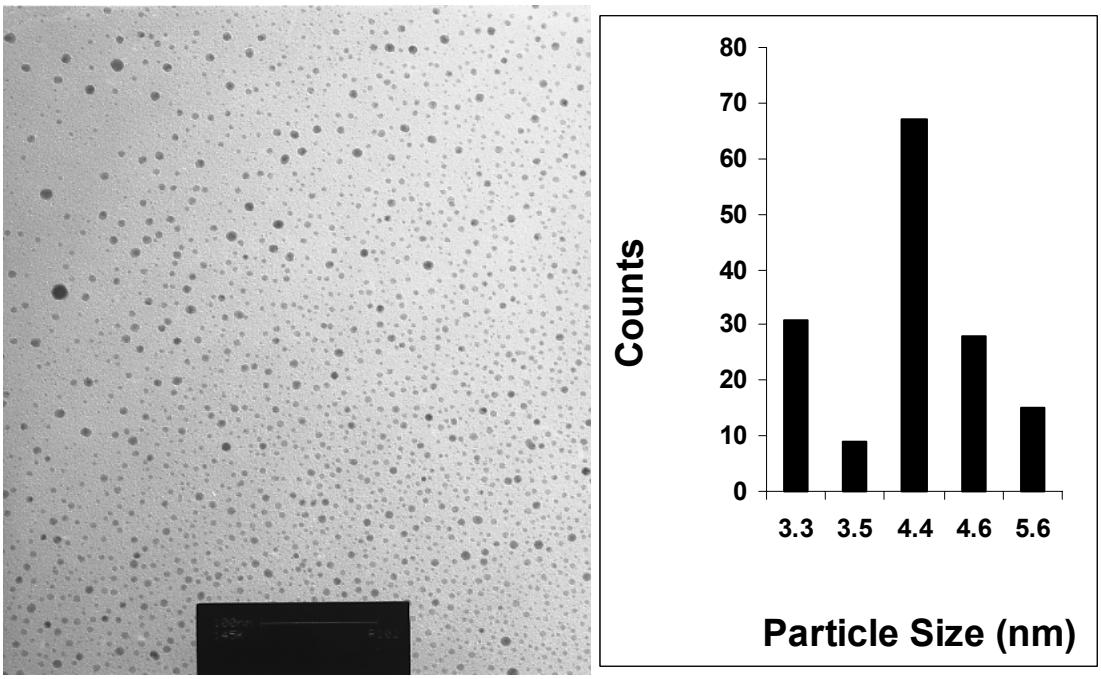


Figure 3.26: DPPP stabilized gold nanoparticles and the corresponding histogram.

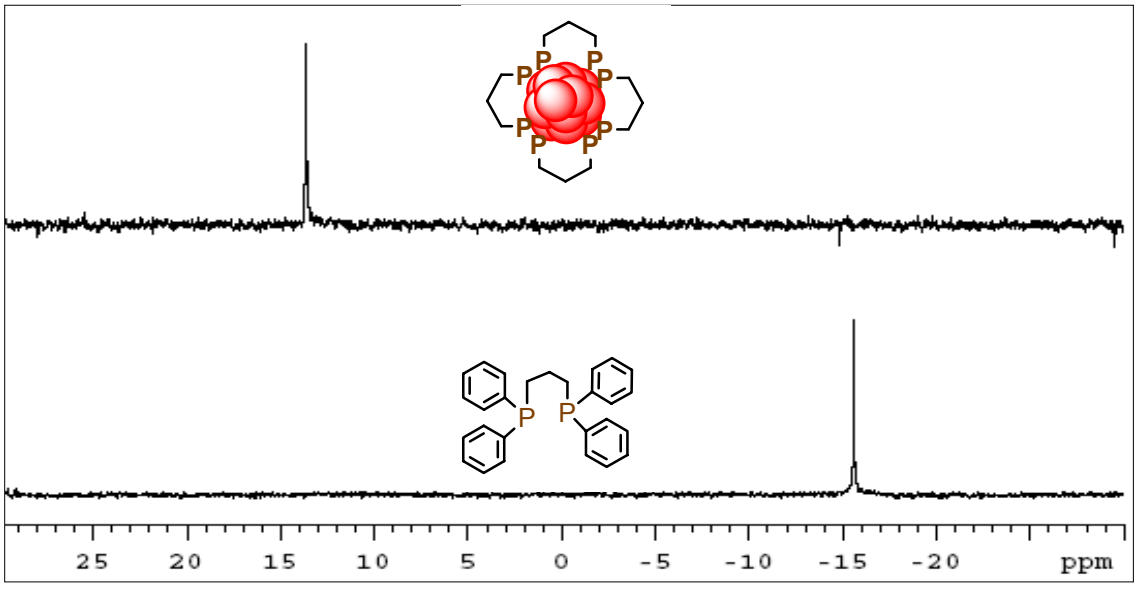


Figure 3.27: Representative ^{31}P NMR spectra of DPPP and the corresponding DPPP-stabilized gold nanoparticles.

Table 3.7. Comparison of UV-vis absorption maxima and particle size analysis of gold nanoparticles in the presence of different surfactant

Entry	Gold Sols	Ligand	UV-vis absorption (λ_{max}: nm)	Particle size (nm)
1	Au-HMTS	TOA	520-525	3.6 (0.4)
2	Au-HMTS	TPP	526-529	3.9 (0.4)
3	Au-HMTS	DPPE	532-537	3.3 (0.6)
4	Au-HMTS	DPPP	530-533	4.3 (0.7)
5	Au-HMTS	DPPB	530-538	4.9 (1.1)

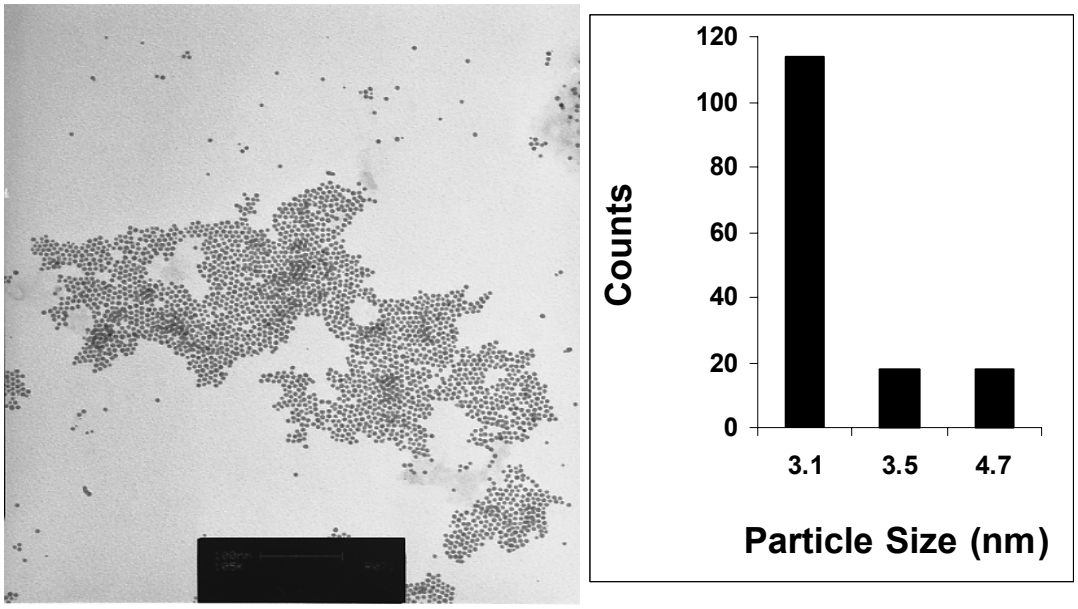


Figure 3.28: DPPE stabilized gold nanoparticles and the corresponding histogram.

3.7 Conclusions

In this section we have described a unique system consisting of hydrophobic, organically capped self-assembled monolayers of gold nanocrystals functionalized with TOA. Specifically we have discussed on the synthesis, characterization, and ligand exchange studies of 3-5 nm average diameter TOA capped gold nanoparticles. The self-assembled gold nanoparticles were achieved by simple one step reduction of chloroauric acid by HMTS, in the presence of TOA. The synthesized gold nanoparticles were allowed to do ligand exchange chemistry for the preparation of highly functionalized nanoparticles and suggest a broaden applicability of the method. The synthesized nanoparticles were characterized by NMR, UV-vis, TEM, XPS, and SEM.

3.8 Experimental section

Chemicals.

Silver acetate, silver nitrate, silver perchlorate, silver tetrafluoroborate, silver heptafluorobutyrate, trioctylamine (TOA), Hydrogen tetrachloroaurate trihydrate ($HAuCl_4.3H_2O$), heptamethyltrisiloxane (HMTS), triphenylphosphine, and were obtained from Aldrich Chemical Company and used without further purification. 1,2-bis(diphenylphosphino)propane from Strem chemical company.. Toluene, THF, benzene, cyclohexane, and dichloromethane were obtained from Fisher scientific company and distilled by Innovative Technology instrument before being used. Acetonitrile was purchased from EMD chemicals (omnisolv, HPLC grade) and used without further

purification. All the reactions were carried out at room temperature under positive pressure of nitrogen.

Experimental Technique.

Microscopic UV-Visible absorption measurements were carried out with a Varian Cary 50-scan spectrophotometer in a10-mm optical path length quartz cuvettes. All spectra shown here are the result of macroscopic measurements performed in standard transmission geometry with unpolarized light impinging upon the surface at normal angle of incidence. Transmission electron microscope (TEM) is a suitable technique used in investigating the size and shape changes of small metallic nanoparticles. The TEM micrographs were obtained with the help of a Philips CM-100 instrument operating at 80 Kv accelerating voltage. TEM samples were prepared by placing a drop of centrifuged reaction mixture on the surface of a 150 mesh (Electron Microscopy Science, Port Washington, PA) copper grid backed with formver and were dried at ambient temperature. The crude reaction mixtures were centrifuged for 10 minutes before deposition on the grid. Particle size analysis was conducted using the Scion Image Beta 4.02 Software (available on the Internet at http://www.scioncorp.com). Images, which have 100 nm scale bar, was chosen to do the particle size analysis. In Scion Image, after setting the unit and known distance the 'Analyze Particle' parameter was used to generate a table of particle diameter. This table was then exported into Microsoft Excel 2000 where statistical analysis and histogram plotting were performed. Scanning electron microscope Amray 1910 (SEM) equipped with EDX was used to conduct the morphological studies of the semisolid product before redispersion. X-ray photoelectron

spectroscopy (XPS) study of the solid was performed with an Omicron Nanotechnology XPS instrument equipped with Mg Kα X-ray source (hυ = 1253.6 eV).

Silver Nanoclusters Synthesis.

The typical synthesis consisted of the following: in a round bottom flask a measured amount of AgOAc (0.2 mmol, 0.032g) suspension was prepared in 50mL toluene. After 10 minutes of stirring, HMTS (1.2mmol, 0.33mL) was added to the silver acetate suspension. The solution was stirred for an additional 10 minutes, after which TOA (0.8mmol, 0.35mL) was injected into the flask. Upon addition of TOA, the colorless solution turned to light yellow and as the reaction progressed it changed to dark yellow. The reaction progress was followed by monitoring the absorption changes in UV-vis spectroscopy at different time intervals. When the absorbance reached its maxima, the total solution was centrifuged and from that one drop was deposited on the TEM grid for morphological analysis. Under similar reaction conditions and identical molar ratios, the reduction of other silver salts, $AgNO_3$, $AgBF_4$, $AgF_7C_4O_2$, and $AgClO_4$ were also investigated. When the reduction of $AgNO_3$ was completed the solution was a reddish brown color. In the $AgBF_4$ reduction the solution was a golden brown color. When $AgF_7C_4O_2$ reduction was completed the solution was a light brown color. The $AgClO_4$ reduction resulted in a dark brown color.

Gold Nanoclusters Synthesis.

A yellow homogeneous solution (λ_{max}: 322 nm) of $HAuCl_4.3H_2O$ (0.008 gm, 0.02 mmol) was prepared in 20 ml acetonitrile. The (0.04-0.12) mmol of TOA was added and the

solution was stirred vigorously at room temperature for 30 minutes. After 30 min stirring, resulted a colorless homogeneous solution. At this point HMTS (0.12 mmol, 0.04 ml) was injected into the solution and rapid stirring was continued. 30 minutes after the addition of HMTS, the colorless solution turned to light purple color. The formation of gold nanoparticles was confirmed by monitoring the UV-vis spectroscopy at different time intervals. When the UV-vis absorption peak touched its maxima, the solution was centrifuged and from that one drop deposited on the formver coated copper carbon grid for TEM analysis.

General Procedure for the Ligand Exchange Reaction.

SAMs of gold nanoparticles were synthesized using 6 equivalents of HMTS (0.12 mmol, 0.04 ml) in the presence of 4 equivalents of TOA (0.08 mmol, 0.04 ml). The particle size was 3.6 ±0.4 nm. To this pre-synthesized SAMs, 4 equivalents (0.08 mmol, 0.02 gm) of TPP were added. After the addition of TPP and stirring for 3h at room temperature, almost all the particles were precipitated out from the solution. The particles were isolated by centrifugation, and washed three times with 20 ml of acetonitrile. Drying in vacuum resulted the product as a dark purple solid. To that dark purple solid, 20-ml of distilled toluene was added and stirred for 2 more hours. After 2h of stirring at room temperature, it was a blue color homogeneous solution. The product was characterized by XPS, UV-vis spectroscopy, ^{31}P NMR spectroscopy, and TEM. Similar place exchange study was carried out for DPPE, DPPP, and DPPB ligands.

3.9 References

1. Alivisatos, A. P. *Science* **1996**, *271*. 933.

2. (a) Andres, R. P. Bielefeld, J. D. Henderson, J. I.; Jones, D. B.; Kolagunta, V. R.; Kubiak, C. P.; Mohoney, W. J.; Osifchin, R. G. *Science* **1996**, *273*, 1690. (b) Harfenist, S. A.; Wang, Z. L.; Alvarez, M. A.; Vermar, I.; Whetten, R.L. *J. Phys. Chem.* **1996**, *100*, 13904. (c) Sun, S.; Andres, S.; Hamann, H. F.; Thiele, J. U.; Baglin, J. E. E.; Thomson, T.; Fullerton. E. E.; Murray, C. B. Terris, B. D. *J. Am. Chem. Soc*. **2002**, *124*, 2884. (d) Murray, C. B.; Norris, D. J.; Bawendi, M. G. *J. Am. Chem. Soc*. **1993**, *115*, 8706.

3. (a) Vossmeyer, T.; Katsikas, L.; Giersig, M.; Popovis, I. G.; Diesner, K.; Chemseddine, A.; Eychmueller, A.; Weller, H. *J. Phys. Chem*. **1994**, *98*, 7665. (b) Weller, H. *Angew. Chem*. **1996**, *35*, 1079.

4. Aiken, J. D., III; Finke, R. G. *J. Mol. Catal. A. Chem*. **1999**, *145*, 1.

5. Herron, N.; Galabrese, J. C.; Farneth, W. E.; Wang, Y. *Science* **1993**, *259*, 1426.

6. (a) Schmid, G. *Chem. Rev*. **1992**, *92*, 1709. (b) Lewis, L. N. *Chem. Rev*. **1993**, *93*, 2693 and references therein.

7. (a) Motte, L.; Billoudet, F.; Lacaze, E.; Douin, J.; Pileni, M. P. *J. Phys. Chem B*. **1997**, *101*, 138. (b) Sarathy, K. V.; Kulkarni, G. U. Rao, C. N. R. *J. Chem. Soc. Chem. Commun*. **1997**, 537. (c) Kim, B.; Tripp, S. L.; Wei, A. *J. Am. Chem. Soc*. **2001**, *123*, 7955. (d) Brousseau, L. C.; Novak, J. P.; Marinakos, S. M.; Feldheim, D. L. *Adv. Mater*. **1999**, *11*, 447. (e) Li, X. M.; de Jong, M. R.; Inoue, K.; Shinkai, S.; Huskens, J.; Reinhoudt, D. N. *J. Mater. Chem*. **2001**, *11*, 1919. (f) Jana, N. R.; Peng, X. *J. Am. Chem. Soc*. **2003**, *125*, 14280.

8. (a) Chen, S.; Fan, Z.; Carroll, D. L. *J. Phys. Chem B*. **2002**, *106*, 10777. (b) Collier, C. P.; Vossmeyer, T.; Heath, J. R. *Annu. Rev. Phys. Chem*. **1998**, *49*, 371. (c) Whetten, R. L.; Khoury, J. T.; Alvarez, M. M.; Murthy, S.; Vermar, I.; Wang, Z. L.; Steohens, P. W.; Cleveland, C. L.; Luedtke, W. D.; Landman, U. *Adv. Mater*. **1996**, *8*, 428. (d) Motte, L.; Billoudet, F.; Pileni, M. P. *Adv. Mater*. **1996**, *8*, 1018. (e) Motte, L.; Billoudet, F.; Pileni, M. P. *J. Phys. Chem*. **1995**, *99*, 16425.

9. (a) Maye, M. M.; Luo, J.; Lim, I. S.; Han, L.; Kariuki, N. N.; Rabinovich, D.; Liu, T.; Zhong, C. J. *J. Am. Chem. Soc*. **2003**, *125*, 9906. (b) Yin, J. S.; Wang, Z. L. *J. Phys. Chem. B* **1997**, *101*, 8979. (c) Heath, J. R.; Knobler, C. M.; Leff, D. V. *J. Phys. Chem. B* **1997**, *101*, 189.

10. (a) Stowell, C.; Korgel, B. A. *Nano Lett*. **2001**, *1*, 595. (b) Petroski, J. M.; Green, T. C.; El-Sayed, M. A. *J. Phys. Chem. A*. **2001**, *105*, 5542. (c) Peng, X.; Wickham, J.; Alivisatos, A. P. *J. Am. Chem. Soc.* **1998**, *120*, 5343.

11. (a) Sun, S.; Murray, C. B.; Weller, D.; Folks, L.; Moser, A. *Science* **2000**, *287*, 1989. (b) Murray, C. B.; Kagan, C. R.; Bawendi, M. G. *Science* **1995**, *270*, 1335. (c) Keely, C. J.; Fink, J.; Brust, M.; Bethell, D.; Schiffrin, D. J. *Nature* **1998**, *80*, 3807. (d) Pahl, K.; Bartelt, M. C.; de la Figuera, J.; Bartelt, N. C.; Hrbek, J.; Hwang, R. Q. *Nature* **1999**, *397*, 238. (e) Park, J.; An, K.; Hwang, Y.; Park, J. G.; Noh, H. J.; Kim, J. Y.; Park, J. H.; Hwang, N. M. Hyeon, T. *Nature* **2004**, *3*, 891

12. (a) Boal, A. K.; Ilhan F.; DeRouchet, J. E.; Thurn, A. T.; Russell, T. P.; Rotello, V. M. *Nature* **2000**, *404*, 746. (b) Murray, C. B.; Kagan, C. R.; Bawendi, M. G. *Annu. Rev. Mater. Sci*. **2000**, *30*, 545.

13. (a) Asher, S. A. U. S. Patents 4,627,689 and 4, 632,517. (b) Schmid, G. *Nanoparticles: From Theory to Application* (Wiley-VCH, Weinheim, 2004). (c) Klabunde, K. J. Nanoscale Materials in Chemistry (Wiley-Interscience, New York, 2001).

14. Kastner, M. A. *Phys. Today* **1993**, 24.

15. (a) Belloni, J.; Mostafavi, M.; Marignier, J. L.; Amblard, J. *J. Imaging Sci*. **1991**, *35*, 68. (b) Mostafavi, M.; Marignier, J. L.; Amblard, J. Belloni, J. *J. Radiat. Phys. Chem*. **1989**, *43*, 605.

16. (a) Kundu, S.; Mandal, M.; Ghosh, S. K.; Pal, T. *J. Colloid Interface Sci*. **2004**, *272*, 134. (b) Sudrik, S. G.; Maddanimath, T.; Chaki, N. K.; Chavan, S. P.; Sonawane, H. R.; Vijayamohanan, K. *Org. Lett*. **2003**, *5*, 2355.

17. (a) El-Sayed, M. A. *Acc. Chem. Res*. **2001**, *34*, 257. (b) Wei, G.; Wang, L.; Liu, Z.; Song, Y.; Sun, L.; Yang, T.; Li, Z. *J. Phys. Chem. B* **2005**, *109*, 23941.

18. (a) Li, P.; Li, J.; Wu, C.; Wu, Q.; Li, J. *Nanotechnology* **2005**, *16*, 1912. (b) Sondi, I.; Sondi, B. S. *J. Colloid Interface Sci*. **2004**, *275*, 177.

19. Brust, M.; Walker, M.; Bethell, D.; Schiffrin, D. J.; Whyman, R. *J. Chem. Soc. Chem. Commun*. **1994**, 801.

20. (a) Cliffel, D. E.; Zamborini, F. P. Gross, S. M.; Murray, R. W. *Langmuir* **2000**, *16*, 9699. (b) Rowe, M. P.; Plass, K. E.; Kim, K.; Kurdak, C.; Zellers, E. T.; Matzger, A. J. *Chem. Mater*. **2004**, *16*, 3513. (c) Yee, C. K. Jordan, R.; Ulman, A. White, H.; King, A.; Rafailovich, M.; Sokolov, J. *Langmuir* **1999**, *15*, 3486. (d) Shon, Y.-S.; Mazzitelli, C.; Murray, R. W. *Langmuir* **2001**, *17*, 7735. (e) Bharathi, S.; Lev, O. *J. Chem. Soc. Chem. Commun*. **1997**, 2303.

21. (a) Stoeva, S.; Klabunde, K. J. Sorensen, C. M.; Dragieva, I. *J. Am. Chem. Soc*. **2002**, *124*, 2305. (b) Selvan, S. T.; Spatz, J. P.; Klok, H. A.; Moller, M. *Adv. Mater*. **1998**, *10*, 132. (c) Schmid, G.; Baumle, M.; Beyer, N. *Angew. Chem. Int. Ed*. **2000**, *39*, 181. (d) Hiramatsu, H.; Osterloh, F. E. *Chem. Mater*. **2004**, *16*, 2509.

22. Bonnemann, H.; Brijoux, W.; Brinkmann, R.; Fretzen, R.; Joussen, T.; Koppler, R.; Korall, B. K.; Neiteler, P.; Richter, J. *J. Mol. Catal*. **1994**, *86*, 129.

23. (a) Chauhan, B. P. S.; Sardar, R. *Macromolecules* **2004**, *37*, 5357. (b) Chauhan, B. P. S.; Rathore, J. S.; Chauhan, M.; Krawicz. A. *J. Am. Chem. Soc*. **2003**, *125*. 2876.

24. Bain, C. D.; Evall, J.; Whitesides, G. M. *J. Am. Chem. Soc*. **1989**, *111*, 7155.

25. Fink, J.; Kiely, C.; Bethell, D.; Schiffrin, D. J. *Chem. Mater*. **1998**, *10*, 922.

26. Kang, S. Y.; Kim, K. *Langmuir* **1998**, *14*, 226.

27. (a) Linnert, T.; Mulvaney, P.; Henglein, A. *J. Phys. Chem*. **1993**, *97*, 679. (b) Makarova, O. V.; Ostafin, A. E.; Miyoshi, H.; Norris, J. R.; Meisel, D. *J. Phys. Chem. B* **1999**, *103*, 9080. (c) Thomas, K. G.; Zajicek, J.; Kamat, P. V. *Langmuir* **2002**, *18*, 3722.

28. Malinsky, M. D.; Kelly, K. L.; Schatz, G. C.; Van Duyne, R. P. *J. Am. Chem. Soc*. **2001**, *123*, 1471.

29. Nuzzo, R. g.; Allara, D. L. *J. Am. Chem. Soc*. **1983**, *105*, 4481.

30. Richard, M. A.; Deutsch, J.; Whitesides, G. M. *J. Am. Chem. Soc*. **1979**, *100*, 6613.

31. Adamson, A. W. *Physical Chemistry of Surface*, 3 rd ed.; Wiley: New York, 1976; Chapter 10.

32. Notoya, T.; Poling, G. W. *Corrosion* **1979**, *35*, 193.

33. Kaelble, D. H. *Physical Chemistry of Adhesion*; Wiley-Interscience; New York, 1971.

34. Prime, K. L.; Whitesides, G. M. *Science* **1991**, *252*, 1164.

35. Soriaga, M. P.; Hubbard, A. T. *J. Am. Chem. Soc*. **1982**, *104*, 3937.

36. Furtlehner, J. P.; Messier, J. *Thin Solid Films* **1980**, *68*, 233.

37. Logunov, S. L.; Ahmadi, T. S.; El-Sayed, M. A.; Khoury, J. T.; Whetten, R. L. *J. Phys. Chem. B* **1997**, *101*, 3713

38. (a) Burda, C.; Chen, X.; Narayanan, R.; El-Sayed, M. A. Chem. Rev. 2005, 105, 1024. (b) Link, S.; Mohamed, M. B.; El-Sayed, M. A. *J. Phys. Chem. B* **1999**, *103*, 3073. (c) Zhu, M.-Q.; Wang, L.-Q.; Exarhos, G. J.; Li, A. D. Q. *J. Am. Chem. Soc*. **2004**, *126*, 2656. (d) Xu, X.-H. N.; Huang, S.; Brownlow, W.; Salaita, K.; Jeffers, R. B. *J. Phys. Chem. B* **2004**, *108*, 15543.

39. Daniel, M.-C.; Astruc, D. *Chem. Rev*. **2004**, *104*, 293.

40. Mcneillie, A.; Brown, D. H.; Smith, W. E.; Gibson, M.; Watson, L. *J. Chem. Soc., Dalton Trans*. **1980**, 767.

41. Berven, C. A.; Clark, L.; Mooster, J. L.; Wybourne, M. A.; Hutchison, J. E. *Adv. Mater*. **2001**, *13*, 109. (b) Sone, J.; Fujita, J.; Ochiai, Y.; Manako, S.; Matsui, S.; Nomura, E.; Baba, T.; Kawaura, H.; Sakamoto, T.; Chen, C. D.; Nakamura, Y.; Tsai, J. S. *Nanotechnology* **1999**, *10*, 135. (c) Maier, S. A.; Brongersma, M. L. Kik, P. G.; Meltzer, S.; Requicha, A. A. G.; Koel, B. E.; Atwater, H. A. *Adv. Mater*. **2001**, *13*, 1507. (d) Mohr, C.; Hofmeister, H.; Radnik, J.; Claus, P. *J. Am. Chem. Soc*. **2003**, *125*, 1905. (e) Willner, I.; Willner, B. *Pure. Appl. Chem*. **2002**, *74*, 1773. (f) Hainfeld, J. F. *Science* **1987**, *236*, 450.

42. (a) Warner, M. G.; Hutchison, J. E. In *Functionalization and Surface Treatment of Nanoparticles*; Baraton, M.-I., Ed.; American Scientific Publishers: San Francisco, 2003; pp 67. (b)

43. Woehrle, G. H.; Brown, O. L.; Hutchison, J. E. *J. Am. Chem. Soc*. **2005**, *127*, 2172.

44. Templeton, A. C.; Wuelfing, W. P.; Murray, R. W. *Acc. Chem. Res*. **2003**, *33*, 27.

45. Wellsted, H.; Sitsen, E.; Caragheorgheopol, A.; Chechik, V. *Anal. Chem*. **2004**, *76*, 2010.

46. John, W. *J. Struct. Biol*. **1999**, *127*, 106.

47. Son, S. U.; Jang, Y.; Yoon, K. Y.; Kang, E.; Hyeon, T. *Nano Lett*. **2004**, *4*, 1147.

48. Zorn, G.; Gotman, I.; Gutmanas, E. Y.; Adadi, R.; Salitra, G.; Sukenik, C. N. *Chem. Mater*. **2005**, *17*, 4218.

49. Wang, Y.; Teng, X.; Wang, J.-S.; Yang, H. *Nano Lett*. **2003**, *3*, 789.

Chapter 4

Polyhydrosiloxane an efficient reagent to control the nucleation and growth of metal nanoparticles: Shape control synthesis of gold nanostructures

Part A
Polymethylhydrosiloxane mediated one-pot synthesis of spherical, prismatic, and rod shaped gold nanocrystals

4.1 Introduction

Synthesis of metal nanostructures has been an active research area for many decades, because of the importance of these materials in biological labeling,[1] catalysis,[2] and information storage.[3] Like their semiconductor cousins (quantum dots), the intrinsic properties of metal nanostructures can be tailored by controlling their size, shape, composition, crystallinity, and structure (solid versus hollow). For example, computational work has predicted that, for silver or gold nanoparticles, the number and position of surface plasmon resonance (SPR) peaks, as well as the effective spectral range for surface-enhanced Raman scattering (SERS), are strongly dependent on the particle shape.[4] Experimentally, the longitudinal SPR modes of silver and gold nanorods have been shown to greatly red-shift with increasing aspect ratio. In addition, arrayed triangular nanoparticles of silver have been demonstrated as effective substrates for SERS in the spectral range from 700 to 800 nm, while spherical nanoparticles of gold are most suitable in the range of 530 to 570 nm.[4] In spite of its fundamental and technological importance (as well as a long history of study), the challenge to synthetically and deterministically control the shape of metal nanostructures has been met with limited success. Design of a generic method for the preparation of metal nanostructures with a broad range of well-defined and controllable morphologies is still

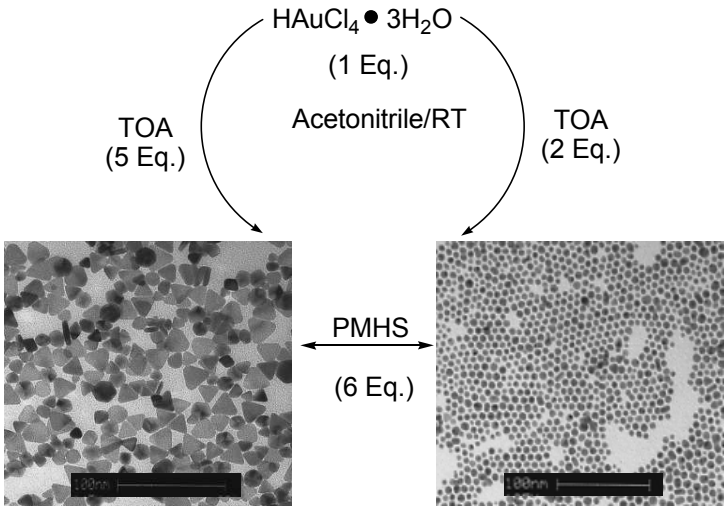
needed in order to fully exploit their peculiar properties and unique applications. Besides giving us novel properties, creating noble nanostructures requires novel understanding of their nucleation and growth process. The nucleation stage for the growth of anistropic shapes plays a key role in determining the size/shape of the resulting nanostructures.

To fully exploit such interesting properties of metal nanoparticles, with highly symmetric shapes, a new method is desirable where the crystal growth can be controlled. In earlier work, various studies have been explored on the size, shape and composition controlled metal nanoparticles.[5] A significant amount of research has already been carried out for cubes,[6] rods,[7] and wires,[8] but little has been accomplished with triangular nanostructures.[9] Thermal and or photochemical methods have been used for the synthesis of metal and semiconductor nanoprisms,[10] while biological, or seed methods, have also been available for the synthesis of triangular gold nanostructures.[11] The limitations of the methods includes, synthesis in aqueous solvents, and over 100 nm size regime of the synthesized nanoprisms.[11,12]

In chapter 3, part B of this dissertation, we have discussed the reducing properties of hydrosiloxane for the generation of gold nanoparticles. This work described the synthesis of self-assembled monolayers of gold nanoparticles using monomeric hydrosiloxane as a reducing agent. We have also successfully investigated the reducing properties of polyhydrosiloxane (PMHS) for the reduction of metal salts such as silver, palladium and platinum.[13] As an extension of the work, here in this chapter we discuss the effect of hydrosiloxane structure (e.g. chain length) on nucleation and growth process, and how it influences the particle morphologies. In this chapter, we describe a single step, high yielding synthetic route to gold nanoparticles employing this novel reducing agent,

PMHS. The versatility of this method is exemplified by this ability to synthesize gold particles with controllable geometry (i.e. nanoprisms, nanoparticles, and nanorods). All this geometries were achieved by simple variation of reducing agent and the surfactant concentration.

4.2 Results and Discussion

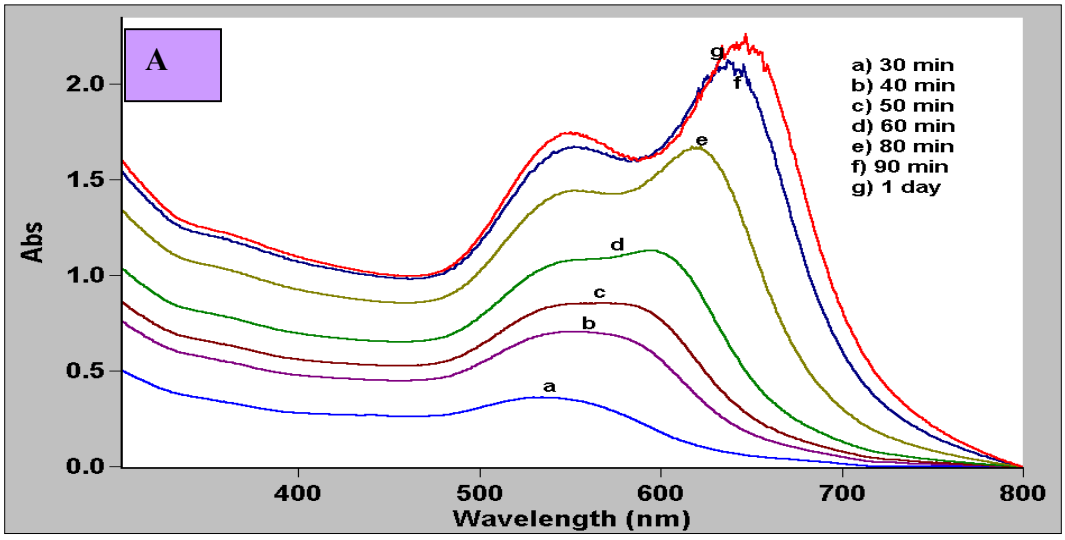


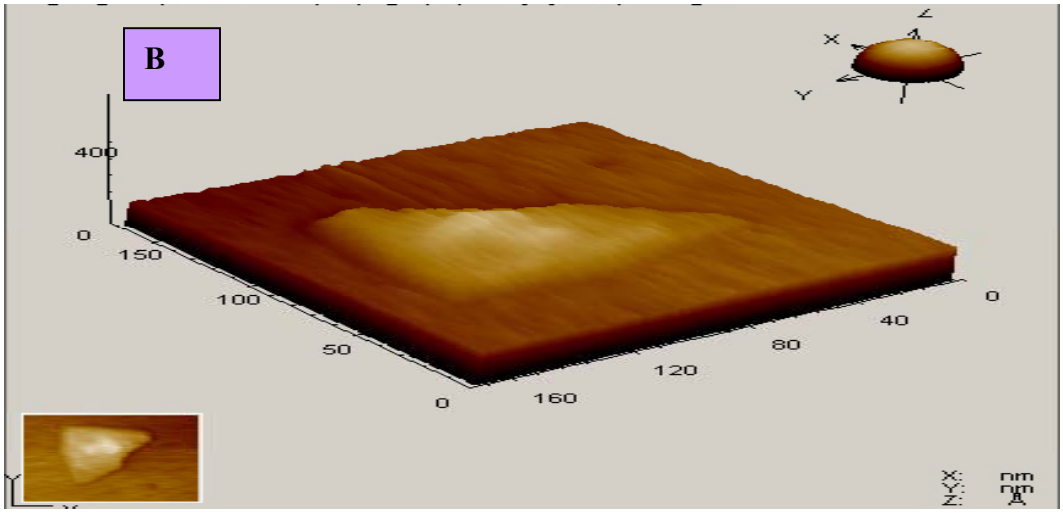
Scheme 4.1: Schematic illustration of the formation of spherical and prismatic gold nanostructures in the presence of different amounts of TOA.

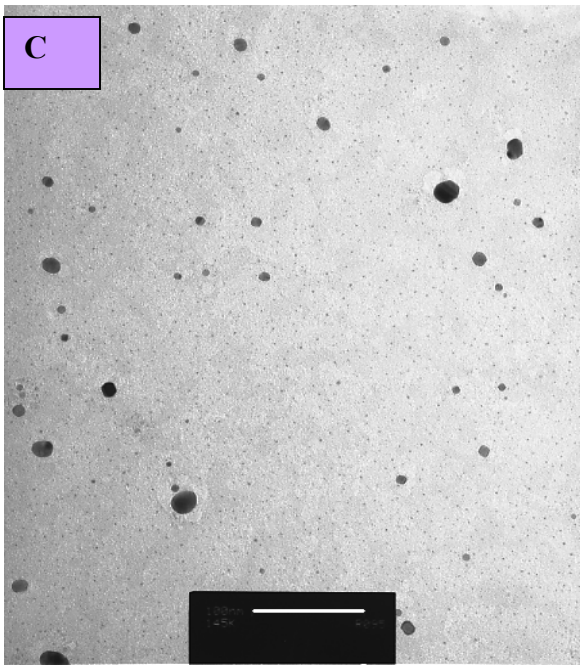
Gold nanoprisms were synthesized from a stirred solution of 0.008 gm of $HAuCl_4.3H_2O$ (0.02 mmol) in 20 ml acetonitrile. The chloroauric acid was completely soluble in acetonitrile and produced a yellow homogeneous solution (λ_{max}: 322 nm). After 30 minutes, TOA (0.10 mmol, 0.043 ml) was added and within another 30 minutes the yellow solution converted to a colorless homogeneous solution. At this juncture, PMHS (0.12 mmol, 0.008 ml) was injected. 30 minutes after the addition of all the reactants, the colorless solution turned purple (λ_{max}: 534 nm). As the reduction

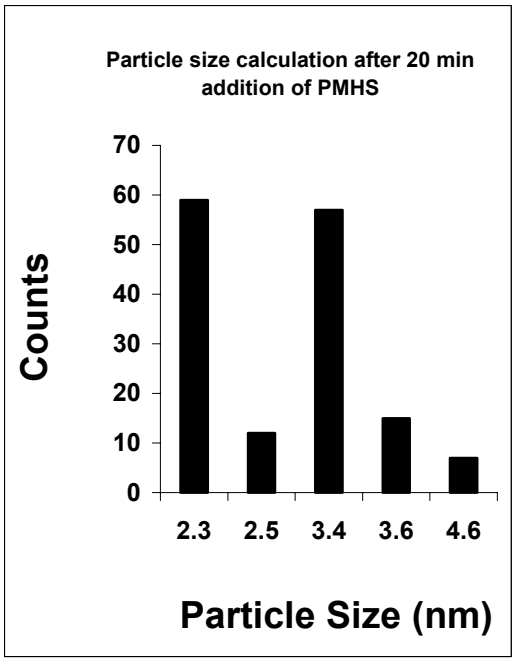
proceeded, the purple color turned to deep purple (λ_{max}: 598 nm) and finally it was a deep blue color solution (λ_{max}: 645 nm). The UV-vis absorption spectra of the reaction mixture were recorded promptly at different time intervals.

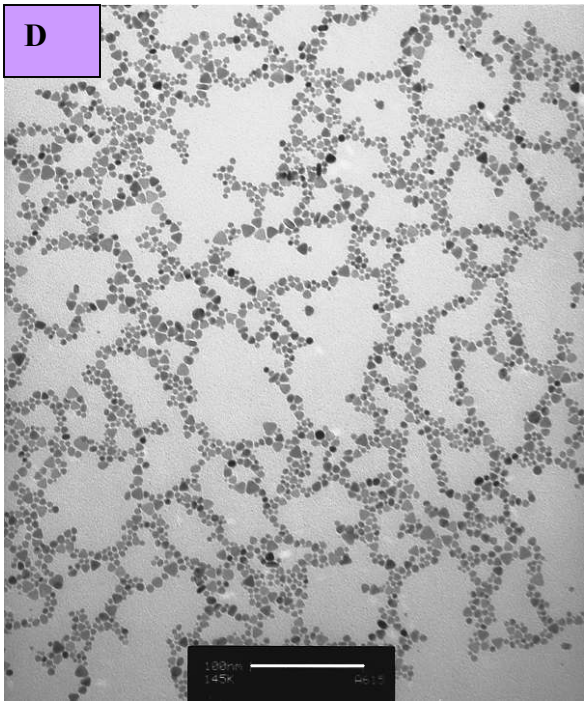
A Philips CM-100 transmission electron microscope, operating at 80 KV, was used to characterize the size and shape of resulting nanocrystals. There were three distinctive stages of nanoprisms formation: induction, growth and termination were identified. All those process were monitored by UV-vis absorption spectroscopy and transmission electron microscopy (Figure 4.1). After 30 minutes of the addition of PMHS, the color of the solution was purple and displayed an absorbance at 534 nm indicates the presence of spherical particles. Within another 10 minutes, the position of the plasmon band (560 nm) changed significantly. The detail TEM studies showed that during the induction period, small spherical gold clusters (1.3-2.3 nm) along with small nanoprisms (5 ± 1 nm edge length) were formed. The nanoprisms were 29 % in abundance respect to the total particles. As the reduction progressed, a second band was observed initially at 598 nm, and this band red shifted with time. This band was assigned to the dipole resonance of the gold nanoprisms that finally appeared at 645 nm in conjunction with another band that appeared at 530 nm. After then no increment on the absorption maxima was observed. The shifts of λ_{max} were most likely due to the increase in nanoprism edge length. The blue solution containing nanoprisms did not show any significant change in intensity of plasmon bands for long period of storage time and was stable under ordinary laboratory condition.

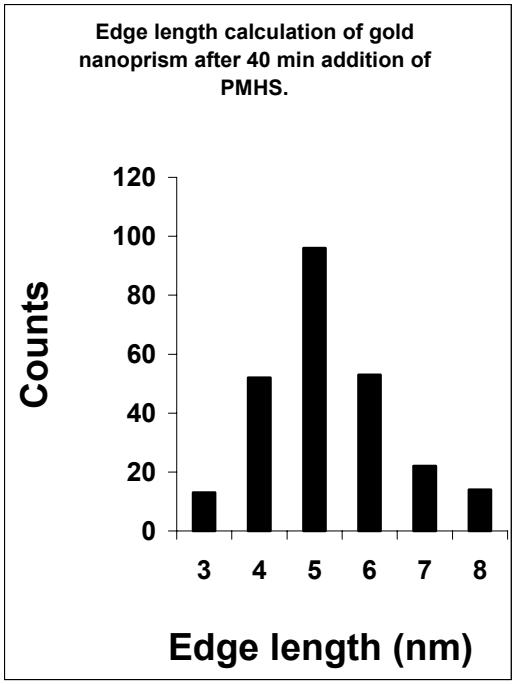

A
a) 30 min
b) 40 min
c) 50 min
d) 60 min
e) 80 min
f) 90 min
g) 1 day
Abs
Wavelength (nm)
2.0
1.5
1.0
0.5
0.0
400
500
600
700
800


B
400
0
150
100
50
0
160
120
80
40
0


C


Particle size calculation after 20 min addition of PMHS
Counts
70
60
50
40
30
20
10
0
2.3
2.5
3.4
3.6
4.6
Particle Size (nm)


D


Edge length calculation of gold nanoprism after 40 min addition of PMHS.
Counts
120
100
80
60
40
20
0
3
4
5
6
7
8
Edge length (nm)

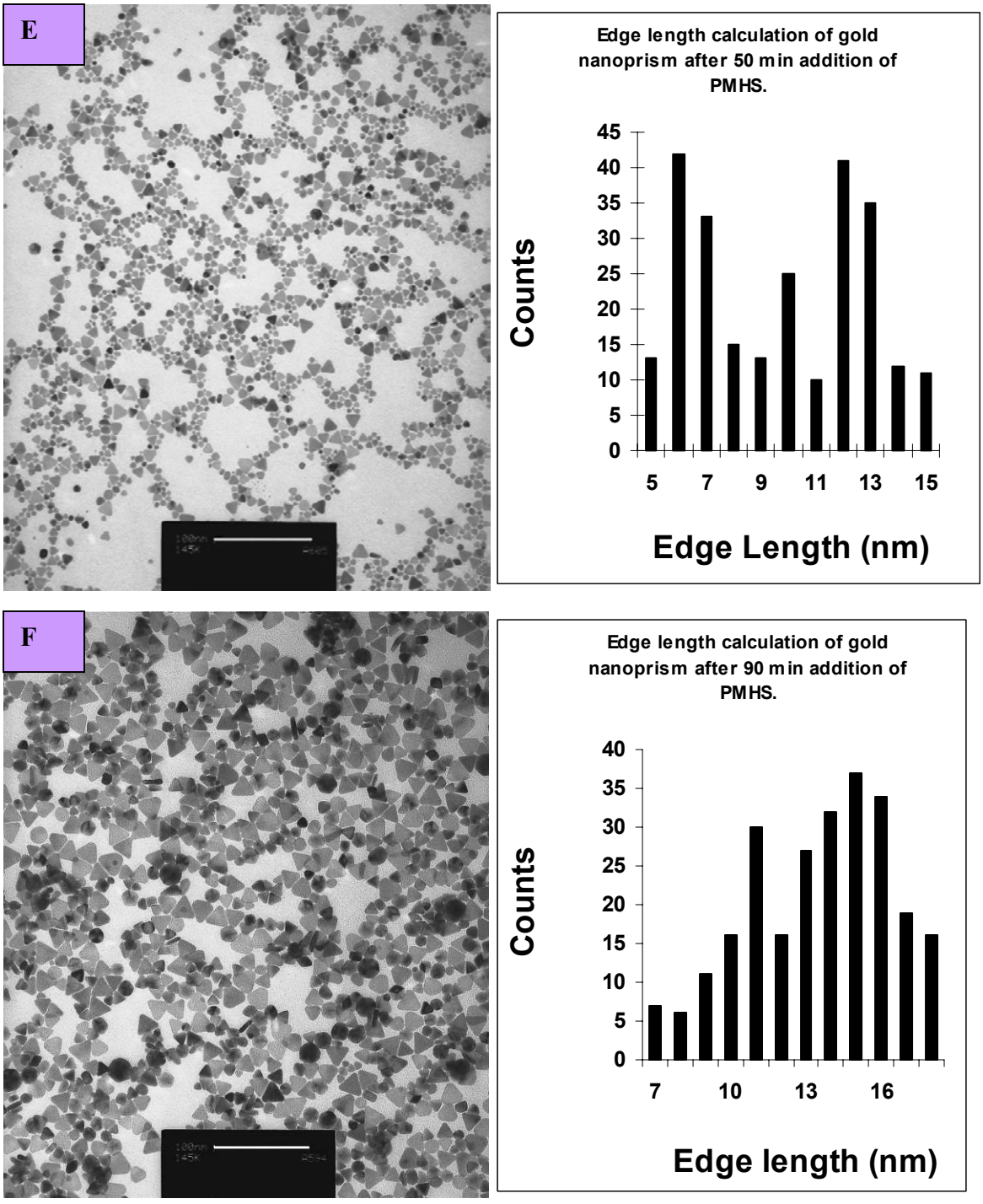


Figure 4.1: (A) UV-vis absorption spectra, (B) AFM image, and TEM analysis of nanoprism formation at different stages of reaction: after (C) 20 min (D) 40 min (E) 50 min and (F) 90 min of PMHS addition. Scale bar is 100 nm.

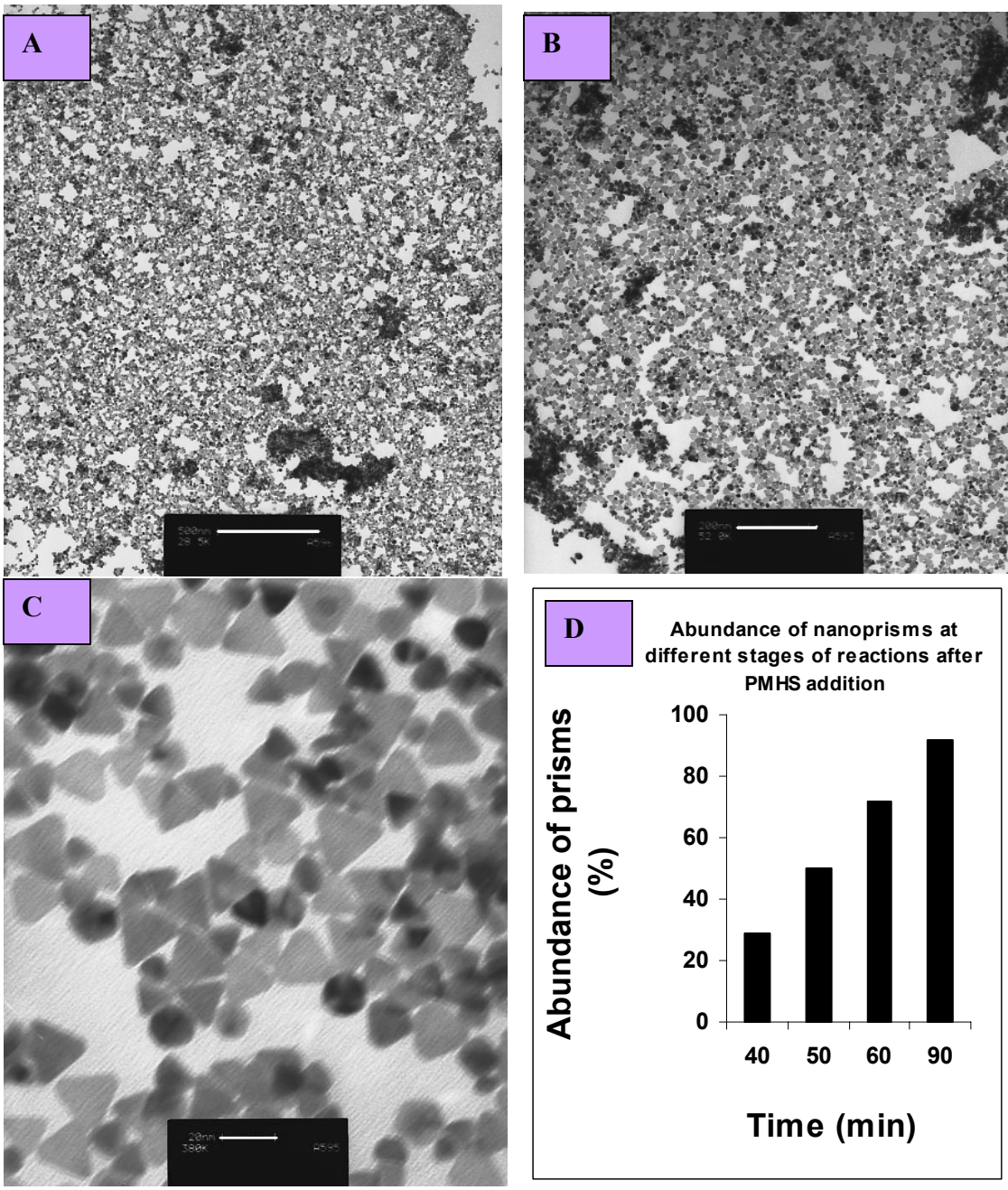


Figure 4.2: TEM analysis of the synthesized gold nanoprisms after 90 min of the addition of PMHS at different scale bar (A) 500 nm, (B) 200 nm, and (C) 20 nm. (D) The abundance of the nanoprisms at different time interval of reaction after PMHS addition.

Table 4.1: Comparison of UV-vis absorption maxima, populations and average edge length of gold nanoprism at different stages of reaction.

Entry	Reaction time (min)	UV-vis Abs. λ_{max} (nm)	Prism Population (%)	Edge length (nm)
1	40	560	29	5±1
2	50	598	50	8 ± 2, 13 ± 2
3	90	550, 645	90	14 ± 3

50 min after the addition of all the reactants, nearly 50 % of the total particles were gold nanoprisms which is significantly higher compare to previous work.[11] The total nanoprism morphology consists two different size distributions, with smaller prisms and the larger prisms having average edge lengths of 8 ± 2 nm and 13 ± 2 nm, respectively. With respect to time, the number of gold nanoprisms in solution gradually increased and at the end of reaction, almost 90% particles were triangular nanoprism with average edge length of 14 ± 3 nm. The TEM analysis gives us an idea about the growth of nanoprisms. After the induction period, it seems that the small nanpoprisms act as seeds and grow into large prisms, with the consumption of small spherical particles. When all the gold ions are reduced, the formation of spherical particles is stopped and the reaction terminates.

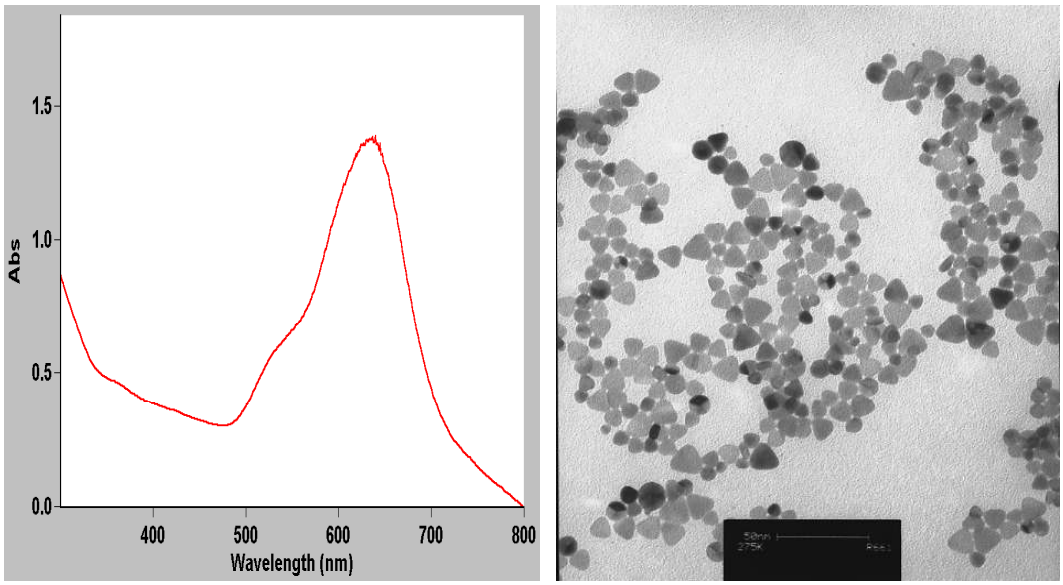


Figure 4.3: UV-vis absorption spectra and TEM image of gold nanoprisms dispersed in water.

It was observed that the particle stability, size, and shape strongly depend on the specific preparation methods and the experimental conditions applied. The solvent exchange studies of the synthesized gold nanoprism were also carried out to determine the property profile of the prism in aqueous solvent. Nanoparticles dispersed in water are useful in many applications starting from fluorescent tags in biology, contrast agents in magnetic resonance imaging (MRI), and green catalysts.[14] Ligand exchange procedures that allow the transfer of nanoparticles from organic solvents into water have therefore attracted considerable attentions. When solvents are removed from metal nanoparticle surface, it is very difficult to redispersed them in the same solvent even though the particles lose their activity and morphology. In this respect, after synthesizing the nanoprism, the acetonitrile was completely evaporated under high vacuum and a light purple color solid was obtained. To that solid, 20-ml distilled water was added and stirred

vigorously for 2h at room temperature. After stirring, it was a homogeneous solution, which was characterized by UV-vis absorption spectra and TEM. In this case we observed the presence of gold nanoparism of 13 ± 5 nm edge lengths and which was comparable to the freshly prepared prisms in acetonitrile, see Figure 4.3. We have observed an effect against this nanoprism stability, especially adsorption on the walls of silica containers for the higher concentration. Although, an advantage of this property can be taken for the application of the particles to the thin films preparation.

To find out the role of surfactant, the similar reduction was carried out in the presence of lower (2 equivalents) and higher (6 equivalents) amounts of TOA. For example, in an experiment, when PMHS (0.12 mmol, 0.008 ml) reduction of $HAuCl_4.3H_2O$ (0.02 mmol, 0.008 gm,) was carried out in the presence of 2 equivalent of TOA (0.04 mmol, 0.02 ml), the reaction mixture turned to purple color (λ_{max}: 520 nm) instead of blue, Figure 4.4. Surprisingly no gold nanoprisms were observed rather of the solution contained self-assembled spherical gold nanoparticles with 3.2 ± 0.5 nm, Figure 4.5.

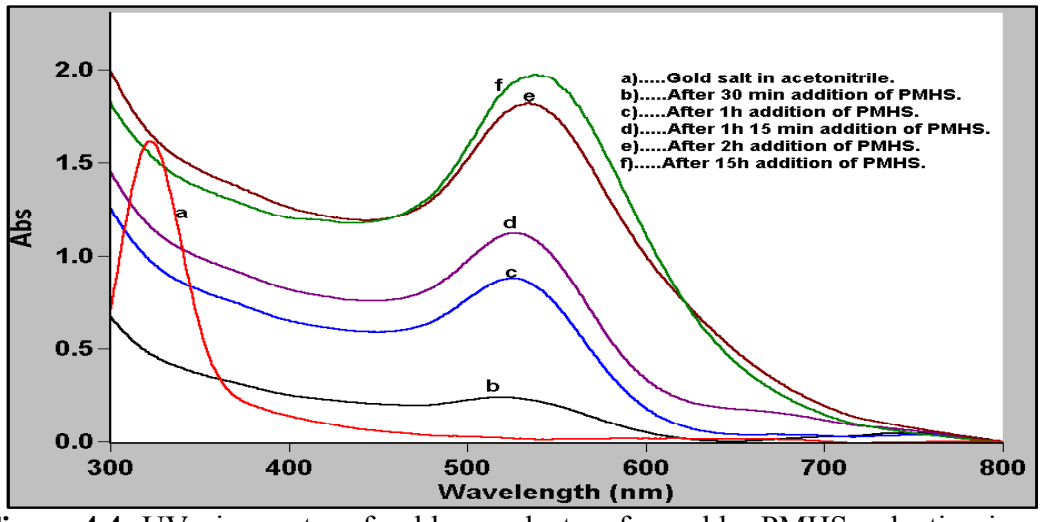


Figure 4.4: UV-vis spectra of gold nanoclusters formed by PMHS reduction in presence of 2 equiv of TOA.

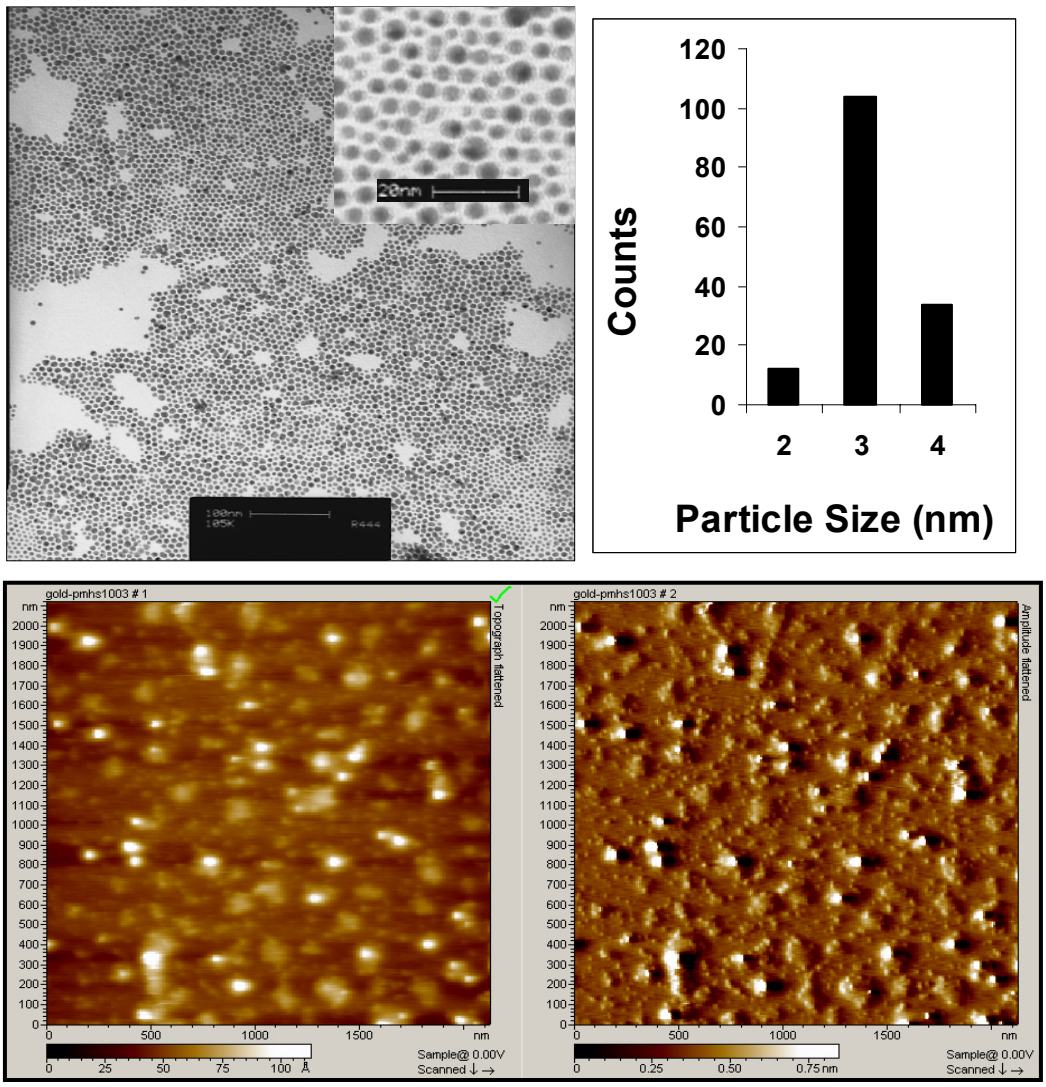


Figure 4.5: TEM image, particles size analysis, and AFM image of gold nanoclusters formed by PMHS reduction in presence of 2 equiv of TOA.

Table 4.2. Shapes of gold nanoparticles and corresponding reaction conditions.

Entry	$HAuCl_4$ Amount (mmol)	Amount of TOA (mmol)	Amount of PMHS (mmol)	Shape	UV-vis absorption (λ_{max}: nm)	Dimension (nm)§
1	0.02	0.04	0.12	Spherical	520	3.4 (0.5)
2	0.02	0.10	0.12	Prismatic	550, 645	14.0 (3.0)
3	0.02	0.12	0.12	Polyhedron	530	9.9 (1.1)
4	0.02	0.10	0.24	Rod	592	14.4 (2.0)

§For nanoparisms, this corresponds to the edge lengths, for rods, this corresponds to the lengths. These dimensions are averaged of 150 particles.

The similar reduction process was investigated in the presence of 6 equivalents of TOA, kept $HAuCl_4$ and PMHS concentration constant. It was observed that, with the increase of the amount of TOA, the rate of reduction was faster but the synthesized particles were not prismatic or spherical in shape. The particles were polyhedrons in shape with averagely 6-nm in size, Figure 4.6.

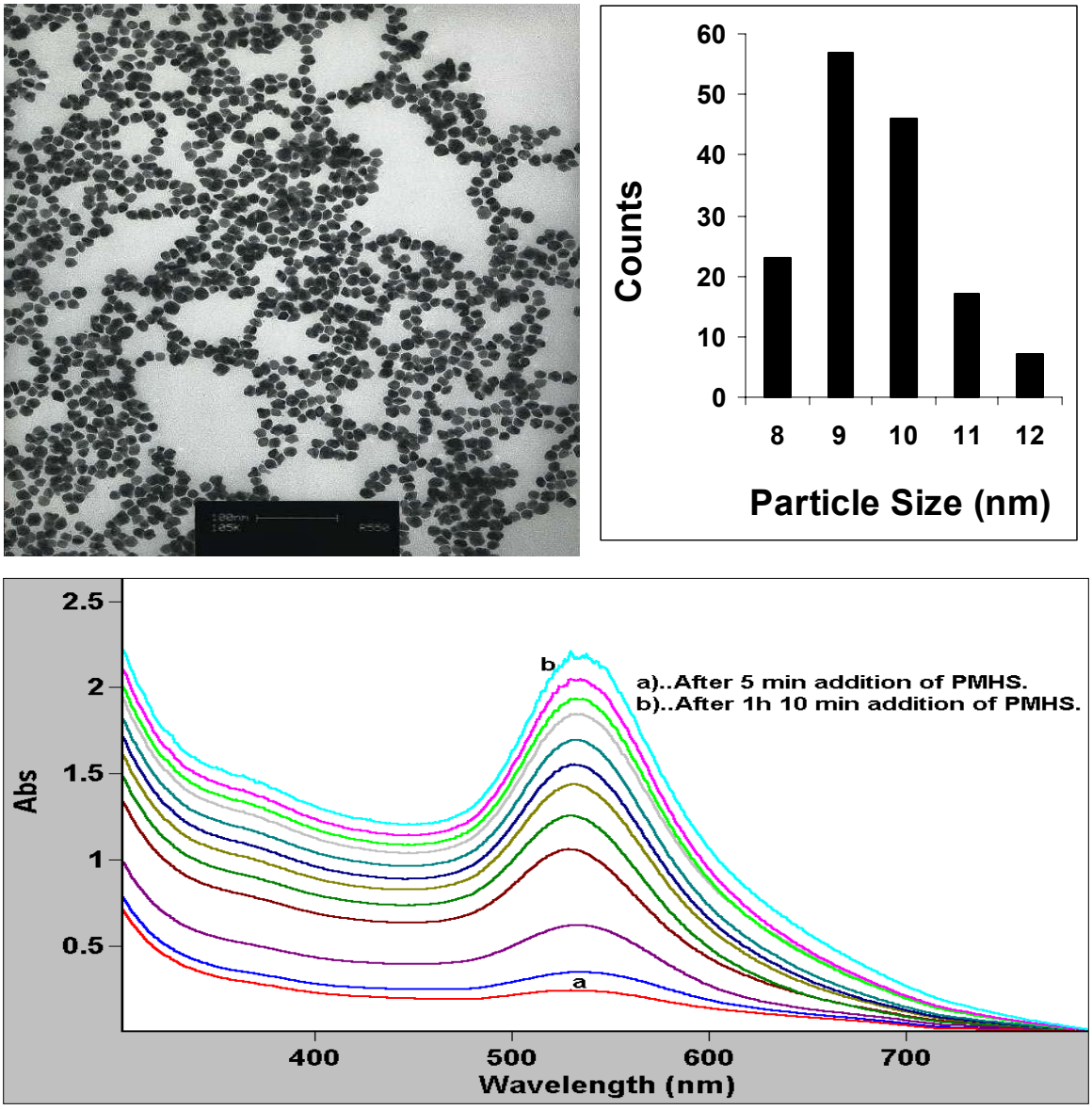
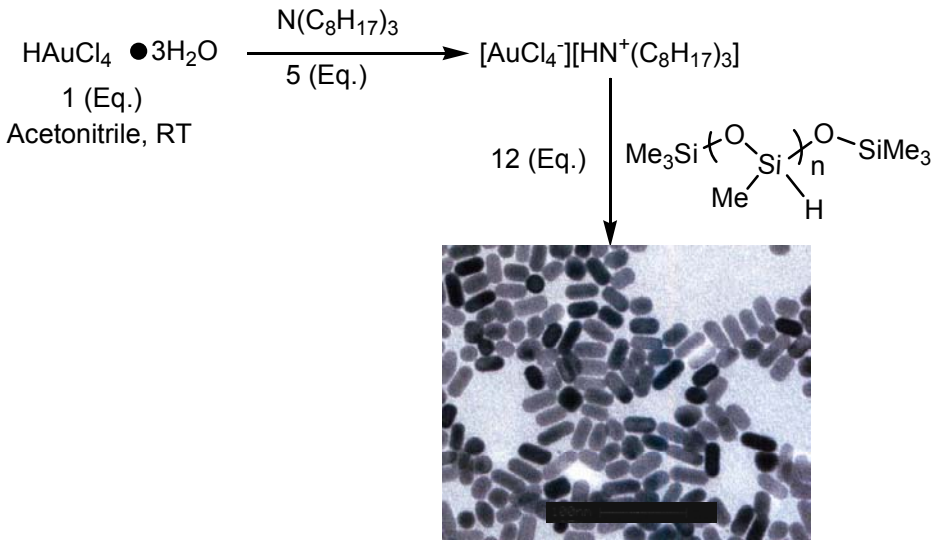


Figure 4.6: TEM image, particles size analysis, and UV-vis absorption spectra of gold nanoclusters formed by PMHS reduction in presence of 4 equiv of TOA

From the above-presented data, it is very clear that the morphology and dimension of the gold nanostructures are strongly depended on the TOA concentration. Eventually it proves that particular synergies are required between nucleation and growth process to generate specific shaped metal nanoparticles. In a recent article, the authors have synthesized different shaped gold nanoparticles by simply varying the concentration of seed, and surfactant.[5e]

Up to this part of chapter 4, we have only discussed the role of surfactant on the particle morphology at a particular hydrosiloxane concentration. The role of PMHS concentration was also investigated in the reaction process. In this part, we discuss the role of PMHS concentration on particle morphology. The gold nanoprisms were obtained in the presence of 5 equivalents of TOA and 6 equivalents of PMHS. We were interested to investigate the particle morphology kept TOA concentration constant (5 equivalents) and increased the PMHS amounts.



Scheme 4.2: Synthetic strategy to polyhydrosiloxane templated gold nanorods.

When the gold salt reduction was carried out in the presence of 5 equivalent of TOA and 12 equivalent of PMHS, surprisingly no nanoprisms were observed instead of the gold nanorods were achieved with very low aspect ratio. Currently research has been focused on one-dimensional nanoparticles such as nanorods since the morphological anisotropy results in very complex physical properties and self assembled behaviors compared to those of spherical nanoparticles.[15] Metal rods have been synthesized by using various methods such as templating,[16] photochemistry,[17]

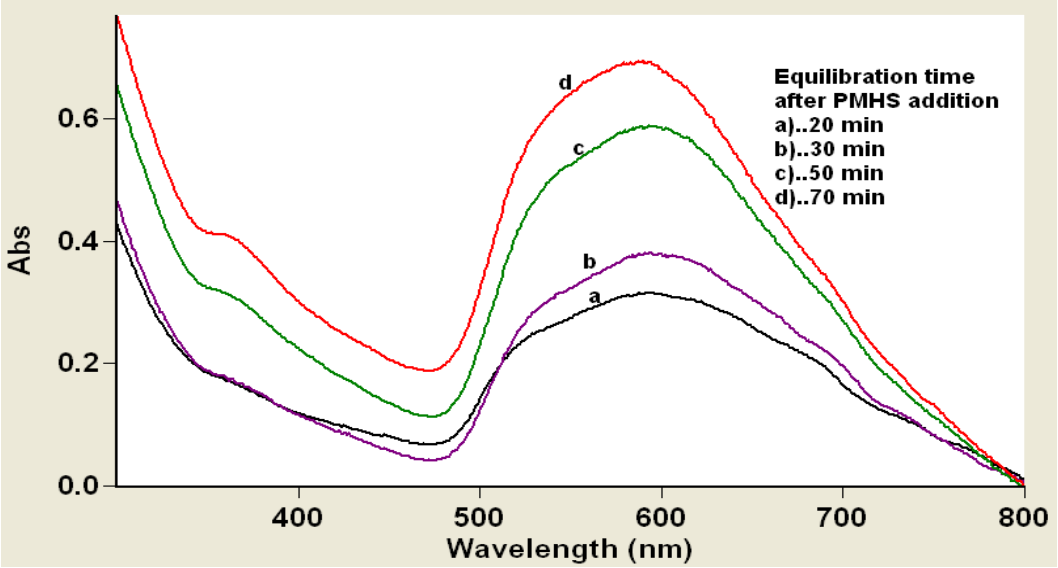


Figure 4.7: UV-vis absorption spectra of the synthesized gold nanorods.

seeding,[18] and electrochemistry.[19] The electrochemical synthesis of gold nanorods provides rods with fairly good uniformity and controlled aspect ratio although its growth mechanism remains elusive. The seed method is also well established on nanorods synthesis but single organic phase step synthesis of gold nanorods with low aspect ratio has not been reported yet.

Briefly, gold nanorods were synthesized from a stirred solution of 0.008 gm of $HAuCl_4.3H_2O$ (0.02 mmol) in 20 ml acetonitrile. After 30 minutes TOA (0.10 mmol, 0.043 ml) was added and within another 30 minutes the yellow solution converted to a colorless homogeneous solution. At this juncture, PMHS (0.24 mmol, 0.016 ml) was injected. After 20 minutes of the addition of PMHS, the colorless solution turned to light purple (λ_{max}: 580 nm). As the reduction proceeded, the light purple color turned to purple (λ_{max}: 587 nm) and finally it was a blue color solution (λ_{max}: 592 nm). After 1h and 10 min of addition of PMHS, no increment of UV-vis absorbance maxima was observed and remained constant for rest of the time, Figure 4.7.

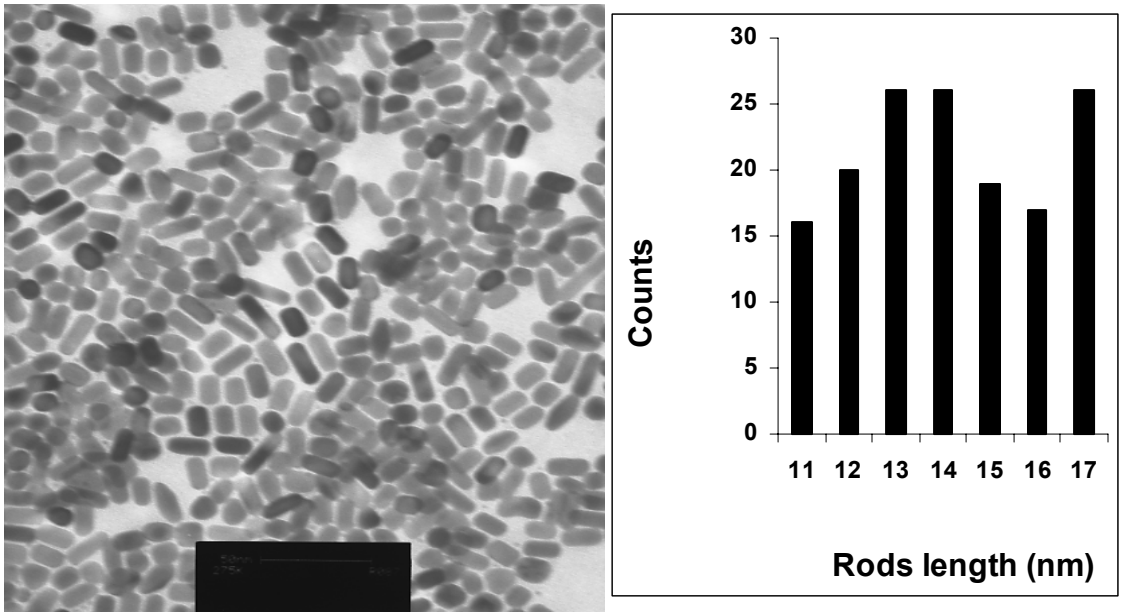


Figure 4.8: TEM image and the average length of synthesized gold nanorods.

At this stage the solution was centrifuged and analyzed by TEM. TEM image, Figure 4.8 shows that the rods are averagely 14.4±2 nm in length with 2.0±0.9 average aspect ratios. It has been observed[19] that the λ_{max} of SP band is strongly dependent on the mean aspect

ratios of gold nanorods. When the aspect ratio increased from 1.8 to 5.2, results in a red shift of the SP bands from 600 to 873.[19] In our synthetic strategy the synthesized nanorods have very low aspect ratio, which correlates its UV-vis absorption maxima at 592-nm region.

4.3 Mechanistic Proposal for different shaped gold nanocrystals

The quantitative treatment of the nucleation process starts from the Gibbs-Thompson equation based on classical theories.[20]

$S_r = S_b \exp(2\sigma V_m/rRT)$, r: radius of the crystals, σ: specific surface energy, V_m: molar volume of the materials, R: the gas constant, T: the absolute temperature. The above equation tells us that for a given monomer concentration, there is a critical size, and the solubility of particles of this size equals exactly to the monomer concentration in the solution. Any crystals/clusters with a size smaller than this critical size should have higher solubility, and thus should be unstable in the solution. In contrast, larger crystals possess low solubility and are stable under the given condition.

The mechanistic proposal for the shape evolution of semiconductor nanocrystals is demonstrated in the literature,[21] but for a particular reduction condition, formation of different shaped gold nanocrystals has not been reported. In this section, we rationalize the experimental results achieved on the formation of different shaped gold nanocryatals. The formation of different shaped gold nanocrystals is totally depended on the formation of monomers in the solution and its growth. It has been known that, essentially at low monomer concentration or long enough growth time, all nanocrystals grow toward the lowest chemical potential environment, and this leads to the generation of only dots. The

requirement of high monomer concentrations for the formation of elongated nanocrystals complicates the nucleation process quite significantly. The critical nuclei can be much smaller than the ones observed for the synthesis of dots. In this extremely small size range, the relative chemical potential is highly size-dependent, and even very sensitive to the configuration of the nuclei. Consequently, certain types of nanoclusters with well-defined morphology, nanoparticles of so-called “mazic sizes”, are observed in the nucleation stage during the synthesis of elongated nanocrystals. The inevitable formation of magic-sized nanoclusters in the nucleation stage for the growth of anisotropic shapes likely plays a key role in the determining the nature of the different shapes nanocrystals.

In our synthetic strategy, it was observed that when the reaction was carried out in the presence of 2 equivalent of TOA, the reduction process was slow and assumed the generation of monomer in the solution was less resulted the formation of self-assembled spherical gold nanoparticles. When the amount of TOA was increased in the reaction mixture (5 equivalent) the reduction was faster compared to the 2 equivalent TOA and formation of gold nanoprisms was observed. As the amine ratio in the reaction mixture was increased, moderate number of nuclei formed, which resulted formation of gold nanoprism due to the activation of Si-H bonds. When the amount of PMHS was increased to double, the formation of gold nanorods was observed. In this case the reduction process was faster compare to previously mentioned two reactions. This entire phenomenon can be explained by formation of “magic-size” nuclei. At a high monomer concentration it can support the growth of a single arm in its 1D growth range, which generates rod-shaped nanocrystals. A median monomer concentration can only support those existing seeds in 3D growth. As a result, the nanocrystals are developed to the

prismatic shape. At low monomer concentration, all those elongated nanocrystals are not compatible with the low chemical potential environment. Consequently, the system can only generate dots.

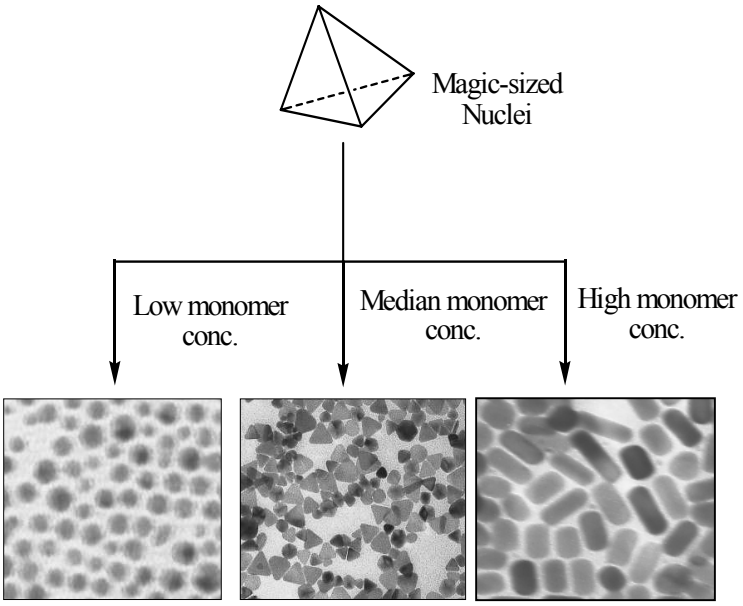


Figure 4.9: Mechanistic proposal for formation of different shapes gold nanocrystals at different monomer concentration (scheme was adapted from ref[21]).

4.4 Conclusion

In this section we have described the room temperature synthesis of different shape gold nanostructures in acetonitrile. This was first example where different shaped gold nanocrystals were successfully synthesized using PMHS as a reducing agent in the presence of surfactant, TOA. The prismatic, spherical, polyhedron, and rod shaped gold nanostructures were obtained by simple variations of reducing agent, and the surfactant concentration. All these nanostructures displayed distinct optical properties and different from each other.

Part B
Morphological conversion of gold nanoprisms to gold nanocubes

4.5 Introduction

The development of nanometer-sized nanoparticles have been focused due to their potential application in fabricating electronics, optical, optoelectronics, and magnetic devices.[1] The intrinsic properties of metal nanoparticles can be tailored by controlling their size, shape, and crystallinity. Recently, researchers have made promising advances that are yielding control over particle size, shape and composition.[2] Triangular nanoprisms showed intense interest due to their unusual optical properties, which is different from the bulk materials. There are some examples present in the literature where spherical metal nanoparticles are subsequently converted to their prismatic shape.[3] On the other hand synthesis of silver or gold nanocubes is quite straightforward. Mostly thermal methods are being used for silver or gold nanocubes synthesis.[6] The formation of metal nanocubes through thermal method is based on the seed growth mechanism, where small spherical nanoparticles has been used to produce different shapes large particles.

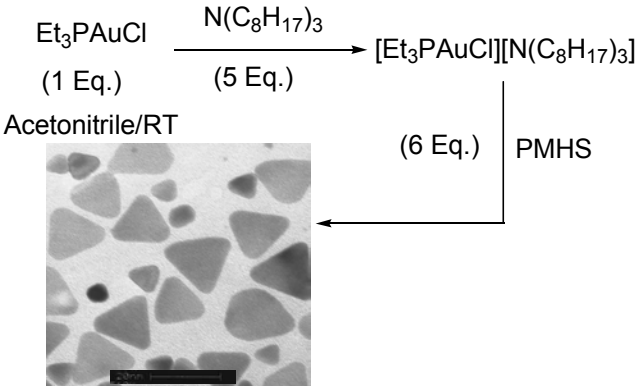
In first part of this chapter, we have discussed the PMHS mediated synthesis of gold nanoprisms from chloroauric acid under a specific reaction conditions. The literature report showed that the gold nanoprisms can only be generated from the reduction of chloroauric acid.[11] However, the formation of gold nanoprisms using other gold salts has not been investigated yet. The reason might be the solubility problem of the other gold

salts or the ligand attach to the gold ion which do not permit the gold nanoprisms formation. In this section we describe the single step synthesis of gold nanoprisms form Et_3PAuCl salt. The synthesis is straightforward, using PMHS as a reducing agent, in the presence of surfactant TOA. Scheme 4.3 is represents the synthetic procedure for generation of gold nanoprisms forms Et_3PAuCl salt. The edge length of the synthesized nanoprisms can be controlled by simple variation of surfactant concentration. The coordination ability of the phosphine ligand on the nanoprisms surface is also described using ^{31}P NMR. To date, no reports are available where gold nanoprisms were used as a seed to synthesize gold nanocubes. The synthesized nanoprisms are then used as a seed to generate the gold nanocubes. This is the first example where gold nanoprisms were successfully converted to the gold nanocubes via a single step method. Both the gold nanoprisms and nanocubes display distinct optical properties under our reaction conditions.

4.6 Results and discussions

Triethylphosphine gold chloride is completely soluble in acetonitrile and produces colorless homogeneous solution. In a typical experiment, Gold nanoprisms were synthesized from a stirred solution of 0.008 gm of Et_3PAuCl (0.02 mmol) in 20 ml acetonitrile. After 30 minutes of stirring, TOA (0.10 mmol, 0.043 ml) was added and after another 30 minutes PMHS (0.12 mmol, 0.008 ml) was injected. 3h after the addition of all the reactants, the color of the solution turned light blue (λ_{max}: 612 nm) and with respect to time the peak intensity gradually increased.12h after the addition of PMHS, no further increament of absorption maxima in UV-vis spectra was observed and resulted a

deep blue color solution (λ_{max}: 622 nm). The deep blue color solution was centrifuged at 1000 rpm for 10 minutes. One drop of centrifuged solution was then deposited on the TEM grid and allowed to air dry at room temperature. A Philips CM-100 transmission electron microscope, operating at 80 Kv, was used to characterize the size and shape of resulting nanoprisms. During the 12h period, the reaction mixture was analyzed by ^{31}P NMR spectroscopy.



Scheme 4.3: Synthetic strategy for the generation of gold nanoprisms fom Et_3PAuCl salt.

The optical spectra of the formation of gold nanoprisms were characterized by UV-vis spectroscopy. At the beginning of the reduction a peak at 612 nm was observed. With time the peak intensity gradually increased and a 10 nm blue shift was observed, Figure 4.10.

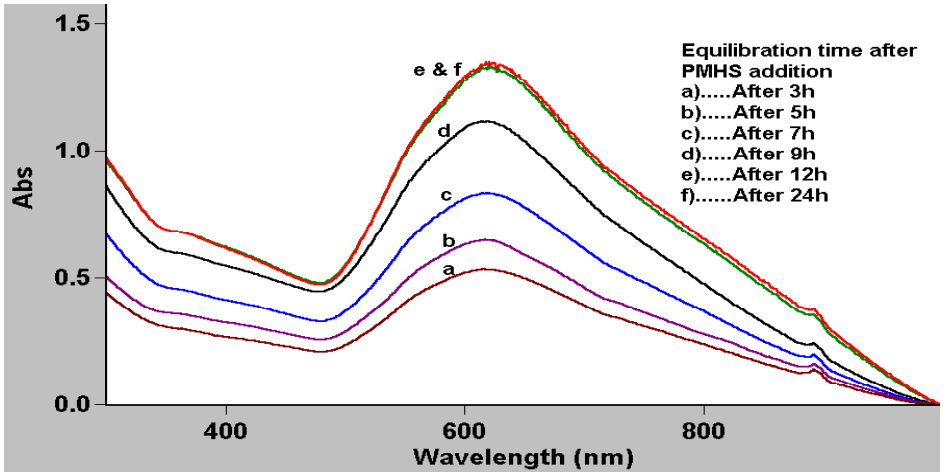


Figure 4.10: UV-vis absorption spectra of the formation of gold nanoprisms from the reduction of Et_3PAuCl salt.

The ^{31}P NMR was used to find out the role of triethylphosphine on the formation and growth of gold nanoprisms. The phosphorus of pure Et_3PAuCl comes at 31.5 ppm. After 3h of addition of PMHS, along with this peak, a new peak was observed at 21.3 ppm. This tells us that some of the gold complex was converted to gold nanoprisms and the phosphine ligands were on the surface of the prisms. After 5h of the addition of all the reagents, the peak at 31.5 completely disappeared and the peak at 21.3 was very strong. As the reaction progressed, no change in this peak position was observed, Figure 4.11.

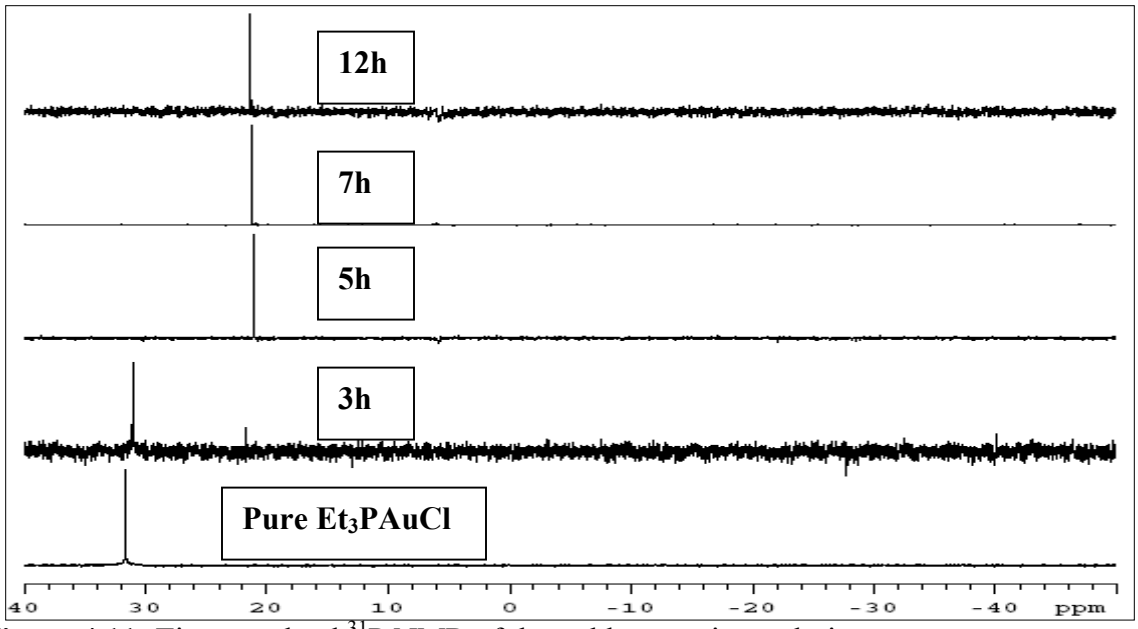


Figure 4.11: Time resolved ^{31}P NMR of the gold nanoprism solution.

One drop of the centrifuged blue solution was deposited on the TEM grid and dried at room temperature. The analysis showed formation of single crystalline gold nanoprisms with average edge length of 11.7±2.8 nm. Almost 95% of the particles were

in well-defined prismatic shape. Figure 6.12 represents the TEM image and the corresponding histogram for edge length calculation of the synthesized nanoprisms. The same solution was also spin coated on mica and analyzed by tapping mode AFM. The AFM data reveals that the nanoprisms are 5 nm in thickness, see Figure 6.12.

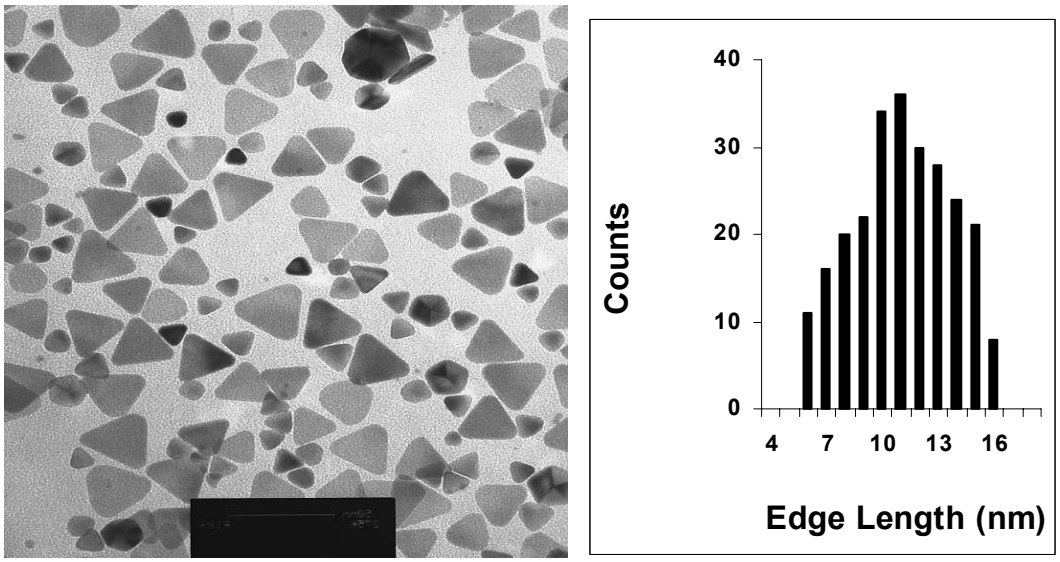


Figure 4.12: TEM image and the corresponding histogram for edge length calculation of gold nanoprisms synthesized from Et_3PAuCl in the presence of 5 equivalent of TOA.

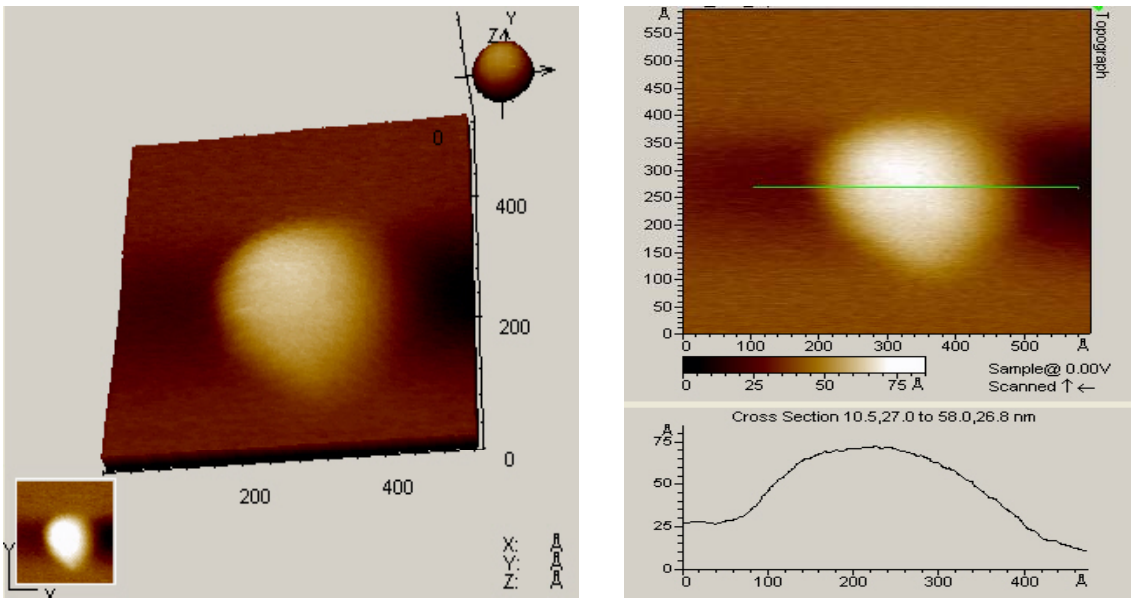


Figure 4.13: AFM image of gold nanoprisms synthesized from Et_3PAuCl in the presence of 5 equivalent of TOA.

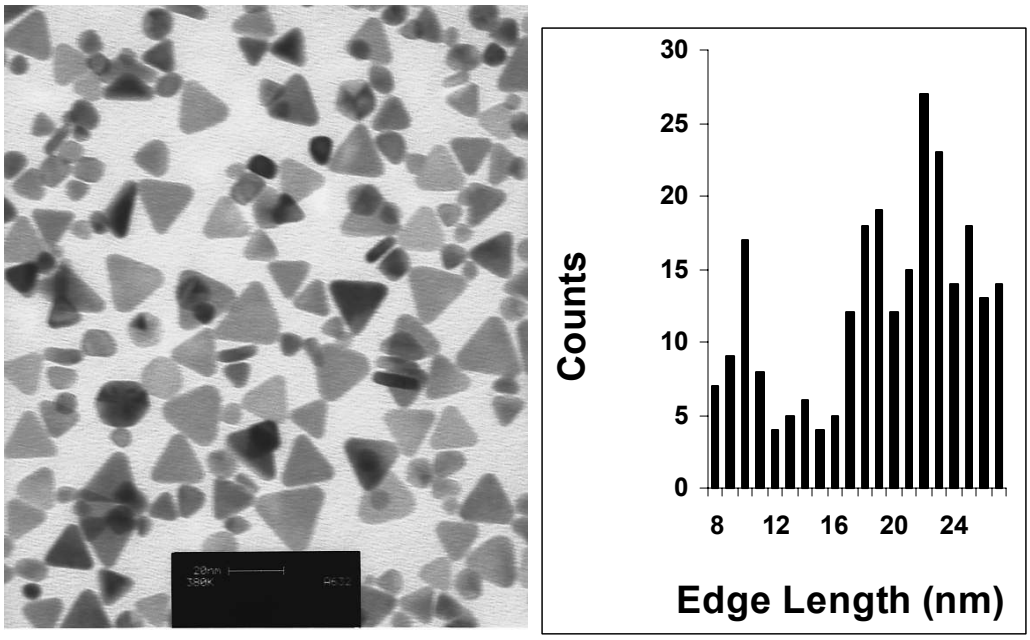


Figure 4.14: TEM image and the corresponding histogram for edge length calculation of gold nanoprisms synthesized from Et_3PAuCl in the presence of 2 equivalent of TOA.

When the similar reduction reaction was carried out in the presence of 2 equivalent of TOA, the gold nanoprisms were also achieved, but the average edge length of the prisms was higher compare to 5 equivalents of TOA. In the case of 2 equivalent of TOA, the population of the prisms was less and they were randomly oriented, see figure 4.14. The average edge length of the prisms was 19.7±5.6 nm. Some of the prisms were truncated in shapes. In this case, the synthesized prisms were not stable in the solution, and after 15 days of reaction they were totally precipitated out from the solution, forming a blue color solid residue. This might happen because of the presence of less amount of surfactant present in the reaction mixture unable to stop the agglomeration process.

From the above experimental data, it is quite clear that the edge length and the population of nanoprisms are strongly related to the amount of surfactant present in the reaction mixture. It was observed that the surfactant ratio has an inverse relationship with

the edge length of nanoprisms. When the concentration of surfactant was less, the corresponding prisms had higher edge length. In addition, lowering the concentration of surfactant results in a decreased number of prisms present in solution.

There is very little number of examples present in the literature where gold nanocubes were synthesized by direct reduction of gold salt. [6] There has not been a single report present in the literature, where metal nanoprisms were converted to the nanocubes morphology by a single step reaction. Here, we describe an efficient route to synthesize the gold nanocubes from presynthesized gold nanoprisms. This method enable us the opportunity to synthesize the nanocubes with a small lateral dimension. Scheme 4.4 represents the synthetic strategy of gold nanocubes formation from gold nanoprisms.

The formation of gold nanoprisms was completed after 12h of addition of PMHS. At this juncture 2 more equivalent of Et_3PAuCl (0.04 mmol, 0.016 gm) was added followed by a gentle stirring for 5 minutes. After then the stirring was stopped and the reaction mixture was left at room temperature. At the initial stage, no significant change of the solution color was observed. After 1h of addition of extra gold salt, the color of the solution changed from deep blue to blue and finally after 3h, it was a purplish blue color solution (λ_{max}: 562 nm). UV-vis absorption spectra of the reaction mixture were recorded promptly. During monitoring, an increased of absorption maxima was observed. After 3h, the crude reaction mixture was deposited on the TEM grid and analyzed by transmission electron microscopy.

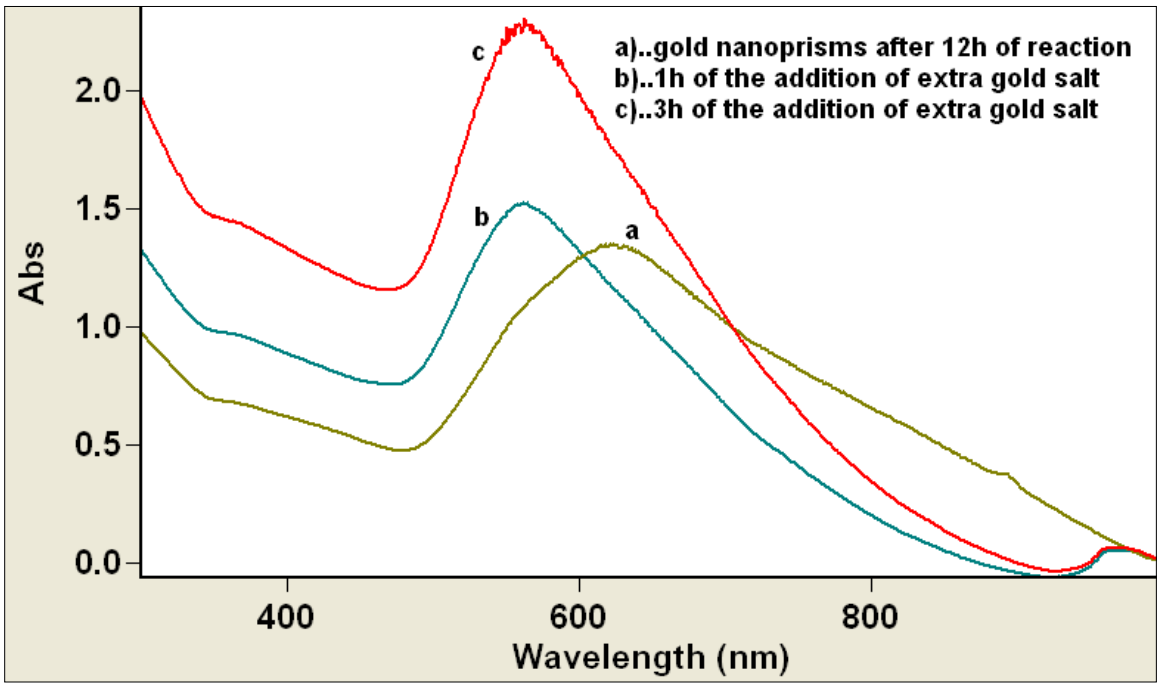
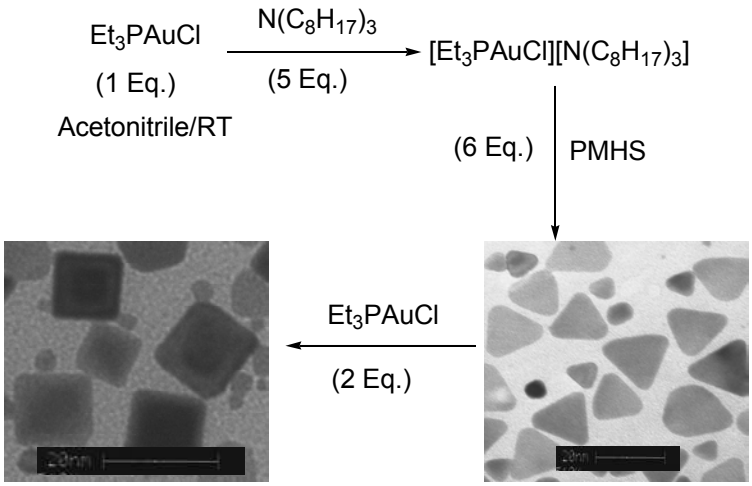


Figure 4.15: Comparison of UV-vis absorbance maxima.



Scheme 4.4: Synthetic strategy for the generation of gold nanocubes from gold nanoprisms.

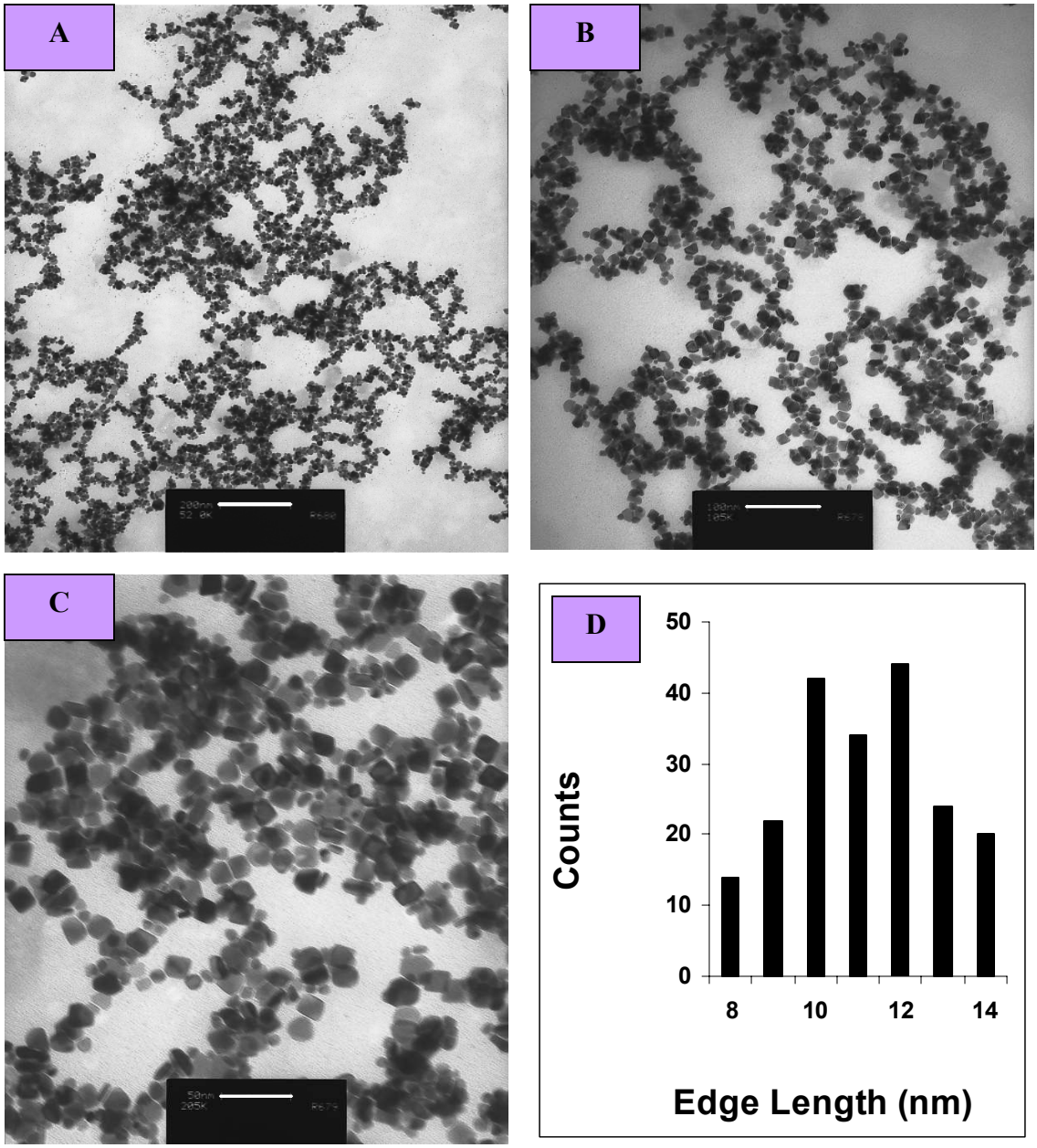


Figure 4.16: TEM image of the gold nanocubes at different magnification; (A) 200 nm, (B) 100 nm, and (C) 50 nm scale bar. (D) the histogram of the nanocubes at 100 nm scale bar.

It was found that the stability of the nanocubes was very poor in acetonitrile and within 2 days almost all the particles were precipitated out resulted a clear solution. On the basis of these preliminary results, we can roughly elucidate the generation and growth process as follows: At the beginning of the addition of extra gold salts, small spherical

nanoparticles were formed and then they deposited on the nanoprisms surface. Due to low amount of surfactants were present in the reaction mixture, it would not able to stabilize the formed nanocubes and eventually they were separated out from the reaction mixture as a precipitate. However, more experimental and theoretical work is underway to understand the formation process.

These gold nanoprisms, and nanocubes should find use in a variety of areas that include photonics, catalysis, and SERS-based sensing. This work and previous demonstrations from other groups[6] make it clear that chemical synthesis of metal nanoparticles with well-defined shapes, sizes and structure is a practical reality. The major requirement seems to be the selection of a capping agent that is able to chemically modify various faces of a metal with an appropriate selectivity.

4.7 Conclusions

In this section we have described the formation of gold nanoprisms from Et_3PAuCl salts, using PMHS as a reducing agent in the presence of TOA. This section is important because it provided a straightforward route to gold nanoprisms with control over edge length, an architectural parameter not accessible via any of the known synthetic methods for such structure. The synthesized prisms were then used as seeds to generate a new architecture, gold nanocubes. This was the first example where gold nanocubes were synthesized from gold nanoprisms.

4.8 Experimental Section:

Materials.

The following chemicals were used as purchased without further purification. Hydrogen tetrachloroaurate trihydrate ($HAuCl_4.3H_2O$), trioctylamine (TOA), polymethylhydrosiloxane (PMHS) were purchased from Aldrich chemical company. Triethylphosphine gold (I) chloride was obtained from Gelest, Inc. Acetonitrile was acquired from EMD chemicals (omnisolv, HPLC grade). All the chemicals were used as received without further purification.

Experimental Technique:

Microscopic UV-Visible absorption measurements were carried out with a Varian Cary 50-scan spectrophotometer in a10-mm optical path length quartz cuvettes. All spectra shown here are the result of macroscopic measurements performed in standard transmission geometry with unpolarized light impinging upon the surface at normal angle of incidence. Transmission electron microscope (TEM) is a suitable technique used in investigating the size and shape changes of small metallic nanoparticles. The TEM micrographs were obtained with the help of a Philips CM-100 instrument operating at 80 Kv accelerating voltage. TEM samples were prepared by placing a drop of centrifuged reaction mixture on the surface of a 150 mesh (Electron Microscopy Science, Port Washington, PA) copper grid backed with formver and were dried at ambient temperature. The crude reaction mixtures were centrifuged for 10 minutes before deposition on the grid. Particle size analysis was conducted using the Scion Image Beta 4.02 Software (available on the Internet at http://www.scioncorp.com). Images, which have 100 nm scale bar, was chosen to do the particle size, populations and edge length

analysis. In Scion Image, after setting the unit and known distance the 'Analyze Particle' parameter was used to generate a table of particle diameter. This table was then exported into Microsoft Excel 2000 where statistical analysis and histogram plotting were performed. ^{31}P NMR spectra (200 MHz) were recorded using the Varian unity NMR instrument.

Synthesis of gold nanoprism.

Gold nanoprisms were synthesized from a stirred solution of 0.008 gm of $HAuCl_4.3H_2O$ (0.02 mmol) in 20 ml acetonitrile. The chloroauric acid is completely soluble in acetonitrile and produced a yellow color homogeneous solution (λ_{max}: 322 nm). After 30 minutes TOA (0.10 mmol, 0.043 ml) was added and within another 30 minutes the yellow solution converted to a colorless homogeneous solution. At this juncture, PMHS (0.12 mmol, 0.008 ml) was injected. After 30 minutes of the addition of PMHS, the colorless solution turned to light purple (λ_{max}: 534 nm). As the reduction proceeded, the light purple color turned to purple (λ_{max}: 598 nm) and finally at the end of the reaction, it was a deep blue color solution (λ_{max}: 645 nm). The UV-vis absorption spectra of the reaction mixture were recorded promptly. A Philip CM-100 transmission electron microscope, operating at 80 KV, was used to characterize the size and shape of resulting nanocrystals. Under similar reaction condition and identical molar ratio, reduction of Et_3PAuCl salt was carried out to synthesize gold nanoprisms.

Synthesis of Self-assembled gold nanoparticles.

The synthesis of gold nanoparticles involves a single step reduction of $HAuCl_4$ by PMHS in the presence of TOA. In the experimental procedure, a yellow colored homogeneous solution (λ_{max}: 322 nm) of $HAuCl_4.3H_2O$ (0.02 mmol, 0.008 gm) was prepared in 20 ml

acetonitrile. After 30 minutes of stirring at room temperature, TOA (0.04 mmol, 0.02 ml) was added followed by vigorous stirring at room temperature for another 30 minutes. After 30 minutes of stirring with TOA, the yellow colored solution converted to a colorless homogeneous solution. At this juncture, PMHS (0.12 mmol, 0.008 ml) was injected into the solution and rapid stirring was continued. After 30 minutes of the addition of PMHS, the colorless solution turned faint purple. The UV-vis spectroscopy showed a plasmon band at 528 nm regions (Figure 1). As the reaction progressed the color of the solution became more intense and a slight blue shift of the absorption maxima was observed. Finally after 2h of the addition of PMHS, it turned to deep purple color solution (λ_{max}: 520 nm). The total solution was then centrifuged and from that one drop was deposited for TEM analysis. The TEM analysis (Figure 1) showed that the particles present in the deep purple color solution displayed 2D-arrangement with average particle size of 3.2 ± 0.5 nm. The interparticle spacing was also calculated and was 2.3 nm. The deep purple color solution was also analyzed by tapping mode AFM.

Synthesis of gold nanorods.

Gold nanorods were synthesized from a stirred solution of 0.008 gm of $HAuCl_4.3H_2O$ (0.02 mmol) in 20 ml acetonitrile. After 30 minutes TOA (0.10 mmol, 0.043 ml) was added and within another 30 minutes the yellow solution converted to a colorless homogeneous solution. At this juncture, PMHS (0.24 mmol, 0.016 ml) was injected. After 20 minutes of the addition of PMHS, the colorless solution turned to light purple (λ_{max}: 580 nm). As the reduction proceeded, the light purple color turned to purple (λ_{max}: 587 nm) and finally at the end of the reaction, it was a blue color solution (λ_{max}: 592 nm).

Synthesis of gold nanocubes.

In this case the gold nanoprisms were synthesized from Et_3PAuCl salt in the presence of 5 equivalents of TOA and 6 equivalents of PMHS. The formation of gold nanoprisms was completed after 12h of addition of PMHS. At this juncture 2 more equivalent of Et_3PAuCl (0.04 mmol, 0.016 gm) was added followed by a gentle stirring for 5 minutes. After then the stirring was stopped and the reaction mixture was left at room temperature. At the initial stage, there was no significant change of the solution color was observed. After 1h of addition of extra gold salt, the color of the solution changed from deep blue to blue and finally after 3h, it was a purplish blue color solution (λ_{max}: 562 nm). UV-vis absorption spectra of the reaction mixture were recorded promptly. During monitoring, an increased of absorption maxima was observed. After 3h, the crude reaction mixture was deposited on the TEM grid and analyzed by transmission electron microscopy.

4.9 References

1. (a) Elghanian, R.; Storhoff, J. J.; Mucic, R. C.; Letsinger, R. L.; Mirkin, C. A. *Science* **1997**, *277*, 1078. (b) Bruchez, M.; Moronne, M.; Gin, P.; Weiss, S.; Alivisatos, A. P. *Science* **1998**, *281*, 2013. (c) Cui, Y.; Wei, Q.; Park, H.; Lieber, C. M. *Science* **2001**, *293*, 1289. (d) Chan, W. C. W.; Nie, S. *Science* **1998**, *281*, 2016.

2. (a) Chauhan, B. P. S.; Rathore, J. S.; Bandoo, T. *J. Am. Chem. Soc*. **2004**, *126*, 8493. (b) Lewis, L. N. *Chem. Rev*. **1993**, *93*, 2693. (c) Schmid, G. *Chem. Rev*. **1992**, *92*, 1709.

3. Sun, S.; Murray, C. B.; Weller, D.; Folks, L.; Moser, A. *Science* **2000**, *287*, 1989.

4. (a) Nikoobakht, B.; El-Sayed, M. A. *Chem. Mater*. **2003**, *15*, 1957. (b) Orendorff, C. J.; Gole, A.; Sau, T. K.; Murphy, C. J. *Anal. Chem*. **2005**, *77*, 3261.

5. (a) Chen, S.; Carroll, D. L.; *Nano. Lett.* **2002**, *2*, 1003. (b) Ahmadi, T. S.; Wang, Z. L.; Green, T. C.; Heglein, A.; El-Sayed, M. A. *Science* **1996**, *272*, 1924. (c) Murray, C. B.; Kagan, C. R.; Bawendi, M C. *Science* **1995**, *270*. 1335. (d) Puntes, V. F.; Krishnan, K. M.; Alivisatos, A. P. *Science* **2001**, *291*, 2115. (e) Sau, T. K.; Murphy, C. J. *J. Am. Chem. Soc***. 2004**, *126*, 8648.

6. (a) Sun, Y.; Xia, Y. *Science* **2002**, *298*, 2176. (b) Feng, J.; Zeng, H. C. *Chem. Mater*. **2003**, *15*, 2829. (c) Hoefelmeyer, J. D.; Niesz, K.; Somorjai, G. A.; Tilley, T. D. *Nano. Lett*. **2005**, *5*, 435. (d) Liu, R.; Oba, F.; Bohannan, E. W.; Ernst, F.; Switzer, J. A. *Chem. Mater*. **2003**, *15*, 4882. (e) Xu, R.; Zeng, H. C. *Langmuir* **2004**, *20*, 9780. (f) Sun, Y.; Wiley, B.; Li, Z.-Y.; Xia, Y. *J. Am. Chem. Soc*. **2004**, *126*, 9399. (g) Jin, R.; Egusa, S.; Schere, N. F. *J. Am. Chem. Soc*. **2004**, *126*, 9900.

7. (a) Cepak, V. M.; Martin, C. R. *J. Phys. Chem. B* **1998**, *102*, 9985. (b) Chen, C.-C.; Chao, C.-Y.; Lang, Z.-H. *Chem. Mater.* **2000**, *12*, 1516. (c) Chang, S.-S.; Shih, C.-W.; Chen, C.-D.; Lai, W.-C.; Wang, C. R. C. *Langmuir* **1999**; *15*, 701. (d) Wei, G.; Zhou, H.; Liu, Z.; Song, Y.; Wang, L.; Sun, L.; Li, Z. *J. Phys. Chem. B* **2005**, *109*, 8738. (e) Vayssieres, L.; Rabenberg, L.; Manthiram, A. *Nano Lett.* **2002**, *2*, 1393. (f) Link, S.; Burda, C.; Nikoobakht, B.; El-Sayed, M. A. *J. Phys. Chem. B* **2000**; *104*, 6152. (g) Yin, M.; Gu, Y.; Kuskovsky, I. L.; Andelman, T.; Zhu, Y.; Neumark, G. F.; O'Brien, S. *J. Am. Chem. Soc.* **2004**, *126*, 6206. (h) Hu, M.; Hillyard, P.; Hartland, G. V.; Kosel, T.; Perez-Juste, J.; Mulvaney, P.; *Nano Lett.* **2004**, *4*, 2493. (i) Gole, A.; Murphy, C. J.; *Chem. Mater.* **2004**, *16*, 3633. (j) Kim, F.; Song, J. H.; Yang, P. *J. Am. Chem. Soc*. **2002**, *124*, 14316.

8. (a) Davidson, F. M., III; Wiacek, R.; Korgel, B. A. *Chem. Mater.* **2005**, *17*, 230. (b) Zhang, D.; Qi, L.; Ma, J.; Cheng, H. *Chem. Mater.* **2001**, *13*, 2753. (c) Wang, J.; Tian, M.; Mallouk, T. E.; Chan, M. H. W.*J. Phys. Chem. B.* **2004**, *108*, 841. (d) Xu,

D.; Shi, X.; Guo, G.; Gui, L.; Tang,Y.*J. Phys. Chem. B.* **2000**, *104,* 5061. (e) Sun, Y.; Gates, B.; Mayers, B.; Xia,Y. *Nano Lett.* **2002**, *2*, 165. (f) Chen, J.; Herricks, T.; Geissler, M.; Xia, Y. *J. Am. Chem. Soc.* **2004**, *126*, 10854.

9. (a) Jin, R.; Cao, Y. C.; Mirkin, C. A.; Kelly, K. L.; Schatz. G. C.; Zheng, J. G. *Science* **2001**, *294*, 1901. (b) Santos, I. P.; Liz-Marzan, L. *Nano Lett*. **2002**, *2*, 903.

10. (a) Sun, Y.; Mayers, B.; Xia, Y. *Nano Lett*. **2003**, *3*, 675. (b) Jin, R.; Cao, Y. C.; Hao, E.; Metraux, G. S.; Schatz, G. C.; Mirkin, C. A. *Nature* **2003**, *425*, 487. (c) Ghezelbash, A.; Sigman, M. B.; Korgel, B. A. *Nano Lett*. **2004**, *4*, 537.

11. (a) Shankar, S. S.; Rai, A.; Ankamwar, B.; Singh, A.; Ahmad, A.; Sastry, M. *Nat. Mater.* **2004**, *3*, 482. (b) Kim, F.; Connor, S.; Song, H.; Kuykendall, T.; Yang, P. *Angew. Chem. Int. Ed. Engl*. **2004**, *43*, 3673. (c) Millstone, J. E.; Park, S.; Shufor, K. L.; Qin, L.; Schatz. G. C.; Mirkin, C. A. *J. Am. Chem. Soc*. **2005**, *127*, 5312.

12. Malikova, N.; Santos, I. P.; Schierhorm, M.; Kotov, N. A.; Liz-Marzan, L. *Langmuir* **2002**, *18*, 3694.

13. (a) Chauhan, B. P. S.; Sardar, R. *Macromolecules* **2004**, *37*, 5136. (b) Chauhan, B. P. S.; Rathore, J. S.; Chauhan, M.; Krawicz, A. *J. Am. Chem. Soc.* **2003**, *125*, 2876. (c) Chauhan, B. P. S.; Rathore, J. S. *J. Am. Chem. Soc*. **2005**, *127*, 5790.

14. (a) Dubertret, B.; Skourides, P.; Norris, D.; Noireaux, V.; Brivanlou, A.; Libchaber, A. *Science* **2002**, *298*, 1759. (b) Perez, J. M.; Josephson, L.; O'Loughlin, T.; Hogemann, D.; Weissleder, R. *Nat. Biotechnol*. **2002**, *20*, 816. (c) Li, Y.; Hong, Z. M.; Collard, D. M.; El-Sayed, M. A. *Org. Lett*. **2000**, *2*, 2385.

15. Creighton, J. A.; Eadon, D. G. *J. Chem. Soc., Faraday Trans.* **1991**, *87*, 3881.

16. Nicewarner-pena, S. R.; Freeman, R. G.; Reiss, B. D.; He, L.; Pena, D. J.; Walton, I. d.; Cromer, R.; Keating, C. D.; Natan, M. J. *Science* **2001**, *294*, 137.

17. Esumi, K.; Matsuhisa, K.; Torigoe, K. *Langmuir* **1995**, *11*, 3285.

18. Sun, Y. G.; Xia, Y. *Adv. Mater*. **2002**, *14*, 80.

19. Yu, Y.-Y.; Chang, S.-S.; Lee, C.-L.; Wang, C. R. C. *J. Phys. Chem. B* **1997**, *101*, 6661.

20. Mullin, J. W. *Crystallization*, Butterworth-Heinemann, Woburn, MA **1997**.

21. Peng, X. *Adv. Mater*. **2003**, *15*, 459.

Chapter 5

Solventfree synthesis and functionalization of monodisperse silver nanoparticles

5.1 Introduction

There is a grate deal of interest in the fabrication of metal nanoclusters due to their potential applications in nonlinear optics,[1] magnetic devices,[2] and sensors.[3] The fundamental physical properties of inorganic naocrystals are closely related to their size, shape and chemical composition.[4] Solution phase synthetic approaches for the creation of various metal nanostructures have been considered with a greater degree of interest,[5] either by preparing them directly in organic media or by transferring them from aqueous to organic medium.[6] In the solution phase synthesis, both the molecular and particle diffusion are fast and it is hard to ignore the coagulative growth of the particles.[7] The second approach is better than the first one for the preparation of well-defined nanoclusters. For the phase transformation of metal nanoparticles form aqueous phase to organic phase, surfactant such as thiols[8] or amines[9] are commonly used. The efficiency of this approach is however limited. When thiol molecules stabilize the nanoparticles, the colloidal surface loses its activity and accessibility for catalytic reactions.[10] There are a few examples present in the literature where semiconductor naocrystals were synthesized by a solventfree approach.[11] The method mainly deals with high temperature decomposition of metallic complexes.

In the past, metallic nanoparticles were synthesized by either one of two methods, viz., the citrate,[12] and Brust[13] methods. The citrate method produces nearly monodisperse particles but the resulting solutions contain fewer nanoparticles and is restricted to water as a solvent. The Brust method suffers from greater polydispersity and higher cost for the phase transfer agents. Generation of silver nanoparticles are of particular interest because of their use in SERS,[14] catalysis,[15] and photographic devices.[16]

To date, no report is available about the room temperature solventfree synthesis of silver nanoparticles from commercially available silver salts. In a recent report,[17] and through out this dissertation, we have discussed the reducing properties of polysiloxane and its oligomeric counter part for generation of silver and gold nanoparticles, which were active and allowed to do the surface modification by organic ligand. Previously polymers were mainly used as a stabilizing agent to stabilize metal nanoparticles,[18] but never been used as solvent as well as a reductant. As we know PMHS is a free flowing colorless liquid and stable at laboratory condition and can be used as a solvent, reducing agent, and stabilizing agent. Based on this hypothesis, in this chapter we demonstrate the room temperature solventfree synthesis of silver nanoparticles using PMHS as a solvent, reducing and stabilizing agent. The Ag^0- PMHS precursor serves as a nanoparticle source and depending on the requirement the semi-solid product can be easily dispersed in different organic solvents such a acetonitrile, THF, DMF, toluene, and cyclohexane. In a recent review, the authors have mentioned that the metal clusters such as Ti, Zr, or V can be stabilized by THF molecules,[19] but there is no report available where silver nanoparticles were stabilized by solvent molecules such as THF, or acetonitrile. The polysiloxane-Ag nanocomposite are easily dispersable in THF, and acetonitrile and produce stable silver organosols. The polysiloxane capped Ag nanoclusters can be considered as “meatball-spaghetti” analog where metal nanoparticles are “meatball” and polysiloxanes are “spaghetti”. Due to very weak interaction between the polysiloxane backbone and metal nanoclusters, one can expect unusual activity and selectivity over the nanoparticles passivated by strong coordinating ligands. We also investigate the surface

grafting properties of the polymer nanoparticle composite in the presence a of strong coordinating ligand such as thiol, amine, acid, or phosphine.

5.2 Results and Discussion

In the experimental procedure, 32 mg (0.2 mmol) silver acetate was taken in a test tube and PMHS (0.072 ml, 1.2 mmol) was injected into it. The mixture was then stirred for 24h at RT. After 24h of stirring a yellowish brown color semi-solid materials was created and to it 2-ml of distilled solvent was added and stirred for another two hours. Depending on the solvent polarity, the concentration of the disperse product varied. The disperse product was then centrifuged and analyzed by different spectroscopic techniques. Scheme 5.1 represents the formation of silver nanoparticles and its stable dispersion in the coordinated solvent.

Before dispersion in the solvent, the semi-solid product was first analyzed by FTIR spectroscopy to determine the true nature of the yellowish materials. In the IR spectra, (Figure 5.1) we can clearly see the presence of Si-H peak at 2165 cm^{-1} region. This tells us that the PMHS is still present in the product and it did not decompose to Si-OH or SiO_2. Moreover we can also see the C-H stretching frequency at 2965 cm^{-1} from the methyl group of PMHS. From the above IR data, it can be inferred that the yellowish brown colored semi-solid product consists of polymer capped silver nanoparticles, that is polysiloxane-Ag(0) nanocomposite.

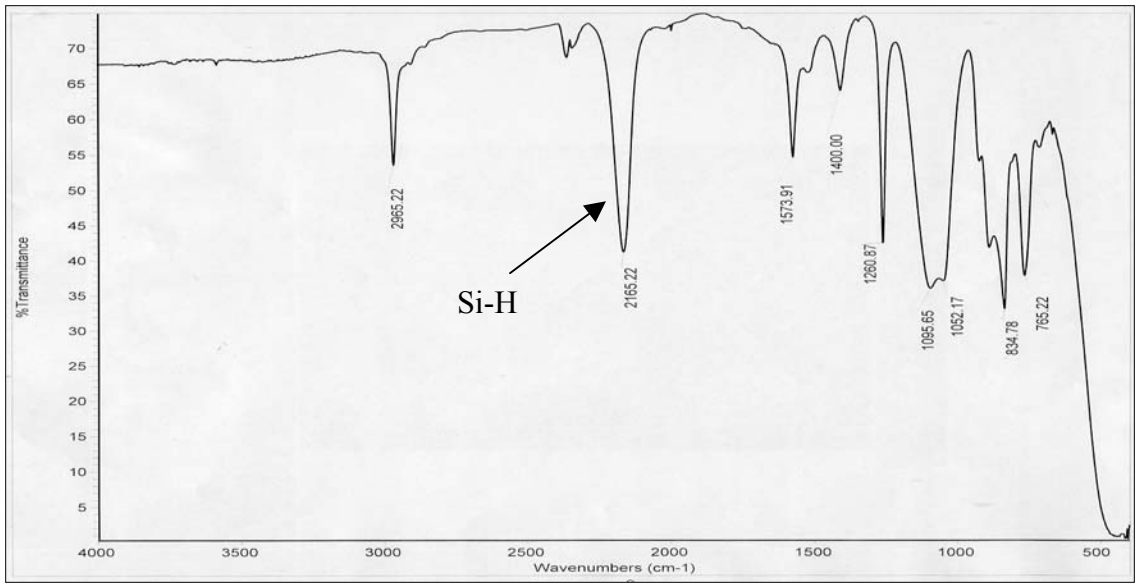
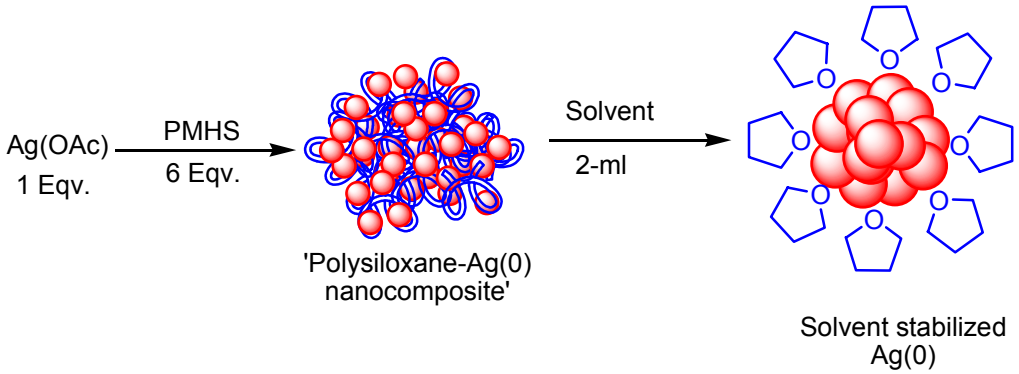


Figure 5.1: FT-IR spectra of the yellowish brawn color semisolid product.

A typical UV-vis spectroscopy of the dispersed semi-solid product in different solvent is shown in Figure 5.2. In this study, six different organic solvents such as acetonitrile, DMF, DMSO, THF, toluene, and cyclohexane were investigated. When non-coordinating solvents such as toluene and cyclohexane were used for the dispersion of polysiloxane Ag(0) nanocomposite, the absorbance of the solution was low. The TEM analysis also showed that the population of the particles in solution was very low. The particle size was also very small and in the range of 2-3 nm. The reason for the small size distribution is due to the fact that the particles which were stabilized by polymer molecules only were able to change their state from semi-solid to stable dispersion.



Scheme 5.1: Synthetic strategy to polysiloxane-Ag(0) nanocomposite and its transformation to soluble organosols.

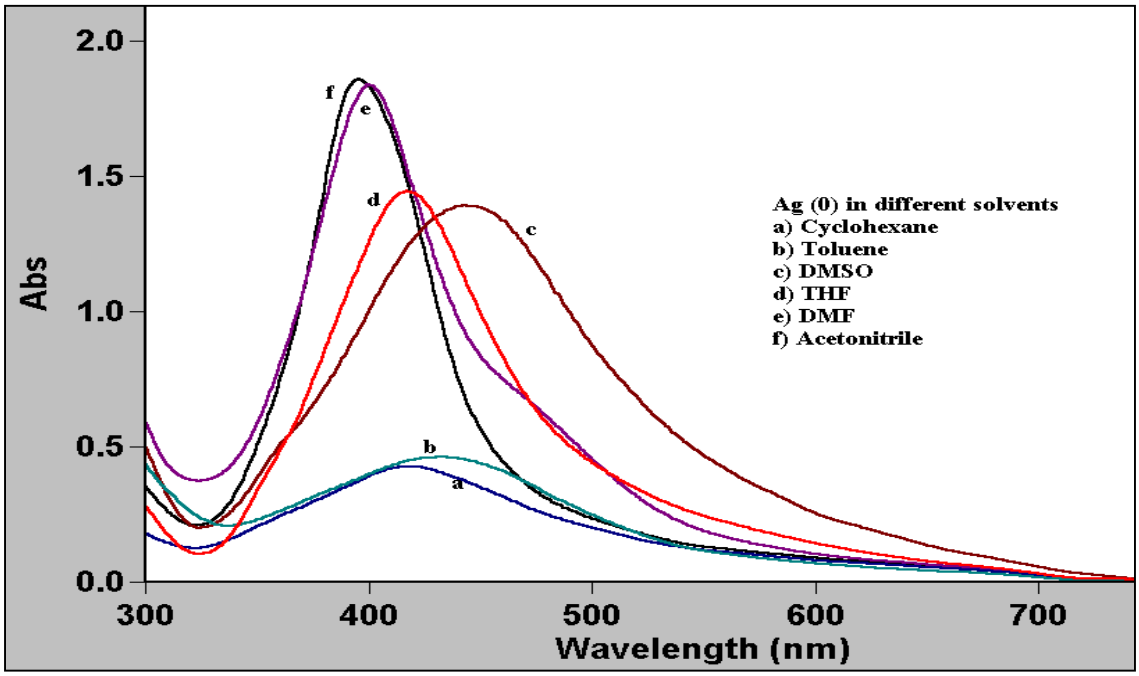


Figure 5.2: UV-vis absorption spectra of disperse silver nanoparticles in different solvent.

After the dispersion of the semi-solid product in different solvents, the silver sols were first analyzed by FT-IR spectroscopy to determine the role of solvents in the particle dispersion. The semi-solid product showed relatively high solubility in the coordinating solvent, such as DMF, acetonitrile, which was clearly observed in the UV-vis

spectroscopic data. In FT-IR for acetonitrile stabilized nanocluster, the –CN stretching frequency occurs at 2408 cm^{-1} whereas the pure acetonitrile is showed at 2295 cm^{-1}, indicting that the cyanide group is coordinated to the silver surface. These IR spectra clearly indicate that the nanoparticles are stabilized by acetonitrile. The observed wave-number increase of 113 cm^{-1} is similar to those observed alkylisocyanide stabilized Pt[20], Pd[21] and Au[22] nanoparticles. The acetonitrile stabilized silver nanoparticles exhibited an intense yellow color and had an absorbance at 395 nm regions in the UV-vis absorption spectrum. One drop of the yellow solution was then deposited on TEM grid for morphological analysis. The TEM data indicated that the particles were monodisperse with an average diameter of 3.9 ± 0.8nm. Figure 5.3 represents the TEM morphogram and the corresponding histogram of acetonitrile stabilized silver nanoparticles.

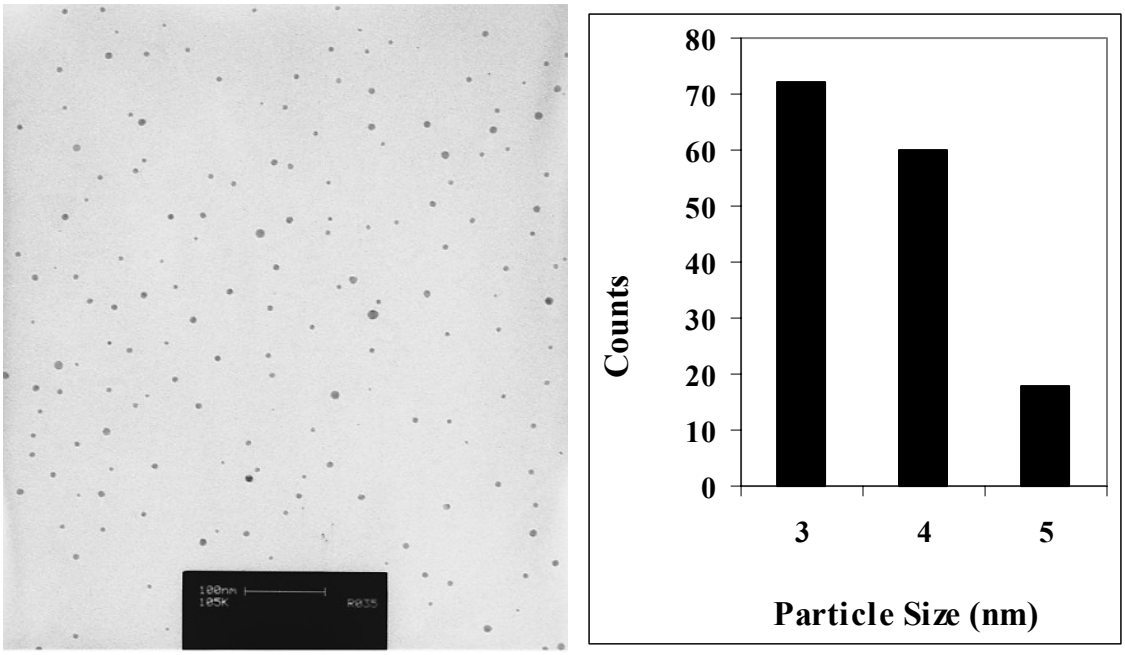


Figure 5.3: TEM image and the corresponding histogram of acetonitrile stabilized silver nanoparticles.

The acetonitrile stabilized Ag(0) was also analyzed by atomic force microscope (AFM). The AFM image (Figure 5.4) that showed the particles were very monodisperse , which correlates with the TEM analysis.

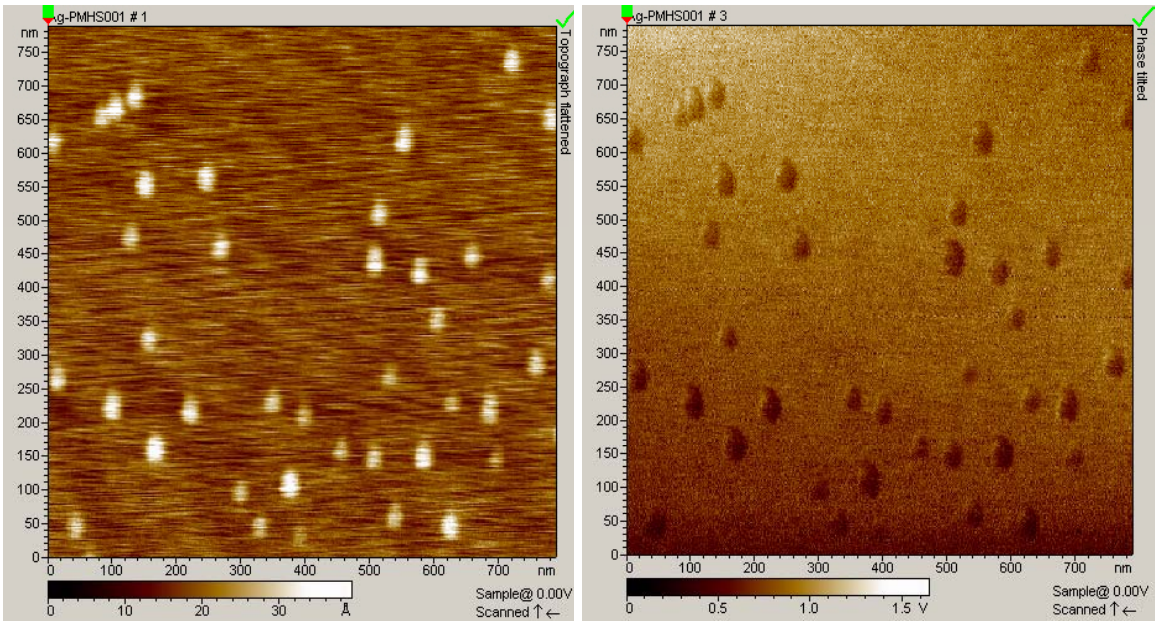


Figure 5.4: AFM image of acetonitrile stabilized silver nanoparticles.

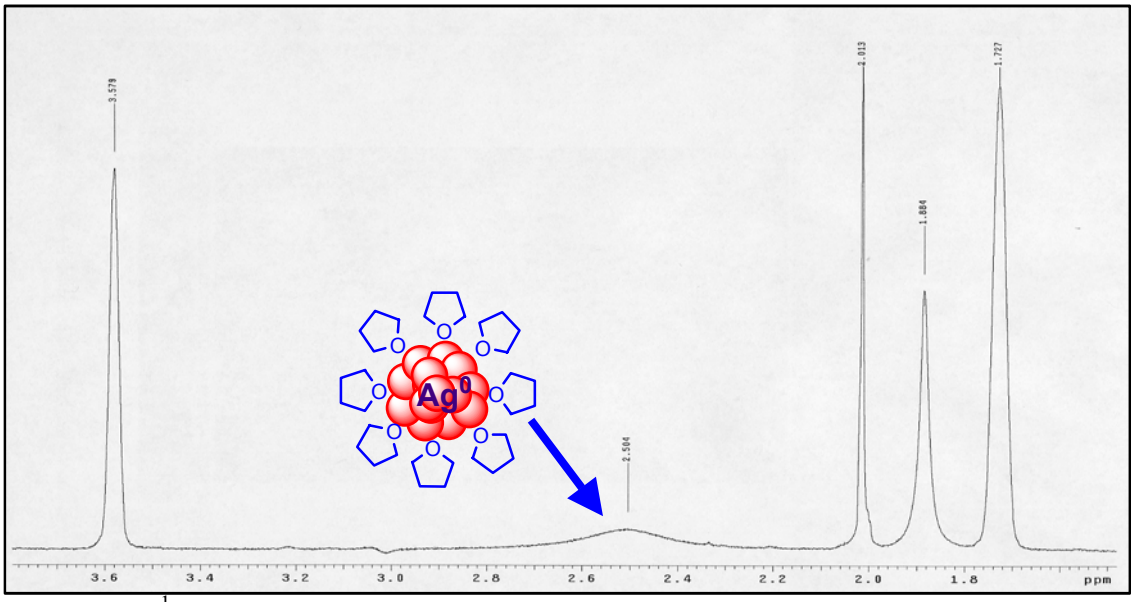


Figure 5.5: ^{1}H NMR of THF stabilized silver nanoparticles.

This solvent coordination phenomenon was also verified by ^{1}H NMR spectroscopy. Before analysis using ^{1}H NMR, the 'polysiloxane-Ag(0)' was stirred with 2-ml of THF-d_8 for 2h and then 0.5-ml was transferred in to the NMR tube for analysis. In ^{1}H NMR the $-OCD_2$ protons of pure THF-d_8 shows at 3.57 ppm, along with this peak, there was a broad new peak appeared at 2.50 ppm corresponds to the coordinated THF molecules, see Figure 5.5. The THF stabilized silver nanoclusters were also analyzed by transmission electron microscope. The data showed particles that were quite monodisperse having 3.1 nm average size with 0.7 nm standard deviation. The THF stabilized particles are stable for long period of time with aggregation or precipitation from the solvent. Figure 5.6 represents the TEM image and the corresponding histogram of THF stabilized silver nanoparticles.

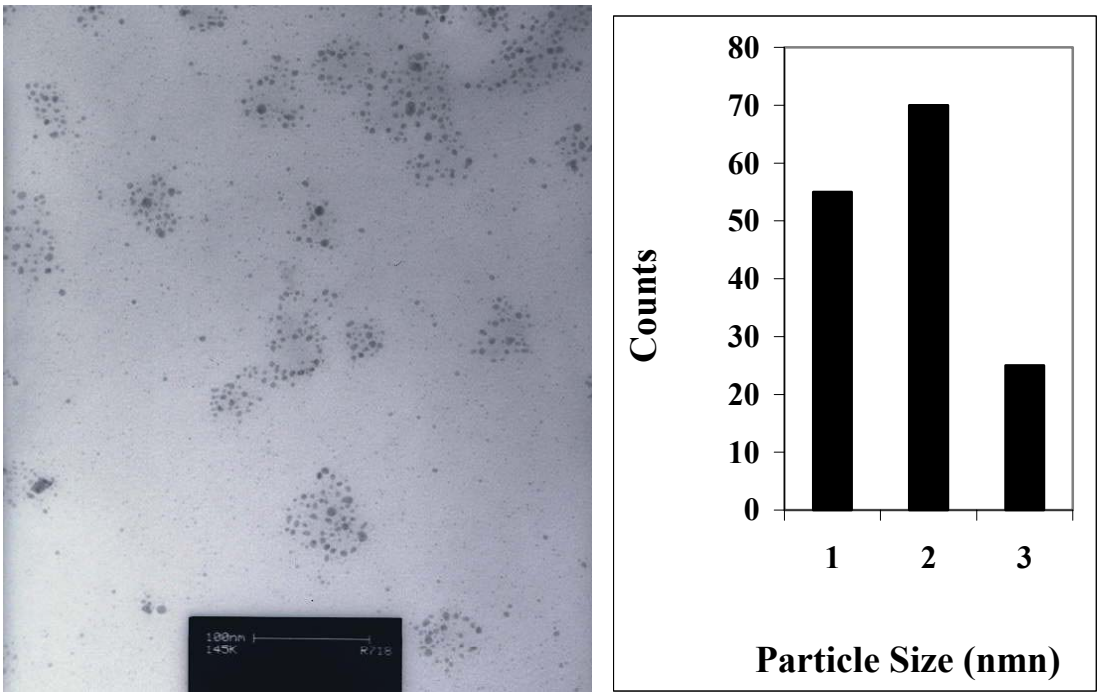


Figure 5.6: TEM image and the corresponding histogram of THF stabilized silver nanoparticles.

A comparative study of the absorption maxima and particle size is compiled in the Table 5.1.

Table 5.1: Comparison of absorption maxima and particle size analysis of silver nanoparticles in different solvents.

Entry	Solvents	Refractive Indices (n)	UV-vis maxima (λ_{max})	Particle size (nm) Std. Dev. (nm)
1	DMSO	1.4360	450	9.5 2.7
2	THF	1.4070	420	3.1 0.7
3	DMF	1.4310	400	4.3 1.4
4	CH_3CN	1.3440	395	3.9 0.8
5	Toluene	1.4960	430	2.3 0.3
6	Cyclohexane	1.4260	420	2.5 1.1

Most of the time it was observed that the synthesized particles were not easily redispersable in organic solvent without any surfactant. The polysiloxane can be easily removed from Ag(0)-PMHS precursor using hexane as a solvent. Hexane is a very non-polar solvent in which only polysiloxane will dissolve not the silver colloids. 2-ml of dry hexane was added to the semi-solid product and stirred for 2h at room temperature. After stirring the reaction mixture was centrifuged and a very faint yellow solution was decanted out. The similar procedure was carried out for at least three times and at this point the hexane solution was completely colorless. After proper washing, a brown solid was obtained and dried under high vacuum and analyzed by FT-IR spectroscopy, where traces of polysiloxane were still observed, Figure 5.7. The brown solid was then dispersed into strong coordinating solvent, such as acetonitrile, THF, DMSO, or DMF

and it was readily dispersable in those solvents but it was not dispersed in toluene or cyclohexane. The peak intensity of the redispersed product was lower compared to the pure Ag(0)-PMHS precursor; the reason might be during the washing step with hexane, some of the product dispersed into it.

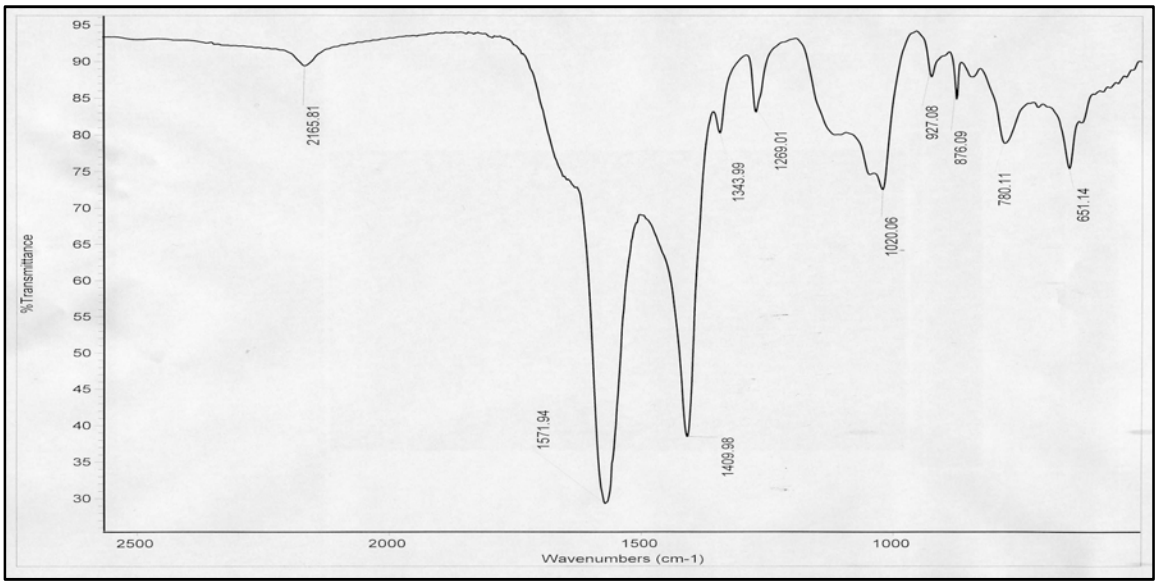
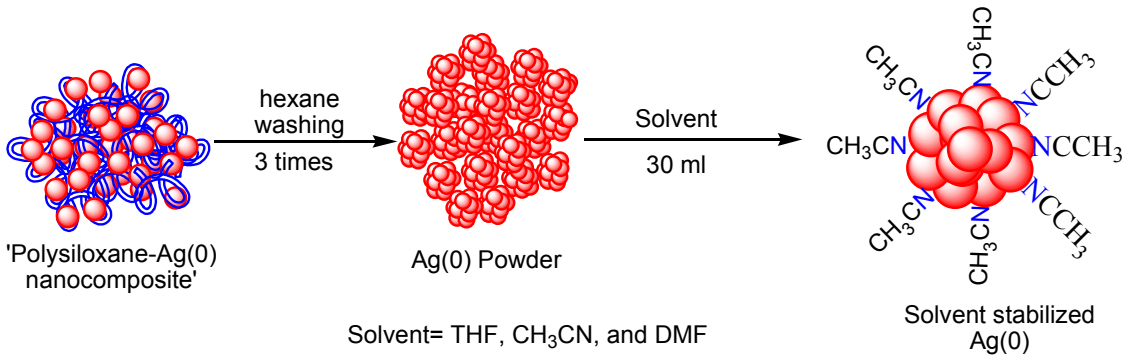


Figure 5.7: Solid state FT-IR of the brown solid after washing with hexane.



Scheme 5.2: Schematic representation of processing of Ag(0) powder and its dispersion in coordinating solvents.

The brown solid was then analyzed by XPS, SEM and EDS. The XPS spectrum of the brown product was carried out determine out the oxidation states of silver present in the powder. Figure 5.8 shows the XPS obtained from the brown solid. The signals of the spectrum indicate the presence of C, Ag, and Si in the synthesized product. A high resolution scan over the 365-385 eV reveals a doublet of the Ag $3d_{5/2}$ peaks at 368.7 and the Ag $3d_{3/2}$ peaks at 374.8 eV corresponding to a peak to peak separation of 5.9 eV due to the presence of Ag (0) states since the peak position, line shapes, and peak to peak distance of the silver doublet are standard measurement of the silver oxidation state.[23]

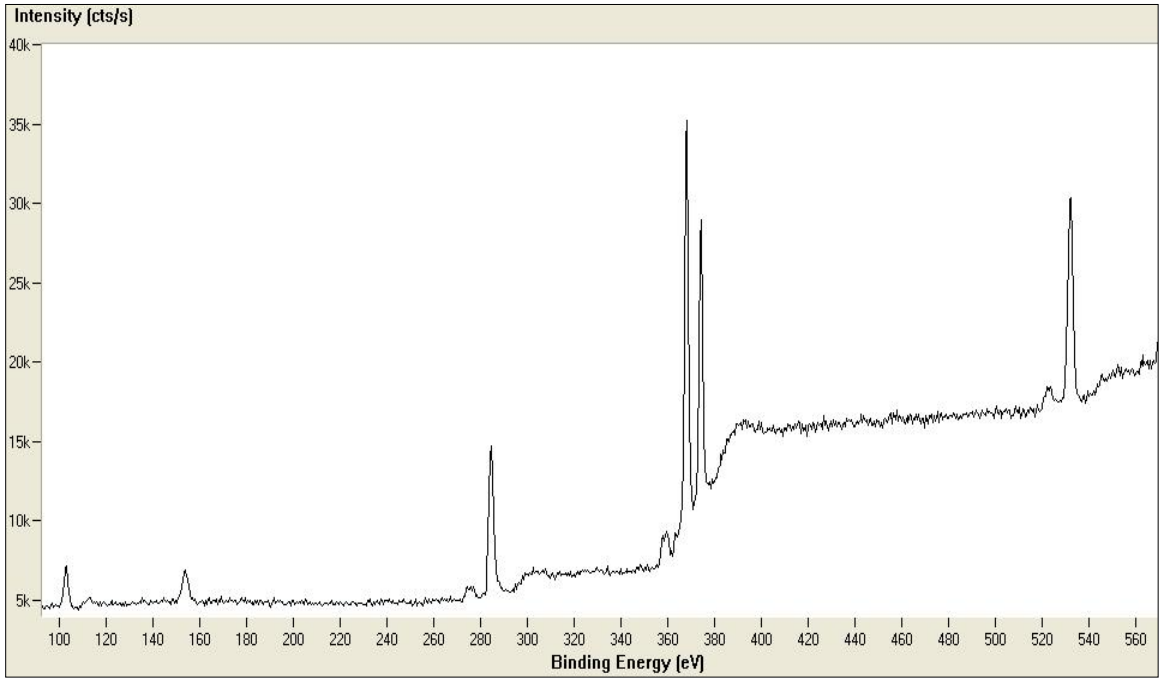


Figure 5.8: XPS spectra of brown solid.

The brown powder was also analyzed by SEM and EDS. The SEM picture shows present of small silver nanoparticles with 50 nm average sizes. The EDS analysis shows 81.53 Wt% silver was present in the brown powder. As we mentioned in the experimental procedure, 6 equivalents of PMHS were used with respect to silver salt, after washing

only 11.2 Wt% of silicon was present. It suggest that the hexane washing was very efficient to in the removal of excess siloxane from the nanoparticle surface.

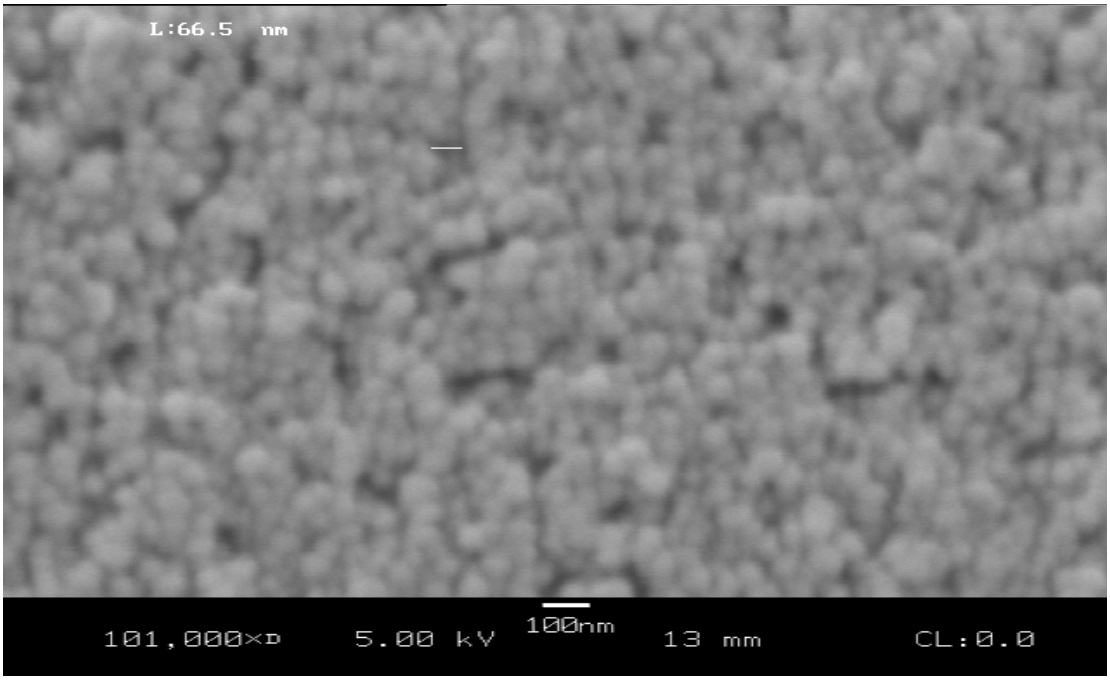


Figure 5.9: SEM image of brown powder.

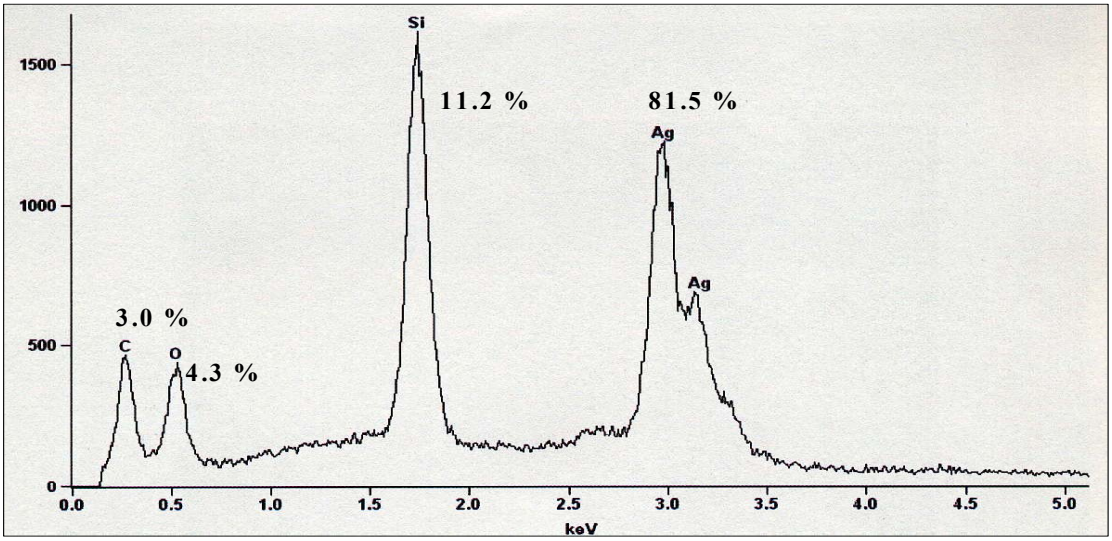


Figure 5.10: EDS analysis of the brown solid.

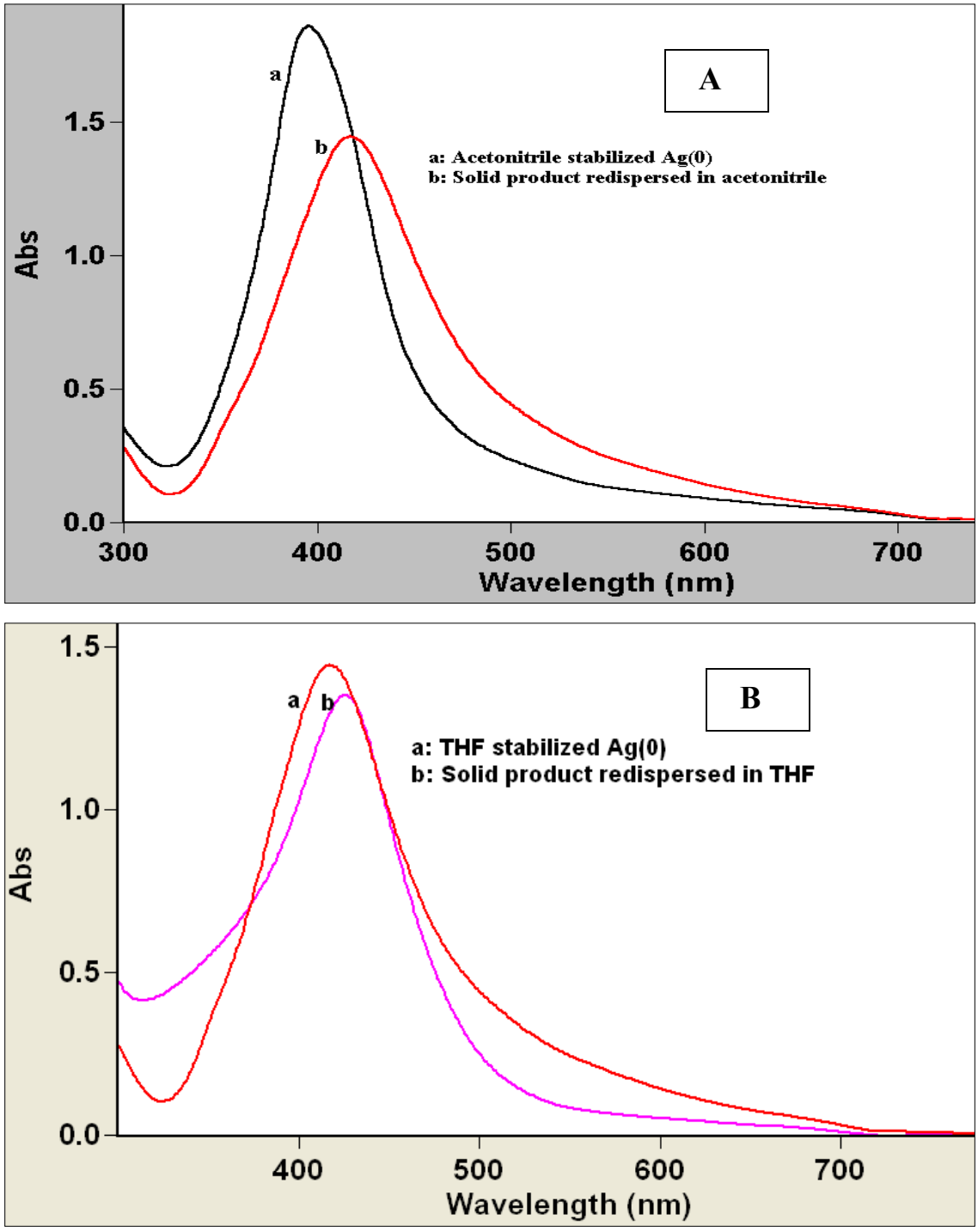


Figure 5.11: UV-vis abs. maxima of brown powder in acetonitrile(A) and THF(B).

The redispersion of brown powder was simple and straightforward. 30 ml of solvent was added to the brown solid and stirred for 2h at room temperature. After 2h of vigorous stirring, the color of the solution was yellow or brown, depending on the solvents. The solution was then analyzed by UV-vis spectroscopy where strong absorption for Ag(0) was observed. The colloidal solution was then analyzed by transmission electron microscopy (TEM). The acetonitrile stabilized (Figure 5.12) particles were large in size with a wide size distribution. This could have happened during the washing with hexane. The hexane washing eventually removed the polysiloxane from silver surface, therefore no effective stabilizing agent was present to stabilize the particles. The active small nanoparticles come closer and formed the bigger particles.

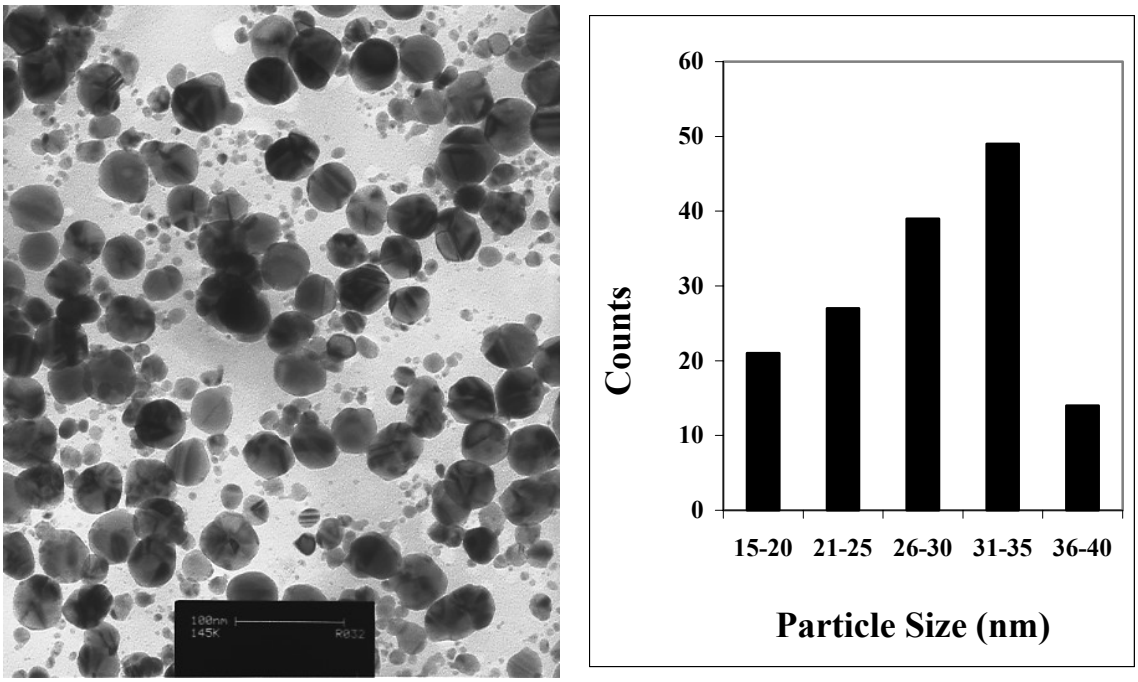
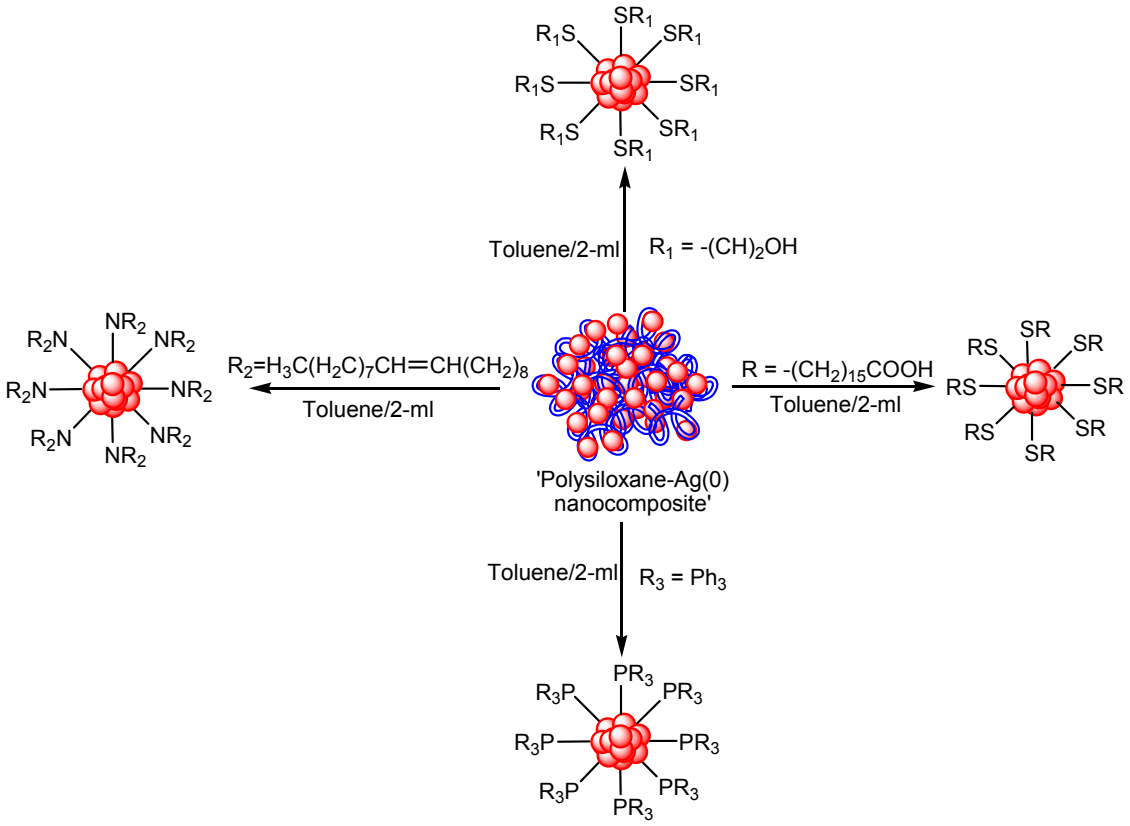


Figure 5.12: TEM image and the corresponding histogram of acetonitrile stabilized brown powder.

5.2 Functionalization of silver nanoparticles



Scheme 5.3: Functionalization of polysiloxane-Ag(0) nanocomposite with different surfactants.

Nanoclusters syntheses have received much attention due to unique size-dependent properties and new collective physical properties. However to fully exploit these properties nanocrystals functionalization is crucial and essential. In general, the key to functionalize nanoparticles is maintenance the original physical properties and in many cases, it is necessary to develop flexible nanocrystal surface chemistry, allowing further, subsequent functionalization. Inorganic-organic nanohybrid can be synthesized by assembling of organic molecules containing functional group, such as thiol, amine, acid,

and phosphine on the three dimensional surface of metal nanoparticles. Surface modification of metallic particles in nanometer size regime with organic molecules yields ordered structure[24, 25] and superstructure.[26] The chemical interactions change the electron density of the metal nanoclusters, there by directly impacting the absorption of the surface bound organic moiety as well as the surface plasmon absorption bond.[27] The borohydride reduction is the most common and widely used for the generation of metallic nanoparticles.[28] After the reduction, a variety of functionalized ligands can be introduced on the nanoparticle surface.[29] However, the disadvantages are the impurities that are introduced by the use of surfactant. Here we discusses the synthesis of functionalized silver nanoparticles from "polysiloxane-Ag(0)" nanocomposites, Scheme 5.3. This method provides us with the opportunity to functionalize of nanocrystals using a variety of ligands. The functionalized silver nanoparticles were stable in toluene for long period of time. In a typical functionalized nanocrystal synthesis procedure, 0.8 mmol (1:4 eqv. based on AgOAc) of ligand was added into the yellowish brown color polysiloxane-Ag(0) nanocomposite materials and stirred for 2h at room temperature. The resulting surfactant capped nanoparticles were then dispersed in 2-ml of toluene for further characterization. The nanoparticle dispersion was first characterized by FT-IR spectroscopy to investigate presence of surfactant on the nanoparticle surface. Figure 5.13 represents the IR comparison of pure oleylamine (A) with amine capped silver nanoparticles (B). The data shows clear formation of silver amine conjugates, where amine is acting as a stabilizing agent. In this study five different surfactants such as triphenylphosphine (TPP), 16-mercaptohexadecanoic acid (MHDA), dodecanoic acid (DDA), oleylamine (OA), and 11-mercapto-1-undecanol (MUN) were investigated.

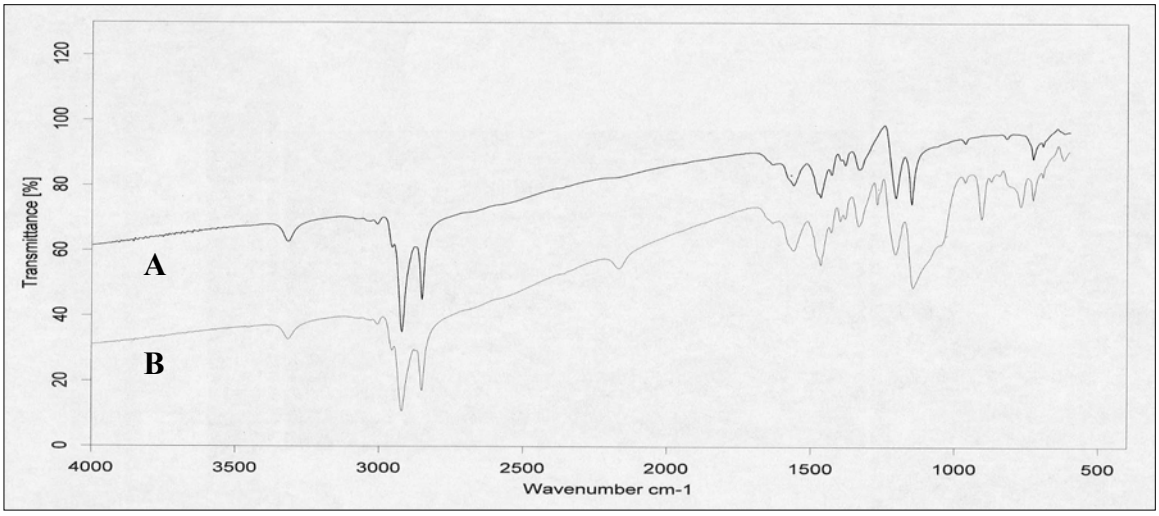


Figure 5.13: FTIR comparison of pure oleylamine (A) and the amine capped nanoparticles.

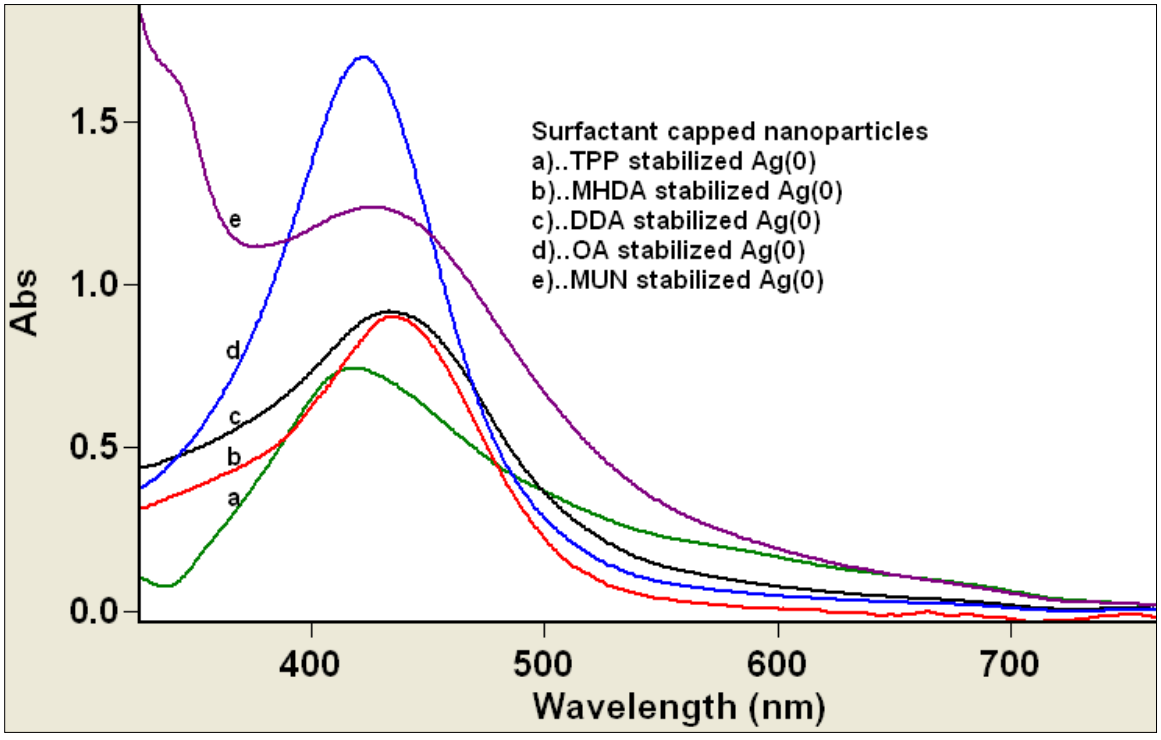


Figure 5.14: UV-vis absorption maxima of silver organosols in the presence of different surfactant.

Table 5.2: Comparison of UV-vis absorption maxima and particle size of silver nanoparticles in the presence of different surfactants.

Entry	Surfactant	UV-vis maxima (λ_{max}) nm	Particle size (nm) Std. Dev. (nm)
1	16-Mercaptohexadecanoic acid	425-435	4.3 (0.5)
2	11-Mercapto-1-undecanol	420-430	3.9 (0.9)
3	Oleylamine	418-422	3.2 (1.0)
4	Triphenylphosphine	414-420	3.9 (1.1)
5	1-Dodecanoic acid	424-434	2.6 (0.7)

Figure 5.14 represents the comparison of UV-vis absorption of the silver organosols in the presence of different surfactant. The concentration of the surfactant capped silver nanoparticles in toluene varied and depended on the solubility of that particular surfactant in toluene. For this dispersion study, toluene was chosen as a solvent because it has no capping action towards the metal nanoparticles. In the beginning of this chapter, it was observed that the dispersibility of the 'polysiloxane-Ag(0)' nanocomposite in toluene was less and the particle populations were also very low. In the presence of surfactant, enhancement of the absorption maxima in toluene was observed, which indicated that the particles, which were capped by surfactant, was soluble in toluene. The oleylamine capped silver nanoparticles exhibited a very high absorbance, which can be explained by the higher solubility of amine in organic solvent. Figure 5.15 represents the TEM images of the different surfactant capped silver nanoparticles.

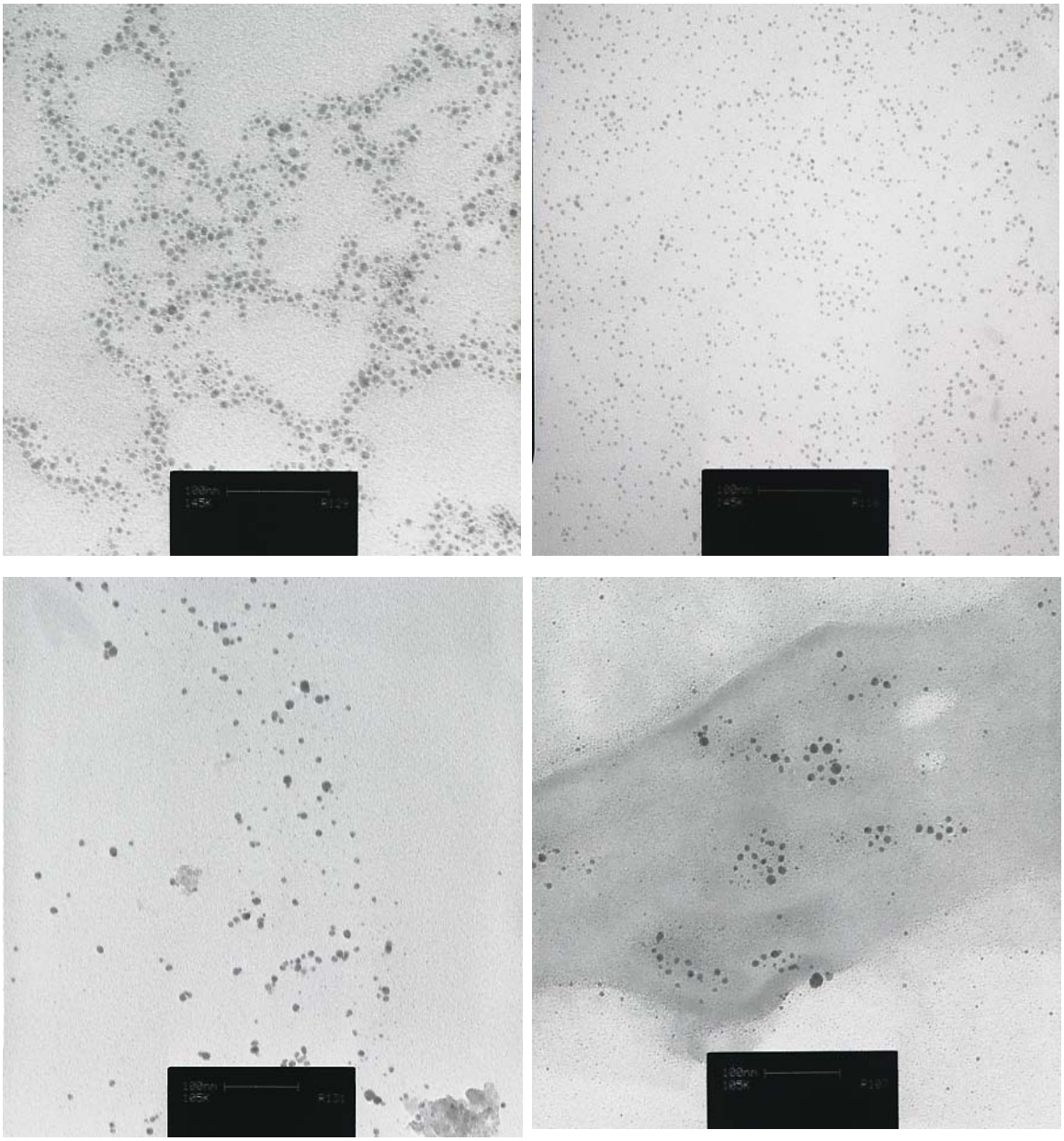


Figure 5.15: TEM images of different surfactant capped silver nanoparticles. (A) OA, (B) DDA, (C) TPP, and (D) MHDA.

5.3 Conclusion

In this chapter, a new facile synthesis for silver nanoparticles is presented. This is the first example where silver nanoparticles were achieved via a solventfree synthesis using PMHS as a solvent, reducing agent, and stabilizer. The key to the success of the single-phase approach is to maintain a tunable activity of the metal precursor. It combines the advantages of a surfactant free synthesis of a weakly stabilized nanoparticle precursor, which produce a stable dispersion in different organic solvents. Subsequent functionalization with a variety of capping ligand is accomplished in a straightforward manner.

5.4 Experimental Section

Preparation of polysiloxane-Ag(0) nanocomposite:

In an experiment procedure AgOAc (32 mg, 0.2 mmol) was taken in a test tube followed by drop-wise addition of PMHS (0.072 ml, 1.2 mmol) via a syringe under vigorous stirring. During stirring, color of the solid turned light yellow and finally after 24h it was yellowish brown color semi-solid materials. At this juncture, 2 ml freshly distilled solvent was added and stirred for another two more hours. Depending on the solvent polarity, the color of the solution varies from yellow to yellowish brown. The solution was the centrifuged and analyzed by UV-vis spectroscopy, TEM, AFM, and NMR.

Surfactant stabilized silver nanoparticles:

The silver nanoparticles can be stabilized by the addition of excess (1:4 eqv. based on AgOAc) of different ligands, which will usually done within 2h of reduction

step. For the preparation of nanoparticles soluble in organic solvents, 16-mercaptohexadecanoic acid, oleylamine, and triphenylphosphine were used. The surfactant capped nanoparticles was prepared via addition of 0.8 mmol of ligand into the yellowish brown color polysiloxane-Ag(0) nanocomposite materials and stirred for 2h at room temperature. The resulting surfactant capped nanoparticles were dispersed in 2-ml of toluene for further characterization.

Experimental Technique:

Microscopic UV-Visible absorption measurements were carried out with a Varian Cary 50-scan spectrophotometer in a10-mm optical path length quartz cuvettes. All spectra shown here are the result of macroscopic measurements performed in standard transmission geometry with unpolarized light impinging upon the surface at normal angle of incidence. Transmission electron microscope (TEM) is a suitable technique used in investigating the size and shape changes of small metallic nanoparticles. The TEM micrographs were obtained with the help of a Philips CM-100 instrument operating at 80 Kv accelerating voltage. TEM samples were prepared by placing a drop of centrifuged reaction mixture on the surface of a 150 mesh (Electron Microscopy Science, Port Washington, PA) copper grid backed with formver and were dried at ambient temperature. The crude reaction mixtures were centrifuged for 10 minutes before deposition on the grid. Particle size analysis was conducted using the Scion Image Beta 4.02 Software (available on the Internet at http://www.scioncorp.com). Images, which have 100 nm scale bar, was chosen to do the particle size analysis. In Scion Image, after setting the unit and known distance the ‘Analyze Particle’ parameter was used to generate a table of particle diameter. This table was then exported into Microsoft Excel 2000

where statistical analysis and histogram plotting were performed. Scanning electron microscope Amray 1910 (SEM) was used to conduct the morphological studies of the semisolid product before redispersion. X-ray photoelectron spectroscopy (XPS) study of the solid was performed with an Omicron Nanotechnology XPS instrument equipped with Mg Kα X-ray source (hυ = 1253.6 eV). ^{1}H NMR spectra (200 MHz) were recorded using the Varian unity NMR instrument. IR studies were carried out by the Magna- IR Spectrometer 550 using a KBr cell.

5.5 References

1. Jose-Yacaman, M.; Perez, R.; Santigo, P.; Benaissa, M.; Gonsalves, K.; Carlson, G. *Appl. Phys. Lett*. **1996**, *69*, 913.

2. Smith, G. B.; Deller, C. A.; Swift, P. D.; Gentle, A.; Garrett, P. D.; Fisher, W. K. *J. Nanopart. Res*. **2002**, *4*, 157.

3. Zamborini, F. P.; Leopold, M. C.; Hickes, J. F.; Kulesza, P. J.; Malik, M. A.; Murray, R. W. *J. Am. Chem. Soc*. **2002**, *124*, 8958.

4. Murray, C. B.; Kagan, C. R.; Bawendi, M. G. *Annu. Rev. Mater. Sci*. **2000**, *30*, 545.

5. (a) Kiwi, J.; Gratzel, M. J. Am. Chem. Soc. 1979, 101, 7214. (b) Peng, Z. A.; Peng, X. G. *J. Am. Chem. Soc*. **2002**, *124*, 3343. (e) Pillai, Z. S.; Kamat, P. V. *J. Phys. Chem. B* **2004**, *108*, 945. (f) Brust, M.; Kiely, C. *J. Colloids and Surfaces A : Physicochem. Eng. Aspects* **2002**, *202*, 175.

6. (a) Sarathy, K. V.; Kulkarni, G. U.; Rao, C, N, R. *J. Chem. Soc. Chem. Commun*. **1997**, 537. (b) Fink, J.; Kiely, C. J.; Bethell, D.; Schiffrin, D. J. *Chem. Mater*. **1998**, *10*, 922. (c) Scott, R. W. J.; Wilson, O. M.; Crooks, R. M. *J. Phys. Chem. B*. **2005**, *109*, 692 and references therein.

7. (a) Jana, N. R.; Gearheart, L.; Murphy, C. J. *Langmuir* **2001**, *17*, 6782. (b) Samia, A. C. S.; Hyzer, K.; Schlueter, J. A.; Qin, C.-J.; Jiang, J. S.; Bader, S. D.; Lin, X.-M. *J. Am. Chem. Soc*. **2005**, *127*, 4126.

8. (a) Kim, B.; Tripp, S. L.; Wei, A. *J. Am. Chem. Soc*. **2001**, *123*, 7955. (b) Oliveira, M. M.; Ugrate, D.; Zanchet, D.; Zarbin, A. J. G. *J. Colloid Interface Sci.* **2005**, *292*, 429. (d) Frenkel, A. I.; Nemzer, S.; Pister, I.; Soussan, L.; Harris, T.; Sun, Y.; Rafailovich, M. H. *J. Chem. Phys*. **2005**, *123*, 184701.

9. (a) Gomez, S.; Philippot, K.; Colliere, V.; Chaudret, B.; Senocq, F.; Lecante, P. *J. Chem. Soc. Chem. Commun*. **2000**, 1945. (b) Schulz-Dobrick, M.; Sarathy, K. V.; Jansen, M. *J. Am. Chem. Soc*. **2005**, *127*, 12816. (c) Hiramatsu, H.; Osterloh, F. E. *Chem. Mater*.**2004**, *16*, 2509.

10. (a) Chauhan, B. P. S.; Rathore, J. S. *J. Am. Chem. Soc*. **2005**, *127*, 5790. (b) Chauhan, B. P. S.; Rathore, J. S.; Bandoo, T. *J. Am. Chem. Soc*. **2004**, *126*, 8493. (c) Chauhan, B. P. S.; Rathore, J. S.; Chauhan, M.; Krawicz, A. *J. Am. Chem. Soc*. **2003**, **125**, 2876.

11. (a) Larsen, T, H.; Sigman, M.; Ghezelbash, A.; Doty, R. C.; Korgel, B. A. *J. Am. Chem. Soc*. **2003**, *125*, 5638. (b) Sigman, M.B.; Ghezelbash, A.; Hanrath, T.; Saunders, A. E.; Lee, F.; Korgel, B. A. *J. Am. Chem. Soc*. **2003**, *125*, 16050. (c) Ghezelbash, A.; Sigman, M.B.; Korgel, B. A. *Nano Lett*. **2004**, *4*, 537.

12. Henglein, A.; Giersig, M. *J. Phys. Chem. B* **1999**, *103*, 9355.

13. Brust, M.; Walker, M.; Bethell, D.; Schiffrin, D. J.; Whyman, R. *J. Chem. Soc., Chem. Commun*. **1994**, 801.

14. (a) Nie, S.; Emory, S. R. *Science* **1997**, *275*, 1102. (b) Nie, S.; Doering, W. E. *J. Phys. Chem. B* **2002**, *106*, 311. (c) Khan, I.; Polwart, E.; McComb, D. W.; Smith, W. E. *Analyst* **2004**, *129*, 950. (d) Michaels, A. M.; Nirmal, M.; Brus, L. E. *J. Am. Chem. Soc*. **1999**, *121*, 9932. (e) Zhang, J.; Li, X.; Sun, X.; Li, Y.; *J. Phys. Chem. B* **2005**, *109*, 12544.

15. (a) Sun, T.; Seff, K.; *Chem. Rev*. **1994**, *94*, 857. (b) Verykios, X. E.; Stein, F. P.; Coughlin, R. W. *Catal. Rev.-Sci. Eng*. **1980**, *22*, 197. (c) Kundu, S.; Mandal, M.; Ghosh, S. K.; Pal, T. *J. Colloid Interface Sci*. **2004**, *272*, 134.

16. (a) Belloni, J.; Mostafavi, M.; Marignier, J. L.; Amblard, J. *J. Imaging Sci*. **1991**, *35*, 68. (b) Mostafavi, M.; Marignier, J. L.; Amblard, J. Belloni, J. *J. Radiat. Phys. Chem*. **1989**, *43*, 605.

17. Chauhan, B. P. S.; Sardar, R. *Macromolecules* **2004**, *37*, 5136.

18. (a) Klingelhofer, S.; Heitz, W.; Greiner, A.; Oestreich, S.; Forster, S.; Antonietti, M. *J. Am. Chem. Soc.* **1997**, *119*, 10116. (b) Maclachlan, M. J.; Ginzburg, M.; Coombs, N.; Coyle, T. W.; Raju, N. P.; Greedan, J. E.; Ozin, G. A.; Manners, I. *Science* **2000**, *287*, 1460. (c) Walker, C. H.; John, J. V. S.; Wisian-Neilson, P. *J. Am. Chem. Soc.* **2001**, *123*, 3846. (d) Mossmer, S.; Spatz, J. P.; Moller, M.; Aberle, T.; Schmidt, J.; Burchard, W. *Macromolecules* **2000**, *33*, 4791. (e) Corbierre, M. K.; Cameron, N. S.; Sutton, M.; Mochrie, S. G. J.; Lurio, L. B.; Ruhm, A.; Lennox, R. B. *J. Am. Chem. Soc.* **2001**, *123*, 10411. (f) Wuelfing, W. P.; Gross, S. M.; Miles, D. T.; Murray, R. W. *J. Am. Chem. Soc.* **1998**, *120*, 12696. (g) Ohno, K.; Koh, K.-m.; Tsujii, Y.; Fukuda, T. *Macromolecules* 2002, 35, 8989.

19. Aiken, J. .D., III; Finke, R. G. *J. Mol. Catal. A: Chem*. **1999**, *145*, 1.

20. Horswell, S. L.; Kiely, C. J.; O'Neil, I. A.; Schiffrin, D. J. *J. Am. Chem. Soc*. **1999**, *121*, 5573.

21. Yonezawa, T.; Imamura, K.; Kimizuka, N. *Langmuir* **2001**, *17*, 4701.

22. (a) Ontka, A. C.; Angelici, R. J. *Langmuir* **1998**, *14*, 1684. (b) Shih, K, C.; Angelici, R. J. *Langmuir* **1995**, *11*, 2539.

23. Kang, S. Y.; Kim, K. *Langmuir* **1998**, *14*, 226.

24. (a) Motte, L.; Billoudet, F.; Lacaze, E.; Douin, L.; Pileni, M. P. *J. Phys. Chem. B* **1997**, *101*, 138. (b) Petroski, J. M.; Green, T. C.; El-Sayed, M. A. *J. Phys. Chem. A* **2001**, *105*, 5542.

25. Lin, Y.; Boker, A.; He, J.; Sill, K.; Xiang, H.; Abetz, C.; Li, X.; Wang, J.; Emrick, T.; Long, S.; Wang, Q.; Balazs, A.; Russell, T. P. *Nature* **2005**, *434*, 55.

26. Yonezawa, T.; Onoue, S. Y.; Kimizuka, N. *Adv. Mater*. **2001**, *13*, 140.

27. (a) Kreibig, U.; Vollmer, M. *Optical Properties of Metal Clusters*; Springer: New York, 1995. (b) Storhoff, J. J.; Lazarides, A. A.; Mirkin, C. A.; Letsinger, R. L.; Mucic, R. C.; Schatz, G. C. *J. Am. Chem. Soc*. **2000**, *122*, 4640. (c) Malinsky, M. D.; Kelly, K. L.; Schatz, G. C.; Van Duyne, R. P. *J. Am. Chem. Soc*. **2001**, *123*, 1471.

28. (a) Mayer, A. B. R.; Antonietti, M. *Colloid Polym. Sci*. **1998**, *276*, 769 and references therein. (b) Balogh, L.; Tomalia, D. A. *J. Am. Chem. Soc*. **1998**, *120*, 7355. (c) Zhao, M.; Sun, L.; Crooks, R. M. *J. Am. Chem. Soc*. **1998**, *120*, 4877. (d) Zhao, M.; Crooks, R. M. *Angew. Chem. Int. Ed. Engl*. **1999**, *38*, 364.

29. (a) Bengo, P.; Polizzi, S.; Battagliarin, M.; Pasquato, L.; Scrimin, P. *J. Mater. Chem*. **2003**, *13*, 2471. (b) Dobrick, M. S.; Sarathy, K. V.; Jansen, M. *J. Am. Chem. Soc*. **2005**, *127*, 12816.